Intracellular chloride and hydrogen ion dynamics in the nervous system

Joseph Valentino Raimondo

Thesis submitted for the degree of
Doctor of Philosophy

Lincoln College
University of Oxford
Trinity Term 2012

Abstract

Synaptic transmission in the nervous system involves the activation of receptor proteins that permit rapid transmembrane fluxes of ions. Ionic gradients across the membrane determine the direction and driving force for the flow of ions and are therefore crucial in setting the properties of synaptic transmission. These ionic gradients are established by a variety of mechanisms, including pump and transporter proteins. However, the gradients can be affected by periods of neural activity, which in turn, are predicted to influence the properties of ongoing synaptic transmission. In this thesis I have examined the concentration gradients of two ions that play a fundamental role in synaptic transmission: chloride ions (Cl^-) and protons (H^+).

Type A γ-Aminobutyric acid receptors ($GABA_A$Rs) are primarily permeable to Cl^- and mediate the majority of fast post-synaptic inhibition in the brain. The transmembrane concentration gradient for Cl^- is therefore a critical parameter in governing the strength of synaptic inhibition. In the first part of the Thesis I use a combination of experimental and theoretical approaches to demonstrate that influxes of Cl^- via activated $GABA_A$Rs can overwhelm a neurons ability to maintain a stable Cl^- concentration gradient. The consequence is that subsequent activation of $GABA_A$Rs results in weaker inhibition or even excitation, which alters how the neuron integrates synaptic inputs. This process is shown to be dependent upon the level of activity of the $GABA_A$R, the post-synaptic cells membrane potential and the cellular compartment into which the Cl^- flows. These principles were extended to demonstrate that popular optogenetic strategies for silencing neural activity have different effects upon $GABA_A$R transmission. A light-activated Cl^- pump was shown to cause substantial accumulations in intracellular Cl, which meant that the strength of synaptic inhibition was significantly reduced following light offset.

In the second part of the Thesis I use electrophysiological and fluorescence imaging techniques to demonstrate that the activation of $GABA_A$Rs during epileptiform activity results in pronounced changes to the transmembrane Cl^- gradient. Indeed, these changes convert synaptic inhibition into synaptic excitation during the course of a seizure event. As part of this work I characterise a novel, genetically-encoded reporter for measuring intracellular Cl^- dynamics in different cell types and subcellular compartments. A significant advantage of this reporter is that it permits the simultaneous quantification of H^+ fluxes, which are also shown to change in an activity-dependent manner and which have been a confounding factor for previous Cl^- reporters.

In the third and final part of the Thesis I use genetically-encoded reporters to investigate activity-dependent changes in intracellular H^+ concentration. I demonstrate that markedly different pH changes occur in neurons and astrocytes during epileptiform activity. Whereas neurons become acidic, astrocytes become alkaline and the dynamics of these pH shifts exhibit a very different temporal relationship with the seizure event.

In conclusion, this thesis demonstrates that the intracellular concentrations of Cl^- and H^+ are dynamic variables that evolve across time and space, in an activity-dependent manner. Changes in the transmembrane gradients of these two ions influence ongoing synaptic transmission. Therefore this work has significant implications for our understanding of network activity and the balance of synaptic excitation and inhibition.

For Mom and Dad,

Acknowledgements

I would like to thank my supervisor Colin, for sharing with me the joy of science. The long hours spent discussing confusing findings or cooking up new experiments with you are moments that I will always cherish. Your warm demeanour, gentle discipline and infectious optimism have made the last four years a very happy time. I've felt like I've been on the bridge of the Starship Enterprise setting forth on a voyage of discovery. Thank you, I've learned so much from you.

I must thank all the basement dwellers of the Akerman lab, you've been an awesome environment of friendship and of intellectual stimulation.

To all the previous and current inmates of Western Rd, first you sheltered me from the storm, then we created our very own maelstrom. It's been both tender and wild, what a perfect combination.

To Mom and Dad, Kee, Tee and Mike thank you for instilling in me a love for the world.

Lastly, Jane thank you for everything you are, I love you very much.

And Knorrox, I'm coming for you dinner...

Contents

1 Introduction **7**

1.1 Neural signalling and the balance between synaptic excitation and inhibition 7
1.2 Synaptic transmission relies on ion gradients 8
1.3 The hippocampal formation and inhibitory circuitry 10
1.4 Synaptic inhibition is mediated by GABAergic transmission 13
1.4.1 $GABA_A$ receptors 13
1.4.2 $GABA_B$ receptors 15
1.4.3 Fast synaptic inhibition is mediated by Cl^- permeable $GABA_A$ receptors 15
1.5 Cl^- gradients show activity dependent changes 18
1.5.1 Long-term changes in the driving force for $GABA_A$Rs 18
1.5.2 Short-term plasticity at $GABA_A$Rs 19
1.5.3 Cl^- accumulation underlies short-term changes to the $GABA_A$R reversal potential 20
1.5.4 An optogenetic silencing tool mediated by transmembrane Cl^- flux. . 22
1.5.5 Intracellular Cl^- accumulation driven by network activity 24
1.6 Intracellular H^+ ion concentration is modulated by activity 25
1.6.1 Baseline pH regulation 25
1.6.2 pH transport mechanisms 26
1.6.3 pH buffering systems 26
1.6.4 pH dynamics during activity 27
1.6.5 Activity-dependent pH shifts in neurons 27
1.6.6 pH affects network excitability 28
1.6.7 Activity-dependent pH shifts in astrocytes 28
1.6.8 Activity-dependent pH shifts in the extracellular space 29
1.7 Techniques for measuring Cl^- and H^+ concentration 29
1.7.1 Measuring intracellular Cl^- concentration 30
1.7.2 Measuring intracellular H^+ concentration 32
1.8 Thesis aims 33

2 Materials and Methods **35**

2.1 Preparation of Slices 35
2.1.1 Organotypic hippocampal slices 35
2.1.2 Acute slices 35
2.2 Plasmids and transfection techniques 36
2.2.1 Ion sensitive genetic reporters 36
2.2.2 Neural silencers 36
2.2.3 Subcloning alternative red fluorescent protein variants into ClopHensor 37
2.2.4 Biolistic gene delivery 37

2.2.5 Viral delivery *in vivo* . . . 37
2.3 Electrophysiological recordings . . . 38
2.3.1 Gramicidin perforated patch recordings . . . 38
2.3.2 Calculating E_{GABAA}, g_{GABAA} and generating Cl^- loads . . . 39
2.3.3 Photoactivation of eNpHR and Arch . . . 40
2.3.4 Estimating E_{GABAA} during seizure episodes . . . 41
2.3.5 Cell-attached recordings . . . 41
2.3.6 Whole-cell recordings . . . 41
2.3.7 Seizure models . . . 42
2.4 Computational models . . . 43
2.4.1 NEURON multi compartment model . . . 43
2.4.2 Matlab single compartment model . . . 45
2.5 Cl^- and pH imaging . . . 47
2.5.1 MQAE based Cl^- imaging . . . 47
2.5.2 Recording intracellular pH . . . 47
2.5.3 Recording intracellular Cl^- and pH using ClopHensor2 . . . 48
2.5.4 Cl^- calibration . . . 49
2.5.5 pH calibration . . . 50
2.6 Drugs . . . 51
2.7 Data analysis and statistics . . . 52

3 Transient changes in the driving force for $GABA_A$Rs 53
3.1 Introduction . . . 53
3.2 Strong $GABA_A$R activation transiently increases intracellular Cl^- . . . 54
3.3 Compartment differences in Cl^- loading . . . 55
3.3.1 Computational modelling of cell compartment differences in Cl^- regulation . . . 58
3.4 Optogenetic silencers generate inhibitory photocurrents . . . 63
3.5 eNpHR activation changes GABAergic transmission . . . 64
3.6 The spatio-temporal dynamics of eNpHR induced Cl^- loads . . . 67
3.7 Modelling eNpHR induced Cl^- loads . . . 69
3.8 eNpHR effects spiking activity post laser activation . . . 71
3.9 Discussion . . . 75

4 Cl^- accumulation during network activity 79
4.1 Introduction . . . 79
4.2 Seizures shift GABA potentials . . . 80
4.3 Seizures shift E_{GABAA} . . . 82
4.4 Shifts in GABA responses differ between compartments . . . 84
4.5 MQAE detects Cl^- shifts . . . 90
4.6 Seizure associated Cl^- accumulation is mediated by $GABA_A$Rs . . . 91
4.7 ClopHensor2 reports Cl^- and pH in neurons . . . 91
4.8 ClopHensor2 calibration . . . 95
4.9 ClopHensor2 detects Cl^- and pH shifts . . . 99
4.10 Quantifying Cl^- accumulation during seizures . . . 102
4.11 Gabazine attenuates seizure associated Cl^- influx . . . 104
4.12 Discussion . . . 106

5 Activity-dependent intracellular pH transients 113
5.1 Introduction . . . 113
5.2 Detecting activity-dependent changes in pH . . . 114
5.3 Calibrating genetically encoded pH sensors . . . 115
5.4 Acidic transients during 0 Mg^{2+} epileptiform activity . . . 117
5.5 Acidic transients during 0 Cl^- epileptiform activity . . . 121
5.6 The kinetics of acidic intracellular transients . . . 123
5.7 Seizures induce alkaline transients in astrocytes . . . 125
5.8 pH transients differ between astrocytes and neurons . . . 129
5.9 A Na^+ / HCO_3^- cotransporter mediates the alkaline transient . . . 131
5.10 Discussion . . . 134

6 General Discussion 143
6.1 Cl^- accumulation shifts E_{GABAA} . . . 143
6.1.1 Optogenetics offer a novel approach for modulating intracellular Cl^- . 145
6.2 Extended effects of neural silencers . . . 146
6.3 Steady-state Cl^- regulatory mechanisms . . . 147
6.4 Short-term alterations in E_{GABAA} . . . 148
6.5 Cl^- accumulation in epilepsy . . . 150
6.5.1 Cl^- accumulation and seizure onset . . . 151
6.5.2 Mechanisms of seizure termination . . . 152
6.6 Activity induced alkaline transients in astrocytes. . . . 154
6.6.1 The intracellular effects of astrocytic alkalinisation . . . 154
6.6.2 The extracellular effects of astrocytic alkalinisation . . . 155
6.7 Concluding remarks . . . 157

List of Figures

1.1 Cells of the hippocampus . . . 12
1.2 The differential expression of Cl^- transporters underlies the change in E_{GABAA} during development . . . 17
1.3 Biphasic responses to intense $GABA_AR$ activation are caused by a rapid shift from hyperpolarising to depolarising E_{GABAA} . . . 22

3.1 Strong $GABA_AR$ activation transiently increases intracellular Cl^- . . . 56
3.2 $GABA_AR$ induced increases in intracellular Cl^- concentration recover . . . 57
3.3 Cell compartments differ in their ability to deal with a Cl^- load . . . 59
3.4 Population data demonstrates that dendrites are more susceptible Cl^- loads than somata . . . 60
3.5 A biophysical model of Cl^- regulation confirms cell compartment differences in susceptibility to a Cl^- load . . . 63
3.6 Optogenetic silencers generate robust inhibitory currents . . . 64
3.7 A light-activated chloride pump, but not a proton pump, causes a sustained change in GABAergic transmission . . . 69
3.8 In vivo virally-driven expression of optogenetic silencers have different effects upon GABAergic transmission in acute slices . . . 71
3.9 The spatio-temporal dynamics of eNpHR induced Cl^- loads . . . 73
3.10 A single compartment model of Cl^- accumulation and extrusion predicted photocurrent induced changes in E_{GABAA} . . . 75
3.11 Optogenetic silencing strategies differ in their effects on synaptically-evoked spiking activity . . . 77

4.1 Epileptiform activity induces a depolarising shift in GABAergic potentials . . . 82
4.2 Epileptiform activity causes a depolarising shift in E_{GABAA} . . . 84
4.3 Seizure induced depolarising shifts in $GABA_AR$ potentials differ between subcellular compartments . . . 86
4.4 Compartment specific differences in seizure induced E_{GABAA} shifts . . . 88
4.5 Detecting Cl^- accumulation during epileptiform activity using the Cl^- sensitive dye MQAE . . . 93
4.6 Seizure associated Cl^- accumulation is mediated by $GABA_ARs$ . . . 94
4.7 ClopHensor2: a genetically encoded Cl^- and pH sensor optimised for neuronal use . . . 97
4.8 Calibrating ClopHensor2 reveals independent pH and Cl^- sensitivity . . . 99
4.9 ClopHensor2 reports rapid Cl^- and pH shifts during epileptiform activity . . . 100
4.10 ClopHensor2 independently reports Cl^- and pH during epileptiform activity . 102
4.11 Quantification of Cl^- accumulation during epileptiform activity using ClopHensor2 . . . 104

4.12 ClopHensor2 reports activity-dependent Cl^- influxes across the somato-dendritic axis . . . 106
4.13 Gabazine attenuates seizure associated Cl^- influx . . . 108

5.1 Genetic reporters of pH detect intracellular pH changes during epileptiform activity . . . 116
5.2 Calibration of pH-sensitive GFP variants . . . 119
5.3 0 Mg^{2+} induced epileptiform activity induces acidic transients in neurons . . . 120
5.4 0 Cl^- induced epileptiform activity induces acidic transients in neurons . . . 122
5.5 The kinetics of acidic transients and epileptiform activity differ between seizure models . . . 125
5.6 Genetic reporters of pH reveal seizure induced intracellular alkaline transients in hippocampal astrocytes . . . 127
5.7 The 0 Mg^{2+} and 0 Cl^- seizure models induce alkaline transients in hippocampal astrocytes . . . 128
5.8 Seizure induced intracellular pH transients differ between hippocampal astrocytes and neurons . . . 131
5.9 The kinetics of seizure induced pH transients differ between cell types . . . 132
5.10 The seizure induced alkaline transient in astrocytes depends on HCO_3^- . . . 133
5.11 S0859 affects astrocytic alkaline transients and 0 Cl^- induced seizures . . . 135

Chapter 1

Introduction

1.1 Neural signalling and the balance between synaptic excitation and inhibition

The remarkable properties of the brain ultimately depend on the coordinated electrical activity of its constituent cells. It has long been asserted that neurons are the basic computational unit of the brain (Cajal, 1899), and the important role played by astrocytes is being increasingly appreciated (Perea et al., 2009). Neurons typically receive hundreds of synaptic inputs from other neurons and the release of neurotransmitter and activation of ligand-gated receptors at these synapses results in the generation of voltage signals in the postsynaptic cell. These input signals are integrated across time and space to determine whether an output is generated in the from of an action potential. This seemingly simple operation lies at the heart of every complex function performed by the brain.

Synaptic inputs differ in terms of the direction and magnitude of effect they have upon the postsynaptic membrane potential. Excitatory inputs work to depolarise the cell membrane potential in order to facilitate action potential generation. Inhibitory inputs meanwhile either hyperpolarise the membrane, or reduce the effect of depolarising currents that occur at the same time, thereby reducing the probability of an action potential. Many factors may differentially effect the strength of inhibitory and excitatory inputs to a neuron and by extension the levels of excitability within a neural network. Indeed, the strength of any particular synaptic connection between two neurons is not a static quantity, but rather a dynamic variable that may be altered by a variety of short and long-term plasticity pro-

cesses.

In the context of these dynamic processes the brain must maintain a delicate balance between excitation and inhibition. This balance is crucial for normal brain function and if it is disturbed, unrestrained hyperexcitability will be the result. Epilepsy is the general term used to describe such hyperexcitability and the primary feature of epileptic activity is the failure of inhibitory systems to contain the generation and spread of neuronal excitation (McCormick and Contreras, 2001).

1.2 Synaptic transmission relies on ion gradients

Ion gradients are fundamental to fast synaptic transmission. When neurotransmitter is released into the synaptic cleft and binds to receptors on the postsynaptic membrane, ions flow down their electrochemical gradient either into, or out of, the cell. The flux of these charged particles results in a change in the membrane potential of the postsynaptic neuron. As such, ion gradients represent the thermodynamic 'currency' that is spent in the process of synaptic transmission. The precise nature of these postsynaptic potentials depends upon the receptors from which they stem. Ligand-gated ion channels bind to specific neurotransmitters and are highly selective as to the type of ion which may traverse the channel pore upon opening. For example, excitatory neurotransmitters generally bind to ionotropic receptors that are permeable to cations such as sodium (Na^+), potassium (K^+) and calcium (Ca^{2+}). This results in an influx of positive ions which depolarise the neuronal membrane. In contrast, inhibitory neurotransmitters often activate receptors which lead to chloride (Cl^-) influx or K^+ efflux which serve to drive the membrane potential toward more negative values.

These ion gradients are established by the actions of ion pumps and transporters in the neuronal membrane. Pumps, such as the Na^+/K^+-ATPase, utilise energy from the hydrolysis of adenosine triphosphate (ATP) in order to move ions into, or out of, the cell. Na^+/K^+-ATPase, arguably the most important neuronal membrane pump, shuttles three Na^+ ions out the cell and two K^+ ions inward, for every molecule of ATP hydrolysed. This process is critical for establishing the transmembrane gradients of Na^+ and K^+ and it has been estimated that the Na^+/K^+-ATPase expends as much as 70% of the ATP utilised by the brain (Bear et al., 2007). Transporters meanwhile are membrane proteins that

typically utilise the transmembrane gradients of other ions, often Na^+ and K^+ gradients established by the Na^+/K^+-ATPase, in order to move ions across the membrane. For instance, transmembrane Cl^- gradients are established by transporter proteins that use the K^+ gradient to transport Cl^- out of the cell (e.g. the family of K^+- Cl^- cotransporters, see Fig. 1.2). Lastly, membrane impermeable, negatively charged proteins also modify the distribution of ions across the cell membrane via electrostatic attraction or repulsion of charged ion species.

Different compartments within the brain contain ions at different concentrations. This is because pumps, transporters, channels and other proteins are often differentially expressed on the borders of the compartments concerned. Three major compartments within the nervous system include the intra-neuronal, intra-astrocytic and extracellular space. Astrocytes are interwoven into the fabric of neuronal networks where, like neurons, they express a host of membrane proteins that establish particular ion gradients across their borders. By affecting ion concentrations within the extracellular space, these cells also modulate the ion gradients that are critical for synaptic transmission. Astrocytes have many roles including providing neurons with metabolites (Pellerin and Magistretti, 1994; Bacci et al., 2002), clearing released neurotransmitter and modulating synaptic plasticity processes (Min and Nevian, 2012; Kang et al., 1998; Henneberger et al., 2010; Perea and Araque, 2010; Yang et al., 2003).

In addition to the cell-type specific control of ion gradients, different subcellular compartments within an individual cell can also show differences in ion concentration. Such subcellular differences may result from the expression pattern of pumps and transporters, or the particular influxes of ion species into different regions of a cell. These regions may be separated by the membranes that surround organelles (e.g. synaptic vesicles or mitochondria) or by simple cell geography (e.g. distal dendrites versus the cell soma). An important question therefore is how ion gradients may be differentially regulated by network activity and in a manner that depends upon the cell-type or the subcellular compartment concerned.

As we have seen, synaptic transmission operates by the activation of receptors that release previously established ion gradients in order to cause voltage changes in the postsynaptic membrane. Recently, optogenetic techniques have been developed which

also utilise the same principle of transmembrane ion movement to control the activity of cells. By expressing microbial opsins, which act as light activated channels or pumps, researchers are able cause the exogenous flux of specific ions, which depolarise or hyperpolarise neurons (Boyden et al., 2005; Zhang et al., 2007). These techniques have had a tremendous impact in the neuroscience field as they enable the optical control of action potential generation in genetically defined subsets of cells. Given that the same ion species are used by neurotransmitter receptors and channels, an important consideration is how optical silencing tools may interact with endogenous signalling systems.

In this thesis I focus on two important ions: chloride (Cl^- and hydrogen (H^+). Both of these ions are critical to fast synaptic inhibition (Farrant and Kaila, 2007). This is because $GABA_A$Rs, the primary mediators of fast inhibition in the brain, are permeable to both Cl^- and HCO_3^- ions (Kaila, 1994). H^+ ion concentrations are intimately linked to HCO_3^- levels because intracellular and extracellular carbonic anhydrases rapidly catalyse the reaction of HCO_3^- and H^+ to H_20 and CO_2. Cl^- and H^+ are often coregulated (Sterling and Casey, 1999; Tabb et al., 1992) and activity driven neuronal processes often involve either the related, or independent, flux of both Cl^- and H^+ ions (Doyon et al., 2011). In the course of this thesis I have investigated how ionic gradients for Cl^- and H^+ are modulated by network activity. In turn, I have examined the reciprocal question: How do changes in the transmembrane gradients for Cl^- and H^+ affect the generation of activity within the nervous system?

1.3 The hippocampal formation and inhibitory circuitry

The work in this thesis was performed on the rat and mouse hippocampal formation. This structure forms part of the limbic system where it is believed to play important roles in both spatial learning and memory consolidation. The hippocampal formation includes the dentate gyrus, the cornu ammonis subdivisions one to four (CA1-CA4), the subiculum and entorhinal cortex (see Fig. 1.1). Neurons within the hippocampus have been shown to fire bursts of action potentials when an animal is in a particular location within its environment (dubbed ‘place cells’) (O’Keefe and Dostrovsky, 1971). In addition, neurons within the subiculum and entorhinal cortex can show a host of interesting spatially dependent behaviours. Individual cells may respond preferentially to the direction in which the

animal is heading ('head-direction cells', (Taube et al., 1990)), the border of the animal's environment ('border cells', (Solstad et al., 2008)) or in a repetitive, spatially defined, triangular pattern ('grid cells', (Hafting et al., 2005)). Consequently the hippocampal formation has been suggested to act as a 'cognitive map' by which animals may navigate their spatial environment (O'Keefe and Dostrovsky, 1971; Moser et al., 2008). It is also well known that damage to the hippocampal formation is associated with loss of episodic memory in both animals and humans. As such, the hippocampus is considered crucial for memory formation, particularly the consolidation of short-term memory into long-term representations (Burgess et al., 2002; Eichenbaum et al., 1992).

At a synaptic level, the hippocampal formation receives inputs from, and projects to, multiple brain areas including cortex, amygdala and thalamus (Andersen et al., 2006). Glutamatergic cell populations conduct excitatory signals through the hippocampal formation via a classic 'trisynaptic pathway' in which primary cells in the entorhinal cortex project to the dentate gyrus using the perforant path, then from the dentate gyrus to CA3 pyramidal cells via mossy cell fibres, and then finally Schaffer collaterals project from CA3 pyramidal cells to pyramidal cells in the CA1 area (Andersen et al., 2006). Neurons in the hippocampal formation also receive inputs from a vast array of inhibitory interneurons. Indeed, at least 21 classes of inhibitory interneuron have been identified in the CA1 region alone, each categorised according to their own pattern of synaptic connectivity, layer-specific location of their somata, characteristic firing patterns and expression of molecular markers (Klausberger and Somogyi, 2008; Somogyi and Klausberger, 2005). For example, axo-axonic cells (Chandelier cells) innervate the axon-initial segment (AIS) of pyramidal cells. Fast-spiking parvalbumin or cholecystokinin expressing basket cells target the soma and proximal dendrites of pyramidal cells, whilst bistratified and oriens-lacunosum molecular interneurons form inhibitory synapses onto the basal and apical dendrites respectively (See Fig. 1.1a). Pyramidal cells are also innervated by neurogliaform cells and Ivy cells, which provide slow inhibitory signals to the apical and proximal dendritic regions (Klausberger and Somogyi, 2008; Somogyi and Klausberger, 2005). Due to their different firing properties and precise spatial targeting, hippocampal interneurons are thought to be critical for shaping pyramidal cell output. As an example, perisomatic targeting basket cells can inhibit Na^+-dependent action potential generation

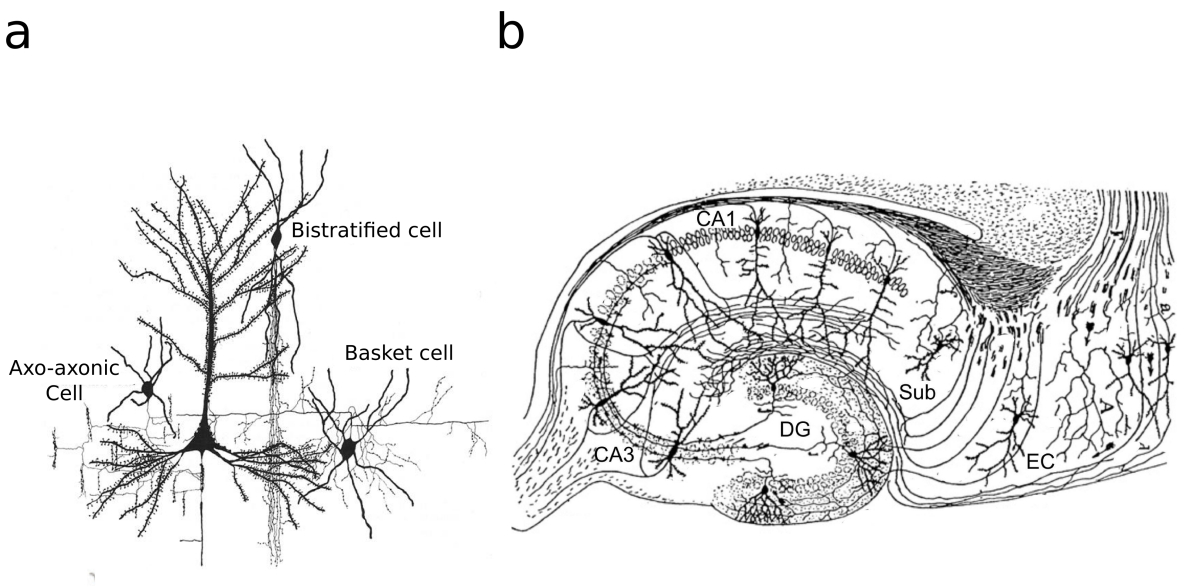

Figure 1.1: Cells of the hippocampus. (a) An example of a mature hippocampal pyramidal neuron. Three presynaptic interneurons and their patterns of connectivity are also depicted. The bistratified cell projects to pyramidal cell dendrites, the basket cell targets the pyramidal cell soma whilst the axo-axonic cell forms synapses onto the axon initial segment. Figure adapted from (DeFelipe and Farinas, 1992). (b) A horizontal slice of the hippocampal formation. Figure adapted from Cajal (1899). DG = dentate gyrus, CA3 = cornu ammonis area 3, CA1 = cornu ammonis area 1, Sub = subiculum, EC = entorhinal cortex.

from the soma and AIS of pyramidal neurons. In contrast, dendritic targeting interneurons have been shown to suppress slower, Ca^{2+}-dependent dendritic spikes (Miles et al., 1996). In addition to simply preventing action potential generation, inhibitory interneurons are also crucial for synchronising activity between neurons in order to generate network oscillations. This oscillatory activity has been suggested to underlie many cognitive functions including information processing, memory encoding and even consciousness (Buzsaki, 2006). It is therefore unsurprising that interneuronal dysfunction is associated with numerous disorders including schizophrenia, bipolar disorder and epilepsy (Benes and Berretta, 2001; Cossart et al., 2001; Dinocourt et al., 2003).

1.4 Synaptic inhibition is mediated by GABAergic transmission

Inhibitory inputs are important for shaping the input-output relationship of neurons and the excitability of neuronal networks. As described above, the importance of inhibition is reflected by the incredible variety of inhibitory interneurons that are strategically placed throughout the nervous system to regulate neural activity (Klausberger and Somogyi, 2008; Somogyi and Klausberger, 2005) and the dramatic proconvulsant effects of agents that block inhibitory signalling (Treiman, 2001). The bulk of inhibitory transmission within the central nervous system is mediated by the neurotransmitter γ-Aminobutyric acid (GABA). Currently, two classes of GABA receptor have been identified; ionotropic $GABA_A$ receptors and metabotropic $GABA_B$ receptors.

1.4.1 $GABA_A$ receptors

$GABA_A$ receptors ($GABA_A$Rs) are members of the 'Cys-loop' superfamily of ligand-gated ion channels, which include the nicotinic acetyl-choline receptors, glycine receptors and 5-HT3 receptors. These receptors are composed of pentameric assemblies of subunits (each with four transmembrane polypeptide sequences) that form a central ion channel, which opens upon neurotransmitter binding. In mammals, nineteen different $GABA_A$ receptor subunit genes have been identified. According to sequence similarity these have been divided into eight classes (six α, three β, three γ, one δ, one ϵ, one θ, one π and three ρ) (Sieghart and Sperk, 2002). $GABA_A$Rs are composed of two α, two β and a fifth subunit that is usually from a different subunit class. The particular subunit composition of $GABA_A$Rs is relevant for the distribution and functional properties of the receptor. The most common arrangement found in the brain is two $\alpha 1$, two $\beta 2$ and a $\gamma 2$ subunit (Benke et al., 2004). These receptors are associated with phasic inhibition and can be located at most GABAergic synapses (Nusser et al., 1996). It is suggested that the γ subunit is crucial for $GABA_A$R clustering at synapses (Farrant and Kaila, 2007). Consistent with this, $GABA_A$Rs where the γ subunit has been replaced by a δ subunit are exclusively found at extrasynaptic sites (Vithlani et al., 2011).

In addition to determining subcellular localisation, subunit composition also governs

the binding and gating properties of $GABA_A$Rs and hence the magnitude and time course of the conductance change elicited in response to GABA exposure. For efficient gating of the pore, two molecules of GABA are required to bind to each of the two interfaces between α and β subunits (Baumann et al., 2003). The group of the $GABA_A$R agonists, benzodiazepines, have a separate binding site at the interface between γ and α subunit. Studies using recombinant $GABA_A$Rs suggest that it is the type of α subunit that controls the sensitivity of the receptor to GABA (Vithlani et al., 2011). The α4 or α6 subunits, which are typically found at extrasynaptic locations, have the highest affinity for GABA, whilst α1-3 and α5 subunits, generally found within synapses, have considerably lower affinity for the neurotransmitter. The α subunit also affects the rates of activation, deactivation and desensitisation with receptors containing the 'extra-synaptic' subunits having far slower kinetics than their 'synaptic' counterparts. Most extra-synaptic $GABA_A$Rs, due to their lack of a γ subunit, are insensitive to benzodiazepines. Due to their particular α subunit composition described above, they also show high affinity to GABA and little desensitisation, which makes them well suited to producing continuous 'tonic' $GABA_A$R currents in response to low-levels of ambient GABA.

Interestingly, subunit composition also appears to affect the rectification properties of $GABA_A$Rs. Receptors which include subunits (α1-3) associated with phasic inhibition show outward rectification as would be predicted by the Goldman-Hodgkin-Katz equation and the unequal transmembrane concentration gradient of Cl^- (Farrant and Kaila, 2007). In contrast, receptors containing the α subunits associated with extrasynaptic localisation appear to show marked inward rectification (Granja et al., 1998), although studies investigating the rectification properties of tonic GABA in acute hippocampal slices have not confirmed this finding (Pavlov et al., 2009).

Whilst most $GABA_A$R subunits assemble as heteromers, ρ subunits, which are predominantly expressed in the retina, can form functional homomeric or heteromeric assemblies. These are insensitive to the classic $GABA_A$R antagonist bicuculline, which is why they are sometimes referred to as $GABA_C$ receptors (Vithlani et al., 2011).

1.4.2 $GABA_B$ receptors

Unlike $GABA_A$Rs, $GABA_B$Rs are metabotropic receptors associated with slow inhibitory effects. $GABA_B$Rs form part of the family of seven transmembrane receptors (7TMRs) whose signalling properties are mediated by guanine nucleotide-binding protein (G-protein) messenger systems (Bettler et al., 2004). Presynaptically, $GABA_B$Rs reduce release of both glutamate and GABA by inhibiting voltage gated Ca^{2+} channels. Postsynaptically, $GABA_B$Rs cause membrane hyperpolarisation by activating G-protein coupled inwardly rectifying K^+ channels (GIRK) (He et al., 2002).

1.4.3 Fast synaptic inhibition is mediated by Cl^- permeable $GABA_A$ receptors

Two variables determine the effect of $GABA_A$R mediated synaptic transmission on the postsynaptic membrane potential. The first is the reversal potential for $GABA_A$Rs (E_{GABAA}), whilst the second is the $GABA_A$R conductance (g_{GABA}). E_{GABAA} is a direct function of the combined ionic gradients for ions that are able to traverse the $GABA_A$ receptor. Open $GABA_A$Rs are approximately four times more permeable to chloride (Cl^-) than to bicarbonate (HCO_3^-) ions (Kaila, 1994). Whilst particular $GABA_A$R subunits have been shown to be relevant for the magnitude and time course of $GABA_A$R conductances, the link between $GABA_A$R subunit composition and relative ionic permeability of the channel has not been investigated.

The ionic gradient for Cl^- is the largest factor in determining the affect of $GABA_A$R activation. Typically, Cl^- is at a much higher concentration outside ($\approx$135 mM) as opposed to inside ($\approx$6 mM) neurons. This transmembrane gradient for Cl^- is established through several mechanisms. Firstly, the resting membrane potential of neurons is approximately -60 mV and, as a negative anion, intracellular Cl^- experiences significant electrostatic repulsion, which acts to extrude Cl^- via any Cl^- permeable channel. Secondly, the K^+-Cl^- cotransporter KCC2, utilises the K^+ gradient established by the Na^+ / K^+-ATPase to further transport Cl^- out of the cell (Blaesse et al., 2009). As a result, the reversal potential for Cl^- (the voltage that needs to be applied across the membrane to precisely counteract the tendency of Cl^- to flow down its concentration gradient) is typically -80 mV, somewhat more negative than the resting membrane potential. However, $GABA_A$R are permeable

to both Cl^- and HCO_3^-. Given the ionic permeabilities described above, E_{GABAA} (typically -70 mV) is much closer to the very negative Cl^- reversal (E_{Cl^-} typically -80 mV) than the considerably more positive HCO_3^- reversal ($E_{HCO_3^-}$; typically -20 mV) (Lambert and Grover, 1995). When γ-Aminobutyric acid (GABA) binds to $GABA_A$Rs, the bulk of anion flux through receptors is Cl^- flowing down its electrochemical gradient from outside to inside the cell (see Fig. 1.3a). This causes the membrane potential hyperpolarisation typical of classic $GABA_A$R mediated inhibition. In addition, by increasing local membrane conductance, activation of $GABA_A$Rs will also reduce or 'shunt' the effect of excitatory inputs occurring at a similar point in space and time.

The above description explains the biophysics of hyperpolarising GABAergic fast inhibition. However, this has dealt with E_{Cl^-} values that are below the resting membrane potential and this is far from always the case. Indeed, under a range of scenarios (see below) E_{Cl^-} can be more positive then the resting membrane potential. If this occurs, $GABA_A$R activation will result in Cl^- efflux and depolarisation. This will remain inhibitory, by virtue of the shunting effect described above, as long as E_{Cl^-} remains negative of the action potential threshold. If E_{Cl^-} exceeds this value, $GABA_A$R mediated transmission becomes excitatory by increasing the probability of action potential generation. In this manner, the intracellular Cl^- concentration $[Cl^-]_i$, by setting E_{Cl^-} and E_{GABAA}, determines the 'mode' of $GABA_A$R operation. The best described example of E_{GABAA} modulation occurs during early development when neurons undergo a shift in the ionic driving force for $GABA_A$Rs from depolarising to hyperpolarising (Ben-Ari, 2002). This change is the result of a developmental decrease in the levels of intracellular Cl^- caused by increased expression of the K^+-Cl^- cotransporter KCC2, which extrudes Cl^-, compared to the Na^+-K^+-$2Cl^-$ cotransporter NKCC1, which normally functions to raise $[Cl^-]_i$ (see Fig. 1.2).

The extent to which GABAergic inputs can move a neuron's membrane potential towards E_{GABAA} is a function of g_{GABA}. g_{GABA} in turn is determined by a host of synaptic parameters including the amount of transmitter released, the number of $GABA_A$Rs present, the $GABA_A$R subunit composition, channel kinetics, phosphorylation state and presence of channel modulators. Whereas E_{GABAA} sets the 'mode', g_{GABA} can be thought of as determining the 'strength' of the GABAergic synapse.

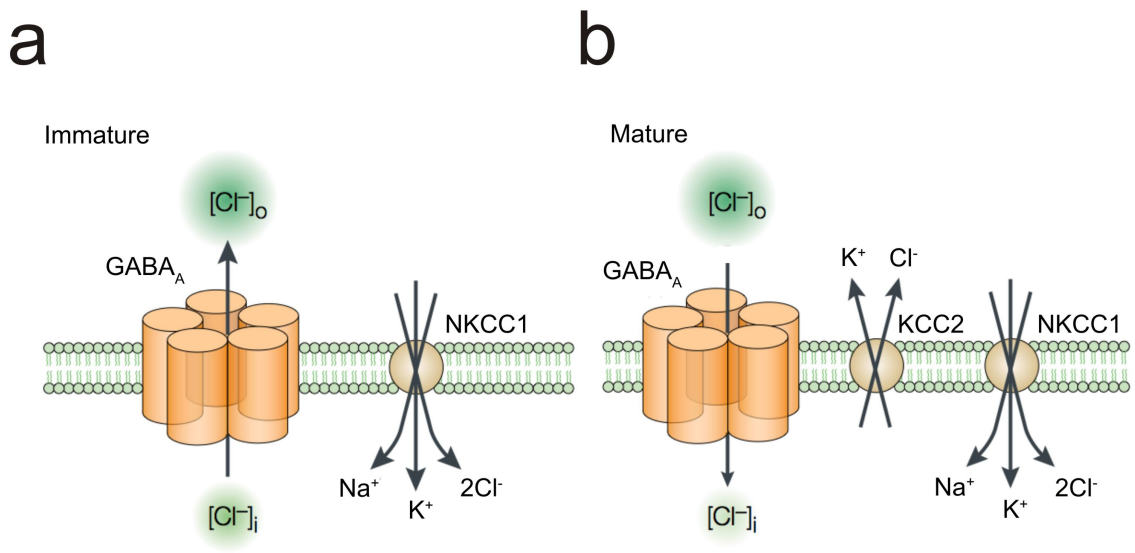

Figure 1.2: The differential expression of Cl^- transporters underlies the change in E_{GABAA} during development. (a) In early development, neurons have a high $[Cl^-]_i$ because the main active Cl^- co-transporter is NKCC1. NKCC1 uses the Na^+ gradient to transport Cl^- into the cell. This leads to a relatively depolarised E_{Cl^-} and thus E_{GABAA}. As a result, $GABA_A$ receptor activation leads to an efflux of Cl^- and depolarisation of the membrane potential. (b) During development the expression and activity of KCC2 increases. KCC2 uses the K^+ gradient to transport Cl^- out of the cell. This leads to a hyperpolarisation of E_{Cl^-} and E_{GABAA}, which means that $GABA_A$ receptor opening typically leads to an influx of Cl^- and hyperpolarisation of the membrane. Figure adapted from Owens and Kriegstein (2002).

1.5 Cl^- gradients show activity dependent changes

1.5.1 Long-term changes in the driving force for $GABA_A$Rs

Alterations to Cl^- and hence E_{GABAA} are known to underlie long-term plastic changes at GABAergic synapses (Wright et al., 2011). For instance, pathological periods of intense network activity, as are characteristic of hyperexcitability disorders such as epilepsy and neuropathic pain, are well know to cause long-term depolarising shifts in E_{GABAA} (Cohen et al., 2002; Pathak et al., 2007; Coull et al., 2005; Lu et al., 2008).

Cohen et al. (2002) were one of the first to uncover such a shift in a subset of hippocampal cells taken from human patients after surgery to treat temporal lobe epilepsy. They were able to show that instead of promoting epileptic activity, application of $GABA_A$R antagonists blocked epileptiform events, which suggests that at least in a significant number of cells, GABAergic transmission had become excitatory. In a similar vein, Rivera et al. (2004)showed that interictal activity, evoked using the low Mg^{2+} model in rat hippocampal slices, switched the driving force of GABAergic post-synaptic potentials from hyperpolarising to depolarising in CA1 pyramidal cells (Rivera et al., 2004). This depolarising shift in E_{GABAA} was correlated with a significant reduction in KCC2 mRNA and protein levels, as well as an increased rate of removal of the Cl^- co-transporter from the cell membrane (Rivera et al., 2004). Similar reductions in KCC2 mRNA and protein were also observed following in vivo kindling (Rivera et al., 2002). Similar studies have shown that long-term depolarising shifts in E_{GABAA} generated by epileptiform activity do correspond with an underlying increase in $[Cl^-]_i$ brought about by either a reduction in the expression of KCC2 (Rivera et al., 2004; Khalilov et al., 2003; Ben-Ari and Holmes, 2005) and/or an increase in NKCC1 expression (Dzhala et al., 2010; Bragin et al., 2009; Palma et al., 2006).

More physiological patterns of activity have also been shown to result in GABAergic plasticity via changes to E_{GABAA}. For example, periods of pre- and postsynaptic spiking can lead to a small 3-4 mV persistent depolarising change in E_{GABAA} (Woodin et al., 2003). A similarly sized shift may be elicited by sustained periods of postsynaptic spiking alone (Fiumelli et al., 2005). In both cases the underlying mechanism involved Ca^{2+} influx via L-type Ca^{2+} channels causing a sustained decrease in KCC2 activity and hence raised

$[Cl^-]_i$. Interestingly, Wang et al. (2006), showed that this kind of GABAergic plasticity could be induced in either direction, either generating depolarising or hyperpolarising shifts in E_{GABAA} depending on the level of Ca^{2+} influx associated with rebound spiking.

Due to the fact that such changes to E_{GABAA} can be generated solely via unspecific postsynaptic spiking (Fiumelli et al., 2005), combined with the fact that over extended periods of time Cl^- is predicted to diffuse and equilibrate throughout a neuron, it seems likely that this form of GABAergic synaptic plasticity is not specific to single synapses. Nonetheless, these changes can have important functional consequences. For instance, Ormond and Woodin (2009) showed that the paired stimulation protocols designed to induce glutamatergic long term potentiation (LTP) also produced depolarising shifts in E_{GABAA}. The resultant reduction in strength of the inhibitory synaptic input occurred in parallel to 'classical' LTP at glutamatergic synapses, with both serving to potentiate synaptic transmission.

The mechanisms underlying synaptic plasticity at GABAergic synapses are not limited to changes in E_{GABAA}. Indeed alterations in GABAergic synaptic conductance (g_{GABA}) are also known to play an important role. Such changes can vary widely in their underlying mechanism. For instance, they may be presynaptic by altering the probability of GABA release (Caillard et al., 1999) or postsynaptic; by altering the number of available post-synaptic $GABA_A$Rs (Nusser et al., 1998) or by modulating the efficacy of the $GABA_A$Rs themselves (Lu et al., 2000).

1.5.2 Short-term plasticity at $GABA_A$Rs

In addition to long-term changes in GABAergic synaptic function, it is well known that post-synaptic responses can also vary on short time scales, as a function of recent pre-synaptic activity (Davies et al., 1990; Fleidervish and Gutnick, 1995; Gupta et al., 2000). At some synapses facilitatory processes dominate under conditions of repeated use and this leads to synaptic enhancement. At other synapses depression prevails and the result of repeated use is a decrease in synaptic strength. In most cases however, multiple processes can co-occur at synapses and the result is a combination of facilitation and depression that depends on the timing of synaptic activation (Tsodyks and Markram, 1997; Varela et al., 1997). Although these processes have been most thoroughly investigated

at glutamatergic synapses, GABAergic synapses are known to display a wide array of short-term plasticity phenomena (Davies et al., 1990; Kirischuk et al., 2002; Fleidervish and Gutnick, 1995; Jiang et al., 2000; Mott et al., 1993), that can be related to the specific interneuron type that is the pre-synaptic source (Gupta et al., 2000; Pouille and Scanziani, 2004). Short-term plasticity phenomena such as these are generally thought to relate to pre-synaptic processes. For instance, synaptic facilitation is typically attributed to residual elevations of pre-synaptic calcium (Ca^{2+}), whilst depression is linked either to depletion of readily releasable synaptic vesicles (Zucker and Regehr, 2002) or the activation of presynaptic $GABA_B$ receptors (Davies et al., 1990; Lambert and Wilson, 1994). However, post-synaptic mechanisms can also contribute to these short-term synaptic plasticity events and these include desensitisation of the post-synaptic receptors (McCarren and Alger, 1985; Overstreet et al., 2000) or changes in the ionic driving force across the post-synaptic receptors. The latter process - transient shifts in the ionic driving force of the post-synaptic $GABA_A$Rs - will be a major focus of this thesis.

1.5.3 Cl^- accumulation underlies short-term changes to the $GABA_A$R reversal potential

Within the glutamatergic system, short-term changes to receptor reversal potentials via breakdown of ionic concentration gradients are not thought to occur. This is because the major ionotropic receptors for glutamate; AMPA, NMDA and Kainate receptors are equally permeable to Na+ and K^+. The concentration gradients across the neuronal membrane for these two ions are diametrically opposed resulting in glutamate receptors having a reversal potential around 0 mV. During periods of intense glutamatergic synaptic activity sodium influx and potassium efflux may reduce their respective concentration gradients at a local level, but as both ion concentrations are perturbed equally this will have no effect on the combined reversal potential for glutamate receptors.

In contrast, GABAergic synapses are potentially unique in that short-term plasticity mechanisms are postulated to include changes in the reversal potential for ionotropic GABA receptors. Previous work has demonstrated that the Cl^- influx that occurs during activation of $GABA_A$Rs is sometimes sufficient to significantly alter E_{GABAA} (Alger and Nicoll, 1979; Staley and Soldo, 1995; Thompson and Gahwiler, 1989*a*). The mecha-

nism is thought to operate as follows: E_{GABAA} is typically close to the neuronal resting membrane potential. This means that relatively small changes to E_{GABAA} can vary the functional effect of $GABA_AR$ activation and consequently neuronal output. As described above $GABA_ARs$ are permeable primarily to Cl^- and to a lesser extent HCO_3^- (Kaila, 1994). This means that at rest, E_{GABAA} (typically -75 mV) is much closer to the very negative Cl^- reversal (E_{Cl^-}; typically -85 mV) than the considerably more positive HCO_3^- reversal ($E_{HCO_3^-}$; typically -20 mV) (Lambert and Grover, 1995). During intense activation of $GABA_ARs$ however, rapid Cl^- influx exceeds Cl^- extrusion mechanisms and a breakdown in the Cl^- gradient occurs (Staley and Proctor, 1999). An equivalent collapse of the HCO_3^- gradient is prevented by the activity of intra- and extracellular carbonic anhydrases, which use CO_2 as a substrate to rapidly regenerate intracellular HCO_3^- (Rivera et al., 2005). As a result E_{GABAA} shifts toward the more positive $E_{HCO_3^-}$ during rapid, repeated activation of $GABA_ARs$. It is therefore likely that such a process could contribute to short-term synaptic depression of GABAergic potentials (McCarren and Alger, 1985).

Not only may inhibitory postsynaptic potentials (IPSPs) be reduced in size, intense $GABA_AR$ activation may cause IPSPs to change from being hyperpolarising to depolarising as E_{GABAA} shifts in a positive direction. Such biphasic responses have been documented previously (Thompson and Gahwiler, 1989*b*,*a*; Alger and Nicoll, 1979; Andersen et al., 1980). As described above they are though to depend on the differential collapse of the opposing concentration gradients of Cl^- and HCO_3^- (see Fig. 1.3)(Staley and Proctor, 1999; Lambert and Grover, 1995). Indeed, Staley and Soldo (1995) have shown that by bocking carbonic anhydrase, the enzyme that maintains intracellular HCO_3^-, with the drug acetazolamide prevents a depolarising response to strong $GABA_AR$ activation. Interestingly, a recent paper argues that this GABA elicited depolarisation is paradoxically accentuated by the activity of the electroneutral co-transporter KCC2 (Viitanen et al., 2010). Following the $GABA_AR$ -mediated accumulation of intracellular Cl^-, this leads to an accelerated extrusion of both Cl^- and K^+ by KCC2. Provided this extrusion of K^+ occurs within a large enough neuronal population, the resultant increase in extracellular K^+ can result in inward K^+ currents that further depolarise the cell membrane (Viitanen et al., 2010; Kaila et al., 1997). It should be noted that such shifts in E_{GABAA} are transient, such that once $GABA_AR$ activity subsides, $[Cl^-]_i$ returns to baseline levels within seconds or

minutes as Cl^- pumps gradually extrude the excess Cl^-(Staley and Proctor, 1999).

Many questions still remain. Firstly, what are the parameters that control a neuron's susceptibility to Cl^- accumulation? Secondly, how do short-term changes in the reversal potential for ionotropic GABA receptors affect synaptic integration and spike timing? These questions will be addressed as part of **Chapter 3** in this thesis.

1.5.4 An optogenetic silencing tool mediated by transmembrane Cl^- flux.

As described previously, optogenetics is a technique which allows the precise control of genetically defined populations of neurons using light Yizhar et al. (2011). Multiple strategies have emerged for rapidly activating or silencing the activity of neurons, all of which use the flux of various ion species in order to control the membrane potential and resistance (Zhang et al., 2007; Chow et al., 2010). One of the most popular silencing strategies uses light-driven Cl^- pumps derived from Natronomonas pharaonis halorhodopsin ('eNpHR'), which move Cl^- into the cell, in order to generate membrane hyperpolarisation (Zhang et al., 2007). Considering, that the transmembrane Cl^- concentration gradient is also the major determinant of E_{GABAA}, it is currently an open question as to whether

---

Figure 1.3 *(facing page)*: Biphasic responses to intense $GABA_AR$ activation are caused by a rapid shift from hyperpolarising to depolarising E_{GABAA}. a) Left, at rest [Cl^-] is typically much higher outside (e.g. 135 mM) as opposed to inside (e.g. 6 mM) neurons. In contrast, [HCO_3^-] is only moderately higher outside (23 mM) as compared to inside (12 mM) the cell. Therefore at a typical resting membrane potential of -60 mV, when GABA (black arrow) binds to ionotropic $GABA_A$ receptors, Cl^- flows into the cell (blue arrow) while HCO_3^- flows out (green arrow). As $GABA_ARs$ are approximately four times more permeable to Cl^- than to HCO_3^- ions (Kaila, 1994), the bulk of anion flux through the receptors is Cl^-. This causes the membrane potential hyperpolarisation (pink region) typical of classic $GABA_AR$ mediated inhibition. Right, with continued $GABA_AR$ activation, Cl^- influx ultimately exceeds Cl^- extrusion mechanisms and a breakdown in the Cl^- gradient occurs (Staley and Proctor, 1999). A corresponding depletion of intracellular HCO_3^- is prevented by the activity of carbonic anhydrase (CA), which uses CO_2 as a substrate to rapidly regenerate HCO_3^-. As a result, E_{Cl^-} and hence E_{GABAA} shift toward the more positive $E_{HCO_3^-}$ causing the late membrane depolarisation (pink region) typical of the biphasic GABAergic response. b) In the presence of carbonic anhydrase inhibitors such as acetazolamide (red cross), the early phase of the membrane potential response to intense $GABA_AR$ activation is similar (left). However, due to the fact that intracellular HCO_3^- cannot be regenerated, the concentration gradient for HCO_3^- efflux is rapidly dissipated (right). As a result, E_{Cl^-}, $E_{HCO_3^-}$ and the membrane potential converge on the same value (in this case -68 mV) and a dynamic electrochemical equilibrium is reached, at which point there is a minimal transmembrane flux of either anion.

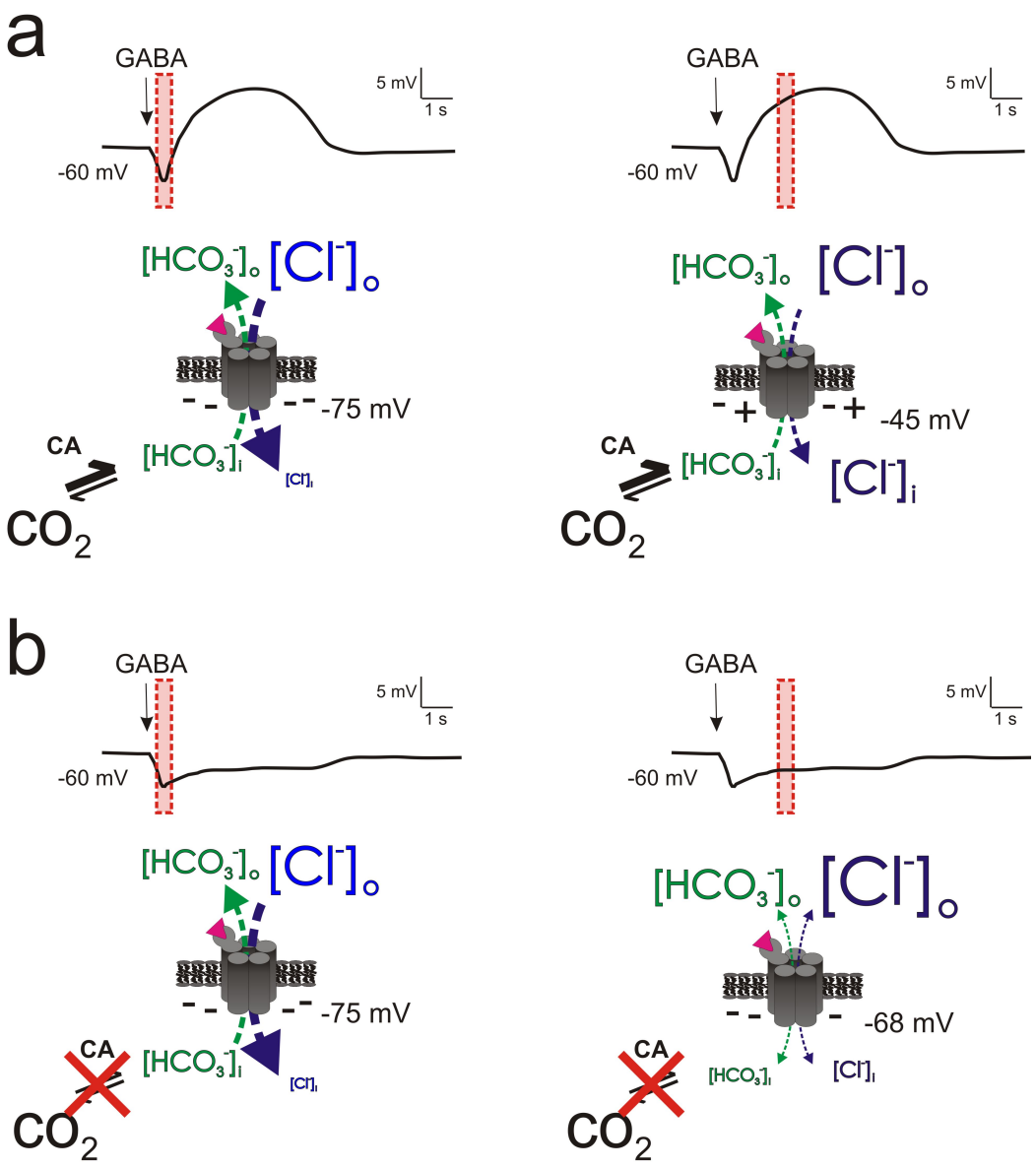
a
GABA
5 mV
1 s
-60 mV
[HCO3-]o
[Cl-]o
-75 mV
CA
[HCO3-]i
[Cl-]i
CO2
GABA
5 mV
1 s
-60 mV
[HCO3-]o
[Cl-]o
-45 mV
CA
[HCO3-]i
[Cl-]i
CO2
b
GABA
5 mV
1 s
-60 mV
[HCO3-]o
[Cl-]o
-75 mV
CA
[HCO3-]i
[Cl-]i
CO2
GABA
5 mV
1 s
-60 mV
[HCO3-]o
[Cl-]o
-68 mV
CA
[HCO3-]i
[Cl-]i
CO2

light driven Cl^- influx mediated by eNpHR is sufficient to alter $[Cl^-]_i$ and consequently GABAergic transmission.

In order to answer this question, **Chapter 3** of this thesis will investigate the effect of eNpHR mediated optogenetic neural silencing on GABAergic transmission. This will be compared to an alternative silencing strategy that employs a light-driven outward H^+ pump ('Arch', derived from *Halorubrum sodomense*) to generate membrane hyperpolarisation (Chow et al., 2010). I will also investigate the utility of employing eNpHR as an 'ion modulator' in order to exogenously control $[Cl^-]_i$. This will be used to investigate Cl^- homoeostasis mechanisms and the effects of short-term changes in E_{GABAA} on synaptic integration.

1.5.5 Intracellular Cl^- accumulation driven by network activity

In order to cause the Cl^- accumulation and transient depolarising shifts in E_{GABAA} described in the studies above, intense $GABA_AR$ activation was elicited either by exogenous application of $GABA_AR$ agonists or high frequency stimulation of GABAergic afferents. Evidence that such short-term changes in E_{GABAA} could occur in vivo, and therefore represent a biologically relevant plasticity mechanism, have come from studies of hyper-active network activity patterns, such as those generated in experimental models of epilepsy. Fujiwara-Tsukamoto et al. (2003), using brief tetanic stimulation of the stratum radiatum of CA1 mini-slices were able to elicit epileptiform afterdischarges lasting up to half a minute. This activity represents the clonic stage of a typical tonic-clonic seizure complex (McCormick and Contreras, 2001). These afterdischarges were shown to be mediated by excitatory GABAergic signalling generated by a transient accumulation of Cl^-. Indeed, even in the presence of complete glutamatergic blockade, GABAergic transmission alone was sufficient to generate afterdischarges (Fujiwara-Tsukamoto et al., 2010).

Several additional studies, using different models of epileptiform activity, have demonstrated a temporary excitatory shift in E_{GABAA} (Fujiwara-Tsukamoto, 2006; Fujiwara-Tsukamoto et al., 2003; Lamsa and Kaila, 1997; Lasztóczi et al., 2011; Perreault and Avoli, 1992). Although this must ultimately represent simultaneous Cl^- accumulation, the manner in which Cl^- increases intra-cellularly is still somewhat uncertain. The most parsimonious

explanation is that the massive GABA release expected during seizures, combined with the concurrent membrane depolarisation that occurs, causes rapid Cl^- accumulation via activated $GABA_A$Rs. This causal link is difficult to establish however, as pharmacological blockade of $GABA_A$Rs during a seizure preclude measurement of $[Cl^-]_i$ using traditional techniques, which rely on evoked $GABA_A$R currents to indirectly estimate Cl^- levels. Direct optical estimation of $[Cl^-]_i$ using the Cl^- sensitive dye MEQ during the tetanic generation of epileptiform afterdischarges has been performed, although this technique does not allow absolute measurement of $[Cl^-]_i$ Isomura et al. (2003). Nonetheless, in the presence of the $GABA_A$R antagonist bicuculline, significant Cl^- accumulation was still observed (Isomura et al., 2003). In addition, Slemmer et al. (2004) showed a very large $GABA_A$R independent intracellular Cl^- increase in response to glutamate application in dissociated cultures. It is clear that direct, absolute measurements of $[Cl^-]_i$ would greatly improve our understanding of how and where activity induced Cl^- fluxes are generated.

1.6 Intracellular H^+ ion concentration is modulated by activity

As discussed above, H^+ ion concentrations are linked to GABAergic transmission through the HCO_3^- buffering mechanisms of neurons and because H^+ and Cl^- ions often move together in cells (Tabb et al., 1992). pH is the negative logarithm of H^+ ion concentration and like Cl^- concentration, intracellular pH in the nervous system has powerful effects upon synaptic transmission and levels of network excitability (Tabb et al., 1992; Drapeau and Nachshen, 1988; Dulla et al., 2005). Furthermore, it is known that pH, like Cl^-, can also be altered by levels of neural activity (Xiong et al., 2000).

1.6.1 Baseline pH regulation

Due to the effect of pH on protein folding and enzymatic activity, it is a critical parameter that needs to be tightly regulated for optimum cell function. In most neurons the reversal potential for H^+ ions is about -20 mV (Chesler, 2003). In addition, intracellular metabolic processes tend to produce acidic byproducts, which means that cells are constantly susceptible to over-acidification. Systems that regulate pH fall into two categories: transporters of H^+ equivalents and buffering systems.

1.6.2 pH transport mechanisms

The family of Na^+/H^+ exchangers, which includes 10 known isoforms (NHE1-10) is one of the primary mechanisms by which cells maintain baseline pH levels. These exchangers utilise the transmembrane Na^+ gradient to extrude protons (Ma and Haddad, 1997; Noel and Pouyssegur, 1995). The presence of intra- and extracellular carbonic anhydrases, which catalyse the reversible reaction of H_20 and CO_2 to HCO_3^- and H^+, mean that HCO_3^- transporters are also and important in controlling pH levels (Maren, 1967). These may be Na^+-dependent or Na^+-independent. Na^+-dependent HCO_3^- transporters (NCBs), like NHEs, NCBs tend to extrude acid using the Na^+ gradient. Depending on their stoichiometry, some NCBs are electroneutral (NCBns) whilst others are electrogenic (NCBes) (Majumdar and Bevensee, 2010; Bevensee et al., 1997; Cooper et al., 2005). Whilst there are certainly exceptions the electroneutral NCBns are mostly expressed in neurons (Cooper et al., 2005), whilst electrogenic NCBe expression is predominantly astrocytic (Majumdar and Bevensee, 2010; Bevensee et al., 1997). This has important implications for cell-type specific pH transients generated in response to the membrane depolarisation as will be discussed in greater detail below. Other transport mechanisms involved in pH regulation include the Na^+ and Cl^- dependent HCO_3^- transporter (NDCBE) (Chen, Kelly, Parker, Bouyer, Gill, Felie, Davis and Boron, 2008), the HCO_3^- and Cl^+ anion exchangers (AEs) (Sterling and Casey, 1999), the ATP driven Ca^{2+} and H^+ ATPases (V-ATPase, SERCA and PMCA) (Pappas and Ransom, 1993; Thomas, 2008; Yu et al., 1993).

1.6.3 pH buffering systems

pH buffering mechanisms can be divided into HCO_3^--dependent and HCO_3^--independent processes. HCO_3^--dependent buffering is a powerful intra- and extracellular buffering system, which uses the carbonic anhydrase (CA) catalysed reaction described above and the fact that CO_2 readily traverses cell membranes to buffer pH changes. The importance of this system is underscored by the plethora of different CA isoforms expressed in the brain. Currently sixteen different isoforms have been described (Supuran, 2008). For example the mitochondrial isoform CA5 is expressed in neurons and astrocytes (Ghandour et al., 2002), CA2 is mostly found intracellularly in astrocytes (Agnati et al., 1995) whilst CA6

has a developmentally regulated intraneural expression pattern (Ruusuvuori et al., 2004). CA4 and CA14 are membrane bound with extracellular actions. Interestingly, they appear to form transport metabolons, which enhance the actions of the AE and NBC exchangers described above (Svichar et al., 2009; Alvarez et al., 2003). HCO_3^--independent intracellular buffers include phosphate and imidazole residues (Burton, 1978).

1.6.4 pH dynamics during activity

Neural activity is known to cause pH transients within neurons, glia and the extracellular space (Chesler, 2003). I will briefly summarise what is known about how these pH shifts are thought to occur.

1.6.5 Activity-dependent pH shifts in neurons

A number of studies using a wide range of experimental preparations have demonstrated that membrane depolarisation and repetitive spiking activity is associated with a fall in neuronal pH (Ahmed and Connor, 1980; Rose and Deitmer, 1995; Schwiening et al., 1993; Trapp et al., 1996; Wang et al., 1994; Pasternack et al., 1993). However, only a single study has attempted to measure intracellular pH transients in the context of epileptiform activity (Xiong et al., 2000).

At least three major processes are likely to be involved in activity-induced neuronal acidification. Firstly, membrane depolarisation is associated with Ca^{2+} influx that must be rapidly extruded to maintain intracellular Ca^+ concentrations in the nanomolar range. This is achieved by the Ca^{2+} /H^+ ATPases (PMCA and SERCA) located in the plasma membrane and endoplasmic reticulum, which will necessarily acidify the cytoplasm in order to remove Ca^{2+} (Schwiening et al., 1993; Makani and Chesler, 2010*b*) Secondly, prolonged neural activity will increase the production of metabolic acids such as CO_2 and lactate (Wang et al., 1994). And thirdly, intense $GABA_AR$ activation has been shown to result in considerable HCO_3^- efflux and a resulting intracellular acidification (Pasternack et al., 1993; Trapp et al., 1996).

1.6.6 pH affects network excitability

Just as increases in neuronal activity have an effect on pH, changes in $[H^+]$ can also influence the nature of ongoing neuronal activity. In other words, there is a reciprocal relationship between pH and neuronal activity. The general consensus is that acidification reduces levels of network excitability, whilst alkalinisation promotes excitation (Chesler, 2003). For instance, NMDA receptors (Tang et al., 1990; Traynelis and Cull-Candy, 1990; Vyklicky et al., 1990), $GABA_A$ receptors (Pasternack et al., 1996; Smart and Constanti, 1982; Takeuchi and Takeuchi, 1967) and voltage gated Ca^{2+} channels (Barnes and Bui, 1991; Iijima et al., 1986; Tombaugh, 1998; Tombaugh and Somjen, 1997) are all modulated by extracellular pH. Whilst acidosis reduces NMDA receptor conductances, it has the opposite effect on $GABA_A$Rs. In addition, acidic shifts promote the release of the inhibitory neurotransmitter adenosine (Dulla et al., 2005) whilst also reducing gap junction coupling (Spray et al., 1981). For these and other reasons it has long been suggested that activity-dependent extracellular and intraneuronal acidification may serve as a local feedback signal that dampens network excitability (Chesler, 2003).

1.6.7 Activity-dependent pH shifts in astrocytes

Periods of elevated neuronal activity result in the depolarisation of nearby glial cells, mainly via an increase of extracellular K^+ concentration (Hösli et al., 1981). However in contrast to neurons, membrane depolarisation of glia leads to an alkaline shift in intracellular pH. For instance, Grichtchenko and Chesler (1994) observed a depolarisation induced alkalinisation in cultures of hippocampal astrocytes after transient elevations of extracellular K^+. These alkalinisations were inhibited by Na^+ free media and removal of HCO_3^- from the buffer solution, whereas extracellular Cl^- and anion transporter inhibition had no effect on the process. A Na^+ and HCO_3^- dependent, depolarisation-induced astrocytic alkalinisation (DIA) has subsequently been confirmed in a variety of studies in both vertebrate and invertebrate systems (Pappas and Ransom, 1994; O'Connor and Sontheimer, 1994; Grichtchenko and Chesler, 1994; Deitmer and Szatkowski, 1990; Chesler and Kraig, 1989). The underlying transporter has been identified as the electrogenic Na^+ HCO_3^- exchanger NBCe1 (Romero et al., 1997). It has a stoichiometry of 1:2, which means that one Na^+ molecule and two HCO_3^- molecules are exchanged every

cycle (Bevensee et al., 1997). As a consequence, upon astrocytic membrane depolarisation, inward transport of HCO_3^- is greatly accelerated resulting in the alkalinisation observed in the studies described above. Although NBCe1 was previously assumed to have an almost exclusive glial expression pattern, it is also expressed to some degree in hippocampal neurons where it is thought to mitigate the acidosis that accompanies extended periods of depolarisation (Svichar et al., 2011).

Although astrocytic alkalinisation has been observed during spreading depression in vivo (Chesler and Kraig, 1989), intracellular astrocytic pH has not previously been measured with respect to epileptiform activity. In **Chapter 5** of this thesis I measure the intracellular pH of both neurons and astrocytes in response to seizures using an in vitro model of epilepsy.

1.6.8 Activity-dependent pH shifts in the extracellular space

Reports of activity-induced extracellular pH shifts go back over 70 years (Dusser de Barenne et al., 1938). For the most part, seizures or electrically stimulated activity are associated with an initial extracellular alkaline shift followed by a prolonged acidosis (Caspers and Speckmann, 1972; Urbanics et al., 1978). A small number of studies have also described a rapid extracellular acidic transient preceding the biphasic response described above (Krishtal et al., 1987). It is logical to assume that pH transients observed in the extracellular space must somehow reflect the combined consequence of intracellular pH transients evoked in astrocytes and neurons. To date however, no study has managed to record both neuronal and astrocytic activity-dependent transients within the same experimental preparation. The data presented in **Chapter 5** will provide a potential explanation for how the temporal features of activity-induced extracellular pH transients are generated.

1.7 Techniques for measuring Cl^- and H^+ concentration

In this introduction I have discussed how both Cl^- and pH are affected by neuronal activity. In addition I have described how neuronal activity itself can generate sizeable shifts in intracellular pH and Cl^- concentration. This reciprocal relationship means that tools to

accurately measure the concentration of these two ions is important for understanding their role during the evolution of both physiological and pathological network states.

1.7.1 Measuring intracellular Cl^- concentration

Prior to the 1980s Cl^- sensitive electrodes were the major available technique for measuring intracellular Cl^- (Mauro, 1954). However, the two main limitations of this technique were the slow detection kinetics and the damage induced by cell impalement. This latter issue meant that the technique was largely confined to use in large cells where cellular injury could be minimised. The advent of patch-clamp technology and the gramicidin perforated patch has allowed the indirect determination of Cl^- concentration via calculation of the reversal potential for $GABA_A$Rs (Kyrozis and Reichling, 1995). Gramicidin pores are permeable to small cations, but importantly not to Cl^-. This means that by adding gramicidin to the microelectrode solution, voltage control of the cell can be achieved without perturbing endogenous intracellular Cl^- levels (Achilles et al., 2007; Gulledge and Stuart, 2003; Brumback and Staley, 2008). An advantage of this technique is that the size and kinetics of $GABA_A$R currents may be precisely determined along with estimates of $[Cl^-]_i$. A disadvantage is that intracellular dialysis of small anions such as H^+, K^+ and Na^+ could potentially affect E_{GABAA}, either by altering intracellular pH or by affecting the thermodynamic gradients for Cl^- transporters such as KCC2 and NKCC1. Although this effect can be minimised by matching the cation concentrations of the internal solution with typical intracellular values.

An alternative electrophysiological approach is to utilise dual cell-attached recordings (Tyzio et al., 2008) to accurately determine both the resting membrane potential and driving force for $GABA_A$Rs in order to calculate E_{GABAA}. Using this technique in comparison with gramicidin perforated patches it has been demonstrated that perforated patches introduce a shunting conductance through the contact between the patch pipette and the cell membrane, which results in erroneously depolarised measures of resting membrane potential (Tyzio et al., 2008). The suggestion is that gramicidin perforated patches, whilst accurately estimating E_{GABAA}, report an erroneous measure of the driving force for $GABA_A$Rs (Tyzio et al., 2008). A major advantage of using dual cell-attached recordings is that they are less invasive. However, these recordings preclude the measurement

of dynamic $GABA_AR$ currents, which are essential for calculating Cl^- loads (Brumback and Staley, 2008). Lastly, all electrophysiological techniques ultimately estimate $[Cl^-]_i$ indirectly via $GABA_AR$ activation. This means that these techniques can not be used to investigate how $GABA_AR$ themselves contribute to establishing E_{GABAA}.

Live cell imaging techniques offer the potential to overcome these limitations by allowing spatial and temporal monitoring of intracellular Cl^- concentration dynamics. The first efforts to use Cl^- imaging made use of the fluorescence of quinolinium-based dyes is quenched by Cl^-. Dyes in this class include 6-methoxy-N-(3-sulfopropyl) quinolinium (SPQ), 6-methoxy-N-ethylquinolium (MEQ) and N-(6-methoxyquinolyl)-acetoethyl ester (MQAE). MQAE, the most popular of the three, is membrane permeable and can easily be loaded into neurons. It is suitable for use with 2-photon microscopy (Marandi et al., 2002), where its fluorescence is Cl^-, but not HCO_3^- sensitive (Koncz and Daugirdas, 1994). Despite these desirable properties, MQAE has significant drawbacks. It is moderately toxic, displays poor signal to noise, bleaches rapidly and suffers from significant cell leakage (Bregestovski et al., 2009). In addition, it does not report Cl^- ratiometrically, which means that fluorescence is susceptible to measurement artefacts caused by variations in excitation path length, indicator concentration, illumination stability, cell thickness, and indicator distribution.

Genetically encoded Cl^- indicators based on mutations of the inherently Cl^- sensitive green fluorescent protein (GFP) offer the potential to overcome many of these issues in addition to providing specific genetic localisation to particular cell-types or subcellular compartments. The most popular and widely used genetically encoded Cl^- indicators are based on fusions of two GFP mutants, yellow fluorescent protein (YFP) and cyan fluorescent protein (CFP), a commonly used fluorescence resonance energy transfer (FRET) donor for YFP. Whereas YFP emission is reduced by Cl^- binding, CFP fluorescence is relatively unaffected. These fusion proteins are therefore useful as ratiometric reporters of intracellular Cl^- concentration. Reporters in this class include ‘clomeleon’ (Kuner and Augustine, 2000) and ‘Cl-sensor’ (Markova et al., 2008). Unfortunately, YFP fluorescence is quenched by both Cl^- and H^+ ions. As a result these YFP fusion proteins are sensitive to both intracellular pH and Cl^- concentration (Jayaraman et al., 2000). This dual sensitivity complicates the interpretation of in vivo measurements using these probes,

particularly as neuronal processes often involve either the related, or independent, flux of both Cl^- and H^+ ions (Tabb et al., 1992; Doyon et al., 2011). Attempts to enhance the Cl^- sensitivity of YFP by inducing mutations in YFP have resulted in matching increases in pH sensitivity. Therefore, genetic reporters that can measure Cl^- independent of pH are greatly sought after.

Recently, Arosio et al. (2010) have reported that GFP-based fusion construct, 'ClopHensor', is able to independently and simultaneously report both intracellular Cl^- and H^+ concentration. A further aim of this thesis, as will become apparent in **Chapter 4**, has been to optimise and adapt this construct for use within the nervous system to directly and accurately measure Cl^- and H^+ ion fluxes in response to network activity.

1.7.2 Measuring intracellular H^+ concentration

Like Cl^-, initial techniques to determine pH relied on pH sensitive microelectrodes (Rose and Deitmer, 1995). Due to their size, the use of microelectrodes to measure pH has been mostly confined to large neurons or the extracellular space (Fedirko et al., 2006). pH-sensitive dyes have also been widely used to measure intracellular pH. Several classes exist, including fluoresceins, benzoxanthenes, rhodols and pyrenes. The fluorescein derivatives, 2'-7'-bis(carboxyethyl)-5(6)-carboxyfluorescein (BCECF) and carboxyseminaphtho -rhodafluor-I (carboxy-SNARF-1) are by far the most popular. These two dyes are suitable for use as ratiometric pH indicators and have desirable optical properties. In addition, both dyes are available as acetoxymethyl (AM) esters, which facilitates intracellular loading without the use of micropipettes. However, fluorescein dyes have a potentially significant disadvantage, which may be particularly relevant to studies of activity-dependent proton fluxes within the nervous system. Fluorescein analogues have been shown to inhibit the Ca^{2+} / H^+ ATPase (Gatto and Milanick, 1993; Chesler, 2003). This ATP dependent transporter extrudes Ca^{2+} in exchange for H^+. As Ca^{2+} influx is a primary feature of neuronal membrane depolarisation, the restoration of low Ca^{2+} via this exchanger is thought to be an important mechanism by which protons accumulate during neuronal activity (Schwiening et al., 1993; Svichar et al., 2011).

Genetically encoded, GFP-based pH reporters offer several potential advantages over the above techniques, including single cell or subcellular targeting, enhanced spatial res-

olution, no fluorophore leakage and reduced interference with the endogenous H^+ transport mechanisms described above (Bizzarri et al., 2009; Gatto and Milanick, 1993). Although GFP-based pH indicators have gained popularity as a marker of synaptic release (Miesenböck et al., 1998), they have not been utilised to study intracellular hydrogen ion fluxes associated with network activity. In **Chapter 5** of this thesis I demonstrate the utility of employing GFP-derived, genetically encoded pH reporters for quantifying intracellular pH transients on the level of single cells.

1.8 Thesis aims

The overall objective of this thesis was to investigate how intracellular concentrations of Cl^- and H^+ modulate, and are modulated by, neural activity. My experimental aims were as follows:

The first aim of this thesis was to examine the conditions under which influxes of Cl^- overwhelm a neuron's ability to maintain a stable Cl^- concentration gradient. The factors that influence this process were investigated, as were the potential consequences of changes in intracellular Cl^- for synaptic integration. This work also involved comparing two popular optogenetic silencing strategies in terms of their effects on intracellular Cl^- concentration and GABAergic synaptic inhibition (**Chapter 3**).

The second aim of this thesis was to investigate the mechanisms and parameters affecting activity-induced Cl^- accumulation during epileptiform activity (**Chapter 4**). To achieve this aim I also sought to develop novel tools for the measurement of dynamic Cl^- concentration changes in neurons.

The third aim of this thesis was to establish the utility of employing GFP-based proton sensors for measuring activity-induced pH transients. These tools were used to measure and compare pH transients in neurons and astrocytes during epileptiform activity (**Chapter 5**).

Chapter 2

Materials and Methods

2.1 Preparation of Slices

2.1.1 Organotypic hippocampal slices

Organotypic slices from 7 day old male Wistar rats (Harlan Laboratories, UK) were prepared as described previously by Stoppini et al. (1991). Animals were killed in accordance with the UK Animals Scientific Procedures Act 1986. After decapitation, rat brains were extracted and quickly placed in cold (4°C) Geys Balanced Salt Solution (GBSS), supplemented with D-glucose (34.7 mM). The hemispheres were separated and individual hippocampi were removed and immediately sectioned into 350μm thick slices on a McIlwain tissue chopper (Mickle, UK). Slices were rinsed in cold dissection media, placed onto Millicell-CM membranes (Millipore, UK) and maintained in culture medium containing 25% Earles balanced salt solution (vol/vol), 49% MEM (vol/vol), 25% heat-inactivated horse serum (vol/vol), 1% B27 (vol/vol, Invitrogen) and 6.2 g/l glucose. Slices were incubated for between 6 and 14 days at 36°C in a 5% CO_2 humidified incubator.

2.1.2 Acute slices

Acute slices were prepared from 3 to 5 week-old male Wistar rats and 5 to 8 week-old CAMKII-cre mice (Jackson laboratory). The animals were killed and the brain rapidly removed and placed in ice-cold (0 to +4°C) artificial cerebro-spinal fluid (ACSF), bubbled with 95 % O_2 / 5 % CO_2. The ACSF was composed of (in mM) NaCl (120), KCl (3), $MgCl_2$ (2), $CaCl_2$ (2), NaH_2PO_4 (1.2); $NaHCO_3$ (23); D-Glucose (11) and the pH was

adjusted to be between 7.38 and 7.42 using NaOH (0.1 mM). Horizontal hippocampal slices (350-400 μm thickness) were cut using a vibrating microtome (Microm HM650V, Carl Zeiss Ltd) and slices were maintained in an interface chamber between humidified carbogen gas (95% O_2, 5% CO_2) and ACSF (at 20-25°C). After recovering for at least 1 h, the slices were mounted on coverslips (coated with 0.1% poly-L-lysine in ultrapure H_2O) before being transferred to the recording chamber.

2.2 Plasmids and transfection techniques

All plasmids were amplified in XL1-Blue competent cells (Stratagene) and extracted using QIAGEN maxiprep kits (Qiagen, USA). Diagnostic restriction digests followed by gel electrophoresis were run to confirm plasmid identity and purity.

2.2.1 Ion sensitive genetic reporters

Cl-Sensor (Markova et al., 2008) was a generous gift from Piotr Bregestovski (Institut de Neuroscience des Systmes, Aix-Marseille Universit, Marseille, France) and was in the pEGFP-C1 expression plasmid (Clontech, USA). deGFP4 (Hanson et al., 2002) in pEGFP-N1 (Clontech, USA) was generously provided by Jim Remington (University of Oregon, USA). ClopHensor (Arosio et al., 2010) in the pcDNA3 expression plasmid was provided by Daniele Arosio (University of Trento; Addgene plasmid 25938).

2.2.2 Neural silencers

eNpHR3.0 (Zhang et al., 2007) was generously provided by Karl Deisseroth (Stanford University, USA). For biolistic transfection of organotypic hippocampal slices the target DNA was either pLenti-hSyn-eNpHR3.0-EYFP (eNpHR3.0 fused to EYFP and driven by the human synapsin 1 promoter, SYN1). For viral injections of CAMKII-cre mice (Jackson Laboratory) adeno-associated virus serotype 2 (AAV2) carrying eNpHR3.0-EYFP was utilised. The viral DNA included the loxP-flanked sequence for eNpHR3.0-EYFP driven by the human elongation factor 1a promoter (EEF1A1).

Arch (Chow et al., 2010) was generously provided by Ed Boyden (Massachusetts Institute of Technology, USA). FCK-Arch-GFP (Arch fused to GFP and driven by the mouse

-CamKII promoter, Camk2a) was used for biolistic transfections. Adeno-associated virus serotype 2 incorporating a loxP-flanked Arch-GFP driven by the cytomegalovirus early enhancer element and chicken beta-actin (CAG) promoter was utilised for injections into CAMKII-cre mice. AAV2 particles were produced at the University of North Carolina Gene Therapy Center Virus Vector Core or the Penn Vector Core, University of Pennsylvania School of Medicine.

2.2.3 Subcloning alternative red fluorescent protein variants into ClopHensor

Subcloning of alternative red fluorescent proteins into ClopHensor was performed by Bradley Joyce within the laboratory of Shankar Srinivas in the department of Physiology, Anatomy and Genetics, University of Oxford. The DsRed monomer in the original ClopHensor (Arosio et al., 2010) was replaced with either mCherry or tandem dimer tomato (tdTomato). The 22 amino acid linker from the original ClopHensor was maintained in both new constructs. In addition, the gene for the new fusion proteins were moved into a new expression vector named pBJ1. This included a the cytomegalovirus early enhancer element and chicken beta-actin promoter (CAG promoter) and employed a human beta globin (HBG) poly-adenylation termination sequence. For plasmid maps see Fig. 4.7.

2.2.4 Biolistic gene delivery

Organotypic hippocampal slices were biolistically transfected after 4 - 7 days in culture. Gold bullets were prepared by precipitating 50 μg of DNA onto 25 mg of 1.6 μm gold particles. A Helios Gene Gun (Bio-Rad, UK), at 100 - 120 psi of helium pressure, was used to propel the coated gold particles into the hippocampal slices. Recordings were then performed 2 - 7 days post transfection, which is equivalent to postnatal days 13 - 21.

2.2.5 Viral delivery *in vivo*

All viral injections were performed by Thomas J. Ellender (Raimondo, Kay, Ellender and Akerman, 2012). Adeno-associated virus serotype 2 carrying the target gene of interest was injected into the hippocampus of anaesthetised CAMKII-cre mice between postnatal

days 14 and 21. Typical coordinates from Bregma for injections into the ventral hippocampus were 3.1 mm lateral, 2.7 mm posterior and 3.25 - 2.25 mm ventral to the surface of brain. Typical titers were approximately 10^{12} IU/ml. Injection volumes were 500 nl. After allowing 2 - 4 weeks for expression, acute horizontal hippocampal slices were prepared as described above.

2.3 Electrophysiological recordings

Hippocampal slices were transferred to a recording chamber and continuously superfused with 95% O_2 5% CO_2 oxygenated artificial cerebro-spinal fluid (aCSF), warmed to 32-35 °C. The composition of the 'standard' aCSF was (in mM): NaCl (120), KCl (3), $MgCl_2$ (2), $CaCl_2$ (2), NaH_2PO_4 (1.2), $NaHCO_3$ (23), D-Glucose (11). The pH was adjusted to be between 7.35 and 7.40 using NaOH. For nominally HCO_3^- free recordings, standard aCSF was used with $NaHCO_3$ replaced by an equimolar amount of HEPES (23 mM). In addition, this aCSF was bubbled with 100% oxygen rather than the normal 95% O_2 5% CO_2 mix.

Neurons or astrocytes within the hippocampal formation were visualised using 20x, 40x or 60x water-immersion objectives (Olympus or Leica) and targeted for recording. In acute hippocampal slices, visualisation of the pyramidal cells was facilitated with infrared differential interference contrast microscopy. Patch pipettes of 3-7 MΩ tip resistance were pulled from filamental borosilicate glass capillaries with an outer diameter of 1.2 mm and an inner diameter of 0.69 mm (Harvard Apparatus Ltd, Hertfordshire, UK), using a horizontal puller (Sutter).

2.3.1 Gramicidin perforated patch recordings

For gramicidin perforated patch recordings (Kyrozis and Reichling, 1995), pipettes were filled with a high KCl internal solution whose composition was (in mM): KCl (135), Na_2ATP (4), 0.3 Na_3GTP (0.3), $MgCl_2$ (2), and HEPES (10). The osmolarity of all internal solutions was adjusted to 290 mOsM and the pH adjusted to 7.38 with KOH. Gramicidin (Calbiochem) was dissolved in dimethylsulfoxide (DMSO, Sigma) to achieve a stock solution of 4 mg/ml. Fresh stock solution was prepared daily. This was then diluted in

internal solution immediately prior to experimentation (10 min before attaining a patch) to achieve a final concentration of 80 μg/ml. The resulting solution was vortexed for 1 min, sonicated for 30 s and then filtered with a 0.45 μm pore cellulose acetate membrane filter (Nalgene). Patch pipettes were back filled with this gramicidin internal solution and mounted to a head stage. Between 80 and 100 psi positive pressure was applied and the pipette tip lowered onto the surface of the target cell. Upon formation of a membrane gigaseal, membrane capacitance was compensated. The perforation progress was evaluated by continuously monitoring the decrease in access resistance. Recordings were started once the access resistance had stabilised between 20 - 50 MΩ (mean Ra $\approx$ 35 MΩ), which usually occurred at around 20 - 40 min from gigaseal. For all experiments except those involving active seizure activity, online series resistance correction of 70% was used. Online series resistance correction was not used in experiments where concurrent epileptiform activity was expected. This is because very large fluctuations in input current often lead to rupture of the gramicidin patch, also known as 'break through'. Break through was detected by observing a dramatic and permanent increase in E_{GABAA} caused by intracellular dialysis of the cell with the high Cl^- internal solution. Recordings were made using an Axopatch 700A amplifier and data acquired using Clampex software (Molecular Devices). Values reported from perforated patch voltage clamp recordings were corrected offline for the liquid junction potential (4.2 mV) between the intracellular and extracellular solution.

2.3.2 Calculating E_{GABAA}, g_{GABAA} and generating Cl^- loads

$GABA_A$Rs were activated by delivering short 'puffs' of GABA (100 μM), through a patch pipette placed close to the soma or over the dendrites and connected to a picospritzer (20 psi for 20 ms; General Valve). To calculate resting E_{GABAA} and g_{GABAA}, $GABA_A$R currents were measured at five different holding potentials (5 mV intervals around the resting membrane potential) in response to a GABA puff. A minimum of 30 s was allowed before each puff in order to allow full recovery of chloride homoeostasis. The peak $GABA_A$R current was plotted as a function of holding potential to generate a current-voltage curve, from which resting E_{GABAA} was defined as the x-intercept value and g_{GABAA} as the slope.

To measure the impact of either photocurrent or $GABA_A$R induced Cl^- loads on E_{GABAA},

it was important to estimate E_{GABAA} from single $GABA_AR$ currents. To achieve this, resting E_{GABAA} and g_{GABAA} were calculated before each experiment (as described above) and these values were then used to estimate E_{GABAA} for a single $GABA_AR$ current by assuming a constant g_{GABAA} across GABA puffs and solving the equation:

$GABA_AR$ current = g_{GABAA} (Holding potential - E_{GABAA})

Cl^- loads were generated either through photoactivation of eNpHR (see below) or via activation of $GABA_ARs$. In the latter case, different sized Cl^- loads were elicited by stepping the membrane voltage to different potentials for 2 s and activating $GABA_ARs$ with a GABA puff (100 ms after the start of the voltage step). Larger depolarising voltage steps resulted in stronger driving forces on the $GABA_AR$ and therefore larger Cl^- loads, which were defined as the area under the $GABA_AR$ current (expressed in pC) after adjusting for the holding current associated with the voltage step. 100 ms after the end of the voltage step (and therefore 2 s after the first GABA puff), or in the case of photoactivation of opsins 250 ms after laser offset, a second GABA puff was delivered to estimate whether E_{GABAA} (measured according to the equation above) had changed as a result of the chloride load.

2.3.3 Photoactivation of eNpHR and Arch

Photoactivation of eNpHR and Arch was achieved via a diode-pumped solid state (DPSS) laser, with a maximum output of 35 mW and a peak at 532 nm (Shanghai Laser Optic Century). The laser was attenuated via a 5% neutral density and coupled to a 1000 μm diameter mulitimode optic fiber via a collimating lens (Thorlabs). The tip of the optic fiber was positioned at an image plane within the microscope in the center of the optical axis, and was directed into the 20x objective lens via a dichroic mirror. This resulted in a spot of light at the brain slice whose diameter was 195 μm, assuming zero tissue scattering. Laser intensity was controlled via a potentiometer on the laser power controller and the output at the tip of the fibre optic was calibrated with an optical power meter (Thorlabs). The timing of laser pulses was controlled via TTL pulses delivered from an analogue to digital (AD) board (Molecular Devices), which were synchronised with the electrophysiology software.

2.3.4 Estimating E_{GABAA} during seizure episodes

Using gramicidin perforated patch recordings cells were held in current clamp mode to record seizure activity. E_{GABAA} could be measured at any point by rapidly switching the recording mode from current-clamp to voltage-clamp and then applying two consecutive voltage ramps, the first under baseline conditions and the second during activation of $GABA_A$Rs as described above. After 3 s in voltage-clamp the cell was returned to current-clamp. I-V plots were constructed and E_{GABAA} defined as the voltage at which the holding current (generated by the first ramp) and the total current (reflecting the holding current plus the current through the activated $GABA_A$Rs) intersected.

2.3.5 Cell-attached recordings

For cell-attached recordings pipettes were back-filled with an internal solution composed of (in mM): K-gluconate (130), NaCl (10), $CaCl_2$ (0.1333), $MgCl_2$ (2), EGTA (1), KCl (4), and HEPES (10). In addition, 2-chloroadenosine (2 μM) was added to the aCSF to reduce spontaneous activity. Patches were established in the loose cell-attached patch configuration (50-150 MΩ). These recordings were used to assess spike probability before and after laser stimulation. Synaptically-evoked spikes were triggered via a bipolar stimulating electrode (Frederick Haer Company) placed in stratum radiatum, 300-400 μm from the recorded cell. Stimulus intensity was set such that spikes (detected during a 200 ms window immediately after the stimulus) were evoked with a probability of approximately 0.4 before laser-activation (i.e. 4 out of 10 trials resulted in at least one spike). The before laser stimulus was delivered 1250 ms before laser onset and the after laser stimulus was delivered 250 ms after laser offset.

2.3.6 Whole-cell recordings

For whole cell recordings pipettes were filled with an internal solution containing (in mM): K-gluconate (130), NaCl (10), $CaCl_2$ (0.1333), $MgCl_2$ (2), EGTA (1), KCl (4), and HEPES (10). These recordings were made in current clamp mode using an Axopatch 1D or Axoclamp 2B amplifier (Axon Instruments). Data was acquired with WinWCP Strathclyde Whole Cell Analysis software (V.3.9.7; University of Strathclyde) and later combined with

imaging data during off-line analysis using MATLAB (MathWorks).

2.3.7 Seizure models

Four seizure models were used: a '0 Mg^{2+} model, a'4-AP model', a 'spontaneous model' and a 0 Cl^- model.

In the '0 Mg^{2+}' model, seizures were induced by switching bath perfusion of slices with normal aCSF to nominally Mg^{2+}-free aCSF. This removes the voltage dependent Mg^{2+} block on NMDA receptors, which predisposes hippocampal slices to periods of synchronised hyperexcitability (Anderson et al., 1986; Mody et al., 1987; Gutiérrez et al., 1999; Avoli et al., 2002).

Using the '4-AP model', seizures were elicited by adding 50 μM 4-aminodpyridine (4-AP) to the bath solution (Perreault and Avoli, 1992). 4-AP is a selective antagonist of the Kv1 (Shaker) family of voltage gated K^+ channels.

The 'spontaneous model' of epilepsy involved utilising hippocampal organotypic slice cultures that were kept in culture for beyond a week. Even in standard aCSF, these slices are known to generate spontaneous seizures (Dyhrfjeld-Johnsen et al., 2010; Berdichevsky et al., 2011; Lillis et al., 2012). This hyperexcitability is thought to be due to increased recurrent connectivity that is established after extended time in culture.

Lastly, in the 0 Cl^- model, seizures were induced by switching the aCSF to nominally Cl^- free aCSF (NaCl, $MgCl_2$ and $CaCl_2$ of standard aCSF replaced with 120 mM sodium D-gluconate, 1 mM $MgSO_4$ and 3 mM calcium D-gluconate, respectively). The 0 Cl^- model of seizures represents the first in vitro model of epilepsy reported in the literature and has since been widely utilised (Yamamoto, 1972; Yamamoto and Kawai, 1969, 1968, 1967; Chamberlin and Dingledine, 1988; Avoli et al., 1990). It is mechanistically similar to the well-described seizure models that use pharmacological blockade of $GABA_A$Rs to reduce the efficacy of GABAergic inhibition (Straub et al., 1996; Hablitz, 1984). Removal of Cl^- from the aCSF has the added advantage of preventing potential Cl^- fluxes that may complicate pH measurements from the pH and Cl^- sensitive genetic reporters such as the Cl-sensor (Markova et al., 2008).

2.4 Computational models

Two computational models investigating Cl^- regulation and accumulation were constructed.

2.4.1 NEURON multi compartment model

In order to investigate whether cell compartment differences in the ability to deal with a Cl^- load could be explained by a limited set of parameters, a multi compartment model of a single pyramidal cell with multiple synaptic inputs was created using the NEURON modelling environment (Hines and Carnevale, 1997). This model was jointly created with Blake Richards. The geometry of the model was based on the reconstruction of a biocytin filled layer 5 medial entorhinal cortex pyramidal cell. It included a soma, axon, 27 basal dendrites and 50 apical dendrites. These structures were modelled as a set of 1949 connected cylinders referred to as 'segments'. The virtual cell received glutamatergic synpases at a density of 0.2 synapses per μm^2 from 44 presynaptic glutamatergic cells, with a mean firing rate of 10 Hz. The virtual cell also received GABAergic synapses at a density of 0.2 synapses per μm^2 innervated by 44 presynaptic cells. Each presynaptic GABAergic cell had a mean firing rate of 40 Hz with spike intervals drawn from a Poisson distribution. This represents a physiologically realistic firing rate for basket cell interneurons (Tamás et al., 2000). A peak synaptic conductance of 0.001 μS was used based on a model of synaptic conductance by Destexhe (1998).

The model also included mechanisms that would dynamically adjust E_{Cl^-} as a function of varying $[Cl^-]_i$, according to the nernst equation (see below). $[Cl^-]_o$ (135 mM), $[K^+]_i$ (3 mM), $[K^+]_o$ (120 mM), $[HCO_3^-]_i$ (10 mM) and $[HCO_3^-]_o$ (25 mM) were assumed to remain constant. $[Cl^-]_i$ for each segment could vary according to transmembrane Cl^- fluxes via activated $GABA_A$Rs, Cl^- transport due to the K^+/Cl^- cotransporter (KCC2) and Cl^- diffusion to and from neighbouring segments of the cell. The parameters defining Cl^- transport via KCC2 were taken from Staley and Proctor (1999) (K_d = 15 mM, V_{max} = 5 mM/s), whilst the diffusion constant was experimentally determined (D = 10 μm^2/s).

The biophysical mechanisms described above were modelled using the following equations:

1. The Cl^- reversal, E_{Cl^-}, as a function of Cl^- concentration gradient across the mem-

brane, as defined by the nernst equation:

$$E_{Cl^-} = -\frac{RT}{F} ln \left(\frac{[Cl^-]_o}{[Cl^-]_i} \right)$$

2. Cl^- flux through activated $GABA_A$Rs was defined as:

$$I_{Cl^-} = g_{GABAA_{Cl}}(V - E_{Cl^-})$$

3. Cl^- extrusion via a uniformly expressed K^+ / Cl^- cotransporter (KCC2) obeyed Michaelis-Menten kinetics (Staley and Proctor, 1999) and was defined by:

$$V_{mm} = \frac{V_{max}[Cl^-]_i}{K_d + [Cl^-]_i}$$

where V_{mm} is the rate of extrusion, V_{max} is the maximum extrusion rate and K_d is the $[Cl^-]_i$ at which extrusion is half maximal. These values were derived from Staley and Proctor (1999).

4. Diffusion of Cl^- within the neuron accounted for segment volumes:

$$Diff_{Cl} = D\frac{\Delta[Cl^-]_i}{L}$$

where $Diff_Cl$ is the rate of diffusion of Cl^-, D is the diffusion constant, L is the distance between segments and $\Delta[Cl^-]_i$ is the concentration gradient between segments.

5. And the $[Cl^-]_i$ of each segment was updated at each time point according to the following equation:

$$\frac{d[Cl^-]_i}{dt} = \frac{I_{Cl}}{L\pi r^2 F} - V_{mm} - Diff_{Cl}$$

2.4.2 Matlab single compartment model

To investigate the interaction between Cl^- loads and subsequent changes in E_{GABAA}, I constructed a single compartment model with Cl^- transport mechanisms similar to those described above (see Section). The model was created using the MATLAB programming environment (MathWorks,USA) and the details of this model were as follows: E_{GABAA} was based on a receptor permeability for Cl^- that is four times that of HCO_3^- (Kaila, 1994). Intracellular and extracellular HCO_3^- concentrations were held constant at 10 mM and 25 mM, respectively (Lambert and Grover, 1995). A stable extracellular Cl^- concentration of 135 mM was used and intracellular Cl^- was able to vary dynamically. E_{GABAA} was calculated at each time-step using the Goldman-Hodgkin-Katz equation.The somatic compartment was modelled as a prolate spheroid with volume (Vol) related to the somatic width (w) and somatic length (l) by the equation below:

$$Vol = \frac{4}{3}\pi l \left(\frac{w}{2}\right)^2$$

To simulate cells of differing volume, somatic length was varied between 12 and 36 μm, whilst somatic width was held constant at 12 μm. These values were based upon measurements from recorded cells and resulted in neuronal cell volumes of between 0.9 and 2.7 pL, which corresponds to the range of somatic volumes reported for rat hippocampal neurons (Ambros-Ingerson and Holmes, 2005). For this model the rate of Cl^- transport by KCC2 was characterised in a more refined manner by describing the transporter's activity in analogy to Ohms law, where current flow is equal to the driving force multiplied by the conductance (Brumback and Staley, 2008). The combined K^+ and Cl^- electrochemical gradient creates the driving force, whilst the transport capacity represents the conductance. The driving force, or change in free energy (ΔG), is a result of the transmembrane concentration gradients of the transported ions:

$$\Delta G = -\frac{RT}{F} ln \left(\frac{[Cl^-]_o[K^+]_o}{[Cl^-]_i[K^+]_i}\right)$$

In order to create a dimensionless term, free energy (ΔG) was normalised to ΔG_{max}.

Using a method similar to that employed by Brumback and Staley (2008), ΔG_{max} was calculated by using the maximum $[Cl^-]_i$ that was measured following a Cl^- load in my recordings (56 mM, see Chapter 3). The transport capacity of KCC2 (V_{mm}) was modelled using Michaelis-Menten kinetics for enzymatic activity (Staley and Proctor, 1999; Russell, 2000).

$$V_{mm} = \frac{V_{max}[Cl^-]_i}{K_d + [Cl^-]_i}$$

Where $[Cl^-]_i$ is the substrate concentration for outward transport of Cl^-, V_{max} is the maximum velocity of Cl^- transport, and K_d is the $[Cl^-]_i$ where transport is half maximal. The values for V_{max} and K_d (5 mM/s and 15 mM) used in the model were taken directly from Staley and Proctor (1999). The velocity of KCC2-mediated Cl^- transport (in mM/s) was therefore calculated by multiplying the normalised driving force ΔG / ΔG_{max} by the conductance term V_{mm} (Brumback and Staley, 2008):

$$V_{KCC2} = \frac{\Delta G}{\Delta G_{max}} V_{mm}$$

A tonic Cl^- current was calculated that would maintain resting $[Cl^-]_i$ at 7 mM in order to achieve a baseline E_{GABAA} of -70 mV. A Cl^- photocurrent of varying amplitude and duration could then be applied and the resulting changes in $[Cl^-]_i$ and hence E_{GABAA} tracked over time using the following equation:

$$[Cl^-]_{(i,t+1)} = [Cl^-]_{(i,t)} + \left[\frac{(I_{tonic} + I_{photocurrent})}{F} - V_{KCC2} Vol\right] \frac{\Delta t}{Vol}$$

It should be noted that Cl^- currents induced via the light activated Cl^- pump, eNpHR, can be maintained in the face of intracellular Cl^- accumulation because of the pumps extremely negative reversal potential (approximately -400 mV) (Seki et al., 2007).

2.5 Cl^- and pH imaging

2.5.1 MQAE based Cl^- imaging

The first technique involved utilising N-(6-methoxyquinolyl)-acetoethyl ester (MQAE), a quinolinium-based Cl^- sensitive dye. This dye is membrane permeable and was loaded into neurons by incubating organotypic hippocampal slices in 95% O_2 and 5% CO_2 bubbled aCSF containing 6 μM MQAE for 10 minutes. Imaging was performed using an Olympus FV300 confocal microscope (Olympus, Japan), custom-converted for two-photon imaging and equipped with a MaiTai-HP Ti:sapphire femtosecond pulsed laser (Newport Spectra-Physics, USA). Images were acquired on a PC using Fluoview software (version 5.0, Olympus, Japan). The two-photon system was mounted on an Olympus BX51 upright microscope equipped with a 20x (NA 0.5) water immersion objective. Fluorescence was detected using an externally mounted PMT (R3896, Hamamatsu, Japan). An excitation wavelength of 750 nm was used and emitted fluorescence between 500-550 nm was collected via a dichroic mirror and custom filter set. Images were exported to the Matlab programming environment where fluorescence intensities were averaged from large regions of interest that included multiple cells. Traces were corrected for bleaching effects by compensating for slow drifts in baseline fluorescence and -Δ F / F values were then calculated.

2.5.2 Recording intracellular pH

Intracellular pH was measured using one of three genetic reporters - E^2GFP (Bizzarri et al., 2006), deGFP4 (Hanson et al., 2002) and Cl-sensor (Markova et al., 2008). For E^2GFP transfected neurons, imaging was performed using an upright Leica SP2 AOBS laser scanning confocal microscope equipped with a 40x water immersion objective (NA 0.8). Sequential excitation of E^2GFP at 458 nm and 488 nm was achieved with a multiline argon laser. Emitted fluorescence was detected between 500 nm and 550 nm using a single photomultiplier tube (PMT) at a constant voltage. To compensate for fluctuations in laser intensity, a custom built laser power sensor (sample rate 10 kHz) was used to record laser power output during imaging (Arosio et al., 2010; Zucker and Price, 2001) and the resulting data was used to correct fluorescence ratios offline. For deGFP4 and

Cl-sensor expressing cells, imaging was performed using an Olympus FV300 confocal microscope (Olympus, Japan), custom-converted for two-photon imaging and equipped with a MaiTai-HP Ti:sapphire femtosecond pulsed laser (Newport Spectra-Physics, USA). Images were acquired on a PC using Fluoview software (version 5.0, Olympus, Japan). The two-photon system was mounted on an Olympus BX51 upright microscope equipped with a 40x water immersion objective (NA 0.80). Fluorescence was detected using two externally mounted PMTs (R3896, Hamamatsu, Japan). An excitation wavelength of 810 nm or 850 nm was used for deGFP4 or Cl-sensor, respectively. Emitted fluorescence from deGFP4 was separated using a dichroic mirror at 495 nm and filtered for detection by the two PMTs at 450-490 nm and 500-550 nm. Emitted fluorescence from Cl-sensor was separated using a dichroic mirror at 510 nm before being filtered for detection at 460-500 nm and 520-550 nm. Images were exported to the Matlab environment where background was subtracted and fluorescence averaged within regions of interest selected from the soma of single neurons or astrocytes. Excitation or emission fluorescence ratios (R_{pH}) were converted to pH values according to calibration curves collected for each construct (see Chapter 5).

2.5.3 Recording intracellular Cl^- and pH using ClopHensor2

The intracellular Cl^- and pH of ClopHensor2 expressing cells were measured as follows. Imaging was performed using an upright Leica SP2 AOBS laser scanning confocal microscope equipped with a 40x water immersion objective (NA 0.8). ClopHensor2 was used as a ratiometric indicator of Cl^- and pH by excitation. The protein was excited sequentially via single-photon excitation at 458, 488 and 594 nm. Emission was collected between 500 and 550 nm by a single photomultiplier tube (PMT) for excitation at 458 and 488 nm, but between 650 and 700 nm by a second PMT during excitation at 594 nm. As described above, a custom built sensor was used to record and correct for fluctuations in laser output power during imaging (Arosio et al., 2010; Zucker and Price, 2001). And images were exported to the Matlab programming environment where background was subtracted and fluorescence averaged within regions of interest selected from the soma of single cells.

ClopHensor2 is a fusion of E^2GFP and tdTomato proteins. E^2GFP is a pH sensitive

protein whose fluorescence is also quenched by Cl^- ions (Bizzarri et al., 2006), while td-Tomato is insensitive to both Cl^- and pH. The excitation spectrum of E^2GFP and hence ClopHensor2 possesses a pH isobestic point at 458 nm (Arosio et al., 2010). The fluorescence at this excitation wavelength is therefore Cl^- sensitive, but not pH sensitive. As such, the ratio of fluorescence elicited by excitation at 458 nm over that acquired at 594 nm ($R_{Cl} = F_{458}/F_{594}$) was converted to intracellular Cl^- concentration according to calibration curves collected in the manner described in Section 2.5.4. In addition, the ratio of fluorescence collected using the two excitation wavelengths 488 and 458 nm ($R_{pH} = F_{488}/F_{458}$) was converted to intracellular pH using the calibration technique described in Section 2.5.5.

2.5.4 Cl^- calibration

Intracellular Cl^- was controlled by equilibrating extra- and intracellular ion concentrations using the K^+ / H^+ exchanger nigericin (10 μM) and the Cl^- / OH^- exchanger tributyltin chloride (10 μM) in a high K^+ containing aCSF. aCSF's of varying [Cl^-] concentration were made by mixing two HEPES buffered aCSF solutions containing 0 mM or 131 mM of chloride, respectively. The 0 mM [Cl^-] solution contained (in mM): potassium D-gluconate (123), HEPES (23), D-glucose (11), NaH_2PO_4 (1.2), $MgSO_4$ (2) and calcium D-gluconate (2). The 131 mM [Cl^-] solution contained (in mM): KCl (123), HEPES (23), D-glucose (11), NaH_2PO_4 (1.2), $MgCl_2$ (2) and $CaCl_2$ (2). Using these two solutions high K^+ containing aCSF solutions of the following Cl^- concentrations were made: 131 mM, 65.5 mM, 32.75 mM, 16.375 mM, 8 mM and 0 mM. aCSF was bubbled with 100% O_2. After each adjustment of Cl^-, at least 15 minutes were allowed for intracellular and extracellular compartments to equilibrate. The Cl^- sensitive fluorescence ratio described above (R_{Cl}) was measured at different intracellular [Cl^-]:

$$R_{Cl} = \frac{S_N}{S_D}$$

S_N and S_D are the numerator and denominator of the calculated fluorescence ratio, respectively. The formation of a 1:1 analyte-sensor complex results in an equilibrium described by the Grynkiewicz equation Grynkiewicz et al. (1985); Arosio et al. (2010), which,

for a Cl^- indicator, can be written as follows:

$$[Cl^-] = K_d^{Cl}\left(\frac{R_{Cl} - R_{free}}{R_{bound} - R_{Cl}}\right)\left(\frac{S_{D,free}}{S_{D,bound}}\right)$$

K_d^{Cl} is the Cl^- dissociation constant, R_{free} is the maximum value of R_{Cl}, reflecting R_{Cl} where no Cl^- is bound to ClopHensor2. In contrast, R_{bound} is the minimum value of R_{Cl}, reflecting R_{Cl} when ClopHensor2 is saturated with Cl^-. In addition, $S_{D,free}$ and $S_{D,bound}$ reflect S_D in its Cl^-- free and Cl^-- bound forms respectively. However, as the fluorescence of tdTomato is insensitive to Cl^-, $\frac{S_{D,free}}{S_{D,bound}} = 1$. Calibration data was then fitted using the following rearranged version of the above equation:

$$R_{Cl} = \frac{[Cl^-]R_{bound} + K_d^{Cl}R_{free}}{K_d^{Cl} + [Cl^-])}$$

This allowed K_d^{Cl}, R_{free} and R_{bound} to be determined and $[Cl^-]_i$ to be calculated from measured fluorescence ratios (R_{Cl}) during subsequent experiments.

2.5.5 pH calibration

In a similar fashion to that described for Cl^-, intracellular pH was controlled by equilibrating extra- and intracellular ion concentrations using the K^+ / H^+ exchanger nigericin (10 μM) and the Cl^- / OH^- exchanger tributyltin chloride (10 μM) in a high K^+ aCSF containing (in mM) potassium D-gluconate (123), HEPES (23), D-glucose (11), NaH_2PO_4 (1.2), $MgSO_4$ (2) and calcium D-gluconate (2) (Boyarsky et al., 1988). pH was adjusted with small aliquots of NaOH and, to avoid CO_2 dependent pH buffering, aCSF was bubbled with 100% O_2. After each adjustment of pH, at least 15 minutes were allowed for intracellular and extracellular compartments to equilibrate. For each indicator, either an excitation (E^2GFP) or emission (deGFP4, Cl-sensor) fluorescence ratio (R_{pH}) was measured at different intracellular pHs:

$$R_{pH} = \frac{S_N}{S_D}$$

S_N and S_D are the numerator and denominator of the calculated pH fluorescence ratio, respectively. The formation of a 1:1 analyte-sensor complex results in an equilibrium described by the Grynkiewicz equation Grynkiewicz et al. (1985); Arosio et al. (2010), which, for a generic pH indicator, can be written as follows:

$$pH_i = pK_a + log\left(\frac{R_{pH} - R_A}{R_B - R_{pH}}\right) + log\left(\frac{S_{D,A}}{S_{D,B}}\right)$$

R_A and R_B are the values of R_{pH} for the ratiometric indicator in its most acidic and basic forms, respectively. Likewise, $S_{D,A}$ and $S_{D,B}$ reflect S_D in its acidic and basic form. pK_a is the acid dissociation constant of the indicator. Calibration data was fitted using the following rearranged version of the above equation:

$$R_{pH} = \frac{R_B 10^{pH - pK_A - log\left(\frac{S_{D,A}}{S_{D,B}}\right)} + R_A}{1 + 10^{pH - pK_A - log\left(\frac{S_{D,A}}{S_{D,B}}\right)}}$$

This allowed the pK_a of each construct to be determined and pH_i to be calculated from measured fluorescence ratios (R_{pH}) during subsequent experiments.

2.6 Drugs

The following drugs were added to the aCSF as required; tetrodotoxin (1 μM, Tocris) - a voltage-gated Na^+ channel blocker, kynurenic acid (2 mM, Sigma) - a broad spectrum glutamatergic receptor antagonist, CGP55845 (5 μM, Tocris) - a $GABA_BR$ anatagonist, gabazine (SR95531 hydrobromide, 20 μM, Tocris) - a $GABA_AR$ antagonist, 4-aminodpyridine (50 μM, Sigma) - a voltage gated K^+ channel blocker, S0859 (50 μM, was kindly provided by Pawel Swietach who sourced the compound from Sanofi-Aventis, formerly Hoechst AG, Hoechst, Germany) - an inhibitor of Na^+ / HCO_3^- cotransport, nigericin (10 μM, Sigma) - a K^+ / H^+ exchanger, and tributyltin chloride (10 μM, Sigma) - a Cl^- / OH^- exchanger.

2.7 Data analysis and statistics

Data analysis was performed using custom-made programs in the MATLAB environment. Some statistical analysis was also performed using GraphPad Prism version 5.0 (GraphPad Software). Data are reported as mean $\pm$ SEM.

Chapter 3

Transient changes in the driving force for $GABA_A$Rs

3.1 Introduction

In the introduction to this thesis I described how the majority of fast synaptic inhibition in the brain is mediated by $GABA_A$ receptors, which are primarily permeable to Cl^-. The transmembrane concentration gradient of Cl^- sets the reversal potential for for $GABA_A$Rs (E_{GABAA}) and as a consequence is a major factor in determining the strength of synaptic inhibition. In the adult nervous system, E_{GABAA} is typically close to the neuronal resting membrane potential. This means that relatively small changes to E_{GABAA} can vary the functional effect of $GABA_A$R activation and consequently neuronal output. Unlike glutamatergic synapses where postsynaptic plasticity mechanisms operate by changing synaptic conductance, GABAergic synapses are unique in that plasticity mechanisms can include changes to E_{GABAA} as well as alterations to synaptic conductance (Wright et al., 2011). Whilst considerable attention has been devoted to describing long term changes in Cl^- regulation, relatively little is known about transient changes in intracellular Cl^- that could occur on the time scale of seconds.

The first aim of this chapter was to confirm previous reports, (Staley and Proctor, 1999; Jin et al., 2005), that the influxes of Cl^- that can accompany strong activation of $GABA_A$Rs may overwhelm a neurons ability to maintain a stable Cl^- concentration gradient. My second aim was to corroborate previous work (Staley and Proctor, 1999), which

described how different subcellular compartments (soma versus dendrites) differ in their susceptibility to $GABA_A$R induced Cl^- accumulation. Thirdly, I aimed to use a biologically realistic computer model to simulate these phenomena as well as investigate how Cl^- loading might effect synaptic integration and spike timing.

Recently two novel strategies have emerged for optically silencing neurons. The first utilises halorhodopsin (eNpHR3.0, 'eNpHR'), a light-driven Cl^- pump, to move Cl^- into a cell (Han and Boyden, 2007; Zhang et al., 2007). The second employs archaerhodopsin ('Arch'), a light-driven proton pump, to transport protons out of a cell (Chow et al., 2010). Both silencing strategies work by generating strong hyperpolarising currents. However, as eNpHR's inhibitory effects are mediated by Cl^- transport, the fourth aim of this chapter was to determine whether the two optogenetic silencers might differ in their effects on GABAergic transmission. Lastly, I sought to establish eNpHR as a tool for optically manipulating $[Cl^-]_i$ with a view to studying how changes in $[Cl^-]_i$ might affect cell function.

3.2 Strong $GABA_A$R activation transiently increases intracellular Cl^- concentration

Previous work has suggested that under certain conditions Cl^- influx via activated $GABA_A$Rs may temporarily 'load' neurons with Cl^- (Staley and Proctor, 1999; Jin et al., 2005). To confirm that intense $GABA_A$R activation can transiently increase $[Cl^-]_i$, GABA was locally applied via a puffer pipette to hippocampal pyramidal neurons in organotypic slice cultures and acute slices (Fig. 3.1a and b). $GABA_A$R currents evoked in this manner were recorded in voltage clamp with positive currents representing Cl^- influx into the cell and negative currents representing efflux. An initial 'loading' GABA puff was followed by a subsequent 'test' GABA puff. The amount of Cl^- loaded into the cell during the 'loading' puff could be varied by changing the membrane voltage at which the GABA puff was applied. More positive membrane voltages, by being further from resting E_{GABAA}, served to increase the driving force for Cl^- across activated $GABA_A$Rs. The second 'test' GABA puff was always applied at the same membrane voltage. In addition, due to the fact that the 'test' puff occurred at the same time with respect to the preceding loading puff, one could assume that the $GABA_A$R conductance generated by the 'test' puff was equivalent

for all sweeps.

Under these conditions, marked differences in the $GABA_AR$ current elicited by the second 'test' puff were observed. This could only be attributed to changes in $[Cl^-]_i$ caused by different amounts of Cl^- moving into the cell during the 'loading' puff (Fig. 3.1). The amount of Cl^- loaded during the first puff could be estimated by calculating the integral of the $GABA_AR$ current trace. Assuming that the $GABA_AR$ conductances elicited by the two consecutive puffs were comparable, I calculated the change in E_{GABAA} that would account for the change in size of the $GABA_AR$ current elicited by the second 'test' puff. In both organotypic and acute slices, the amount of Cl^- loaded by the first puff was proportional to the subsequent change in E_{GABAA} measured 2 s later (Figure 3.1). This demonstrates that large influxes of Cl^- through $GABA_ARs$ can overwhelm a neuron's ability to maintain a stable $[Cl^-]_i$ gradient.

To determine whether these increases in $[Cl^-]_i$ caused by $GABA_AR$ activation were transitory, I systematically varied the times of the second 'test' puff (Fig. 3.2). The $GABA_AR$ currents were observed to recover over a period of 15 s, which indicated representing a recovery in the underlying $[Cl^-]_i$.

3.3 Cell compartments differ in their ability to deal with a Cl^- load

In order to investigate whether compartments of a neuron differ in their ability to deal with a Cl^- load, a similar experiment to that described in Figure 3.2 was performed. However, in this case the puff of GABA to 'load' the neuron with Cl^- and the subsequent 'test' puff were both either directed over the dendrite or over the soma of the neuron (see schematic in Fig. 3.3a). Whilst Cl^- influx elicited by puffing over the dendrites had an obvious effect on the size and direction of the current evoked by the 'test' puff (Fig. 3.3b), a minimal effect was seen when similar amounts of Cl^- were loaded over the soma (Fig. 3.3c). Population data confirmed this difference. Although a prior Cl^- load was significantly correlated with a change in $[Cl^-]_i$ for both dendritic and somatic application of GABA (r = 0.8102 and 0.6114 respectively, $P < 0.0001$ Pearson correlation), the slope of the the linear fit was steeper (21.07 ± 1.210 mM/nC) for $GABA_AR$ currents elicited over the dendrites as opposed to

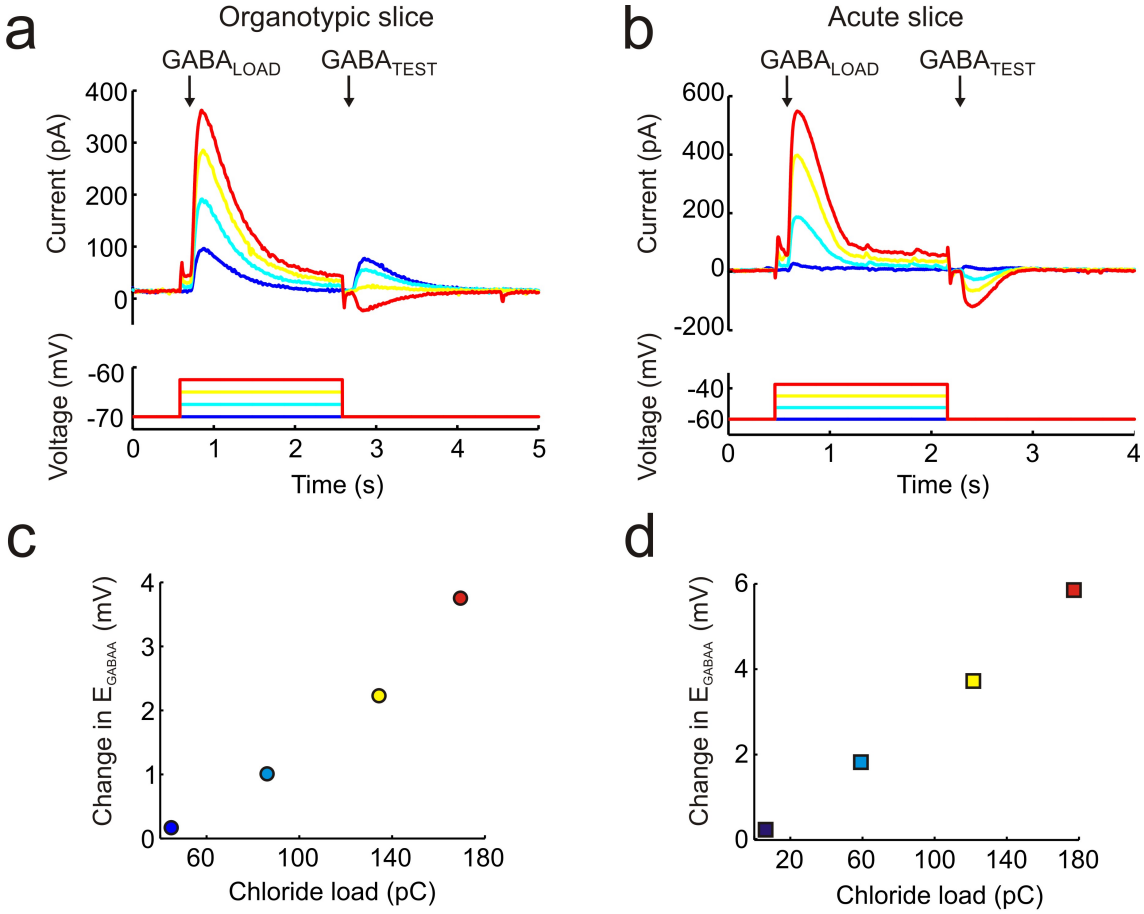

Figure 3.1: Strong $GABA_A$R activation transiently increases intracellular Cl^- (a) Gramicidin perforated patch voltage clamp recording from a CA3 pyramidal neuron in an organotypic hippocampal slice. Different sized Cl^- loads were elicited by stepping the membrane voltage to different potentials for 2 s and activating $GABA_A$Rs simultaneously with a GABA puff (100 μM; 100 ms after the start of the voltage step). Larger depolarising voltage steps resulted in stronger driving forces on the $GABA_A$R and therefore larger Cl^- loads. 100 ms after the end of the voltage step (and therefore 2 s after the first 'loading' GABA puff) a second 'test' GABA puff was delivered to estimate whether E_{GABAA} had changed as a result of the Cl^- load. Note that larger Cl^- loads can switch the direction of the $GABA_A$R current from outward to inward. (b) Similar data for a subicular pyramidal neuron recorded from an acute hippocampal slice (aged 4 weeks). Note again that larger Cl^- loads switch the direction of the $GABA_A$R current from outward to inward. (c) and (d) show the change in E_{GABAA} caused by the different Cl^- loads in the recordings from the cells in a and b, respectively (colour-coded by trace).

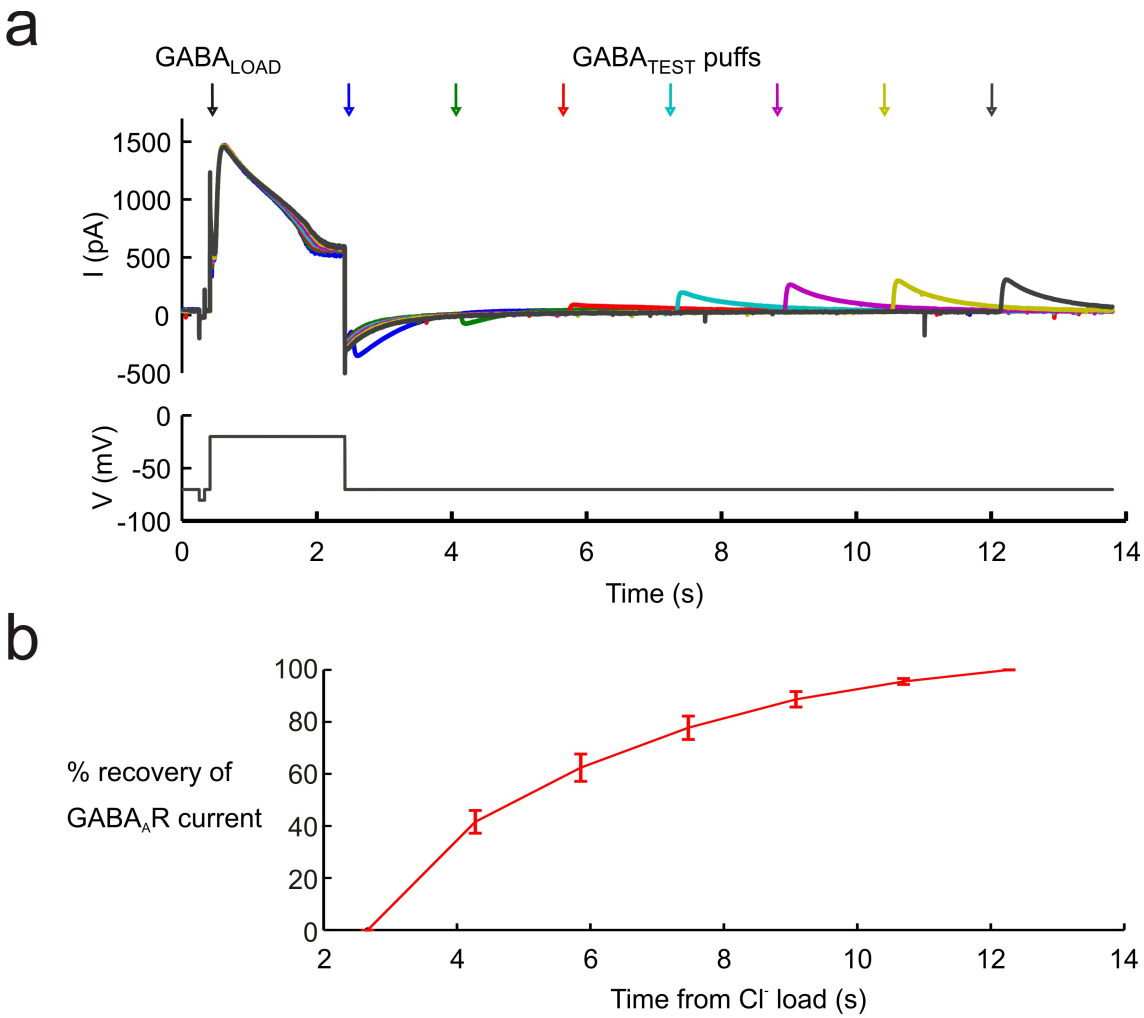

Figure 3.2: $GABA_AR$ induced increases in $[Cl^-]_i$ recover over time. a) A 'loading' puff of GABA was followed by a 'test' puff. Each colour represents a different recording sweep and thus a different interval between the 'load' puff and the 'test' puff. The $GABA_AR$ currents were observed to recover over a period of 15 s representing a recovery in the underlying $[Cl^-]_i$. b) Population data from 4 CA3 pyramidal neurons confirmed the recovery of $GABA_AR$ currents over time.

the soma (4.393 $\pm$ 0.8946 mM/nC) (P ¡ 0.0001, t test, Fig. 3.4a).

This data was collected using a nominally HCO_3^- free aCSF solution to ensure that $GABA_A$R currents could be attributed purely to Cl^-. The fact that $GABA_A$Rs are also partially permeable to bicarbonate (Kaila, 1994) led us to test whether reintroducing physiological levels of HCO_3^- could affect the differences in subcellular Cl^- loading observed. The experiment was therefore repeated with bicarbonate containing artificial cerebrospinal fluid (aCSF) in both organotypic and acute slices (Fig. 3.4b and c). In organotypic slices containing HCO_3^-, the slope of the linear fit was 37.84 $\pm$ 4.384 mM/nC for dendrites vs 5.851 mM/nC for somata (P ¡ 0.0001, t test, Fig. 3.4b). Similarly in acute slices in the presence of HCO_3^-, the slope was steeper at 72.20 $\pm$ 10.46 mM/nC for the dendritic compartment compared to the somatic compartment (16.02 $\pm$ 1.040 mM/nC) (P ¡ 0.0001, t test, Fig. 3.4c). These experiments confirm that dendrites are more susceptible to Cl^- loads than somatic compartments.

3.3.1 Computational modelling of cell compartment differences in Cl^- regulation

In order to investigate whether cell compartment differences in the ability to deal with a Cl^- load could be explained by a limited set of parameters, I generated a biophysical model of Cl^- regulation in the NEURON modelling environment (Hines and Carnevale, 1997).

Constructing the model: Mechanisms and Parameters

The geometry of the model was based on the reconstruction of a biocytin filled layer 5 medial entorhinal cortex pyramidal cell. It included a soma, axon, 27 basal dendrites and 50 apical dendrites. These structures were modelled as a set of 1949 connected cylinders referred to as ‘segments’. The virtual cell received glutamatergic synpases at a density of 0.2 synapses per μm^2 innervated by 44 presynaptic glutamatergic cells firing at 10 Hz Wilson and McNaughton (1994). The virtual cell also received GABAergic synapses at a density of 0.2 synapses per μm^2 innervated by 44 presynaptic cells. Each presynaptic GABAergic cell would fire at 40 Hz in a Poisson manner (Fig. 3.5a, top) - a physiologically plausible firing rate for basket cell interneurons (Tamás et al., 2000). A maximum synaptic conductance of 0.001 μS was used as defined in a model of synaptic

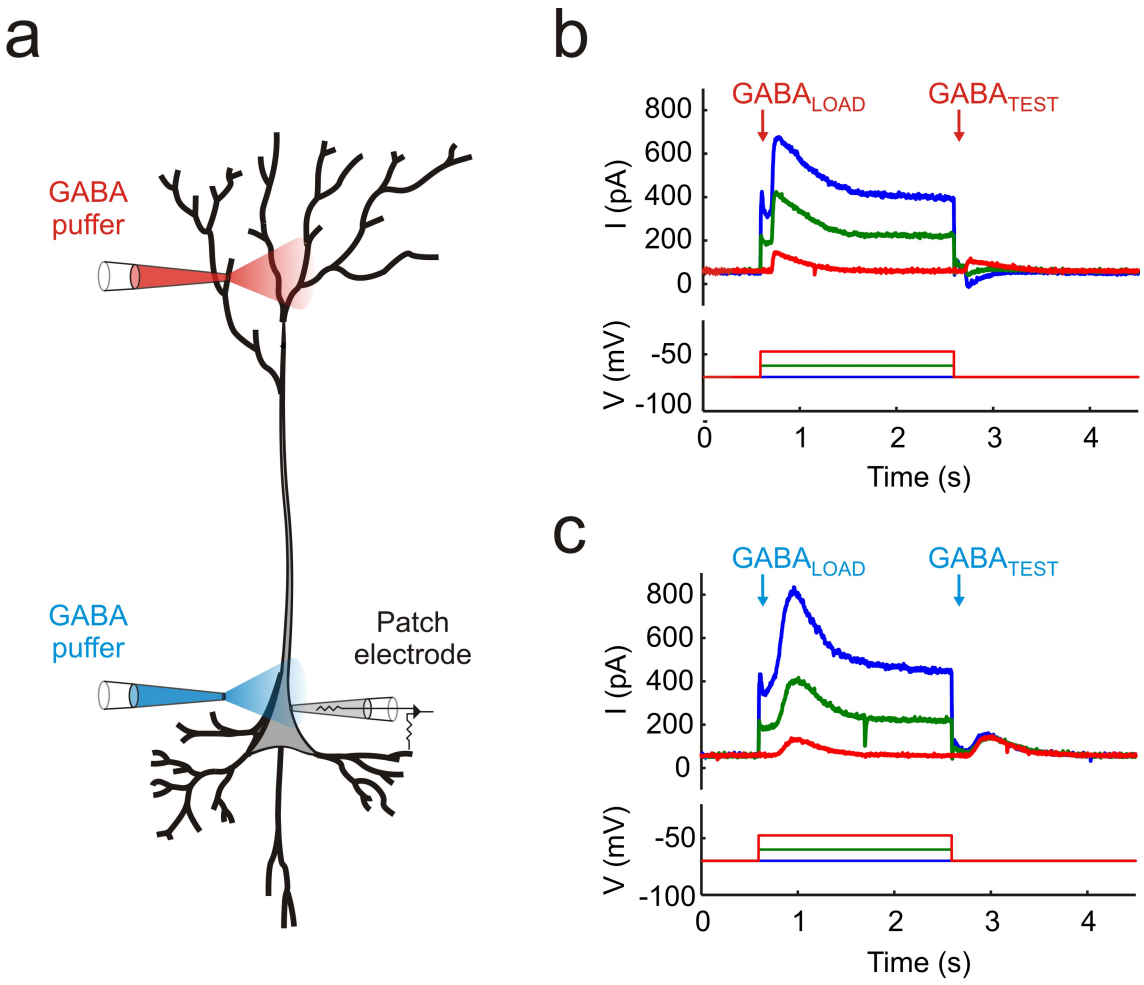

Figure 3.3: Cell compartments differ in their ability to deal with a Cl^- load. Recording from a CA3 pyramidal neuron revealed that a Cl^- load over the dendrites increased $[Cl^-]_i$ to a greater extent than a similar load over the soma. a) As in Fig. 3.2, $GABA_AR$ activation was evoked by local application of GABA. This was either applied to the dendrites (red) or soma (blue). b) When the puffer pipette was positioned over the dendrites, increasing amounts of Cl^- loaded by the first puff affected the size and direction of $GABA_AR$ currents to the second 'test' puff. c) This effect was not evident when similar Cl^- loads were evoked by puffing over the soma.

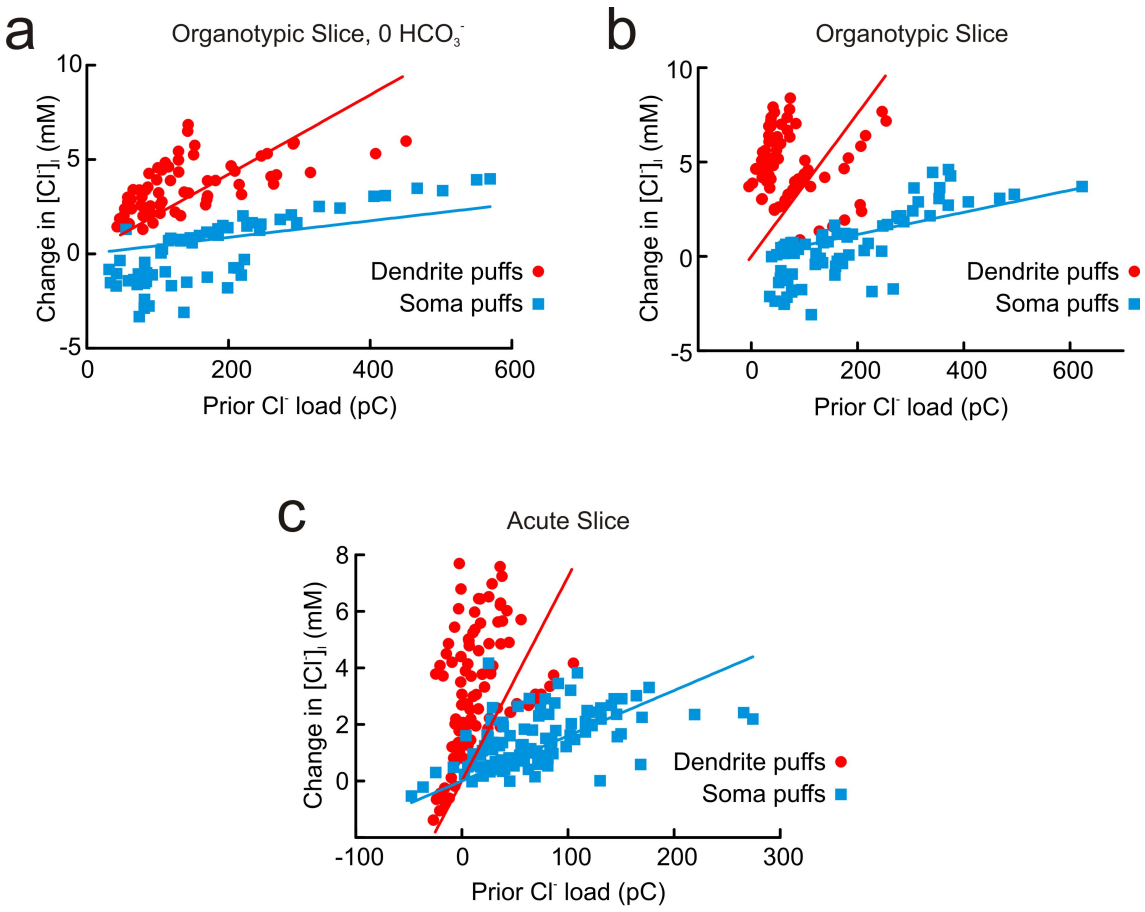

Figure 3.4: Population data demonstrates that the dendrites of hippocampal pyramidal neurons are more susceptible to a Cl^- load than their soma. This was the case for experiments performed in HCO_3^- free aCSF in organotypic slices (a), HCO_3^- containing media in organotypic slices (b) and HCO_3^- containing aCSF in acute slices.

conductance by Destexhe (1998).

The model was able to dynamically adjust E_{GABAA}as a function of fluctuating $[Cl^-]_i$ according to the nernst equation. $[Cl^-]_o$ (135 mM), $[K^+]_i$ (3 mM), $[K^+]_o$ (120 mM), $[HCO_3^-]_i$ (10 mM) and $[HCO_3^-]_o$ (25 mM) were assumed to remain constant. $[Cl^-]_i$ for each segment could vary according to transmembrane Cl^- flux via activated $GABA_A$Rs, Cl^- transport due to the K^+/Cl^- cotransporter (KCC2) and Cl^- diffusion to and from neighbouring segments of the cell. The parameters defining Cl^- transport via KCC2 were taken from Staley and Proctor (1999) (K_d = 15 mM, V_{max} = 5 mM/s), whilst the diffusion constant for Cl^- was based on an approximate experimental estimation (D = 10 μm^2/s).

Executing the model

In order to compare the effects of different neuronal compartments, the model was executed in two different anatomical modes. In the first, all the GABAergic inputs were placed on the soma ('somatic' inhibition). In the second, the same number of GABAergic inputs were all placed on the dendrites ('dendritic' inhibition).

When the somatic inhibition was run, GABAergic inputs directed over the soma caused a negligible shift in $[Cl^-]_i$. In contrast, the same GABAergic inputs directed over the dendrites caused a substantial increase in $[Cl^-]_i$ within the dendritic compartment (Fig. 3.5a, bottom). As KCC2 expression was uniform within the model, all differences in Cl^- loading were attributable to volume differences between the compartments.

For the two anatomical modes, the model was run either with $[Cl^-]_i$ fixed at its initial value (Fig. 3.5b, black) or with $[Cl^-]_i$ able to fluctuate due to the transmembrane flux of Cl^- (Fig. 3.5b, pink). Interestingly, when predicted spike times were calculated they were markedly different between fixed and dynamic Cl^-, but only when GABAergic inputs were directed over the dendrites (Fig. 3.5b, left) and not when inputs were directed over the soma (Fig. 3.5b, right).

These computational simulations and the experimental data described previously both argue that small volume compartments, such as dendrites, are most susceptible to changes in intracellular Cl^- and E_{GABAA}.

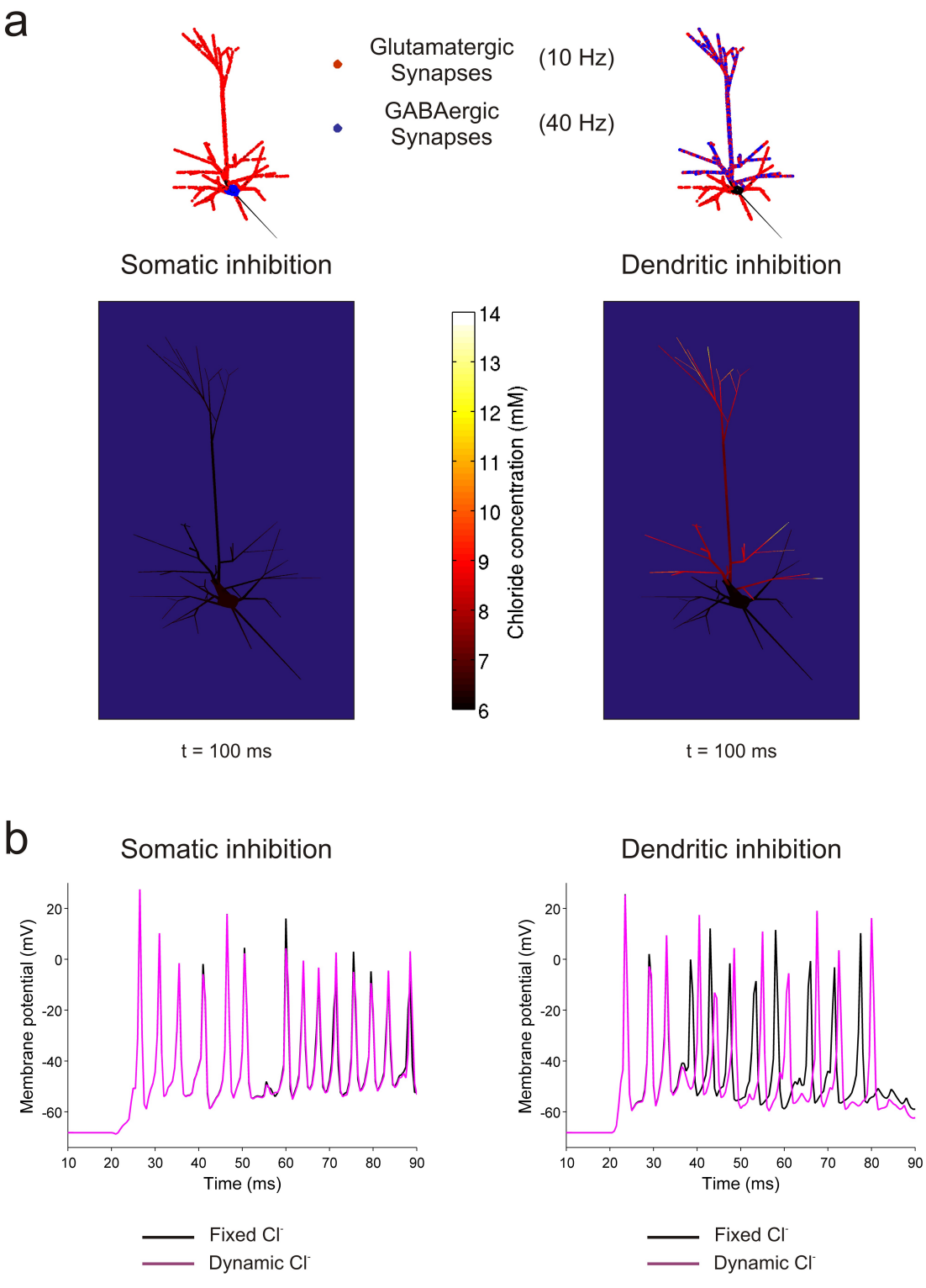
a
Glutamatergic Synapses (10 Hz)
GABAergic Synapses (40 Hz)
Somatic inhibition
Dendritic inhibition
Chloride concentration (mM)
14
13
12
11
10
9
8
7
6
t = 100 ms
t = 100 ms
b
Somatic inhibition
Dendritic inhibition
Membrane potential (mV)
Time (ms)
Fixed Cl-
Dynamic Cl-

3.4 Optogenetic silencers generate inhibitory photocurrents

The potential for concentration gradients to collapse is not only relevant for endogenous network activity, but also for experimental manipulations that use the flux of ions to control activity. Multiple strategies have emerged for rapidly silencing the activity of neurons, all of which use the transmembrane movement of various ion species in order to hyperpolarise the cell membrane. The two most successful silencing strategies have used light-driven chloride pumps (Han and Boyden, 2007; Zhang et al., 2007), which move chloride into the cell and more recently proton pumps, which move protons out of the cell and thus generate a hyperpolarising effect (Chow et al., 2010). I set out to explore how light activated ion fluxes may interact with endogenous signalling systems. More specifically, given that neurons are susceptible to collapses in Cl^- gradients, do light-activated pumps cause significant shifts in E_{GABAA}? For these experiments I utilised the latest light-driven inward Cl^- pump (*Natronomonas pharaonis* halorhodopsin, eNpHR3.0 or eNpHR)Gradinaru et al. (2010) and a popular light-driven outward H^+ pump (Archaerhodopsin-3 from *Halorubrum sodomense*, Arch) (Chow et al., 2010). eNpHR3.0-EYFP or Arch-GFP were expressed in pyramidal neurons from hippocampal organotypic slice cultures or acute slices using biolistic transfection or viral injection respectively. To confirm their function in these systems, transfected cells were patched and stimulated with a 532 nm laser, which reliably evoked outward photocurrents consistent with previous reports (Gradinaru et al., 2010;

Figure 3.5 *(facing page)*: A biophysical model of Cl^- regulation predicts cell compartment differences in susceptibility to a Cl^- load, which impacts the spike times generated by synaptic inputs. a) Two separate simulations were generated, which were identical in every respect except for the location of GABAergic inputs. In the first simulation, 'Somatic inhibition' (left), GABAergic inputs were exclusively targeted to the soma. In the second simulation, 'Dendritic inhibition' (right), the neuron received the same number of inputs but they were exclusively targeted to the dendrites. The GABAergic inputs were then 'turned on' using physiologically plausible firing rates. After 100 ms $[Cl^-]_i$ had hardly changed in the soma of the first simulation. However, the second simulation showed marked increases in $[Cl^-]_i$, particularly in structures of small volume such as the apical dendrites. b) In order to assess the potential impact on the spiking activity of the cell in response to a barrage of inputs the simulations were executed either with $[Cl^-]_i$ fixed at its initial value (black traces) or with $[Cl^-]_i$ able to fluctuate in accordance with transmembrane fluxes of Cl^- (pink traces). Allowing dynamic fluctuations in $[Cl^-]_i$ affected spike times when GABAergic synapses were directed over the dendrites (right) but not when those inputs were directed over the soma (left).

Chow et al., 2010) (Fig. 3.6a). The amplitude of photocurrents was directly proportional to the laser intensity (Fig. 3.6d). This relationship was statistically indistinguishable for both eNpHR and Arch, suggesting that a particular laser power would generate photocurrents of comparable amplitude under my recording conditions (P = 0.7074, Analysis of Covariance). The photocurrents exhibited fast onset and offset kinetics as has been shown previously (Madisen et al., 2012; Mattis et al., 2012) (Fig. 3.6b). The time constant for both Arch and eNpHR onset and offset were comparable and fast ($<$10 ms, on average, Fig. 3.6c). As described below, activated photocurrents consistently inhibited action potential generation in response to somatic current injection (Fig. 3.6a, bottom).

3.5 A light-activated chloride pump, but not a proton pump, causes a change in GABAergic transmission.

To test whether eNpHR has sustained effects upon GABAergic transmission I performed voltage clamp recordings using the perforating agent gramicidin, which preserves intracellular Cl^-. Brief puffs of GABA (100 μM) were used to compare E_{GABAA} before, and after, light-activation of the pumps. Resting E_{GABAA} values did not differ between the eNpHR-expressing (mean of -68.7 $\pm$ 1.2 mV, n = 18 cells) and Arch-expressing (mean of -68.5 $\pm$ 1.0 mV, n = 13 cells) neurons (P = 0.89, t test). However, I found that eNpHR-activation for 15 s consistently changed the amplitude and/or polarity of $GABA_A$R currents, such that $GABA_A$R currents that were outward before laser-activation often became strong

Figure 3.6 *(facing page)*: Optogenetic silencers generate robust inhibitory currents. (a) Left, eNpHR3.0-EYFP or Arch-GFP expressing pyramidal cells were patched and activated with a 532 nm laser. Right, a voltage clamp recording from a eNpHR expressing neuron demonstrates that laser stimulation generates robust outward currents. Bottom, in current clamp mode the same photocurrents are seen to reliably inhibit action potential generation in response to somatic current injection. b) Voltage clamp recordings from a neuron expressing Arch (top) and a separate neuron expressing eNpHR3.0 (bottom) immediately following laser onset (left) and immediately following laser offset (right). Activation and deactivation kinetics could be fitted with a single exponential function (red). (b) Population data shows that the time constant for both Arch and eNpHR onset and offset are comparable and fast ($<$10 ms, on average). (c) Mean photocurrent amplitude plotted as a function of laser power for Arch- and eNpHR3.0-expressing neurons. This relationship was statistically indistinguishable for the two optical silencers, suggesting that a particular laser power would generate photocurrents of comparable amplitude under the recording conditions (P = 0.7074, Analysis of Covariance) used here.

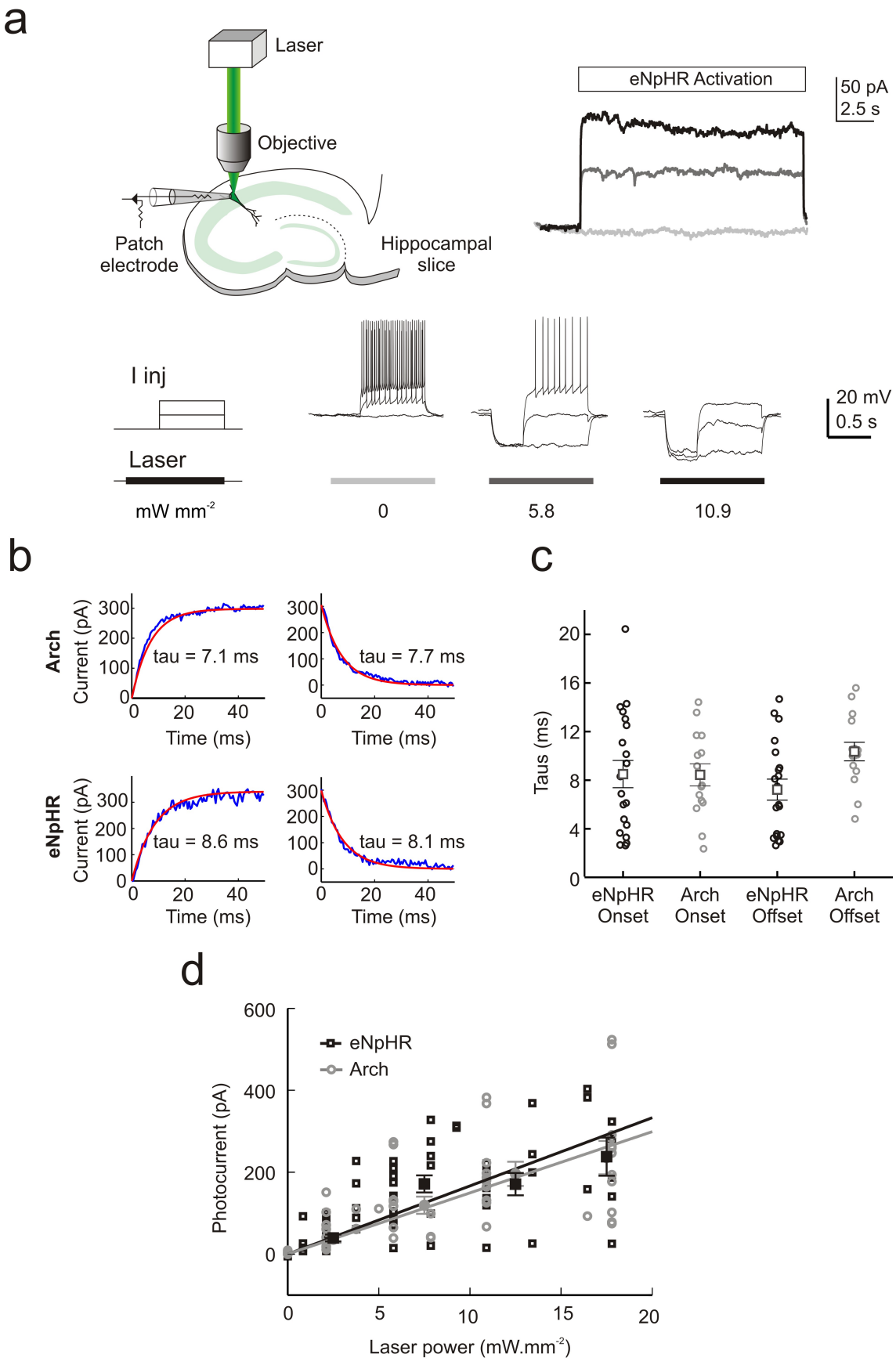
a
Laser
Objective
Patch electrode
Hippocampal slice
eNpHR Activation
50 pA
2.5 s
I inj
Laser
20 mV
0.5 s
mW mm-2
0
5.8
10.9
b
Arch
eNpHR
Current (pA)
tau = 7.1 ms
tau = 7.7 ms
tau = 8.6 ms
tau = 8.1 ms
Time (ms)
c
Taus (ms)
eNpHR Onset
Arch Onset
eNpHR Offset
Arch Offset
d
eNpHR
Arch
Photocurrent (pA)
Laser power (mW.mm-2)

inward currents after laser-activation (measured 250 ms after laser offset; Fig. 3.7a), consistent with the light-driven accumulation of intracellular Cl^-. This was not the case for Arch-expressing cells, which showed stable $GABA_A$R currents across a range of photocurrents (Fig. 3.7b).

Functionally relevant laser intensities were chosen by assessing the ability of the photocurrents to inhibit spiking in response to somatic current injections via the recording pipette (see Fig. 3.7a and b, bottom). First, I injected a range of current steps in current clamp (1 s duration) without any laser-activation, from which I defined a threshold somatic current (the minimum current that evoked spiking; mean of 112 $\pm$ 25 pA, which generated a mean spike rate of 4.1 0.8 Hz, n = 12) and a strong somatic current (twice the amplitude of the threshold current; mean of 224 $\pm$ 50 pA, which generated a mean spike rate of 13.3 2.6 Hz). An intermediate laser intensity produced the minimum mean photocurrent (104 $\pm$ 17 pA, range 40 - 230 pA) required to inhibit all spiking activity in response to the threshold somatic current. A higher laser intensity produced the minimum mean photocurrent (207 $\pm$ 35 pA, range 90 - 400 pA) required to inhibit all spiking in response to the strong somatic current injection.

The effect upon $GABA_A$R currents was quantified by estimating E_{GABAA} for individual GABA puffs and relating this to the size of the photocurrent (Fig. 3.7c; see Materials and Methods). This revealed a strong positive correlation between the size of the eNpHR photocurrent and the change in E_{GABAA}, (r = 0.70, $P <$ 1x10-19, Pearson Correlation). The slope of the linear fit for the eNpHR data indicated an 8.8 mV shift in E_{GABAA} per 100 pA of mean photocurrent (Fig. 3.7e). Mean eNpHR photocurrents of between 90 and 400 pA, which effectively blocked spiking activity evoked by somatic positive current injection (Fig. 3.7a,b), generated an average E_{GABAA} shift of 19.7 $\pm$ 1.7 mV ($P <$ 1x10-14, *t* test). Modest mean eNpHR photocurrents of between 25 and 50 pA also generated a significant change in E_{GABAA} of 4.8 $\pm$ 1.0 mV (P = 0.0004, *t* test). In contrast, Arch-expressing cells exhibited much more stable E_{GABAA} across a range of photocurrents (Fig. 3.7e); the slope of the linear fit for the Arch data was -0.4 mV per 100 pA of mean photocurrent, with a small negative correlation between Arch photocurrent and the change in E_{GABAA}, (r = -0.2213, P = 0.023, Pearson Correlation). The slope of the linear fits for the two optical silencers were highly statistically different ($P <$ 0.0001, Analysis of Covariance).

To determine whether the effect of eNpHR photocurrents upon E_{GABAA} was evident in different experimental preparations, I examined neurons from mice that had received in vivo viral delivery of one of the optical silencers, via injections into the hippocampus. These neurons, recorded in acute hippocampal slices, also showed a strong relationship between eNpHR photocurrent and change in E_{GABAA} (r = 0.50, $P < 0.0001$, Pearson Correlation; linear fit of 8.9 mV per 100 pA of photocurrent; n = 7 cells; Fig. 3.7d and Fig. 3.8a), which was statistically indistinguishable from neurons with plasmid-driven eNpHR expression in organotypic slices (P = 0.89, Analysis of Covariance). Meanwhile, neurons with viral-expression of Arch showed stable E_{GABAA} across a range of photocurrents (r = -0.07, P = 0.68, Pearson Correlation; linear fit of -0.2 mV per 100 pA of photocurrent; n = 6 cells; Fig. 3.7d and Fig. 3.8b).

3.6 The spatio-temporal dynamics of eNpHR induced Cl⁻ loads

To quantify the time scale of the effects of eNpHR-activation on E_{GABAA}, I estimated E_{GABAA} at different times after laser-activation. The rate of recovery of E_{GABAA} had a time constant of 14.7 $\pm$ 3.2 s, on average (Fig. 3.9a,c,e). In addition, varying the duration of the light-activation period revealed that changes in E_{GABAA} were closely related to the duration of the photocurrent and were evident for relatively short photocurrents (Fig. 3.9b,d,f). Significant positive shifts in E_{GABAA} were detected following photocurrents of just 500 ms duration (2.41 $\pm$ 0.5 mV change in E_{GABAA}, P = 0.0014, t test) and showed an incremental relationship with longer photocurrents. The depolarising shifts in E_{GABAA} that resulted from shorter periods of eNpHR-activation were comparable to the shifts associated with prolonged activation of $GABA_A$Rs (Fig. 3.4), supporting the conclusion that Cl^--dependent changes in E_{GABAA} are a fundamental feature of mature GABAergic transmission.

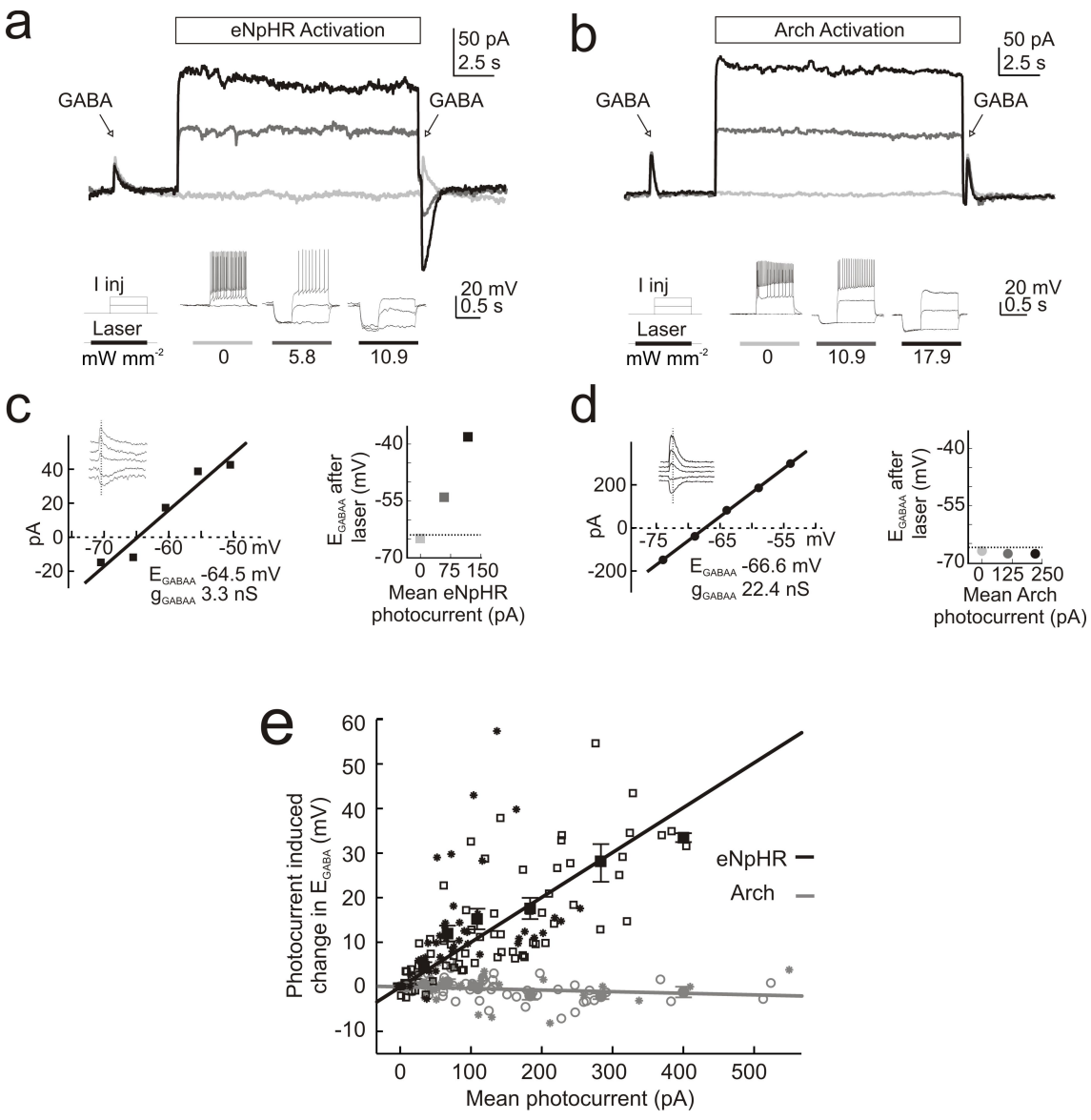
a
eNpHR Activation
50 pA
2.5 s
GABA
GABA
I inj
Laser
mW mm-2
0
5.8
10.9
20 mV
0.5 s
b
Arch Activation
50 pA
2.5 s
GABA
GABA
I inj
Laser
mW mm-2
0
10.9
17.9
20 mV
0.5 s
c
pA
40
20
0
-20
-70
-60
-50 mV
EGABAA -64.5 mV
gGABAA 3.3 nS
EGABAA after laser (mV)
-40
-55
-70
0 75 150
Mean eNpHR photocurrent (pA)
d
pA
200
0
-200
-75
-65
-55 mV
EGABAA -66.6 mV
gGABAA 22.4 nS
EGABAA after laser (mV)
-40
-55
-70
0 125 250
Mean Arch photocurrent (pA)
e
Photocurrent induced change in EGABA (mV)
60
50
40
30
20
10
0
-10
0
100
200
300
400
500
Mean photocurrent (pA)
eNpHR
Arch

3.7 A single compartment model confirms the experimentally observed effect of eNpHR photocurrents on E_{GABAA}

To investigate the interaction between eNpHR induced Cl^- load and subsequent change of E_{GABAA}, I constructed a single compartment model with realistic Cl^- transport mechanisms, as in Section 3.3.1. The single compartment was intended to represent a pyramidal cell soma and hence its volume was assumed to be a prolate spheroid (rugby ball) (see Materials and Methods). To simulate cells of differing volume, somatic length was varied between 12 and 36 μm whilst somatic width was held constant at 12 μm, in line with our own measurements. This resulted in typical neuronal cell volumes of between 0.905 and 2.714 pl, which match the range of somatic volumes reported in the literature (Ambros-Ingerson and Holmes, 2005). For each instance of the model with a particular volume, a tonic Cl^- current was calculated that would maintain resting $[Cl^-]_i$ at 7.0158 mM for an initially stable E_{GABAA} of -70 mV. A Cl^- photocurrent of varying amplitude and duration could then be applied and the resulting changes in $[Cl^-]_i$ and hence E_{GABAA} tracked over time.

In agreement with our experimental observations from a range of cell somata, E_{GABAA} increased steadily over the course of the modelled photocurrent before recovering there-

---

Figure 3.7 *(facing page)*: A light-activated chloride pump, but not a proton pump, causes a sustained change in GABAergic transmission. a) Top, gramicidin perforated patch voltage clamp recording from a CA3 pyramidal neuron expressing eNpHR3.0-EYFP. $GABA_AR$ currents were measured before and after eNpHR-activation using three different laser intensities: 'zero' (light grey), 'intermediate' (dark grey) and 'higher' (black). Note the change in direction of current flow through the $GABA_AR$ as a function of eNpHR-activation. Bottom, laser intensities were selected by assessing their effectiveness in silencing spikes evoked by somatic current injection in current clamp. b) Recordings from a neuron expressing Arch-GFP. All conventions as in 'a'. Note the consistent $GABA_AR$ current for different levels of Arch-activation. c) and d) Estimating the effects of photocurrents on E_{GABAA} for the eNpHR cell in 'a' (c) and Arch cell in 'b' (d). $GABA_AR$ IV plots (left) were used to calculate the resting E_{GABAA} and $GABA_AR$ conductance (g_{GABAA}), which were then used to estimate E_{GABAA} for individual GABA puffs delivered after different mean photocurrents (right; symbol colours correspond to data in 'a' and 'b'). e) Summary of the change in E_{GABAA} associated with different eNpHR (black symbols) and Arch (grey symbols) photocurrents. Square and circle symbols indicate data from neurons recorded in organotypic hippocampal slices that had been biolistically transfected. Stars indicate data from neurons recorded in acute hippocampal slices, with virally-induced expression of opsins.

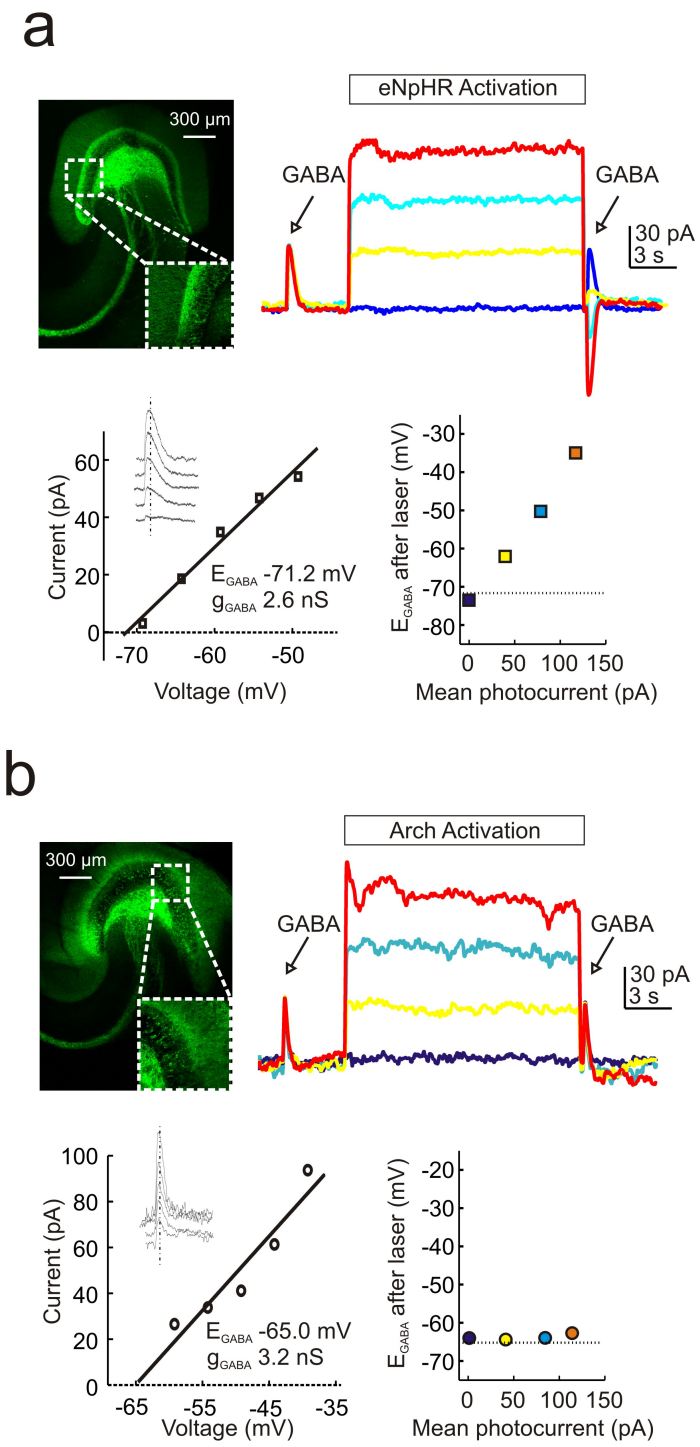
a
eNpHR Activation
300 µm
GABA
GABA
30 pA
3 s
Current (pA)
60
40
20
0
-70
-60
-50
Voltage (mV)
E_GABA -71.2 mV
g_GABA 2.6 nS
E_GABA after laser (mV)
-30
-40
-50
-60
-70
-80
0
50
100
150
Mean photocurrent (pA)
b
Arch Activation
300 µm
GABA
GABA
30 pA
3 s
Current (pA)
100
80
60
40
20
0
-65
-55
-45
-35
Voltage (mV)
E_GABA -65.0 mV
g_GABA 3.2 nS
E_GABA after laser (mV)
-20
-30
-40
-50
-60
-70
0
50
100
150
Mean photocurrent (pA)

after. A soma length of 24 μm resulted in E_{GABAA} shifting by 9.1 mV by the end of the 15 s photocurrent, matching the size of shift demonstrated experimentally (see Fig. 3.7e). As depicted by Fig. 3.10b, photocurrent induced changes in E_{GABAA} were predicted to be proportional to the magnitude of the photocurrent induced. This matched my experimental observations (Fig. 3.7e). In addition, the model predicted that lengthy photocurrents should result in depolarising shifts in E_{GABAA} that stabilise after approximately 40 s. This trend was also evident in my experimental data (Fig. 3.9b and f). Finally, the plateau value of E_{GABAA} reached during a prolonged photocurrent (Fig. 3.10c) was predicted to be dependent on both the kinetics of Cl^- transport and the size of the photocurrent concerned.

3.8 Optogenetic silencing strategies differ in their effects on synaptically-evoked spiking activity.

One prediction is that light-activated shifts in E_{GABAA} could effect spiking activity. It is possible that if E_{GABAA} were to become sufficiently depolarised, GABA activation alone might be able to trigger action potential generation. Indeed, I found that eNpHR has sustained effects upon GABAergic transmission when performing current clamp recordings using the perforating agent gramicidin, which preserves intracellular chloride. Under these conditions I found that a brief puff of GABA (100 μM) normally generated a hyperpolarising response, but when the same puff was delivered after a period of eNpHR-activation, a depolarising response and action potentials could be generated (n = 5 cells; Fig. 3.11c).

To compare the effects of optogenetic silencing strategies upon synaptically-evoked

Figure 3.8 *(facing page)*: In vivo virally-driven expression of optogenetic silencers have different effects upon GABAergic transmission in acute slices. a) Top left, a 2-photon image showing widespread expression of eNpHR3.0-EYFP in the dentate gyrus. Top right, gramicidin perforated patch voltage clamp recording from an eNpHR3.0-expressing neuron in this slice. $GABA_AR$ currents were measured before and after eNpHR-activation for 15 s, at four different laser intensities. Bottom left, $GABA_AR$ IV plots were used to calculate the resting E_{GABAA} and $GABA_AR$ conductance (g_{GABAA}), which were then used to estimate E_{GABAA} for individual GABA puffs delivered after different mean photocurrents (bottom right). b) Top left, a 2-photon image showing widespread expression of Arch-GFP in the dentate gyrus. Top right, recordings from an Arch-expressing neuron in this slice. Bottom left and right, all conventions as in a. Note the stable $GABA_AR$ current following different levels of Arch-activation.

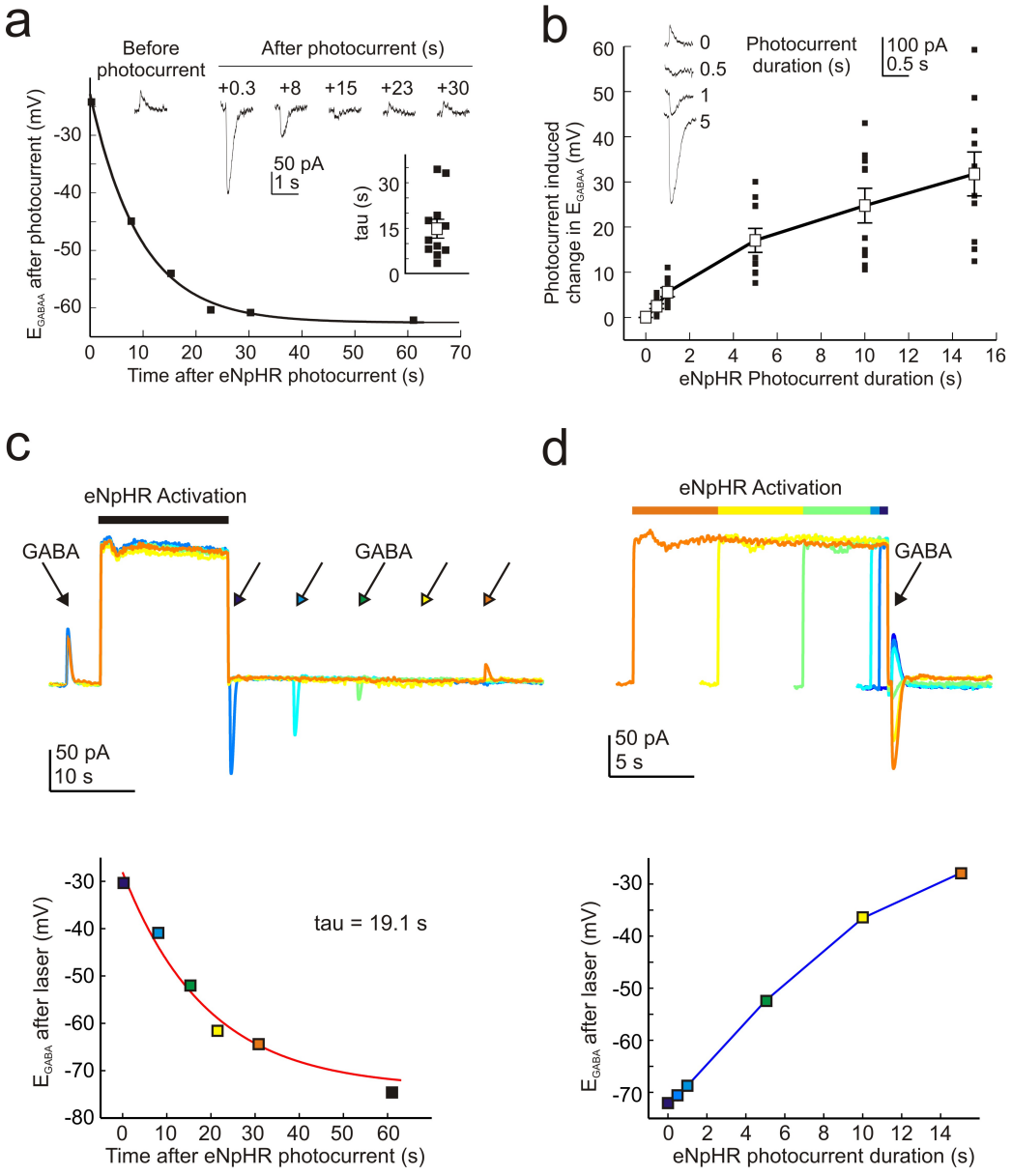
a
Before photocurrent
After photocurrent (s)
+0.3
+8
+15
+23
+30
50 pA
1 s
tau (s)
E_{GABAA} after photocurrent (mV)
Time after eNpHR photocurrent (s)
b
0
0.5
1
5
Photocurrent duration (s)
100 pA
0.5 s
Photocurrent induced change in E_{GABAA} (mV)
eNpHR Photocurrent duration (s)
c
eNpHR Activation
GABA
GABA
50 pA
10 s
E_{GABA} after laser (mV)
tau = 19.1 s
Time after eNpHR photocurrent (s)
d
eNpHR Activation
GABA
50 pA
5 s
E_{GABA} after laser (mV)
eNpHR photocurrent duration (s)

action potential activity, we performed cell-attached recordings from neurons within the pyramidal cell layer of rat hippocampal organotypic brain slices, which had been biolistically transfected with either eNpHR3.0-EYFP or Arch-GFP. Postsynaptic spikes were elicited by delivering brief electrical stimuli to the Schaffer collateral pathway. This stimulus recruits convergent monosynaptic and polysynaptic excitatory and inhibitory postsynaptic potentials (Pouille and Scanziani, 2001). Spike probability was measured before and after a 15 s period of laser-activation (532 nm, mean intensity 19.4 $\pm$ 3.4 mW.mm^{-2}). Separate perforated patch recordings confirmed that these conditions resulted in robust hyperpolarising photocurrents in both eNpHR- and Arch-expressing neurons, which were similar in amplitude (mean eNpHR photocurrent 237 $\pm$ 46 pA; mean Arch photocurrent 235 $\pm$ 40 pA; Fig. 3.6d). However, I found marked differences in terms of how cells responded to synaptic input in the period following light-activation. In eNpHR-expressing cells the mean spike probability increased significantly from 0.37 $\pm$ 0.05 before laser-activation, to 0.82 $\pm$ 0.04 after laser-activation (n = 10 cells, P = 0.00015, paired t test; Fig. 3.11a). The mean stimulus-evoked spike rate (measured over 200 ms) also increased from 1.9 $\pm$ 0.3 Hz before laser-activation to 5.5 $\pm$ 0.9 Hz after laser-activation (P = 0.005, paired t test). This was in contrast to recordings from Arch-expressing cells, which had a comparable spike probability before and after laser-activation, even when the highest laser intensities were used (see example cell in Fig. 3.11b; range of 7.9 to 76.1 mW.mm^{-2}). For a population of Arch-expressing cells the spike probability be-

---

Figure 3.9 *(facing page)*: The spatio-temporal dynamics of eNpHR induced Cl^- loads. a) Gramicidin perforated patch voltage clamp recording from a CA3 neuron expressing eNpHR3.0-EYFP in an organotypic hippocampal slice. Traces show $GABA_AR$ currents recorded at different times after a 15 s photocurrent, on different trials. E_{GABAA} versus time after photocurrent is plotted for this cell and the recovery is well fitted by a single-exponential function. Inset plot shows the distribution of time constants of E_{GABAA} recovery for a population of eNpHR-expressing cells. b) Traces from the same neuron as in 'a' showing $GABA_AR$ currents recorded after photocurrents of different durations. Plot illustrates the change in E_{GABAA} as a function of photocurrent duration for all eNpHR-expressing cells. c) Traces (top) from a representative eNpHR-expressing neuron in an acute slice showing $GABA_AR$ currents recorded at different times after a photocurrent, on different trials. E_{GABAA} versus time after photocurrent is plotted (bottom) for this cell and the recovery is well fitted by a single-exponential function as in 'a'. d) Traces (top) from the same cell as in 'c' showing $GABA_AR$ currents recorded after photocurrents of different durations. The plot (bottom) shows the change in E_{GABAA} in this cell as a function of photocurrent duration.

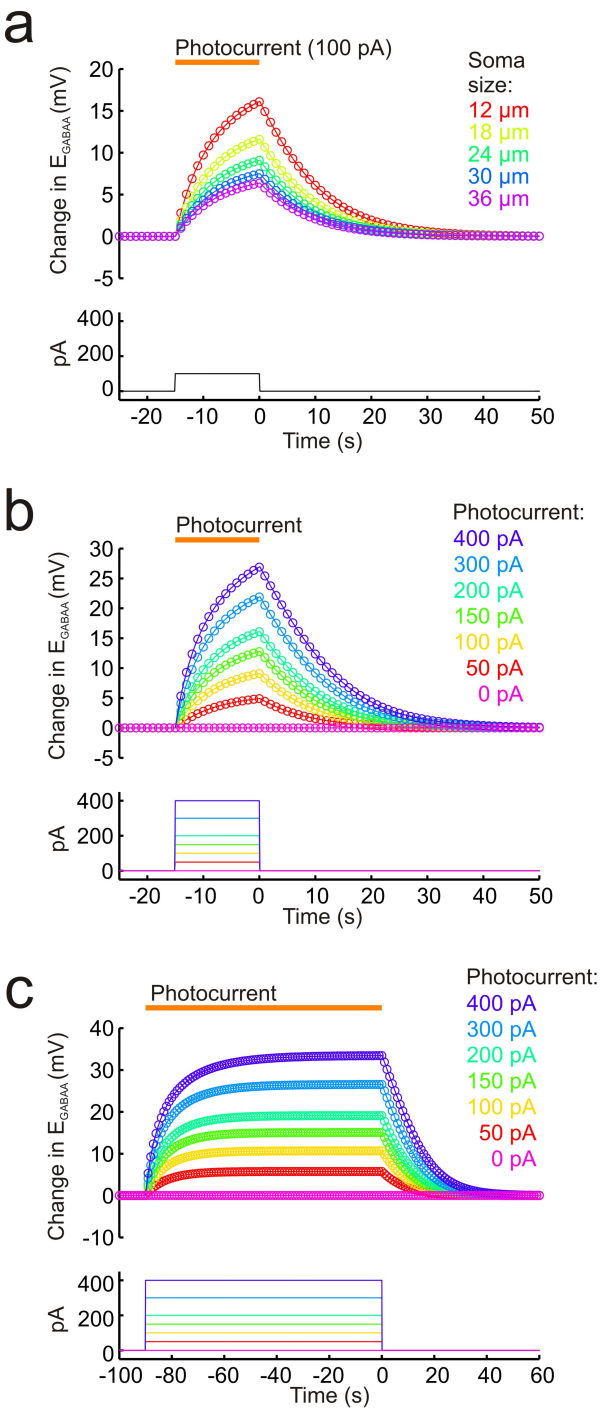
a
Photocurrent (100 pA)
Soma size:
12 µm
18 µm
24 µm
30 µm
36 µm
Change in E_{GABAA} (mV)
pA
Time (s)
b
Photocurrent
Photocurrent:
400 pA
300 pA
200 pA
150 pA
100 pA
50 pA
0 pA
Change in E_{GABAA} (mV)
pA
Time (s)
c
Photocurrent
Photocurrent:
400 pA
300 pA
200 pA
150 pA
100 pA
50 pA
0 pA
Change in E_{GABAA} (mV)
pA
Time (s)

fore laser-activation was 0.43 $\pm$ 0.04 and the equivalent measure was 0.45 $\pm$ 0.05 after laser-activation (n = 12 cells, P = 0.74, paired t test; Fig. 3.11b). The mean stimulus-evoked spike rate was also stable for Arch-expressing cells at 2.15 $\pm$ 0.2 Hz before laser-activation and 2.3 $\pm$ 0.3 Hz after laser-activation (P = 0.64, paired t test).

3.9 Discussion

In this chapter I have confirmed previous reports (Staley and Proctor, 1999; Jin et al., 2005) that strong activation of $GABA_A$Rs causes Cl^- influxes that are large enough to overwhelm a neurons ability to maintain stable Cl^- concentration gradients. In addition, consistent with prior findings (Staley and Proctor, 1999), I have demonstrated that dendrites, due to their smaller volume, are more susceptible to Cl^- loads than neuronal somata.

In these experiments, intense $GABA_A$R application was elicited by pharmacological activation of receptors with exogenous GABA. Such a manipulation would presumably activate both synaptic and extra-synaptic $GABA_A$Rs. In addition, $GABA_A$R activation would be expected to last over longer periods than might occur during physiological patterns of network activity. Finally, large Cl^- loads were generated by artificially increasing the driving force for $GABA_A$Rs by holding the neuronal membrane at depolarised voltages. During normal patterns of activity a similar process might enhance Cl^- accumulation. This would include any mechanism that depolarises the neuronal membrane coincident with

---

Figure 3.10 *(facing page)*: A single compartment model of Cl^- accumulation and extrusion predicted photocurrent induced changes in E_{GABAA}. a) A 100 pA Cl^- photocurrent was applied to somata of varying volumes for 15 s. Soma volume was modelled as a prolate spheroid (rugby ball), the soma width was held constant at 12 μm whilst soma length was varied between 12 and 36 μm. For all somata, E_{GABAA} was seen to increase steadily over the course of the modelled photocurrent and then gradually recovered when the photocurrent ended. A soma length of 24 μm resulted in E_{GABAA} shifting by 9.1 mV by the end of the 15 s photocurrent, which matched the size of shift demonstrated experimentally (see Fig. 3.7e). b) The photocurrent induced change in E_{GABAA} was proportional to the magnitude of the photocurrent induced. 15 s Cl^- photocurrents of varying size (between 0 and 400 pA) were applied to soma of 24 μm length (as in 'a'). Also note that E_{GABAA} recovered over the period of 20 to 40 s following termination of the photocurrent. c) Modelling photocurrents of 90 s in duration demonstrated that depolarising shifts in E_{GABAA} stabilise after approximately 40 s, at values dependent on the size of the induced photocurrent.

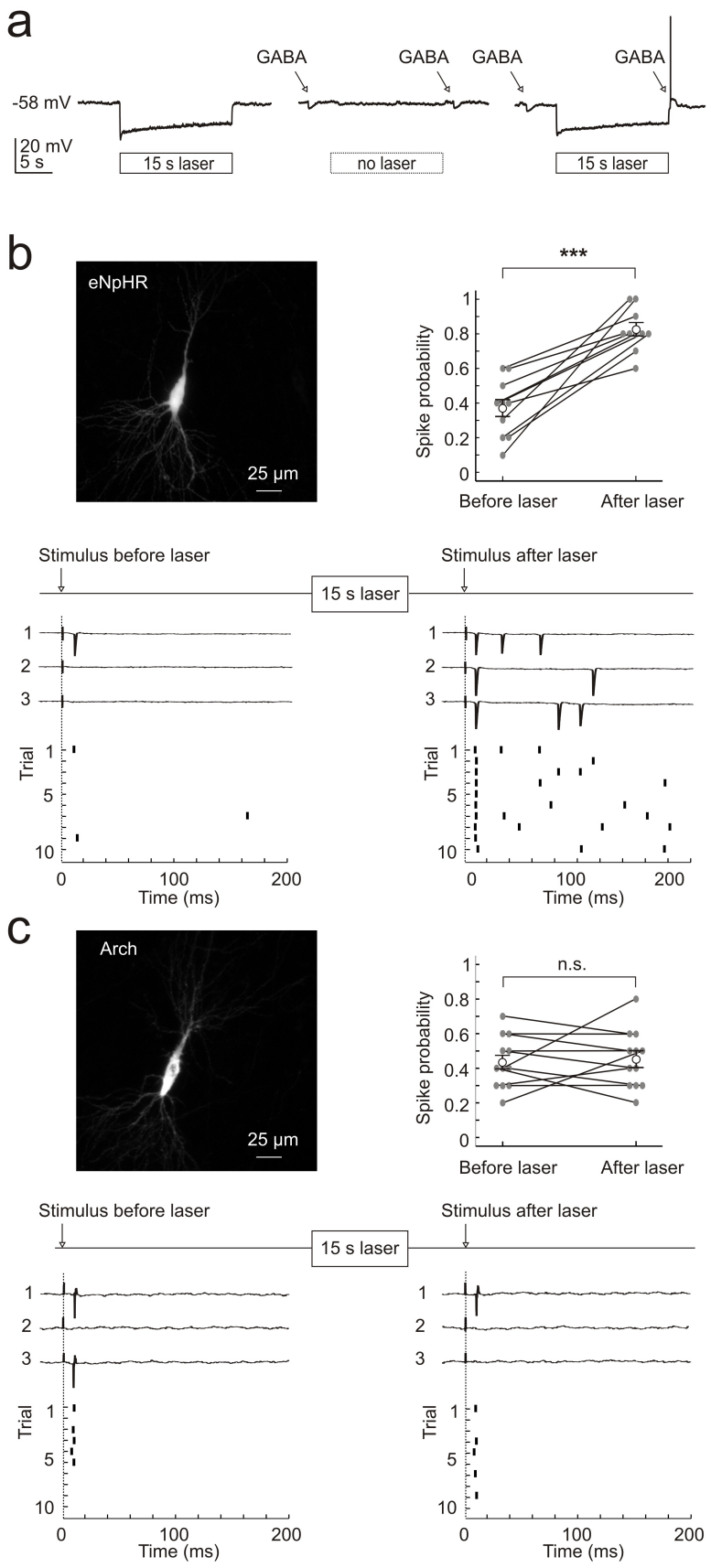
a
GABA
GABA
GABA
GABA
-58 mV
20 mV
5 s
15 s laser
no laser
15 s laser
b
eNpHR
25 µm
***
Spike probability
Before laser
After laser
Stimulus before laser
15 s laser
Stimulus after laser
Trial
Time (ms)
c
Arch
25 µm
n.s.
Spike probability
Before laser
After laser
Stimulus before laser
15 s laser
Stimulus after laser
Trial
Time (ms)

the arrival of GABAergic synaptic inputs, such as simultaneous glutamatergic activation or back-propagating action potentials. That said, previous work has demonstrated that $GABA_AR$ activation alone, without exogenously increasing the driving force for Cl^- influx by voltage clamp, is sufficient to cause considerable Cl^- accumulation (Staley and Soldo, 1995). This is ultimately because $GABA_ARs$ are permeable to HCO_3^- as well as Cl^-. Compared to E_{Cl^-}, the reversal for HCO_3^- ($E_{HCO_3^-}$) is considerably more positive (Lambert and Grover, 1995). This means that during strong activation of $GABA_ARs$, $E_{HCO_3^-}$ can provide the thermodynamic drive for continued Cl^- accumulation and a collapse in the Cl^- gradient. A corresponding collapse of the HCO_3^- gradient is prevented by the activity of intra- and extracellular carbonic anhydrases, which use CO_2 as a substrate to rapidly regenerate intracellular HCO_3^- (Rivera et al., 2005).

In this chapter I also described a model of a pyramidal cell with realistic Cl^- transport mechanisms and biologically relevant glutamatergic and GABAergic synaptic inputs. The model revealed a Cl^- accumulation-dependent change in spike timing, which is in keeping with previous reports using dialysis or computer models (Saraga et al., 2008; Valeeva et al., 2010), and has shown that modest shifts in E_{GABAA} affect the spiking behaviour of cells. Consistent with my experimental data, the model showed that the functional effects of Cl^- shifts were more likely to occur when GABAergic inputs were directed over the dendrites as opposed to the soma. This is because a given Cl^- load will result in a

---

Figure 3.11 *(facing page)*: Optogenetic silencing strategies differ in their effects on synaptically-evoked spiking activity. a) Perforated patch current clamp recording from a eNpHR-expressing neuron. Laser-activation (10.9 $mW.mm^{-2}$ laser for 15 s) evoked a sustained hyperpolarising response (left). In the absence of laser-activation, GABA puffs elicited hyperpolarising responses (middle). However, the same GABA puff generated a depolarising response and action potential when delivered 250 ms after laser-activation (right). b) Top left, confocal image of a CA3 pyramidal neuron expressing eNpHR3.0-EYFP ('eNpHR'). Bottom, cell-attached recordings from this cell showing synaptically-evoked spiking before (left) and after (right) eNpHR-activation (15 s, 532 nm, 7.9 $mW.mm^{-2}$). Spike probability was set to approximately 0.4 before laser-activation (measured over 10 trials). The before stimulus was delivered 1250 ms before laser onset and the after stimulus was delivered 250 ms after laser offset. Top right, summary of spike probability for eNpHR cells (n = 10; error bars, s.e.m.; $^{***}P < 0.001$). c) Top left, a CA3 pyramidal neuron expressing Arch-GFP ('Arch'). Bottom, cell-attached recordings from this cell showing synaptically-evoked spiking before (left) and after (right) Arch-activation (15 s, 532 nm, 76.1 mW mm-2). Top right, summary of spike probability for Arch cells (n = 12; n.s., non-significant, $P = 0.74$). All conventions as in 'b'.

larger change in $[Cl^-]_i$ and hence E_{GABAA} in a small compartment, as compared to a large cellular compartment.

In the latter half of this chapter I asked whether light-activated proteins that use ion fluxes can also impact $[Cl^-]_i$ and E_{GABAA}. I demonstrated that the two most popular optogenetic strategies for silencing neuronal activity differ in their effects on GABAergic transmission. Silencing neural activity with a Cl^- pump (eNpHR), but not a proton pump (Arch), altered GABAergic synaptic transmission beyond the period of silencing and in a manner that altered the subsequent excitability of the network. The effects upon E_{GABAA} were related to the size and duration of the eNpHR photocurrent. This is entirely consistent with what is known about eNpHRs ion selectivity. The fact that its photocurrents can be maintained in the face of intracellular Cl^- accumulation is presumably a function of its extremely negative reversal potential (approximately -400 mV) (Seki et al., 2007). Proton pumps meanwhile have been reported to generate modest changes in pH, which are rapidly stabilised (Chow et al., 2010) and appear to be tightly regulated by efficient buffering and transport mechanisms (Staley and Proctor, 1999; Chesler, 2003). My slice recordings establish an important difference between optical silencing strategies, which are directly relevant to ex vivo and in vitro experiments, and may be helpful in interpreting future in vivo experiments where it is more challenging to record directly from a silenced neuron and to dissect network effects. While the effect upon GABAergic inhibition is evident immediately after silencing, it remains to be seen whether this could influence processes that have their effect over a longer time scale (via mechanisms such as synaptic plasticity). The effects of eNpHR are consistent with reports of depolarizing shifts in the driving force for $GABA_A$Rs described in this chapter and elsewhere in the literature (Staley and Proctor, 1999; Jin et al., 2005). Finally, my observations confirm the use of eNpHR as a modulator of Cl^-, which will be invaluable in exploring the role of this ion in synaptic transmission, development and pathology.

Chapter 4

Intracellular chloride accumulation during network activity

4.1 Introduction

The previous chapter demonstrated how exogenous activation of $GABA_A$Rs is sufficient to cause Cl^- accumulation and a depolarization in the reversal potential for these receptors. It also investigated how the E_{GABAA} of different subcellular compartments might vary in response to a given Cl^- load.

In order to evoke the transient depolarising shifts in E_{GABAA} described above, strong $GABA_A$R activation was elicited by exogenous application of $GABA_A$R agonists. Published evidence that such short-term changes in E_{GABAA} might occur in vivo, and therefore represent a biologically relevant plasticity mechanism, have come from studies of hyper-active network activity patterns, such as those generated in experimental models of epilepsy. Several additional studies, using different in vitro models of epileptiform activity, have demonstrated a temporary excitatory shift in E_{GABAA} (Fujiwara-Tsukamoto, 2006; Fujiwara-Tsukamoto et al., 2003; Lamsa and Kaila, 1997; Lasztóczi et al., 2011; Perreault and Avoli, 1992).

In this Chapter I set out to confirm previous reports that epileptiform activity, at least in vitro, is associated with a transient shift in GABAergic signalling from being hyperpolarising and inhibitory, to becoming depolarising and excitatory. In order to investigate the mechanisms underlying this change I developed electrophysiological and imaging based

techniques to measure E_{GABAA} and intracellular Cl^- dynamics during epileptiform activity. Previous methods used to measure activity induced Cl^- fluxes have had several important limitations. Firstly, electrophysiological techniques have relied on evoked $GABA_AR$ currents to indirectly estimate Cl^- levels. As such, the contribution of endogenous activation of $GABA_ARs$ can not be investigated because pharmacological blockade of these receptors will preclude the measurement of subsequent $[Cl^-]_i$. Secondly, the massive synaptic bombardment that occurs during seizure activity also complicates attempts to calculate specific Cl^- mediated currents using electrophysiological methods. Thirdly, imaging based methods for measuring intracellular Cl^- are either unable to provide absolute measurements or suffer from substantial complications related to pH sensitivity (Bregestovski et al., 2009; Raimondo, Irkle, Wefelmeyer, Newey and Akerman, 2012). In this Chapter I present a new genetic reporter that is able to determine absolute intracellular concentrations of Cl^- and pH simultaneously in neurons. This reporter is an optimised version of ClopHensor (Arosio et al., 2010), which I have named ClopHensor2.

Using this and other tools, I have characterised seizure associated intracellular Cl^- changes in hippocampal neurons. I determined the mechanism behind observed increases of Cl^- and investigated whether various subcellular compartments (soma versus dendrites) differ in their response to seizure induced Cl^- accumulation.

4.2 Epileptiform activity induces a depolarising shift in GABAergic potentials

In the first set of experiments, I set out to address whether depolarising shifts in E_{GABAA} are a fundamental feature of epileptiform activity. Epileptiform activity was induced using three separate, well established, in vitro models of epilepsy; the '0 Mg^{2+}' model, the '4-AP' model and the 'spontaneous' model (see Fig. 4.1a). The '0 Mg^{2+}' model involves omission of Mg^{2+} from the brain slice perfusate. This removes the voltage dependent Mg^{2+} block on NMDA receptors, which predisposes hippocampal slices to periods of synchronised hyperexcitability (Anderson et al., 1986; Mody et al., 1987; Gutiérrez et al., 1999). These seizures lasted on average 205 $\pm$ 45 s, (n = 11). Seizures were elicited using the '4-AP' model by adding 50 μM 4-aminodpyridine (4-AP) to the bath solution

(Perreault and Avoli, 1992). 4-AP is a selective antagonist of the Kv1 (Shaker) family of voltage gated K^+ channels. Seizures produced in this manner had a mean duration of 222 $\pm$ 55 s, (n = 7). Lastly, hippocampal organotypic slice cultures that are allowed to mature for beyond a week are known to generate spontaneous seizures (Dyhrfjeld-Johnsen et al., 2010; Berdichevsky et al., 2011; Lillis et al., 2012). This hyperexcitability is presumably due to the enhanced connectivity that occurs with extended culture durations. These spontaneous seizures lasted on average 115 $\pm$ 30 s (n = 19).

In all cases, seizure onset was characterised by a pronounced membrane potential depolarisation upon which occurred high-frequency, low-amplitude discharges (see Fig. 4.1a). For analysis purposes the onset of the seizure was defined as the time at which the membrane potential depolarised beyond a 'threshold' set at 30 mV above the cells resting membrane potential ('baseline'). The end of the seizure was defined as the point at which the membrane potential returned to baseline for the first time after the start of the seizure. Beyond this point however, numerous after-discharges were often observed. These are rhythmic bursts of activity, which occur from a relatively hyperpolarised membrane potential.

Recordings from pyramidal neurons in the CA3 region of organotypic hippocampal slice cultures were made using the perforating agent gramicidin, which preserves intracellular Cl^- concentration (see Materials and Methods). Membrane potential was measured in current clamp mode and $GABA_AR$ potentials evoked by delivering short puffs of GABA (100 μM) every 10 s in the presence of $GABA_BR$ blockade (CGP55845, 5 μM). $GABA_AR$ potentials were defined as the maximum GABA induced membrane potential deviation (excluding triggered action potentials), caused by the puffs. As demonstrated in Fig. 4.1, prior to seizure onset $GABA_AR$ potentials were hyperpolarising (-78.65 $\pm$ 1.799 mV, in the '0 Mg^{2+}' model, -74.25 mV $\pm$ 2.667 for the '4-AP' model and -77.10 $\pm$ 2.586 mV for spontaneously generated seizures). However, in all three seizure models, after seizure onset and for a substantial period following seizure offset, GABA became markedly depolarising in nature. Indeed, as depicted in Fig. 4.1b, during the seizure period GABA application could independently generate action potentials indicating that the $GABA_AR$ reversal potential exceeded the action potential threshold. Immediately following the seizure GABAergic potentials were markedly depolarising (-58.83 $\pm$ 1.427 mV

for '0 Mg^{2+}' seizures, -53.16 $\pm$ 2.830 mV utilising the '4-AP' model and -61.05 $\pm$ 2.292 mV for spontaneous seizures). This depolarising shift in $GABA_AR$ potentials was highly significant with $P < 0.0001$ for the '0 Mg^{2+} and 'spontaneous' conditions, and $P = 0.003$ for the '4-AP' seizure model (paired *t* tests, Fig. 4.1c). This change was temporary as GABAergic potentials gradually returned to baseline values within 5 minutes following the end of the seizure. Recovery potentials for '0 Mg^{2+}' seizures were -77.71 $\pm$ 1.352 mV, -68.90 $\pm$ 3.692 mV for '4-AP' seizures and -77.06 $\pm$ 2.195 mV for spontaneously generated seizures. As evidence of full recovery, there was no significant difference between pre-seizure and recovery GABAergic potentials for the three seizure models ($P = 0.5030$, $P = 0.2163$ and $P = 0.9657$, paired *t* test).

4.3 Epileptiform activity causes a depolarizing shift in the reversal potential for $GABA_AR$ receptors

The evoked GABA potentials are a function of g_{GABAA}, E_{GABAA} and the underlying resting membrane potential at the time the $GABA_ARs$ are activated. As a result, a change in measured GABA potential could be generated by changes in any of these three variables. Therefore, to better investigate the mechanisms underlying the seizure-associated alteration in $GABA_AR$ signalling, I performed a separate series of experiments to directly

---

Figure 4.1 *(facing page)*: Epileptiform activity induces a depolarising shift in GABAergic potentials. Three in vitro models of epilepsy were utilised. The '0 Mg^{2+}' model (left), the '4-AP' model (centre) and the 'spontaneous' model (right). Perforated patch recordings were made from CA3 pyramidal neurons and $GABA_AR$-mediated potentials elicited every 10 s before, during, and after a seizure episode by delivering a puff of GABA (100 μM) via a patch pipette positioned over the cell soma. a) In current clamp mode the membrane potential of CA3 pyramidal cells were recorded (black trace). The value of $GABA_AR$ potentials were defined as the maximum GABA induced membrane potential deviation (excluding triggered action potentials), caused by the GABA puff (green circles). Note how $GABA_AR$ potentials become depolarising following seizure onset and gradually recover to baseline following seizure offset. b) Representative GABA potentials corresponding to the grey bars in 'a'. In all three seizure models, $GABA_AR$ potentials are hyperpolarising before seizure onset but become markedly depolarising by the time of seizure offset (defined as the first time the membrane potential returns to baseline after the start of the seizure). In many cases the depolarising GABA potentials were sufficient to generate action potentials. c) Population data demonstrates this depolarising shift in $GABA_AR$ potential and its subsequent recovery (**$P < 0.01$, ***$P < 0.001$, paired *t* test).

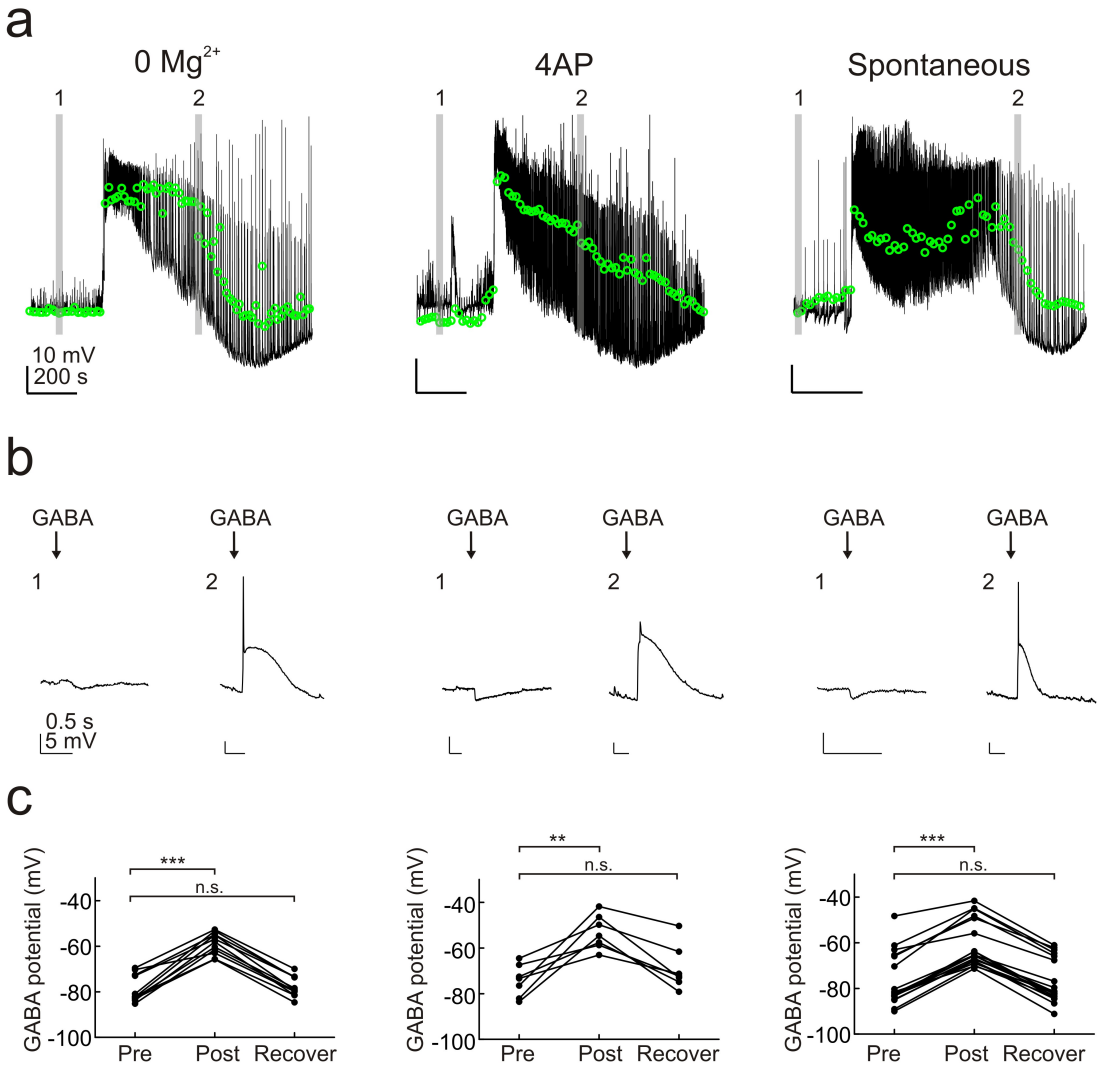
a
0 Mg2+
4AP
Spontaneous
1
2
10 mV
200 s
b
GABA
0.5 s
5 mV
c
GABA potential (mV)
-40
-60
-80
-100
***
n.s.
**
Pre
Post
Recover

measure E_{GABAA} prior to, and immediately following, seizure activity. By rapidly switching from current-clamp to voltage-clamp mode during gramicidin recordings, E_{GABAA} could be calculated using voltage ramp protocols. As shown in Fig. 4.2 seizure activity produced a pronounced shift in E_{GABAA}. Population data presented in Fig. 4.2d demonstrate that in the first 20 s following the end of recorded seizures (mean duration 81.56 $\pm$ 20.22 s), there was a highly significant positive shift in E_{GABAA}, 47.29 $\pm$ 2.092 mV, $P < 0.0001$. Within 80 - 100 s, E_{GABAA} recovered to baseline levels (P = 0.8685 as compared to pre-seizure levels, *t* test).

4.4 Seizure induced depolarising shifts in $GABA_AR$ responses differ between subcellular compartments

In the previous chapter I showed experimentally and with computer models that cell compartments differ in their susceptibility to Cl^- accumulation. This work showed that for a given Cl^- load, small volume compartments experienced a greater shift in $[Cl^-]_i$ and E_{GABAA} than larger volume compartments. In order to investigate whether seizure induced shifts in $GABA_AR$ potentials might differ between subcellular compartments, a similar experiment to that described in Section 4.2 was performed. Whereas previously

---

Figure 4.2 *(facing page)*: Epileptiform activity causes a depolarising shift in E_{GABAA}. a) A recording in which E_{GABAA} was measured prior to and immediately following seizure activity. Dashed boxes indicate example E_{GABAA} measurements before the seizure (1), shortly after the seizure terminated (2) and (3), and later following recovery (4). E_{GABAA} values are represented by the circles. To measure E_{GABAA} without contamination from ongoing spiking activity, TTX was applied roughly 2 min after seizure onset (horizontal black bar). b) E_{GABAA} was measured by rapidly switching the recording mode from current-clamp (CC) to voltage-clamp and then applying two consecutive voltage ramps, the first under baseline conditions (black line; - GABA) and the second during activation of $GABA_AR$s (grey line; + GABA). After 2 s in voltage-clamp the cell was returned to current-clamp. E_{GABAA} measurements were made every 10 s. c) IV plots for measurements for the four the time points represented by the boxes in 'a'. E_{GABAA} was defined as the voltage at which the holding current (generated by the first ramp; black line) and the total current (reflecting the holding current plus the current through the activated $GABA_AR$s; grey line) intersected. Note that E_{GABAA} was at hyperpolarised values prior to the seizure (1), switched to depolarising values during the seizure (2) and (3), before recovering to pre-seizure values afterwards (4). d) Summary of the change in E_{GABAA} relative to the baseline recorded before seizure activity commenced. Within 80-100 s following seizure offset, E_{GABAA} values had returned to baseline levels.

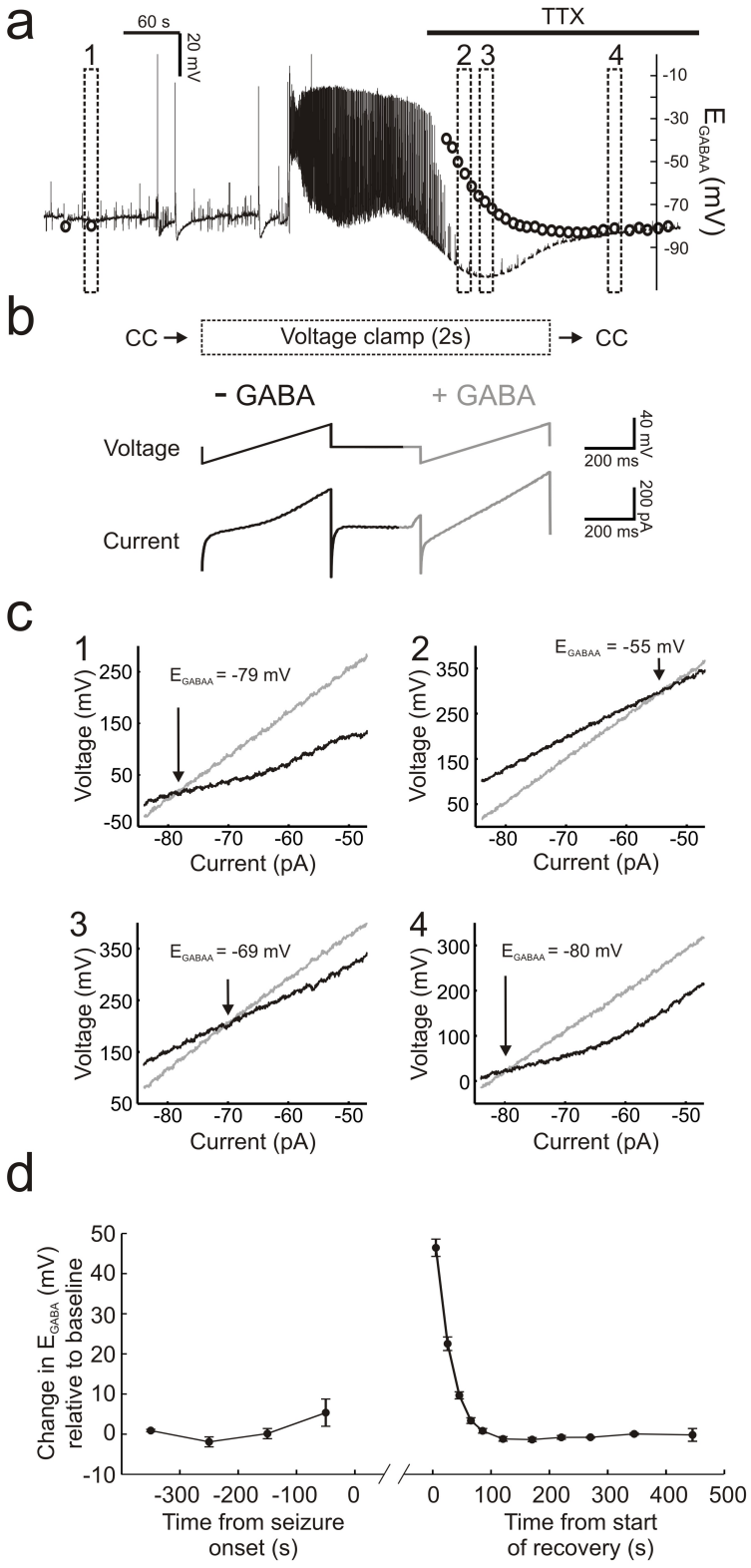
a
60 s
20 mV
TTX
1
2 3
4
-10
-30
-50
-70
-90
E GABAA (mV)
b
CC
Voltage clamp (2s)
CC
- GABA
+ GABA
Voltage
Current
40 mV
200 ms
200 pA
200 ms
c
1
E GABAA = -79 mV
2
E GABAA = -55 mV
3
E GABAA = -69 mV
4
E GABAA = -80 mV
Voltage (mV)
Current (pA)
d
Change in E GABA (mV) relative to baseline
Time from seizure onset (s)
Time from start of recovery (s)

a single, soma-directed, GABA puffer pipette was used, in this version of the experiment two GABA puffer pipettes were utilised simultaneously. The first puffed GABA onto the soma and the second puffed GABA onto the apical dendrites (approximately 150 μm from the soma). This arrangement allowed $GABA_AR$ potentials to be elicited every 5 s at alternating subcellular locations before, during and following epileptiform activity.

Evoked $GABA_AR$ potentials were typically hyperpolarising at both somatic and dendritic locations prior to seizure onset. As demonstrated in Fig. 4.3, the seizure induced depolarising shift was actually larger for $GABA_AR$ potentials elicited over the soma, as compared to the dendrites. In an effort to prevent potential errors introduced by the puffer pipettes evoking different sized conductances, a steady hyperpolarising current was sometimes applied to ensure that pre-seizure GABA potentials were also depolarising. This allowed pre-seizure GABA potentials to be matched in size by adjusting the position of the puffer pipettes as in Fig. 4.3b. Once again, a difference between somatic and dendritic GABA potentials in the post-seizure period could be observed (Fig. 4.3b). Population data employing only those cases where dendritic pre-seizure GABA potentials were larger than their somatic counterparts confirmed that the seizure induced depolarising shift was greater in amplitude when GABA potentials were evoked over the soma (see Fig. 4.3c). The difference between somatic and dendritic GABA potentials during the 30 s prior to seizure onset was -2.569 $\pm$ 0.4789 mV but following the end of the seizure the difference between soma and dendrites had moved to 4.326 $\pm$ 1.667 mV. This represented a statistically significantly difference ($P < 0.0001$, *t* test).

Figure 4.3 *(facing page)*: Seizure induced depolarising shifts in $GABA_AR$ potentials differ between subcellular compartments. a) An example of a spontaneous seizure recorded from a CA3 pyramidal neuron. GABA potentials were elicited every 5 seconds by puffing GABA (100 μM) either over the soma (blue) or apical dendrites (red). Whilst somatic and dendritic $GABA_AR$ potentials were hyperpolarising preceding the onset of epileptiform activity (1), immediately following a seizure somatic $GABA_AR$ potentials became comparatively more positive than their dendritic counterparts (2). b) Somatic current injection via the recording pipette was used to ensure that pre-seizure $GABA_AR$ potentials were matched (3). Again, following the seizure, GABA potentials evoked at the soma were more depolarised then those at the dendrites (4). c) Population data based only on cases where dendritic pre-seizure $GABA_AR$ potentials were larger than their somatic counterparts. Post seizure, the somatic GABA response was significantly more depolarised than the dendritic GABA response ($^*P < 0.05$, *t* test). This difference between the compartments disappeared within 3 minutes following the end of the seizures.

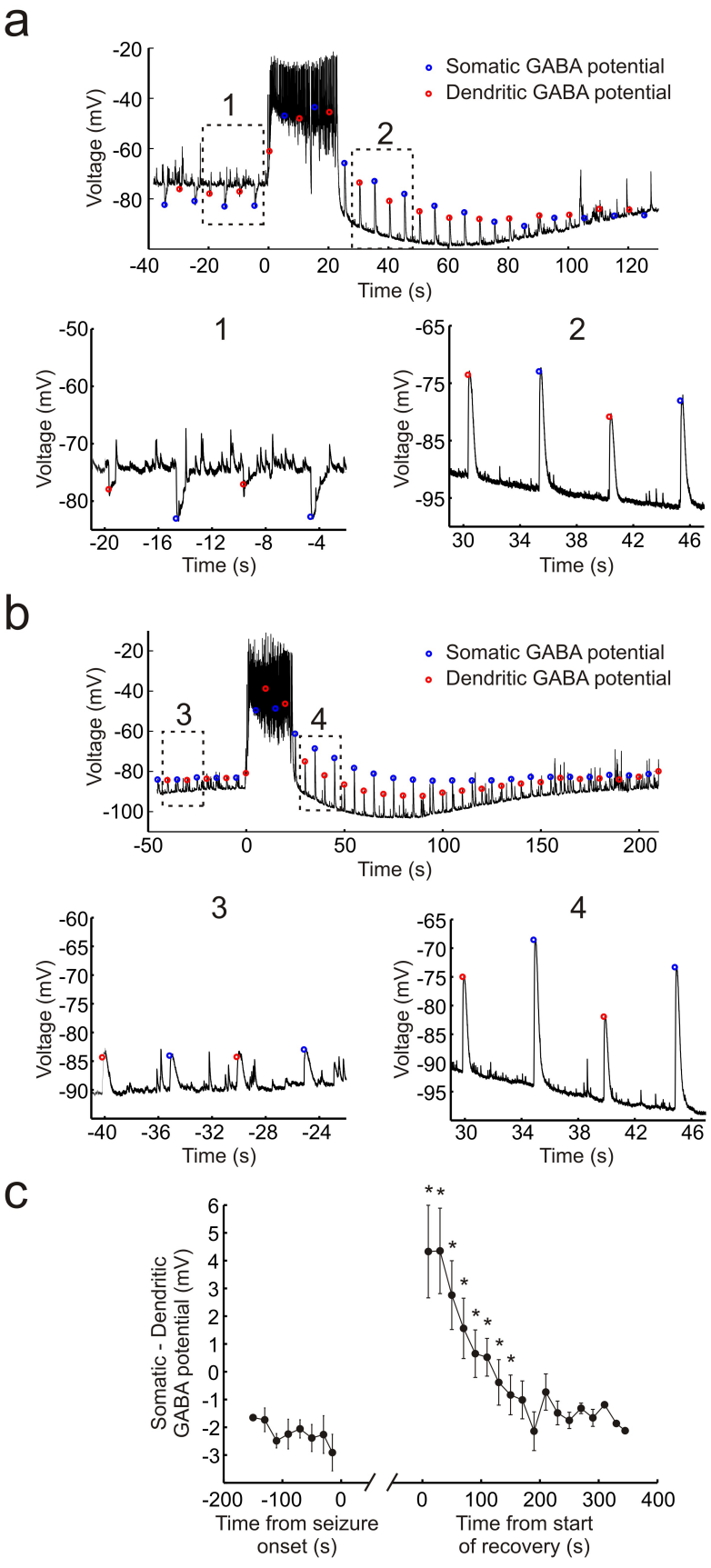
a
Somatic GABA potential
Dendritic GABA potential
Voltage (mV)
Time (s)
1
2
b
3
4
c
Somatic - Dendritic GABA potential (mV)
Time from seizure onset (s)
Time from start of recovery (s)

To further probe subcellular compartment differences in how E_{GABAA} might fluctuate in response to epileptiform activity, a similar experiment to that described in Section 4.3 was performed. As in Section 4.4, two puffer pipettes were used; one placed over the soma and another over the dendrites (approximately 150 μ from the soma). By rapidly switching from current-clamp to voltage-clamp mode, and by puffing GABA at two separate locations along the somatodendritic axis, E_{GABAA} could be calculated dynamically at both somatic and dendritic locations. Fig. 4.4 demonstrates that the activity induced depolarising shift in E_{GABAA} described in Section 4.3 was actually more pronounced in the somatic as compared to the dendritic compartment of CA3 hippocampal pyramidal cells. Although both compartments experienced a substantial depolarising shift in E_{GABAA} (Fig. 4.4d,e), the E_{GABAA} change in the first 20 s following seizure activity was 47.62 $\pm$ 2.16 mV over the soma but 34.07 $\pm$ 2.93 mV over the dendrites. This represented a statistically significant difference (P = 0.0007, t test).

In summary, the combination of current-clamp and voltage-clamp recordings show that during seizure activity, E_{GABAA} tends to move more depolarising in the soma than the dendrites. This is counter to the observations made in the previous chapter.

Figure 4.4 *(facing page)*: Compartment specific differences in seizure induced E_{GABAA} shifts. a) A recording in which somatic and dendritic E_{GABAA} were measured during seizure activity. Dashed boxes indicate example E_{GABAA} measurements before the seizure (t1), shortly after the seizure (t2), and later following recovery (t3). Somatic E_{GABAA} values are represented by the blue circles whilst dendritic E_{GABAA} is marked by the red circles. Note that directly following the seizure, somatic E_{GABAA} is more depolarised than dendritic E_{GABAA}. To measure E_{GABAA} without contamination from ongoing spiking activity, TTX was applied about 2 min after seizure onset (horizontal black bar). b) As in Fig. 4.2, E_{GABAA} was measured by rapidly switching the recording mode from current-clamp (CC) to voltage-clamp and then applying two consecutive voltage ramps, the first under baseline conditions (black line; - GABA) and the second during activation of $GABA_A$Rs (grey line; + GABA) either on the soma or on the apical dendrites (approximately 150 μm from the soma). After 2 s in voltage-clamp the cell was returned to current-clamp. E_{GABAA} measurements were made every 10 s. c) IV plots for somatic (top) and dendritic (bottom) measurements for the three time points represented by the boxes in 'a'. E_{GABAA} was defined as the voltage at which the holding current (generated by the first ramp; black line) and the total current (reflecting the holding current plus the current through the activated $GABA_A$Rs; grey line) intersected. Note that both somatic and dendritic E_{GABAA} were at hyperpolarised values before the seizure (t1), switched to depolarising values during the seizure (t2), and recovered to preseizure values (t3). d) and e) Population data depicting a small but significant difference in the seizure induced positive shift in E_{GABAA} between somatic and dendritic compartments. ($^*P < 0.05$, t test).

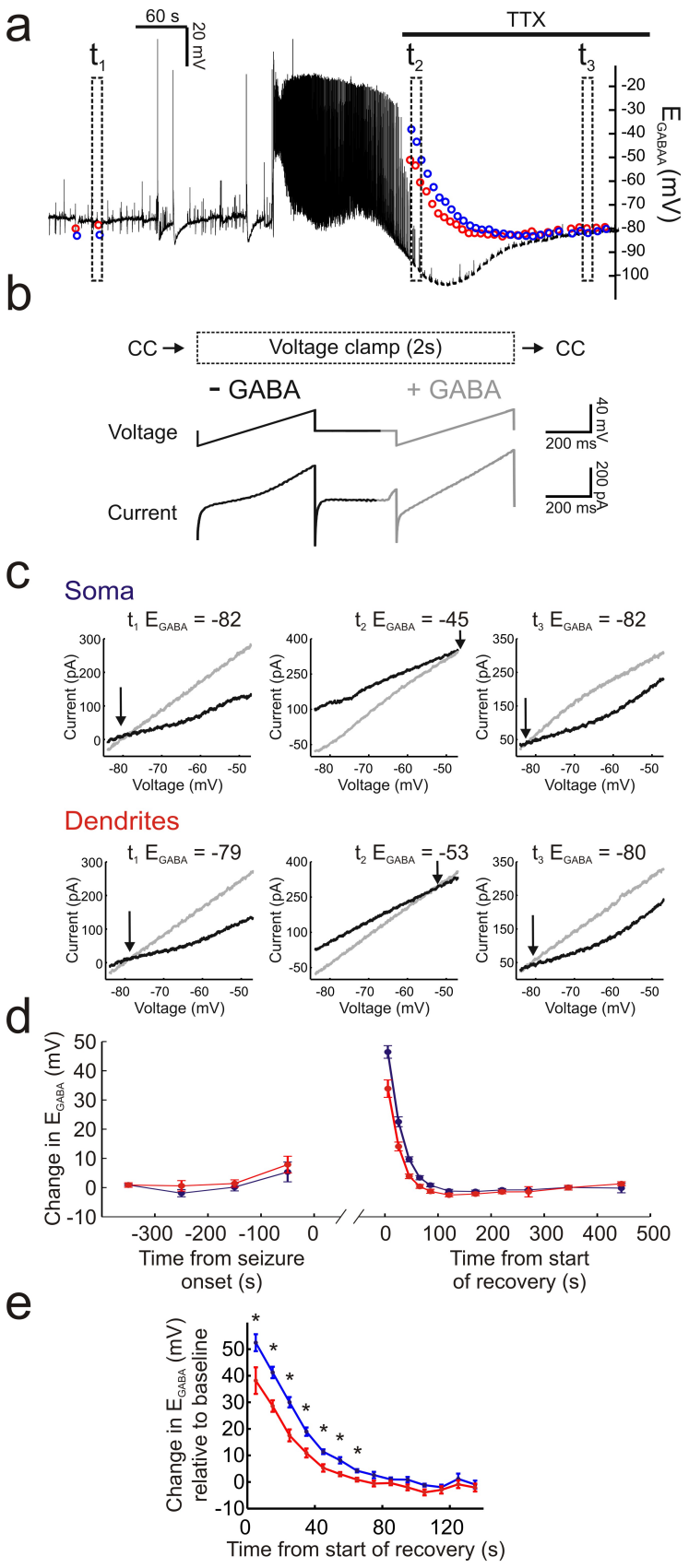
a
60 s
20 mV
TTX
t1
t2
t3
-20
-30
-40
-50
-60
-70
-80
-90
-100
EGABAA (mV)
b
CC
Voltage clamp (2s)
CC
- GABA
+ GABA
Voltage
Current
40 mV
200 ms
200 pA
200 ms
c
Soma
t1 EGABA = -82
t2 EGABA = -45
t3 EGABA = -82
Current (pA)
Voltage (mV)
Dendrites
t1 EGABA = -79
t2 EGABA = -53
t3 EGABA = -80
d
Change in EGABA (mV)
Time from seizure onset (s)
Time from start of recovery (s)
e
Change in EGABA (mV) relative to baseline
Time from start of recovery (s)

4.5 Detecting Cl^- accumulation during epileptiform activity using the Cl^- sensitive dye MQAE

The previous electrophysiological techniques (gramicidin perforated patch and exogenous GABA application) made it possible to measure changes in Cl^- dependent parameters (e.g. GABA potentials or E_{GABAA}) before and after seizure activity. These techniques have several limitations including the fact that they do not measure Cl^- changes directly and they provide limited access to different cellular compartments. For these reasons I was keen to establish an imaging based method to report Cl^- concentration.

The first imaging technique I adopted involved the use of N-(6-methoxyquinolyl)-acetoethyl ester (MQAE) a quinolinium-based Cl^- sensitive dye. This dye is membrane permeable and was loaded into pyramidal neurons by incubating organotypic hippocampal slices in 6 μM MQAE for 10 minutes. MQAE is suitable for use with 2-photon microscopy (Marandi et al., 2002), where its fluorescence has been shown to be Cl^-, but not HCO_3^- sensitive (Koncz and Daugirdas, 1994). Due to the relatively poor signal to noise properties of the dye, it was necessary to average fluorescence signal from multiple cells at a time. And during the recordings a single neuron was whole cell patched in order to provide simultaneous readout seizure activity. As demonstrated in Fig. 4.5a, average MQAE fluorescence signal from the CA3 pyramidal layer quenched during a seizure episode, which reflects an increase in intracellular Cl^-. Between 25 s and 35 s after the onset of epileptiform activity, MQAE fluorescence normalised to baseline fluorescence decreased by 1.77 $\pm$ 0.14 percent (n = 32 seizures, $P < 0.0001$, *t* test).

In an attempt to measure MQAE fluorescence signal over the dendrites, regions of interest were selected that were outside the pyramidal cell layer and presumably over the dendrites of the pyramidal neurons (mean distance was 72.82 $\pm$ 4.26 μm, Fig. 4.5b and c). The mean MQAE fluorescence normalised to baseline fluorescence for these 'dendritic' regions decreased by just 0.4385 $\pm$ 0.07 percent during seizure activity (Fig. 4.5c). This was statistically different to the change measured directly over the pyramidal cell bodies ($P < 0.0001$, *t* test). An important caveat however, is that MQAE is known to rapidly leak out of cells (Koncz and Daugirdas, 1994; Marandi et al., 2002). In addition, as Fig. 4.5a and b demonstrate, I could not resolve dendrites in these images and therefore

the exact source of the signal measured in the 'dendritic' regions of interest is uncertain.

4.6 Seizure associated Cl^- accumulation is mediated by $GABA_A$Rs

An advantage of imaging based techniques to detect intracellular Cl^- changes, as opposed to electrophysiological methods which rely on current flow through activated $GABA_A$Rs, is that $GABA_A$Rs can be pharmacologically blocked without interfering with Cl^- estimation. It was hypothesised that the seizure induced Cl^- accumulation described above is mediated by Cl^- influx across $GABA_A$Rs during the intense synaptic activity and membrane depolarisation that accompanies seizure episodes. In order to test this, I evoked seizures with a combination of 0 Mg^{2+} aCSF and 20 μM gabazine, which blocks $GABA_A$Rs. As is evident in Fig. 4.6c, seizure episodes triggered in this manner were significantly shorter (30.78 $\pm$ 3.77 s) than controls (49.13 $\pm$ 5.38 s), P = 0.032, t test. Nevertheless, the gabazine completely abolished the MQAE fluorescence change associated with control seizures in 0 Mg^{2+} (Fig. 4.6). Between 25 and 35 s post seizure onset the mean MQAE fluorescence normalised to baseline fluorescence was -0.3322 $\pm$ 0.064 (n = 15 seizures), as compared to 1.77 $\pm$ 0.14 percent in controls. This difference was statistically significant ($P < 0.0001$, t test) and consistent with the conclusion that $GABA_A$Rs mediate Cl^- influx during seizure activity.

4.7 ClopHensor2: a genetically encoded Cl^- and pH sensor optimised for neurons

MQAE is probably the most promising synthetic Cl^- sensitive dye. However, it is associated with a number of significant limitations. Firstly, the dye is moderately toxic, bleaches rapidly and experiences significant cell leakage (Bregestovski et al., 2009). In addition, it does not report Cl^- ratiometrically, which means that fluorescence is susceptible to measurement artefacts caused by variations in excitation path length, indicator concentration, illumination stability, cell thickness, and indicator distribution.

Genetically encoded Cl^- indicators based on mutations of the inherently Cl^- sensitive green fluorescent protein (GFP) offer the potential to overcome many of these issues

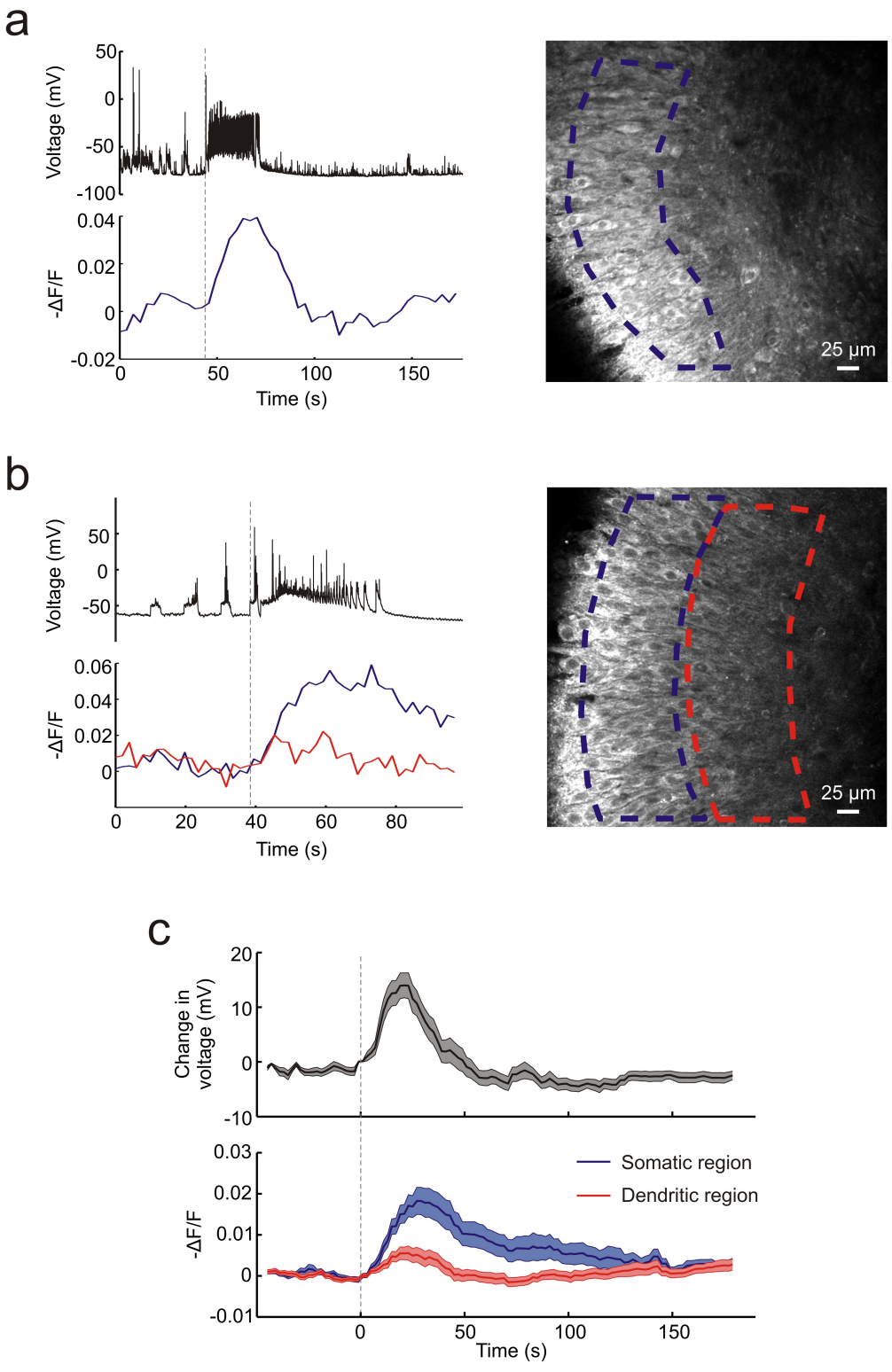
a
Voltage (mV)
50
0
-50
-100
-ΔF/F
0.04
0.02
0
-0.02
0
50
100
150
Time (s)
25 µm
b
Voltage (mV)
50
0
-50
-ΔF/F
0.06
0.04
0.02
0
0
20
40
60
80
Time (s)
25 µm
c
Change in voltage (mV)
20
10
0
-10
-ΔF/F
0.03
0.02
0.01
0
-0.01
Somatic region
Dendritic region
0
50
100
150
Time (s)

in addition to providing specific genetic localisation to particular cell-types or subcellular compartments. The most popular and widely used genetically encoded Cl^- indicators are based on fusions of two GFP mutants, yellow fluorescent protein (YFP) and cyan fluorescent protein (CFP), a commonly used fluorescence resonance energy transfer (FRET) donor for YFP. Whereas YFP emission is reduced by Cl^- binding, CFP fluorescence is relatively unaffected. These fusion proteins are therefore useful as ratiometric reporters of intracellular Cl^- concentration. Reporters in this class include 'Clomeleon' (Kuner and Augustine, 2000) and 'Cl-sensor' (Markova et al., 2008). Unfortunately, YFP fluorescence is quenched by both Cl and H^+ ions. As a result these YFP fusion proteins are sensitive to both intracellular pH and Cl^- concentration (Jayaraman et al., 2000). This dual sensitivity complicates the interpretation of in vivo measurements using these probes, particularly as neuronal processes often involve either the related, or independent, flux of both Cl^- and H^+ ions (Tabb et al., 1992; Doyon et al., 2011).

Recently Arosio et al. (2010) engineered a novel fusion protein capable of independently and simultaneously measuring Cl^- and pH. Named 'ClopHensor', this reporter is based on the fusion of a well described pH and Cl^- sensitive GFP mutant E^2GFP with the pH and Cl^- insensitive monomer DsRed (Fig. 4.7b). The uniform expression of both E^2GFP and DsRed is critical to ClopHensor's function as a ratiometric reporter of these two ions. The original characterisation of ClopHensor was conducted in heterologous non-neuronal cells. In order to test whether ClopHensor could be used to measure Cl^- and H^+ concentrations in neurons I biolistically transfected hippocampal slices with

---

Figure 4.5 *(facing page)*: Detecting Cl^- accumulation during epileptiform activity using the Cl^- sensitive dye MQAE. a) Right, an organotypic hippocampal slice was bulk loaded with 6 μM MQAE for 10 minutes and resulted in bright staining of neurons when imaged by 2-photon microscopy. Left and top, a whole cell patch clamp recording of a nearby pyramidal neuron provides a readout of 0 Mg^{2+} induced seizure activity. Left and bottom, MQAE fluorescence averaged from the somatic region of pyramidal cells as indicated by the dashed blue line. Note how the MQAE fluorescence is quenched (shown here as an increase in $-\Delta F/F$) during seizure activity indicating an increase in intracellular $[Cl^-]_i$. b) Same conventions as in 'a', but with a second region of interest over the dendrites of pyramidal neurons (red trace and red dashed line). Note how the MQAE fluorescence change for the 'dendritic' region is smaller than that over the cell somata (blue trace and blue dashed line). c) Population data depicting a seizure associated change in MQAE fluorescence, which is more pronounced over somatic regions (blue) as opposed to the putatively dendritic regions (red). The shaded areas indicate s.e.m.

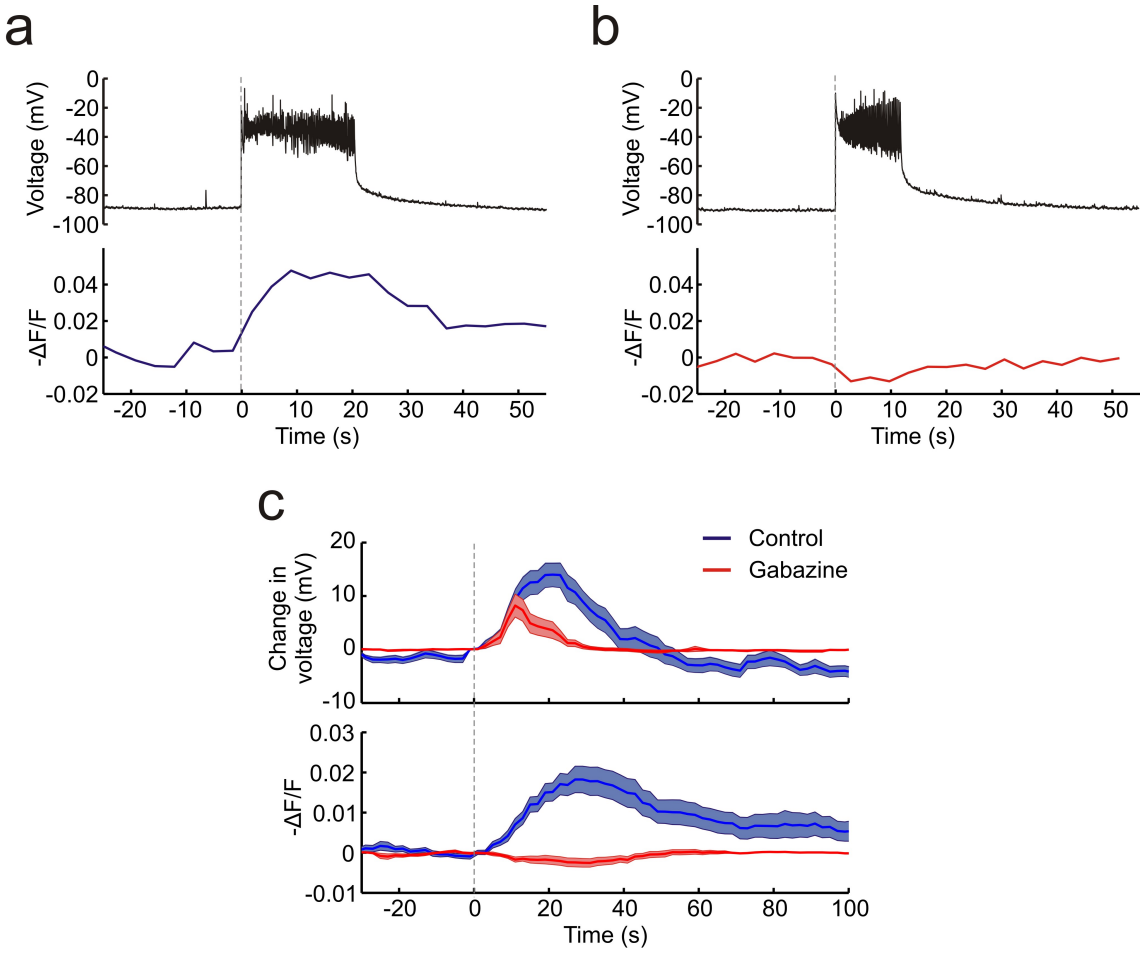

Figure 4.6: Seizure associated Cl^- accumulation is mediated by $GABA_A$Rs. a) Top, a whole cell patch of a pyramidal neuron in current clamp mode provided a read out of seizure activity. Bottom, simultaneous MQAE fluorescence signal change from a region of interest that included multiple CA3 neuronal cell bodies normalised to baseline fluorescence. Epileptiform activity was evoked using 0 Mg^{2+} aCSF. Seizure onset was correlated with a decrease in MQAE fluorescence or a positive shift in -ΔF/F, which reflects an increase in intracellular Cl^-. b) Recordings from the same slice as in 'a' but with bath application of 20 μM gabazine. In this case epileptiform activity was not associated with an increase in -ΔF/F. c) Population data demonstrates that 20 μM gabazine prevents the seizure associated increase in -ΔF/F ($P < 0.0001$, t test).

ClopHensor expressing plasmids. As depicted in Fig. 4.7a, expression of this construct in neurons resulted in uniform E^2GFP expression but highly heterogeneous and aggregated DsRed expression. This is consistent with previous reports that DsRed is susceptible to aggregation issues particularly within fusion proteins (Shaner et al., 2005).

In an attempt to address this issue I designed two new fusion proteins where the DsRed monomer in the original ClopHensor was replaced with either mCherry or tandem dimer tomato (tdTomato), Fig. 4.7d and f. The 22 amino acid linker from the original ClopHensor was maintained in both new constructs. The new fusion proteins were expressed using a different plasmid which included a combination of the cytomegalovirus early enhancer element and chicken beta-actin promoter (CAG promoter) and employed a human beta globin (HBG) poly-adenylation termination sequence. Interestingly, the E^2GFP-mCherry fusion suffered from similar (albeit reduced) aggregation issues as the original ClopHensor (Fig. 4.7c). In contrast, the E^2GFP-tdTomato fusion protein expressed uniformly with no visible difference in localisation between E^2GFP and tdTomato (Fig. 4.7e). This uniform expression in neurons suggests that this construct will afford ratiometric reporting of Cl^- and H^+. We have named this new fusion protein ClopHensor2.

4.8 Calibrating ClopHensor2 confirms independent pH and Cl^- sensitivity

As demonstrated in Fig. 4.7 and Fig. 4.8a, ClopHensor2 showed robust expression in primary hippocampal neurons following biolistic transfection. I then assessed the ability of ClopHensor2 to independently report steady-state Cl^- and pH. The reporter was used as a ratiometric indicator of Cl^- and pH by excitation. The protein was excited sequentially via single-photon excitation at 458, 488 and 594 nm using a confocal microscope. Emission was collected between 500 and 550 nm by a single photomultiplier tube (PMT) for excitation at 458 and 488 nm, and between 650 and 700 nm by a second PMT during excitation at 594 nm. Calibration was performed by systematically varying extracellular Cl^- and pH in the presence of proton and Cl^- permeable ionophores known to equilibrate intra- and extracellular concentrations of these two ions (see Materials and Methods). The excitation spectrum of E^2GFP possesses a pH isobestic point at 458 nm (Arosio et al.,

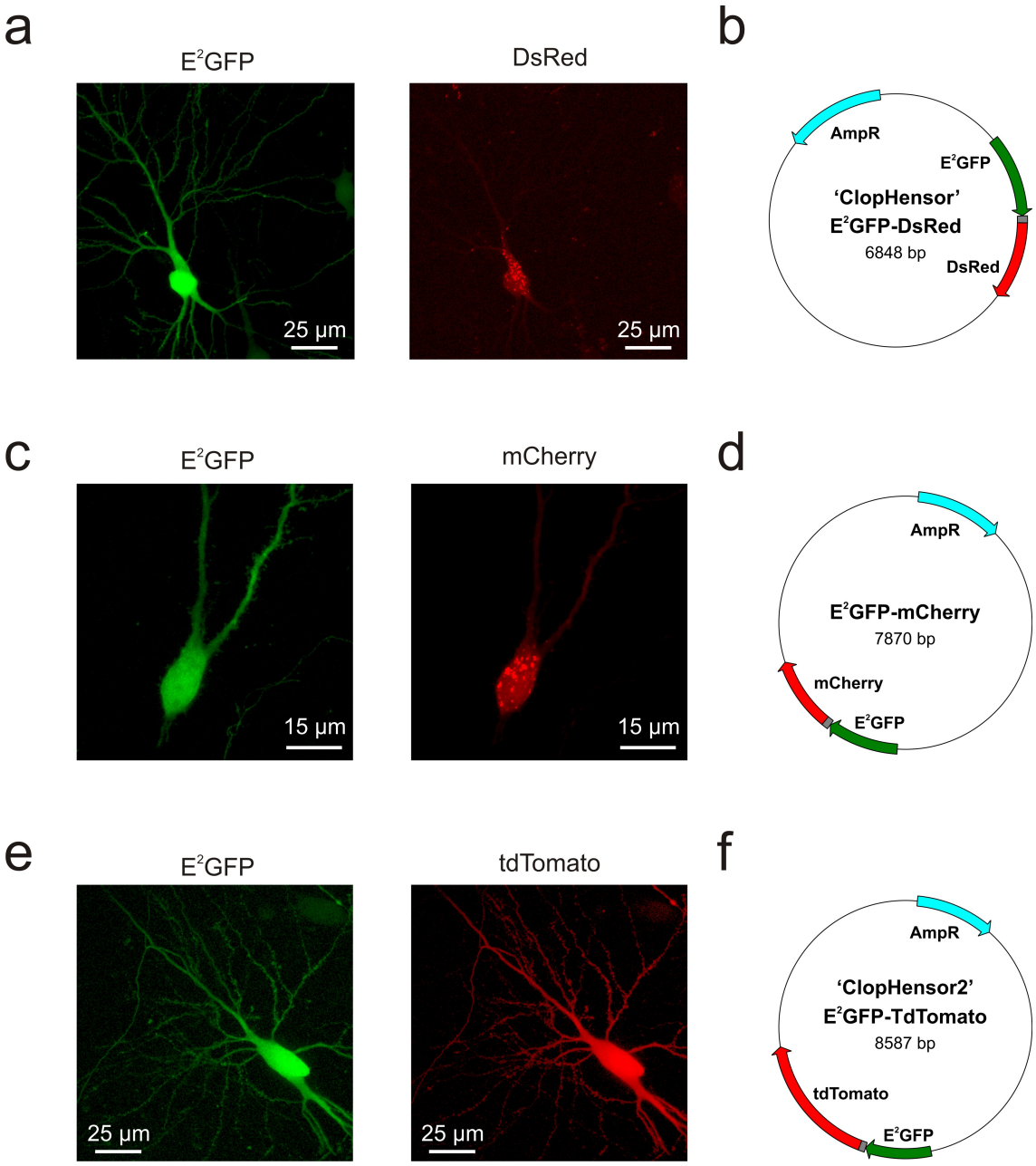
a
E²GFP
DsRed
25 µm
25 µm
b
AmpR
E²GFP
'ClopHensor'
E²GFP-DsRed
6848 bp
DsRed
c
E²GFP
mCherry
15 µm
15 µm
d
AmpR
E²GFP-mCherry
7870 bp
mCherry
E²GFP
e
E²GFP
tdTomato
25 µm
25 µm
f
AmpR
'ClopHensor2'
E²GFP-TdTomato
8587 bp
tdTomato
E²GFP

2010). Fluorescence signal at this excitation wavelength is Cl^- sensitive, but not pH sensitive. As such, the ratio of fluorescence elicited by excitation at 458 nm over that acquired at 594 ($R_{Cl} = F_{458}/F_{594}$) was shown to depend on intracellular Cl^- with a K_d of 18.4 mM (Fig. 4.8b). Furthermore, the relationship between R_{Cl} and intracellular Cl^- concentration was confirmed to be independent of pH within the physiological range. Systematically varying the intracellular pH (6.8 - 7.6) did not affect the Cl^- calibration curve (Fig. 4.8d). In addition, the ratio of fluorescence collected using the two excitation wavelengths 488 and 458 nm ($R_{pH} = F_{488}/F_{458}$) was shown to depend on intracellular pH with a pK_a of 7.27 (Fig. 4.8c). Systematically varying the intracellular Cl^- (0 - 131 mM) did not affect the pH measurements. Therefore, R_{pH} did not depend on intracellular Cl^- concentration (Fig. 4.8e).

The calibration curves presented in Fig. 4.8 allowed absolute neuronal Cl^- concentration and pH to be determined independently and simultaneously from fluorescence ratios (R_{Cl} and R_{pH}), independent of protein expression levels. This establishes ClopHensor2 as an important new tool for identifying Cl^- and H^+ dynamics in neurons.

Figure 4.7 *(facing page)*: ClopHensor2: a genetically encoded Cl^- and pH sensor optimised for neuronal use. a) A CA3 pyramidal cell neuron biolistically transfected with 'ClopHensor' - a E^2GFP-DsRed fusion protein. Left, E^2GFP imaged using a 488 argon laser and fluorescence emission collected between 500 and 550 nm. Note the uniform expression of the green fluorescent protein. Right, DsRed imaged using a 594 laser and emitted fluorescence collected between 650 and 700 nm. This revealed marked intracellular aggregation and poor localisation of DsRed with E^2GFP, possibly indicating cleavage of the fusion protein in neurons. b) A map of the plasmid containing the original ClopHensor construct including a cytomegalovirus early enhancer element (CMV promoter) and bovine growth hormone (bGH) poly-adenylation termination sequence. c) A CA3 pyramidal cell expressing the E^2GFP-mCherry fusion protein imaged in the same manner as 'a'. Similar aggregation issues affect the red fluorophore in this construct. d) The plasmid map containing the gene for the E^2GFP-mCherry fusion protein. This plasmid uses the cytomegalovirus early enhancer element and chicken beta-actin promoter (CAG promoter) and employs a human beta globin (HBG) poly-adenylation termination sequence. e) A CA3 pyramidal cell expressing the E^2GFP-tdTomato fusion protein ClopHensor2. This cell was imaged using the same acquisition parameters as in 'a' and 'c'. Note the homogenous expression of both E^2GFP and tdTomato indicating good co-localisation of the two fluorophores. f) ClopHensor2 plasmid map, which is identical to that in 'd' apart from mCherry being replaced by tdTomato.

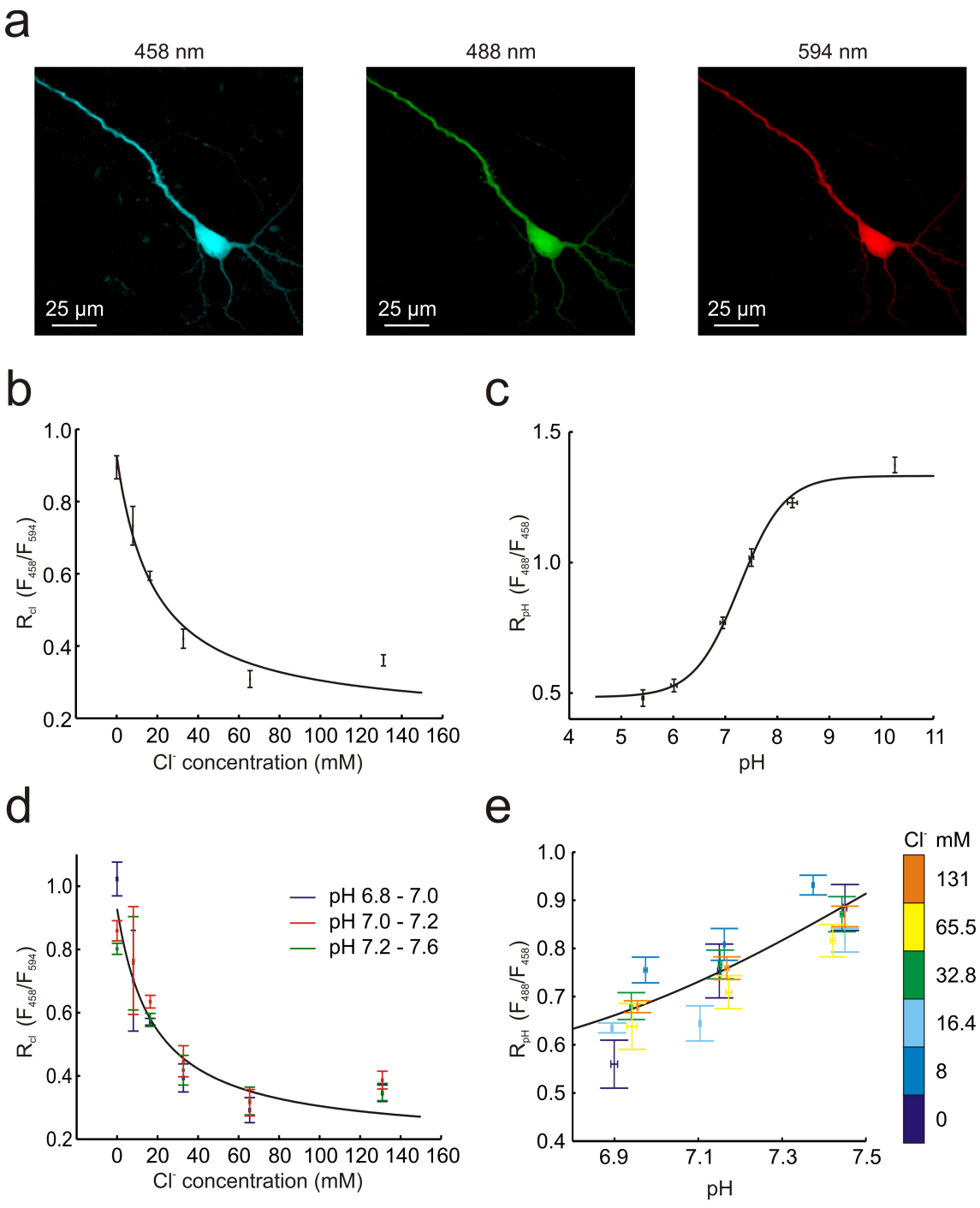
a
458 nm
488 nm
594 nm
25 µm
25 µm
25 µm
b
R_{cl} (F_{458}/F_{594})
Cl⁻ concentration (mM)
c
R_{pH} (F_{488}/F_{458})
pH
d
R_{cl} (F_{458}/F_{594})
pH 6.8 - 7.0
pH 7.0 - 7.2
pH 7.2 - 7.6
Cl⁻ concentration (mM)
e
R_{pH} (F_{488}/F_{458})
pH
Cl⁻ mM
131
65.5
32.8
16.4
8
0

4.9 ClopHensor2 reports rapid Cl^- and pH shifts during epileptiform activity

To investigate whether ClopHensor2 could be used to detect Cl^- and pH changes during neuronal network activity at a single cell level, I combined whole-cell patch clamp recordings with simultaneous confocal imaging in hippocampal brain slices (Fig. 4.9a). ClopHensor2 was delivered by biolistic DNA transfection methods (Fig. 4.9b). Epileptiform activity was generated using the 0 Mg^{2+} seizure model, which resulted in periods of synchronized neuronal discharges (Fig. 4.9c). Similar to the technique used during MQAE imaging, neuronal activity was monitored by performing whole-cell current clamp recordings from nearby pyramidal neurons ($<$200 μm between somata). This provided precise information regarding seizure onset, offset and intensity, without disrupting the physiology of the imaged neuron. Neurons expressing ClopHensor2 were imaged using the acquisition settings described in the previous section. With this arrangement I found that seizure episodes were associated with marked Cl^- and pH transients in neurons (Fig. 4.9c). During individual seizure events, neurons experienced significant increases in intracellular Cl^- and H^+ concentrations, which were transient and typically recovered before

---

Figure 4.8 *(facing page)*: Calibrating ClopHensor2 reveals independent pH and Cl^- sensitivity. a) Confocal images of a hippocampal CA3 pyramidal neuron expressing ClopHensor2. Panels from left to right depict fluorescence collected following excitation with 458, 488 and 594 nm respectively. b) Calibration curve relating the Cl^- sensitive excitation fluorescence ratio (R_{Cl}) of ClopHensor2 expressing neurons to their intracellular Cl^- concentration. Excitation was delivered at two separate wavelengths (458 and 594 nm) and emitted light was collected between 500 and 550 nm for 458 nm excitation and between 650 and 700 nm during excitation with the 594 nm laser. Intracellular Cl^- was systematically varied by controlling extracellular Cl^- in the presence of a Cl^- permeable ionophore (see Materials and Methods). Data was fit using established equations (Grynkiewicz et al., 1985; Arosio et al., 2010) and K_d found to be 18.4 mM. c) Calibration curve relating the pH sensitive excitation fluorescence ratio (R_{pH}) of neurons expressing ClopHensor2 to their intracellular pH. In order to measure R_{pH}, excitation was delivered sequentially at two separate wavelengths (458 and 488 nm) and emitted light collected from a single window (500 and 550 nm). Intracellular pH was manipulated by adjusting extracellular pH in the presence of a proton permeable ionophore. Data was fit using established equations (Grynkiewicz et al., 1985; Arosio et al., 2010) also see Materials and Methods, and pK_a was found to be 7.27. d) Adjusting intracellular pH within the physiological range had no affect on the R_{Cl} Cl^- calibration curve. e) Similarly, adjusting intracellular Cl^- had a negligible affect on the calibration of R_{pH}. This demonstrates that within neurons, ClopHensor2 is able to accurately report intracellular Cl^- and pH simultaneously.

the next seizure event.

In order to confirm the ability of ClopHensor2 to independently measure Cl^- and pH dynamics in neurons, I performed measurements using two separate models of epileptiform activity in the same brain slice preparation. The first utilised the '0 Cl^-' model of epilepsy. $GABA_A$ receptors are primarily permeable to Cl^- (Hamill et al., 1983). Therefore, by removing Cl^- from the aCSF, one is able to profoundly reduce the efficacy of GABAergic inhibition (Yamamoto, 1972; Yamamoto and Kawai, 1968, 1967, 1969; Avoli et al., 1990; Chamberlin and Dingledine, 1988). In addition, without Cl^- in the aCSF, the seizure induced Cl^- influx that has been shown to occur during other models of epilepsy would be predicted not to occur in response to 0 Cl^- induced seizures. Indeed, as is demonstrated in Fig. 4.10b, periods of 0 Cl^- induced epileptiform activity actually resulted in moderate Cl^- efflux and not C^- influx. In other words, each seizure event was associated with a flux of intracellular Cl^- into the extracellular space. pH measurements performed simultaneously with ClopHensor2 showed that acidic intracellular transients still occurred during each seizure event. Replacing the bath solution with standard Cl^- containing aCSF followed by '0 Mg^{2+}' aCSF enabled 0 Mg^{2+} seizures to be subsequently induced in the same brain slice (Fig. 4.10c). Under these conditions clear increases in $[Cl^-]_i$ were associated with each seizure event as were the acidic pH transients. seizure associated Cl^- increases could be recorded. This demonstrates the ability of ClopHensor2 to independently report Cl^- and pH during network activity. The remainder of this Chapter will focus on Cl^- fluxes during epileptiform activity as determined by ClopHensor2 measurements.

Figure 4.9 *(facing page)*: ClopHensor2 reports rapid Cl^- and pH shifts during epileptiform activity. a) A schematic of the experimental setup. A hippocampal pyramidal neuron transfected with ClopHensor2 was imaged using single-photon confocal microscopy. This allowed dynamic measurement of intracellular Cl^- and pH. A whole cell patch recording from a neighbouring neuron (cell somata $<$200 μm apart) provided simultaneous readout of seizure activity within the hippocampal slice. b) A confocal image of two CA3 pyramidal neurons expressing ClopHensor2. The dashed rectangle demarcates the region of interest used to estimate intracellular Cl^- and pH. c) Dynamic, simultaneous intracellular Cl^- (upper trace) and pH (lower trace) measurements imaged from the neuron in 'b' . A neuron in close proximity was whole cell patched and the membrane potential recorded over time in current clamp mode (upper trace). Perfusion of the slice with 0 Mg^{2+} induced periods of epileptiform activity characterised by membrane depolarisation and high frequency firing, the onset of which is depicted by dashed lines. Note the Cl^- influx and acidic pH shifts that were closely associated with epileptiform activity.

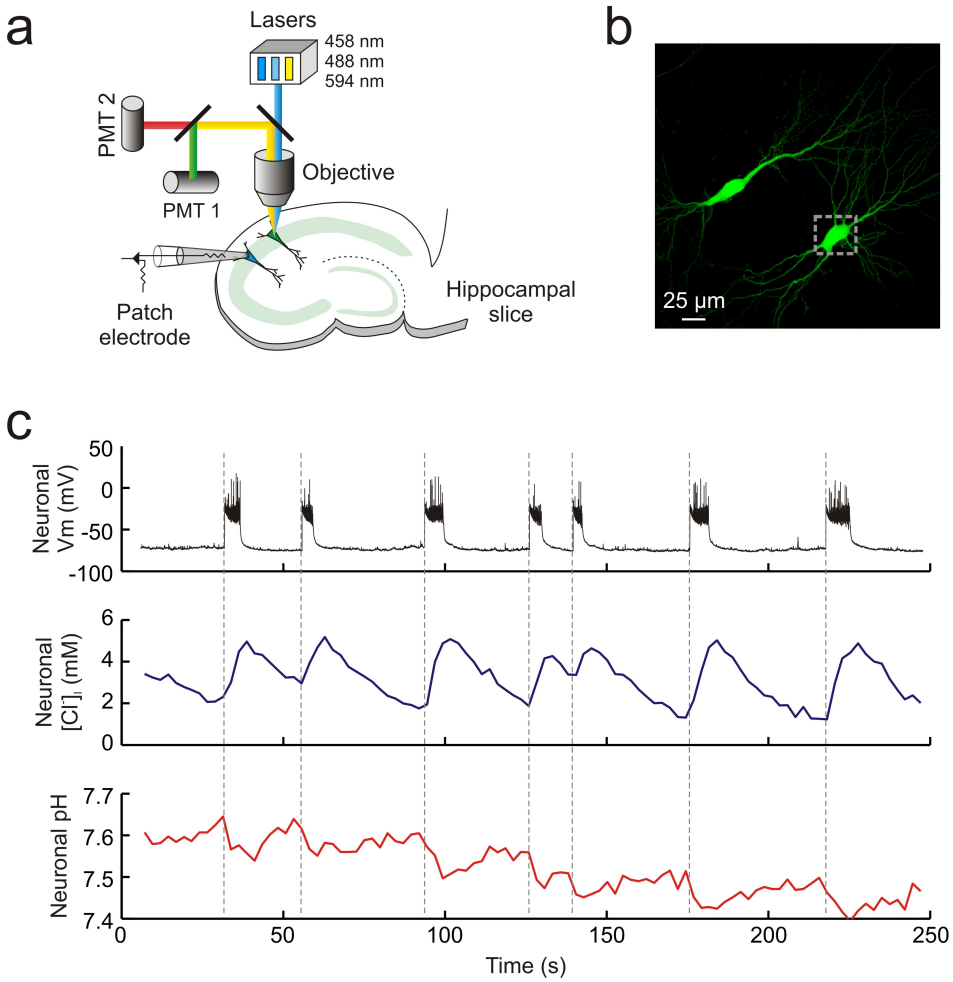
a
Lasers
458 nm
488 nm
594 nm
PMT 2
Objective
PMT 1
Patch
electrode
Hippocampal
slice
b
25 µm
c
Neuronal
Vm (mV)
50
0
-50
-100
Neuronal
[Cl⁻]i (mM)
6
4
2
0
Neuronal pH
7.7
7.6
7.5
7.4
0
50
100
150
200
250
Time (s)

Seizure induced pH transients will be the subject of Chapter 5.

4.10 Absolute quantification of Cl^- accumulation during epileptiform activity using ClopHensor2

Electrophysiological techniques are unable to measure Cl^- fluxes during seizure activity due to the concurrent heavy synaptic bombardment of cells. Techniques utilising synthetic Cl^- sensitive dyes are not ratiometric and hence are unable to make absolute measurements of Cl^- concentration. Even genetic reporters of Cl^- (clomeleon and Cl-sensor) are unable to directly measure Cl^- concentration changes during seizure activity as it is well known that these reporters are also sensitive to pH changes (Markova et al., 2008). This is important as it is well established that pH fluctuates during network activity (Raimondo, Irkle, Wefelmeyer, Newey and Akerman, 2012). Utilising the newly developed ClopHensor2 I made the first absolute measurements of intracellular Cl^- concentration changes in neurons during epileptiform activity (Fig. 4.11). Epileptiform activity was found to be associated with an increase of intracellular Cl^- concentration that was dependent upon the length of the seizure. Seizures that lasted between 10 and 20 s caused, on average, a 3.84 $\pm$ 0.28 mM (n = 54 seizures) increase in intracellular Cl^- from a mean baseline of 9.997 $\pm$ 0.54 mM. Even rapid bursts of activity on the order of 1 or 2 seconds caused detectable increases in intracellular Cl^- (Fig. 4.11b). For instance, seizures lasting between 1 and 5 s caused, on average, a 1.6 $\pm$ 0.13 mM maximum increase in intracellular Cl^- concentration ($P < 0.0001$, *t* test).

Figure 4.10 *(facing page)*: ClopHensor2 independently reports Cl^- and pH during epileptiform activity. a) A confocal image of a CA3 pyramidal neuron expressing ClopHensor2. Panels from left to right depict fluorescence collected following excitation with 458, 488 and 594 nm respectively. b) Dynamic, simultaneous intracellular Cl^- (middle trace) and pH (lower trace) measurements from the neuron in 'a' during '0 Cl^-' induced seizure activity. A whole cell patch of a nearby pyramidal neuron in current clamp mode provided a readout of seizure activity (upper trace). Dashed lines indicate seizure onset. Note, the modest seizure-associated Cl^- *efflux* that accompanied the acidic pH transients. c) In contrast, during subsequent induction of '0 Mg^{2+}' seizures, ClopHensor2 was able to register substantial Cl^- influx in tandem with the acidic transients. Same conventions as in 'b'. This demonstrates the ability of ClopHensor2 to independently report Cl^- and pH during seizure activity.

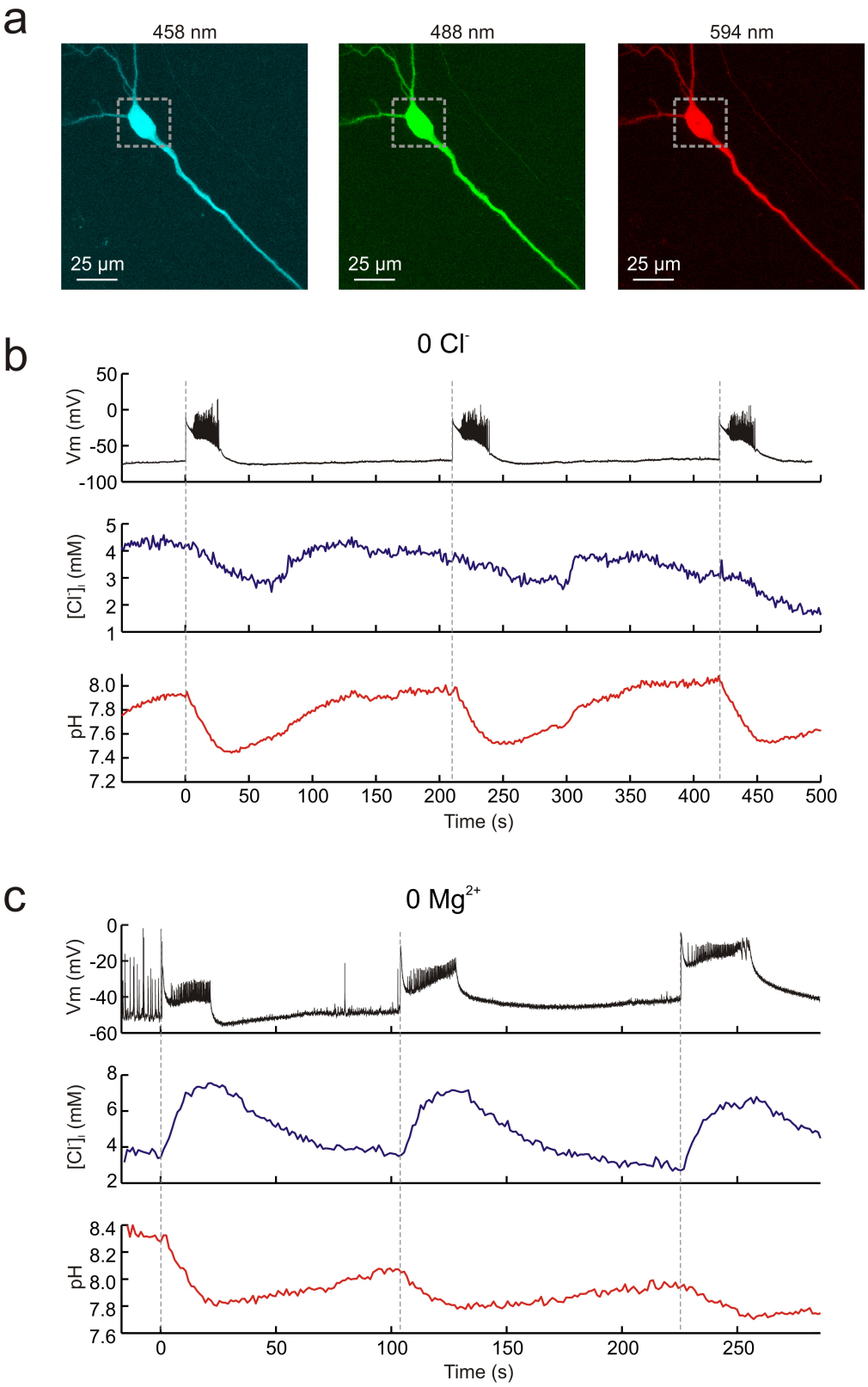
a
458 nm
488 nm
594 nm
25 µm
25 µm
25 µm
b
0 Cl⁻
Vm (mV)
[Cl⁻]i (mM)
pH
Time (s)
c
0 Mg2+
Vm (mV)
[Cl⁻]i (mM)
pH
Time (s)

ClopHensor2 allows the absolute measurement of Cl^- concentration across time and space. I took advantage of this property to investigate seizure associated Cl^- shifts in various subcellular compartments. In particular, I focussed on whether there were differences between somatic and dendritic compartments in terms of seizure associated Cl^- dynamics. Previous sections in this Chapter have used alternative techniques to explore potential differences along the somato-dendritic axis in terms of epileptiform activity induced Cl^- accumulation. Using ClopHensor2 I measured Cl^- changes from regions of interest at different distances from the cell soma (Fig. 4.12). Seizure associated increases in Cl^- were reliably detected along the entire somato-dendritic axis. The mean maximum change in $[Cl^-]_i$ within 10 μm of the soma was 3.93 $\pm$ 0.39 mM (n = 26 seizures) compared to 6.23 $\pm$ 0.50 mM (n = 19 seizures) for regions of interest $>$ 100 μm from the cell body. This difference was statistically significant with P = 0.0007, t test, Fig. 4.12c. This suggests that Cl^- accumulation occurs throughout the somato-dendritic axis during epileptiform activity.

4.11 Gabazine attenuates seizure associated Cl^- influx

In section 4.6 of this Chapter I demonstrated that 20 μM gabazine blocked seizure associated Cl^- influx as measured by MQAE imaging. In order to confirm this effect, I repeated this experiment using ClopHensor2, which allowed more reliable, absolute measurements of intracellular Cl^- changes. As shown in Fig. 4.13, 20 μM gabazine markedly reduced Cl^- influx during epileptiform activity. For instance, during control 0 Mg^{2+} induced seizures lasting between 10 and 20 s, the mean maximum change in intracellular Cl^- was

Figure 4.11 *(facing page)*: Quantification of Cl^- accumulation during epileptiform activity using ClopHensor2. a) Top, a whole cell patch of a neuron in close proximity to that depicted in 'c' was held in current clamp mode and provided a readout of epileptiform activity. Bottom, imaging data from ClopHensor2 reports intracellular Cl^-. Note the increases in intracellular Cl^- correlate closely with the onset of seizure activity. b) An enlargement of the dashed box in 'a'. Even relatively brief periods of epileptiform activity lasting less than 5 s result in measurable increases in intracellular Cl^-. c) A confocal image of the hippocampal pyramidal neuron expressing ClopHensor. The dashed box represents the region of interest used in acquiring the data in 'a' and 'b'. d) Population data plots the maximum recorded shift in Cl^- against seizure duration. Note how the seizure induced shift in Cl^- concentration increases incrementally with seizure duration.

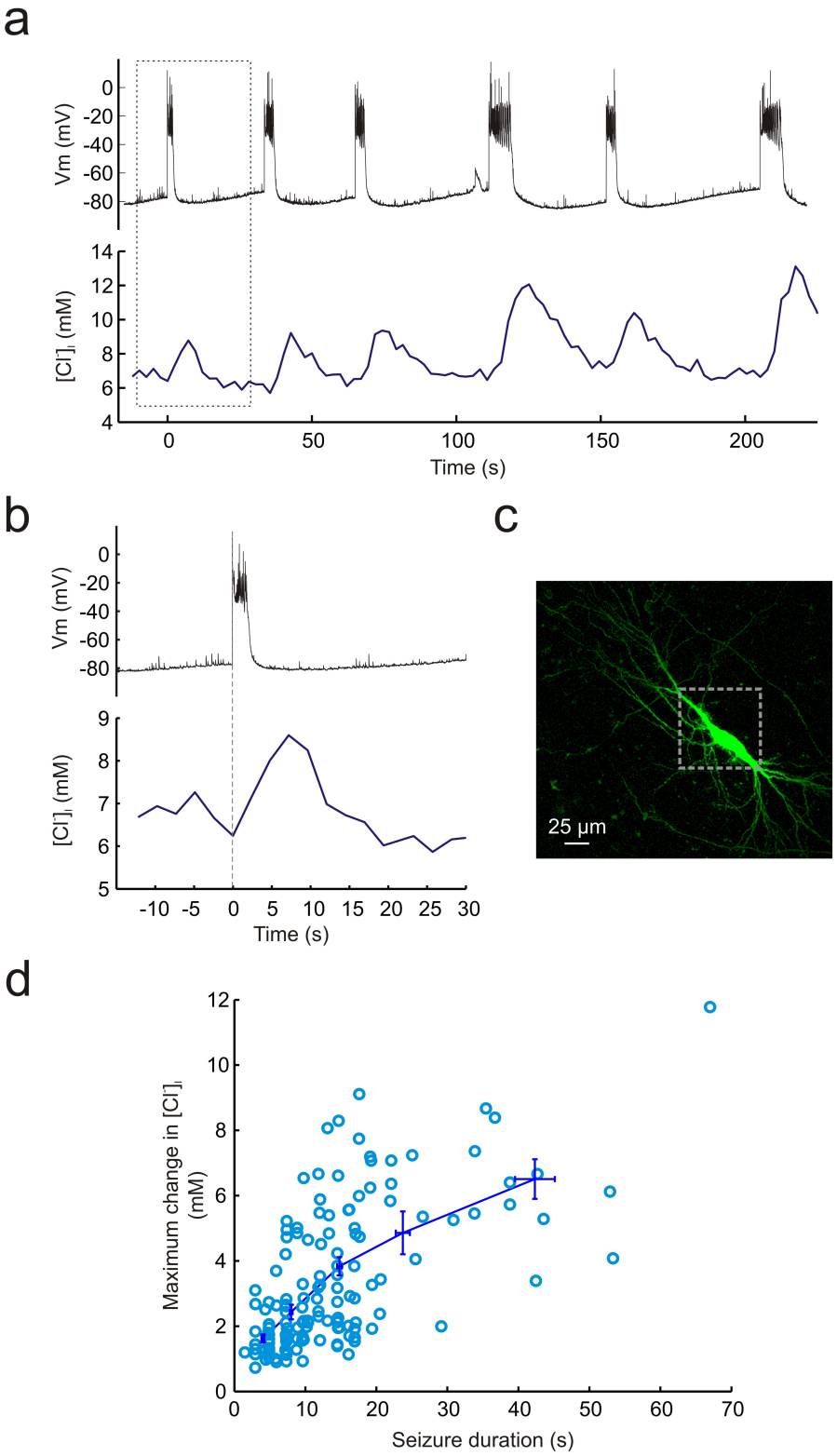
a
Vm (mV)
0
-20
-40
-60
-80
[Cl]i (mM)
14
12
10
8
6
4
0
50
100
150
200
Time (s)
b
Vm (mV)
0
-20
-40
-60
-80
[Cl]i (mM)
9
8
7
6
5
-10 -5 0 5 10 15 20 25 30
Time (s)
c
25 µm
d
Maximum change in [Cl]i (mM)
12
10
8
6
4
2
0
0 10 20 30 40 50 60 70
Seizure duration (s)

3.84 $\pm$ 0.28 mM (n = 54 seizures). In contrast, in 20 μM gabazine, seizures lasting between 10 and 20 s only produced a 0.82 $\pm$ 0.29 mM (n = 13 seizures) positive shift in $[Cl^-]_i$ ($P < 0.0001$, *t* test). Along with previous data presented in this chapter, this confirmed that seizure associate Cl^- accumulation is mediated by the $GABA_A$Rs.

4.12 Discussion

This chapter began by confirming previous reports (Fujiwara-Tsukamoto, 2006; Fujiwara-Tsukamoto et al., 2003; Lamsa and Kaila, 1997; Lasztóczi et al., 2011; Perreault and Avoli, 1992) that in vitro models of epilepsy are associated with an excitatory shift in GABAergic signalling. This was assessed by exogenously applying GABA via a puffer pipette to evoke $GABA_A$ potentials. These were hyperpolarising prior to seizure onset but became markedly depolarising and even excitatory after extended periods of epileptiform activity. As $GABA_A$ receptors are primarily permeable to Cl^- the most likely explanation for this phenomenon is a seizure associated increase in intracellular Cl^- and a consequent depolarising shift in E_{GABAA}. Employing sophisticated electrophysiological protocols involving rapid switching between voltage and current clamp mode, I was able to measure E_{GABAA} before and immediately after seizure episodes. This revealed seizure induced depolarizing shifts in E_{GABAA}, upward of 30 mV.

Electrophysiological techniques cannot measure Cl^- changes directly but are restricted to inferring $[Cl^-]_i$ indirectly via quantification of E_{GABAA}. This requires stable baseline membrane conductances in order to calculate $GABA_A$R currents accurately. However, due to the extensive synaptic input that accompanies epileptiform activity, electrophysiological techniques can only measure E_{GABAA} before and for a limited period during the

---

Figure 4.12 *(facing page)*: ClopHensor2 reports activity-dependent Cl^- influxes across the somato-dendritic axis. a) A confocal image of a CA3 hippocampal pyramidal cell expressing ClopHensor2. Regions of interest utilised for Cl^- estimation and their respective distances from the cell soma are depicted in red and cyan. b) Top, a current clamp trace from a separate neuron in close proximity to the cell in 'a' provides readout of seizure activity. Bottom, dynamic measurements of $[Cl^-]_i$ for the two regions of interest in 'a'. Note the prominent seizure associated intracellular Cl^- increases observed in both regions. c) Population data comparing the maximum seizure associated change in $[Cl^-]_i$ against distance from the soma. Note the tendency for regions furthest from the cell soma to experience slightly larger seizure associated Cl^- increases.

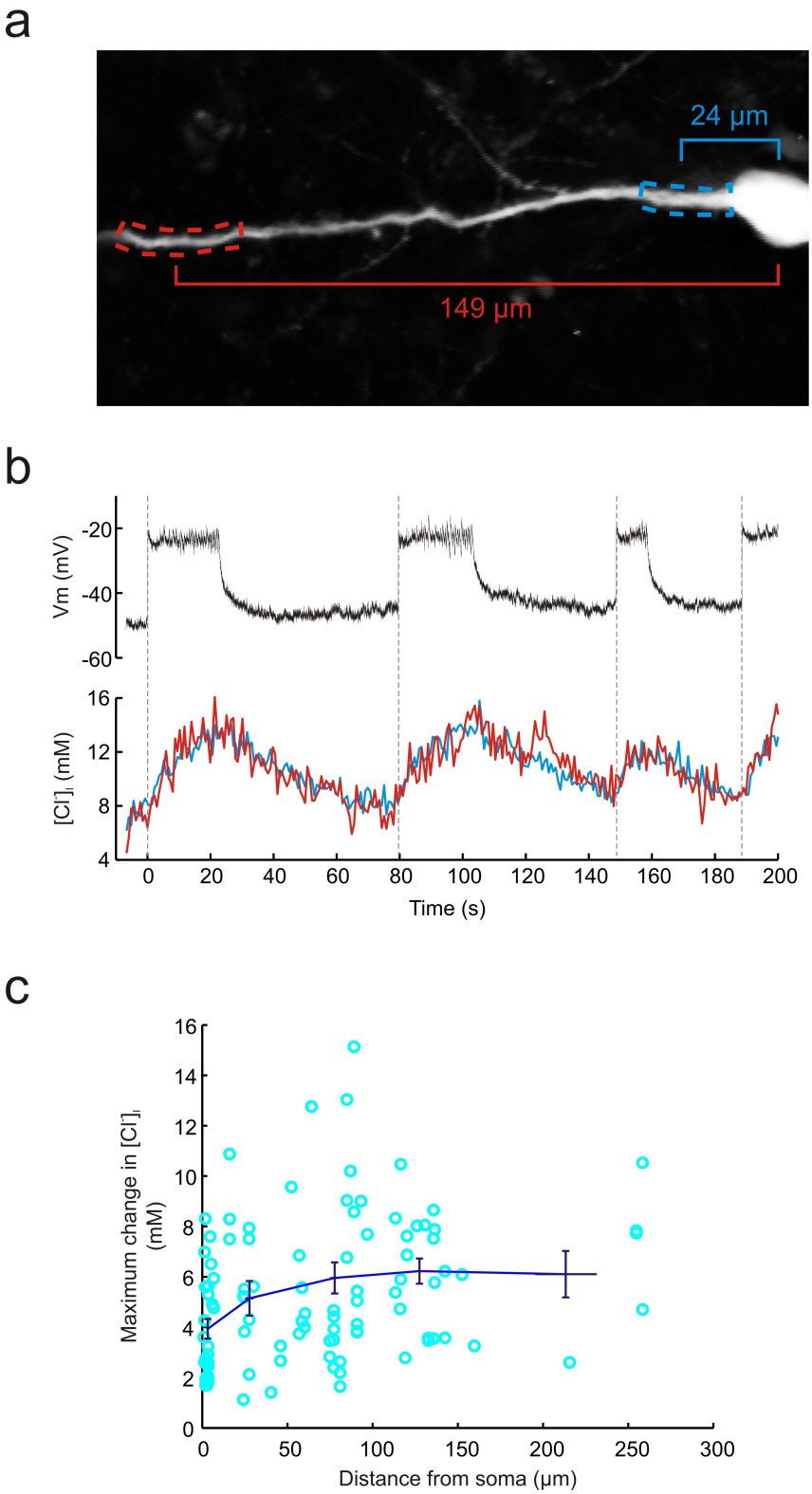
a
24 µm
149 µm
b
Vm (mV)
-20
-40
-60
[Cl]i (mM)
16
12
8
4
0
20
40
60
80
100
120
140
160
180
200
Time (s)
c
Maximum change in [Cl]i (mM)
16
14
12
10
8
6
4
2
0
0
50
100
150
200
250
300
Distance from soma (µm)

latter stages of a seizure episode. In order to directly estimate Cl^- accumulation throughout seizures themselves, I employed two different imaging methods. The first made use of the Cl^- sensitive dye MQAE, whilst the second method involved the development and utilisation of a novel genetic reporter of Cl^-, ClopHensor2.

Experiments with MQAE demonstrated a relative increase in Cl^- during epileptiform activity. However, MQAE (like all currently available dyes) is not ratiometric, which means that Cl^- estimates are susceptible to measurement artefacts induced by variations in excitation path length, indicator concentration, illumination stability, cell thickness, and indicator distribution. Furthermore, not being ratiometric, MQAE can not report absolute Cl^- concentrations without laborious within cell calibrations. Additional issues associated with the dye include, toxicity, rapid bleaching and significant cell leakage (Bregestovski et al., 2009).

In order to overcome these issues I sought to utilise a ratiometric genetic reporter of Cl^-. Despite addressing many of the problems associated with Cl^- sensitive dyes, the best characterised reporters in this class, clomeleon and Cl-sensor (Kuner and Augustine, 2000; Markova et al., 2008), display substantial sensitivity to pH. It is well established that pH can fluctuate as a function of neural activity (Xiong et al., 2000). As a result, pH induced artefacts in Cl^- estimation are a major drawback of these reporters. Recently a novel genetic indicator (ClopHensor) has been developed by Arosio et al. (2010) that potentially addresses this issue by affording simultaneous measurement of both Cl^- and pH.

Despite its potential I demonstrated that ClopHensor does not express well in neurons. At least in this cell type, it appears to have inherited many of the protein aggregation issues associated with monomeric DsRed' (Shaner et al., 2005). This problem has been experienced by other investigators (Arosio and Wefelmeyer, personal communication).

Figure 4.13 *(facing page)*: Gabazine attenuates seizure associated Cl^- influx. a) Current clamp recording from a nearby CA3 pyramidal neuron provided readout of seizure activity. Bottom, readout of intracellular Cl^- fluctuations as determined by imaging a cell expressing ClopHensor2. Note the seizure associated increases in intracellular Cl^-. b) The similar recordings to those in 'a' but performed in the presence of 20 μM gabazine. Note how epileptiform activity is no longer correlated with discernible shifts in intracellular Cl^-. c) Population data demonstrating the effect of 20 μM gabazine on seizure induced Cl^- influx.

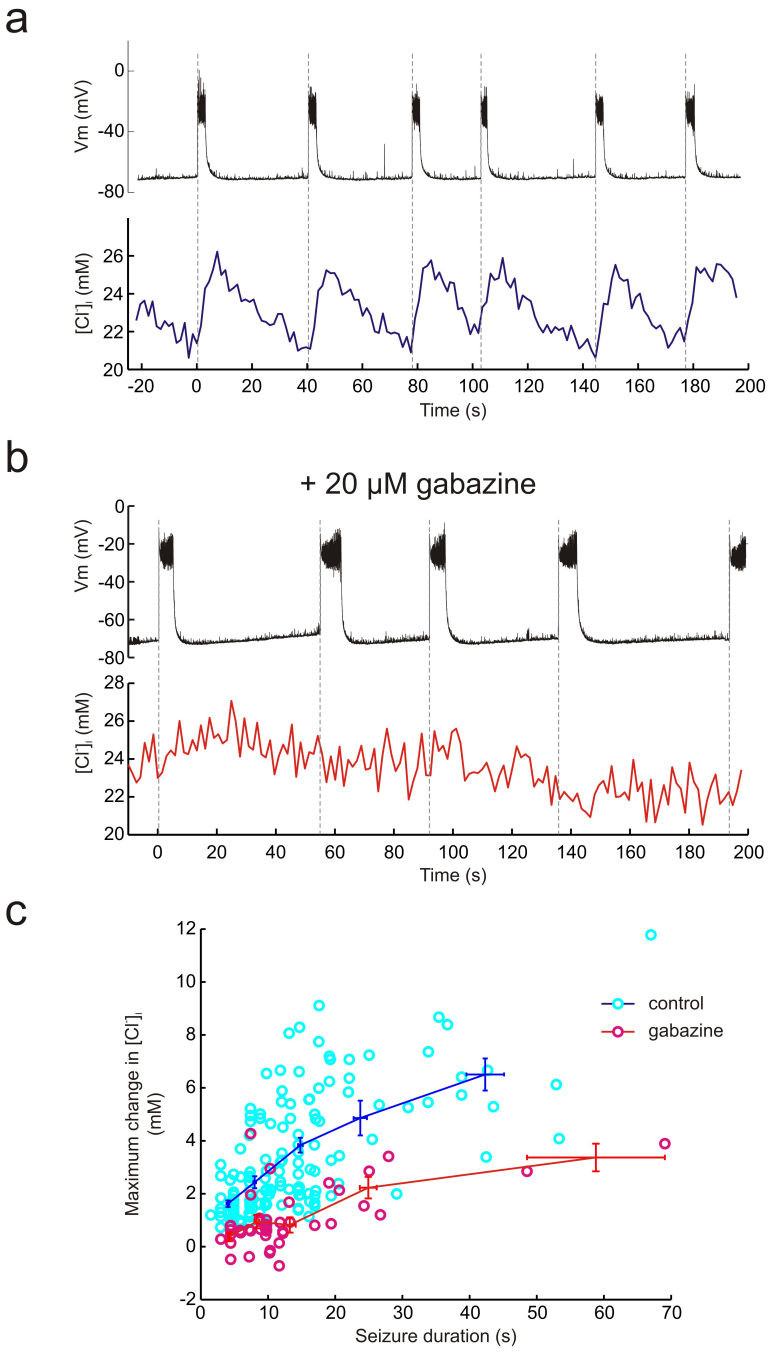
a
Vm (mV)
0
-40
-80
[Cl]i (mM)
26
24
22
20
-20 0 20 40 60 80 100 120 140 160 180 200
Time (s)
b
+ 20 µM gabazine
Vm (mV)
0
-20
-40
-60
-80
[Cl]i (mM)
28
26
24
22
20
0 20 40 60 80 100 120 140 160 180 200
Time (s)
c
Maximum change in [Cl]i (mM)
12
10
8
6
4
2
0
-2
0 10 20 30 40 50 60 70
Seizure duration (s)
control
gabazine

Intriguingly, despite being a 'fusion protein', the colocalisation of E^2GFP and monomeric DsRed (the two linked proteins that make up ClopHensor), was found to be extremely poor. Indeed, if the two proteins were truly fused, one would expect E^2GFP to form part of the DsRed induced aggregations. This suggests that post translational cleavage of the reporter protein may also occur in neurons.

It is well known that DsRed is susceptible to aggregation issues, particularly as a fusion partner (Shaner et al., 2005). As such, we sought to replace DsRed with red fluorophores that have been optimised for use in fusion proteins. To achieve this, mCherry or tdTomato was substituted for DsRed within ClopHensor, while preserving the original amino-acid linking sequence. I found that the E^2GFP-mCherry fusion experienced similar aggregation problems as the original ClopHensor. However, E^2GFP-tdTomato showed no signs of aggregation or colocalisation issues when expressed in neurons suggesting that this is an optimal fusion ratiometric reporting of Cl^- and pH. I have named this optimised sensor ClopHensor2.

Using this novel reporter I was able to dynamically and simultaneously measure absolute Cl^- and H^+ concentrations in neurons during epileptiform activity. Seizures lasting more than 40 seconds resulted in an absolute increase of intracellular Cl^- of roughly 6 mM. On a mean $[Cl^-]_i$ baseline of 9 mM and assuming a constant extracellular concentration of Cl^- (135 mM; plus a stable transmembrane HCO_3^- gradient), this would translate to a 10 mV increase of E_{GABAA} from -65 mV to -55 mV. This is a considerably smaller shift than the upward of 30 mV increases in E_{GABAA} observed following epileptiform activity when utilising electrophysiological techniques. There are several possible explanations for this difference. Firstly, due to technical time constraints, somewhat shorter seizures were selected for the imaging experiments than for the electrophysiological experiments (approx 40 s vs 80 s). Secondly, changes to $[Cl^-]$ in the extracellular space would be expected to contribute to changes in E_{GABAA} but would not be detected by the imaging method. Lastly, it is possible that voltage clamp errors involving series resistance may have contributed to an overestimation of E_{GABAA}.

Mechanistically, the most parsimonious explanation for Cl^- accumulation during seizures is that massive endogenous GABA release, combined with concurrent membrane depolarization, causes rapid Cl^- influx via activated $GABA_A$Rs. Until now however, this causal

link has been difficult to establish as pharmacological blockade of $GABA_A$Rs during a seizure would preclude the measurement of $[Cl^-]_i$ using traditional techniques, which rely on evoked $GABA_A$R currents to indirectly estimate Cl^- levels. Direct, optical technologies for estimating $[Cl^-]_i$ using the Cl^- sensitive dye MEQ during the tetanic generation of epileptiform afterdischarges has been performed previously (Isomura et al., 2003). Although this technique does not allow absolute measurement of $[Cl^-]_i$, it was reported that significant Cl^- accumulation was still observed in the presence of the $GABA_A$R antagonist bicuculline (Isomura et al., 2003). In addition, Slemmer et al. (2004) showed a very large $GABA_A$R independent intracellular Cl^- increase in response to glutamate application in dissociated cultures. Therefore, considerable uncertainty has existed in terms of the underlying mechanism behind seizure induced Cl^- accumulation. By using both MQAE and ClopHensor2 based imaging methods, I have been able to show that 20 μM gabazine markedly reduces Cl^- increases during epileptiform activity. It is possible that the difference between my observations and prior work can be accounted for by the fact that the Cl^- estimation techniques used by both (Isomura et al., 2003) and Slemmer et al. (2004) were susceptible to pH artefacts Vasseur et al. (1993). These findings serve to confirm the integral role that $GABA_A$Rs play in mediating seizure induced intracellular Cl^- accumulation.

In this chapter various techniques were utilised in order to determine whether subcellular compartments (soma vs dendrites) might differ in terms of epileptiform activity induced increases in intracellular Cl^-. This is important as compartment specific modulation of the action of soma versus dendritically targeted interneurons could have consequences for the evolution of ongoing network activity. The electrophysiological methods that employed gramicidin perforated patches, and either soma or dendrite directed puffs of GABA, revealed a slightly larger increase in somatic E_{GABAA} compared to dendritic E_{GABAA} during seizure activity. Using MQAE, a similar pattern emerged although considerable leakage of the dye meant that confident fluorescence measurements from dendritic structures could not be attained. Use of ClopHensor2 to make absolute estimates of Cl^- changes in the two subcellular compartments produced a somewhat contradictory picture. Intracellular Cl^- increases were similar or greater in size as a function of distance from the soma.

The most likely explanation for the observed difference between imaging and electrophysiological techniques stems from the fact that $GABA_A$Rs are permeable to $HC0_3^-$ as well as Cl^-. HCO_3^- would influence electrophysiological measures of E_{GABAA}, whilst imaging methods would not report $HC0_3^-$. In addition, whilst gramicidin pores are impermeable to Cl^- this is not the case for small anions such as hydrogen. Therefore, whilst gramicidin perforated patches will leave intracellular Cl^- concentrations unperturbed, pH (and by extension HCO_3^- levels) will be affected by the patch pipette internal solution. It is well known that seizure activity is associated with significant intracellular acidification (Xiong et al., 2000), which is predicted to reduce HCO_3^- concentration and hence have a hyperpolarising affect on E_{GABAA}. A gramicidin perforated patch is better able to clamp pH and HCO_3^- during a seizure at the soma than within the dendrites. It is therefore likely that during a perforated patch recording the ability of seizure induced acidification to hyperpolarise E_{GABAA} would be stronger in the dendritic compartment. In contrast, ClopHensor2 measurements leave intracellular Cl^- and pH unperturbed. It is therefore likely that this technique provides a more accurate picture of Cl^- and pH changes during epileptiform activity.

The results presented in this chapter confirm that Cl^- accumulation occurs throughout neurons during seizure activity. This means that as a seizure progresses, $GABA_A$R mediated inhibition will weaken before ultimately becoming excitatory. As part of the following chapters, I will discuss how these findings can inform our understanding of how seizures start, propagate and eventually terminate.

Chapter 5

Activity-dependent intracellular pH transients

5.1 Introduction

In the previous chapter I investigated how intracellular Cl^- concentrations change as a function of neuronal activity. It is known however, that neuronal processes often involve either the related, or independent, flux of both Cl^- and H^+ ions (Tabb et al., 1992; Doyon et al., 2011). Indeed, H^+ and Cl^- are linked via their mutual association with HCO_3^-. Intra- and extracellular carbonic anhydrases catalyse the reversible reaction of HCO_3^- and H^+ to H_20 and CO_2. Therefore any cellular process that modifies pH will effect intracellular HCO_3^- concentration (and vice versa). Intracellular HCO_3^- in turn is linked to Cl^- via Cl^-/HCO_3^- co-transporters and the combined permeability of $GABA_A$Rs to both Cl^- and HCO_3^- (Sterling and Casey, 1999; Kaila, 1994). Furthermore, as shown for Cl^- in the previous chapter, it is known that intracellular pH both affects neuronal activity, and is itself altered by neuronal activity (Chesler, 2003). For these reasons the experiments described in this chapter sought to investigate intracellular pH dynamics at the single cell level and in the context of heightened network activity.

Such an investigation requires tools for the accurate measurement of intracellular pH during evolving network activity. Previous work investigating the effect of spiking activity and neuronal depolarization on intracellular pH has relied either on pH-sensitive micro-electrodes or pH-sensitive fluorescent dyes (Rose and Deitmer, 1995; Xiong et al.,

2000). Genetically encoded, GFP-based pH reporters offer several potential advantages over these techniques, including single cell or subcellular targeting, enhanced spatial resolution, no fluorophore leakage and reduced interference with endogenous H^+ transport mechanisms (Bizzarri et al., 2009; Gatto and Milanick, 1993). Although GFP-based pH indicators have gained popularity as a marker of synaptic release (Miesenböck, 1998), they have not been utilised to study intracellular H^+ ion fluxes associated with network activity. Therefore, the first aim of this chapter was to establish and characterise the utility of employing GFP-based, genetically encoded pH indicators for investigating activity-dependent pH changes at the single-cell level.

Only one previous study has measured intracellular pH fluxes during an in vitro model of epilepsy (Xiong et al., 2000). The absolute values that were reported for pH changes in this study were likely to be affected by the imaging techniques that were adopted. Therefore, the second aim of this chapter was to accurately quantify neuronal pH transients using genetic pH reporters in two separate models of epileptiform activity.

Finally, a third aim of this chapter was to use genetic reporters to compare pH dynamics in different cell types. Previous work using microelectrode recordings has suggested that astrocytes and neurons might differ in their pH responses to depolarisation (Bevensee et al., 1997; Grichtchenko and Chesler, 1994; Pappas and Ransom, 1994; Chesler, 2003). However, astrocytic intracellular pH responses have not been measured during epileptiform activity. For this reason, I set out to quantify and characterise seizure induced pH changes in hippocampal astrocytes.

5.2 Detecting activity-dependent changes in pH using genetic reporters

To investigate whether genetic reporters of pH can be used to detect the effect of neuronal network activity upon intracellular pH at a single cell level, I combined whole-cell patch clamp recordings with simultaneous two-photon or single-photon confocal imaging in hippocampal brain slices (Fig. 5.1). The intracellular pH of individual pyramidal neurons within the CA1 and CA3 regions was measured using one of three genetically encoded ratiometric pH sensors: E^2GFP (Bizzarri et al., 2006), deGFP4 (Hanson et al.,

2002) or Cl-sensor (Markova et al., 2008), which were delivered by biolistic DNA transfection methods. Hyper-active network states were generated using seizure models that result in periods of synchronized neuronal discharges (see Materials and Methods). The effects upon neuronal activity were monitored by performing whole-cell current clamp recordings from nearby pyramidal neurons ($<$200 μm between somata). This provided precise information regarding seizure onset, offset and intensity, without disrupting the physiology of the imaged neuron (Fig. 5.1c). With this arrangement I found that seizure episodes were associated with marked acidic pH transients in neurons. The acidic pH transient typically began at the onset of the seizure (Fig. 5.1c) and pH continued to decrease before reaching a minimum at, or shortly following, the end of the seizure. The pH then recovered to baseline levels in the period between seizure events. Across slices and experiments the network events varied in terms of duration and the signal to noise of the pH measurements was sufficient to detect acidic transients associated with relatively brief periods of network activity, lasting on the order of 5 s (see example in, Fig. 5.1c).

5.3 Calibrating genetically encoded pH sensors in hippocampal neurons

I next assessed the ability of each pH sensor to report pH under our imaging conditions. deGFP4, E^2GFP, and Cl-sensor showed robust expression in primary hippocampal neurons following biolistic transfection (Fig. 5.2a-c). Each genetic reporter was calibrated by systematically varying extracellular pH in the presence of a proton-permeable ionophore, to achieve known intracellular pH values (see Materials and Methods). E^2GFP was used as a ratiometric pH indicator by excitation. The protein was excited sequentially via single-photon excitation at 458 nm and 488 nm, with emission collected between 500 and 550 nm using a single PMT. The ratio of fluorescence collected using the two excitation wavelengths (R_{pH} = F488 / F458) was shown to depend on intracellular pH with a pK_a of 7.56 (Fig. 5.2a, right). deGFP4 was employed as a ratiometric pH indicator by emission. A two-photon laser at 810 nm was used to excite the protein, whilst emission was simultaneously recorded at 450-490 nm and 500-550 nm by two separate PMTs. The fluorescence ratio between these emission windows ($R_{pH} = F_{500\text{-}550} / F_{450\text{-}490}$) was found

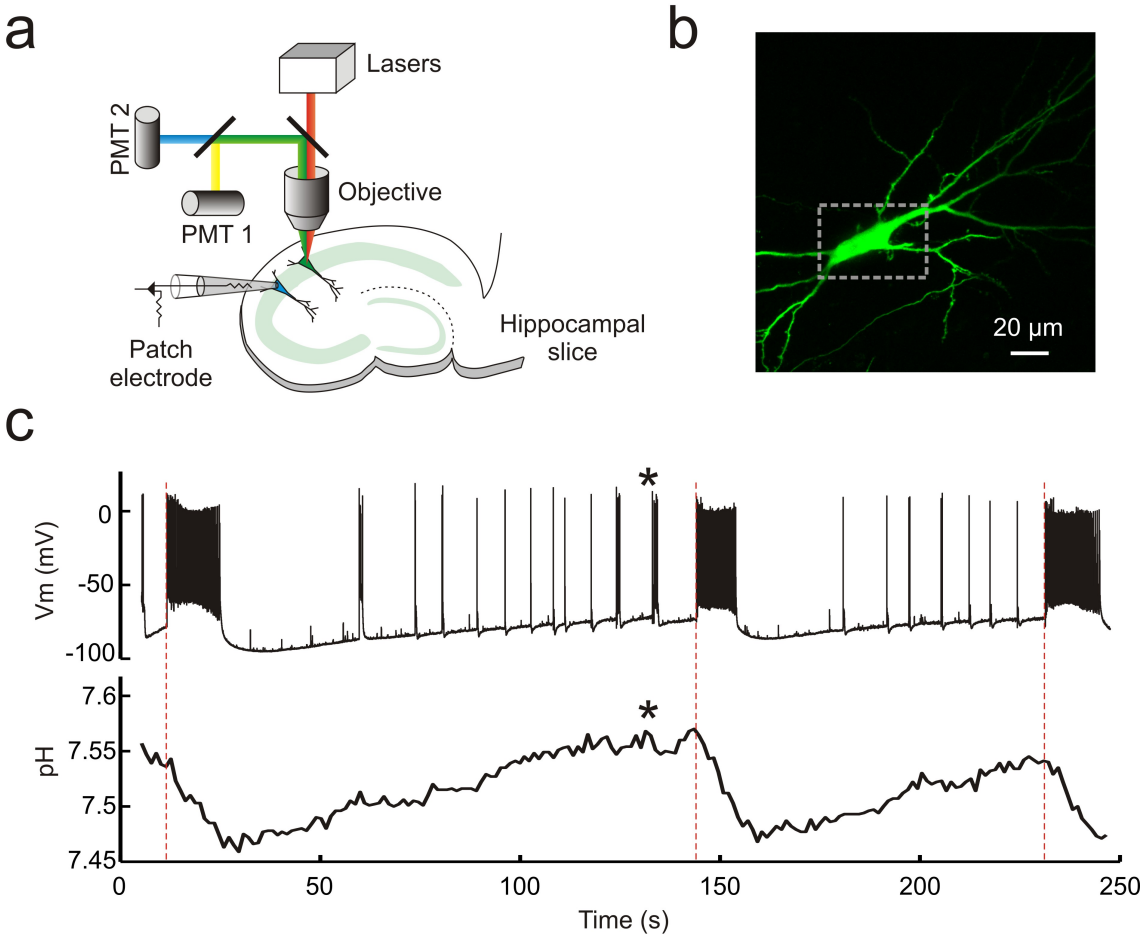

Figure 5.1: Genetic reporters of pH detect intracellular pH changes during epileptiform activity. a) A schematic of the experimental setup. A hippocampal pyramidal neuron transfected with a genetically encoded pH indicator was imaged using either two-photon or single-photon confocal microscopy. This allowed dynamic measurement of intracellular pH. A whole cell patch recording from a neighbouring neuron (cell somata $<$200 μm apart) provided simultaneous readout of seizure activity within the hippocampal slice. b) A confocal image of a CA3 pyramidal neuron expressing the pH indicator E^2GFP. The dashed rectangle demarcates the region of interest used to estimate intracellular pH. c) Dynamic intracellular pH measurements imaged from the neuron in b (lower trace). A neuron in close proximity was whole cell patched and the membrane potential recorded over time in current clamp mode (upper trace). Perfusion of the slice with 0 Mg^{2+} induced periods of epileptiform activity characterised by membrane depolarisation and high frequency firing, the onset of which is depicted by red dashed lines. Note the marked acidic shifts in pH that are associated with epileptiform activity. Even brief periods of activity were associated with detectable acidic transients (indicated by asterisks).

to be dependent upon intracellular pH with a pK_a of 7.42 (Fig. 5.2b, right). Cl-sensor was also utilised as a ratiometric pH indicator by emission. This reporter was excited at 850 nm, whilst emission was simultaneously recorded at 460-500 nm and 500-550 nm by two separate PMTs. Once again, the fluorescence ratio ($R_{pH} = F_{500\text{-}550} / F_{460\text{-}500}$) was strongly dependent upon intracellular pH, with a pK_a of 7.73 (Fig. 5.2c, right). Under these imaging conditions the noise associated with the pH signal was found to be different for the three reporters ($P < 10^{-7}$, one-way ANOVA). Comparing the root mean square (RMS) noise of the intracellular pH signal under baseline conditions revealed that E^2GFP exhibited the least noise (RMS = 0.01 $\pm$ 0.001 pH), then Cl-sensor (RMS = 0.02 $\pm$ 0.001 pH), and deGFP4 exhibited the greatest signal noise (RMS = 0.04 $\pm$ 0.004 pH). Nevertheless, for all three pH indicators, the calibration curves presented in Fig. 5.2 allowed absolute neuronal pH to be determined from fluorescence ratios (R_{pH}), independent of protein expression levels.

5.4 Genetic pH reporters reveal acidic intracellular transients during 0 Mg^{2+} induced epileptiform activity

Previous work using pH-sensitive electrodes or dyes has shown that neurons exhibit acidic shifts during heightened network activity (Rose and Deitmer, 1995; Xiong et al., 2000). Here I made use of pharmacological models of temporal lobe epilepsy to examine whether the ratiometric genetic reporters were able to capture dynamic shifts in pH during seizure activity. Omission of Mg^{2+} from the brain slice perfusate removes the voltage dependent Mg^{2+} block on NMDA receptors, which predisposes hippocampal slices to periods of synchronised hyperexcitability (Anderson et al., 1986; Mody et al., 1987; Gutiérrez et al., 1999) and resulted in ictal-like seizure events of different durations (mean duration of analysed seizures was 32.3 $\pm$ 1.6 s). Using this epilepsy model, I was able to demonstrate that the genetic pH reporters E^2GFP and deGFP4 are able to detect a highly significant negative shift in pH during epileptiform activity (E^2GFP: $P < 10^{-10}$, n = 40, deGFP4: $P < 10^{-7}$, n = 19, *t* test). As Fig. 5.3a and Fig. 5.3b demonstrate, intracellular pH for CA3 pyramidal neurons decreased from baseline following the onset of epileptiform activity and reached a minimum at, or shortly following, seizure cessa-

a

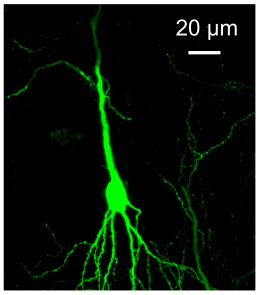

E^2GFP

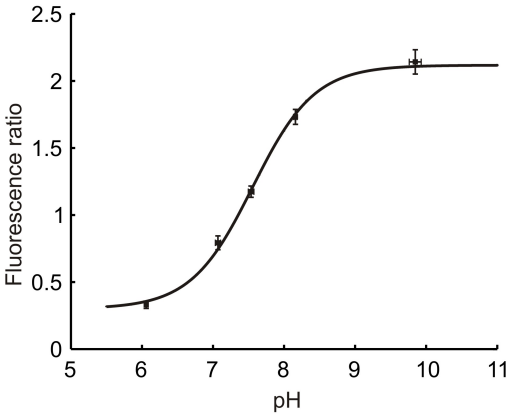

b

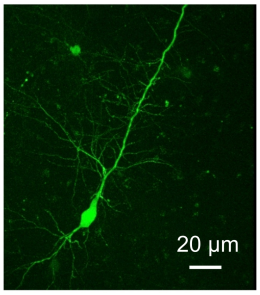

deGFP4

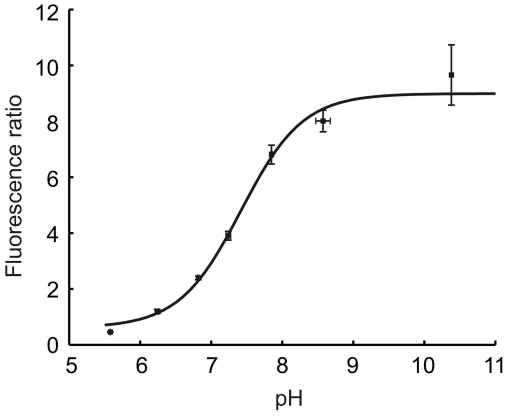

c

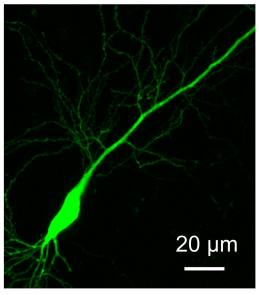

Cl-sensor

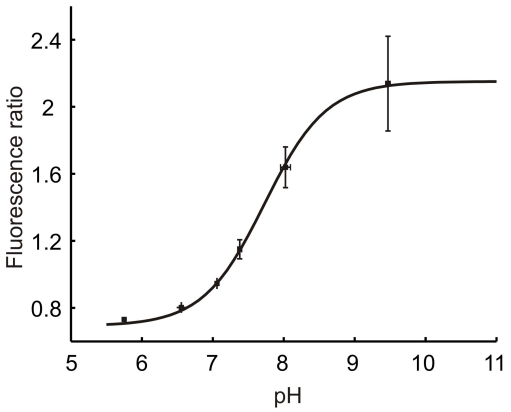

tion. Neuronal pH then gradually re-alkalinised to pre-seizure levels. To compare the pH responses recorded by the two pH reporters, I investigated the relationship between seizure length and the amplitude of maximum pH shift. When utilising both E^2GFP and deGFP4 I observed a strong negative correlation between seizure duration and maximum pH change (E^2GFP: r = -0.8270, $P < 0.0001$, deGFP4: r = -0.6056, $P = 0.0060$, Pearson Correlation, Fig. 5.3c). This relationship was indistinguishable for the two genetic reporters ($P = 0.4534$, Analysis of Covariance), which corroborated the magnitude of the pH shifts that were detected. As such, a linear fit could be applied to the pooled data from both probes and revealed a seizure-associated population shift of -0.005 pH units per second of seizure duration (Fig. 5.3c). When the maximum pH shift from individual seizures was adjusted for a typical seizure duration of 30 s, the mean pH shift for E^2GFP neurons was -0.19 $\pm$ 0.01 (n = 40) and the mean pH shift for deGFP4 neurons was -0.21 $\pm$ 0.03 (n = 19) (Fig. 5.3d).

Figure 5.2 *(facing page)*: Calibration of pH-sensitive GFP variants. a) A confocal image of a hippocampal CA3 pyramidal neuron expressing E^2GFP (left). Calibration curve relating the fluorescence ratio of E^2GFP expressing neurons to their intracellular pH (right; n = 4). E^2GFP was used as an excitation ratiometric reporter, with excitation at two separate wavelengths (458 nm and 488 nm) and emitted light collected from a single wavelength window (500-550 nm). Intracellular pH was systematically varied by controlling extracellular pH in the presence of a proton-permeable ionophore (see Materials and Methods). Data was fit using established equations (Grynkiewicz et al., 1985; Arosio et al., 2010) and pK_a was found to be 7.56. b) A confocal image of a hippocampal CA3 pyramidal neuron expressing deGFP4 (left). Calibration curve relating the fluorescence ratio of deGFP4 expressing neurons to their intracellular pH (right; n = 7). deGFP4 was used as an emission ratiometric reporter, with excitation at a single wavelength (810 nm) and emission collected simultaneously at two separate windows (450-490 nm and 500-550 nm). The pH response properties of deGFP4 revealed a pK_a of 7.42. c) A confocal image of a hippocampal CA1 pyramidal neuron expressing Cl-sensor (left). Calibration curve relating the fluorescence ratio of Cl-sensor expressing neurons to their intracellular pH (right; n = 7). Cl-sensor was used as an emission ratiometric reporter, with excitation at a single wavelength (850 nm) and emission collected simultaneously at two separate windows (460-500 nm and 520-550 nm). The pH response properties of Cl-sensor revealed a pK_a of 7.73.

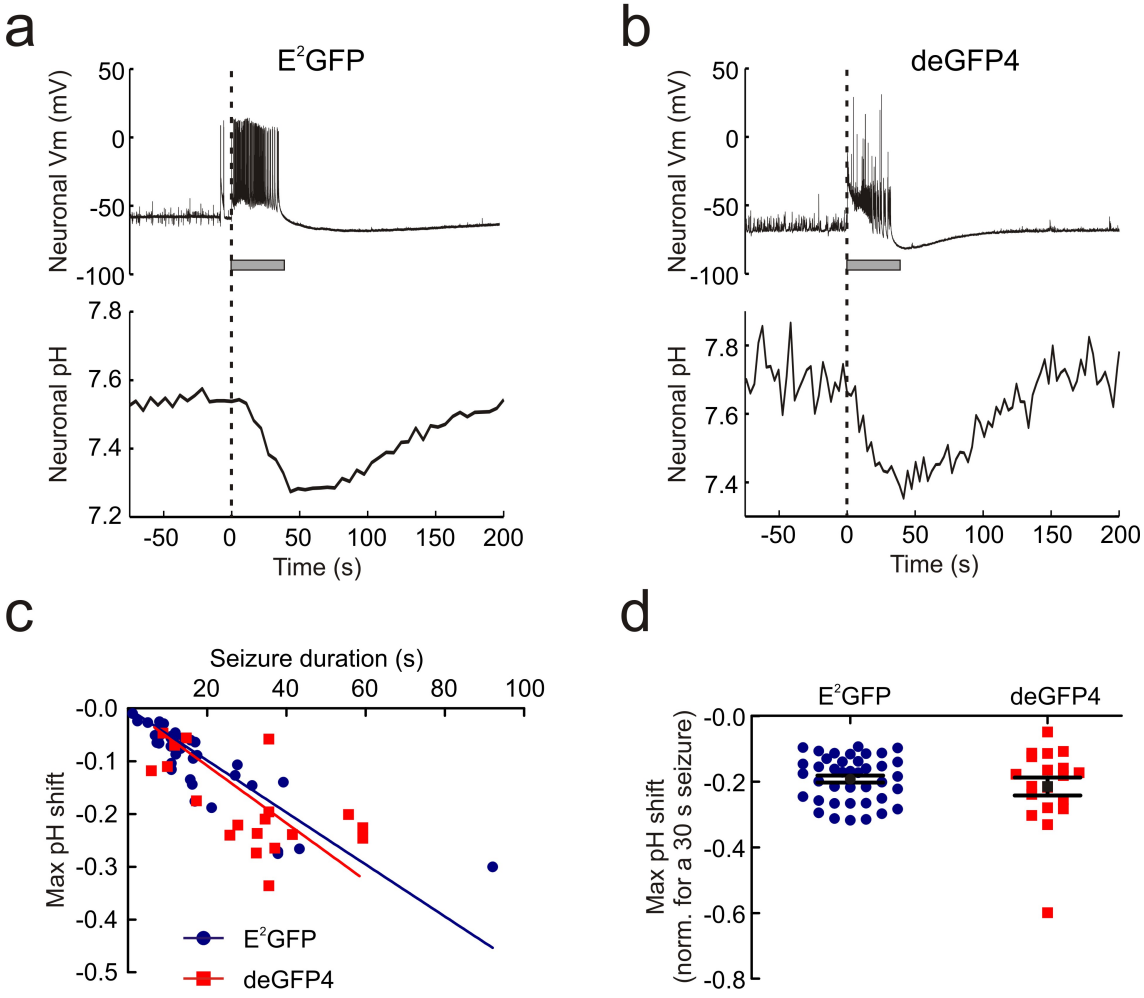

Figure 5.3: 0 Mg^{2+} induced epileptiform activity induces acidic transients in neurons. a) The intracellular pH of a hippocampal CA3 pyramidal neuron transfected with E^2GFP recorded during an episode of 0 Mg^{2+} induced epileptiform activity. The onset of epileptiform activity (dashed line) is correlated with the start of a decrease in intracellular pH. The pH continues to decrease during the seizure and reaches a minimum around the time of seizure termination (seizure duration is depicted by the horizontal grey bar), and then recovers to baseline in the post-seizure period. b) Seizure-associated acidic transients of a similar amplitude were recorded from neurons expressing the pH reporter deGFP4. Although note the greater variance in the signal with this reporter. c) The magnitude of intracellular acidic transients was directly proportional to seizure duration. This relationship was not dependent on the pH reporter used (P = 0.4534, Analysis of Covariance). d) Maximum pH shifts normalised to a 30 s seizure had an average amplitude of 0.20 $\pm$ 0.1 pH units. This was not different for the two pH reporters (P = 0.3581, t test).

5.5 Genetic pH reporters reveal acidic intracellular transients during 0 Cl^- induced epileptiform activity

Having established the ability of genetically encoded reporters to show pH changes during 0 Mg^{2+} seizures, I was interested to test their performance in other models of hyperexcitability. $GABA_A$Rs are primarily permeable to Cl^- (Hamill et al., 1983). Therefore, by removing Cl^- from the aCSF, one is able to profoundly reduce the efficacy of GABAergic inhibition (Yamamoto, 1972; Yamamoto and Kawai, 1968, 1967, 1969; Avoli et al., 1990; Chamberlin and Dingledine, 1988). Removal of Cl^- from the aCSF has the added advantage of preventing potential Cl^- fluxes that may complicate pH measurements from the pH and Cl sensitive genetic reporter Cl-sensor (Markova et al., 2008). Using the 0 Cl^- seizure model I was able to demonstrate that the genetic pH reporters Cl-sensor and deGFP4 are also able to measure a highly significant negative shift in pH during epileptiform activity (Cl-sensor: $P < 0.0001$, n = 40, deGFP4: $P < 0.0001$, n = 48, paired t test). The pH response to 0 Cl^- seizure activity was qualitatively similar to that observed in response to 0 Mg^{2+} induced seizures, with activity causing an acidic transient that reached its maximum near the end of epileptiform episodes, before returning to baseline levels between seizure events (Fig. 5.4a, b). Once again a strong relationship between seizure length and the size of maximum pH shift was apparent for both Cl-sensor and deGFP4 expressing neurons (Cl-sensor: r = -0.5751, P = 0.0001, deGFP4: r = -0.4575, P = 0.0011, Pearson Correlation, Fig. 5.4c). The relationship between seizure length and maximum pH shift was statistically indistinguishable for the two sensors (P = 0.4534, Analysis of Covariance), indicating that the values reported were accurate. And when a linear fit was applied to the pooled data this revealed a seizure-induced population shift of -0.0043 pH units per second of seizure (Fig. 5.4c). When the maximum pH shift from individual seizures was adjusted for a seizure duration of 30 s, the mean pH shift for Cl-sensor neurons was -0.16 $\pm$ 0.01 (n = 40) and for deGFP4 neurons the mean was -0.15 $\pm$ 0.01 pH units (n = 48; Fig. 5.4d).

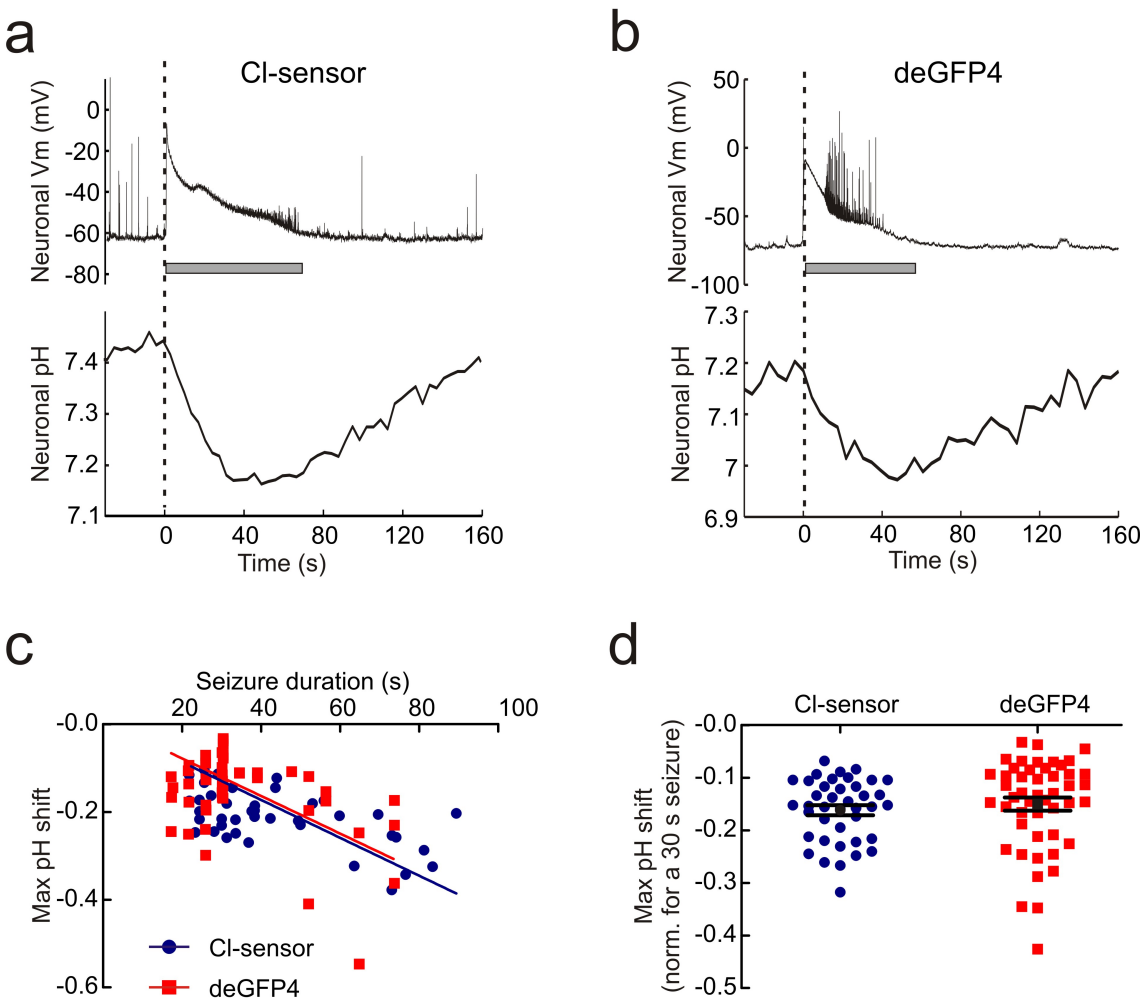

Figure 5.4: 0 Cl^- induced epileptiform activity induces acidic transients in neurons. a) The intracellular pH of a hippocampal CA1 pyramidal neuron transfected with Cl-sensor recorded during an episode of 0 Cl^- induced epileptiform activity. Similar to the 0 Mg^{2+} model, the seizure onset (dashed line) is correlated with the start of a decrease in intracellular pH. The pH continues to decrease during the seizure, reaches a minimum around the time of seizure termination, and then recovers to baseline during the post-seizure period. b) Similar acidic transients were associated with Cl^- induced epileptiform activity in neurons expressing the pH reporter deGFP4. c) The magnitude of intracellular acidic transients was directly proportional to seizure duration. This relationship was not dependent on the pH reporter (P = 0.2721, Analysis of Covariance, Analysis of Covariance). d) Maximum pH shifts normalised to a 30 s seizure had an average amplitude of 0.16 $\pm$ 0.1 pH units. This did not depend on the pH reporter being used (P = 0.4726, t test).

5.6 Genetic reporters reveal differences in the kinetics of acidic intracellular transients

Having established the accuracy and sensitivity of the genetic pH reporters, I investigated whether they were able to detect differences in the kinetics of different seizures. I had observed that 0 Cl^- induced seizures tended to show a maximum depolarising shift in the membrane potential at the onset of the seizure. In contrast, 0 Mg^{2+} induced seizures tended to reach maximal membrane depolarisation at later stages of the seizure (Fig. 5.4a, b). Indeed, across the population data the time of peak membrane potential depolarisation relative to seizure duration occurred significantly earlier in 0 Cl^- (27.0 $\pm$ 1.3% of seizure duration, n = 88) as compared to 0 Mg^{2+} seizures (70.9 $\pm$ 3.2% of seizure duration, n = 59; $P < 0.0001$, *t* test, Fig. 5.5c). To address whether these different seizure kinetics were associated with different intracellular pH dynamics I examined the time course of the acidic transients recorded, pooling data across the three genetic reporters. Consistent with the membrane potential measurements, I found that the time of the maximum pH shift occurred significantly earlier for 0 Cl^- seizures than for 0 Mg^{2+} seizures (P = 0.0031, *t* test, Fig. 5.5d). In the case of 0 Cl^- the maximum acidic shift was reached at 109.7 3.2% of seizure duration (n = 88), whereas in the case of 0 Mg^{2+} the maximum acidic shift was reached at 130.5 7.0% (n = 59) of seizure duration. Similarly, intracellular pH returned to baseline more rapidly in the 0 Cl^- model than the 0 Mg^{2+} model. pH recovered by 279.4 $\pm$ 12.1% of seizure duration following 0 Cl^- seizures (n = 58), whereas it required until 391.5 $\pm$ 26.7% of seizure duration to recover following 0 Mg^{2+} seizures (n = 31, $P < 0.0001$, *t* test, Fig. 5.5e). These data are consistent with the time course of membrane depolarisation recorded in the two epilepsy models (Fig. 5.5c) and indicate that the genetic reporters are able to capture differences in the kinetics of activity-dependent pH changes.

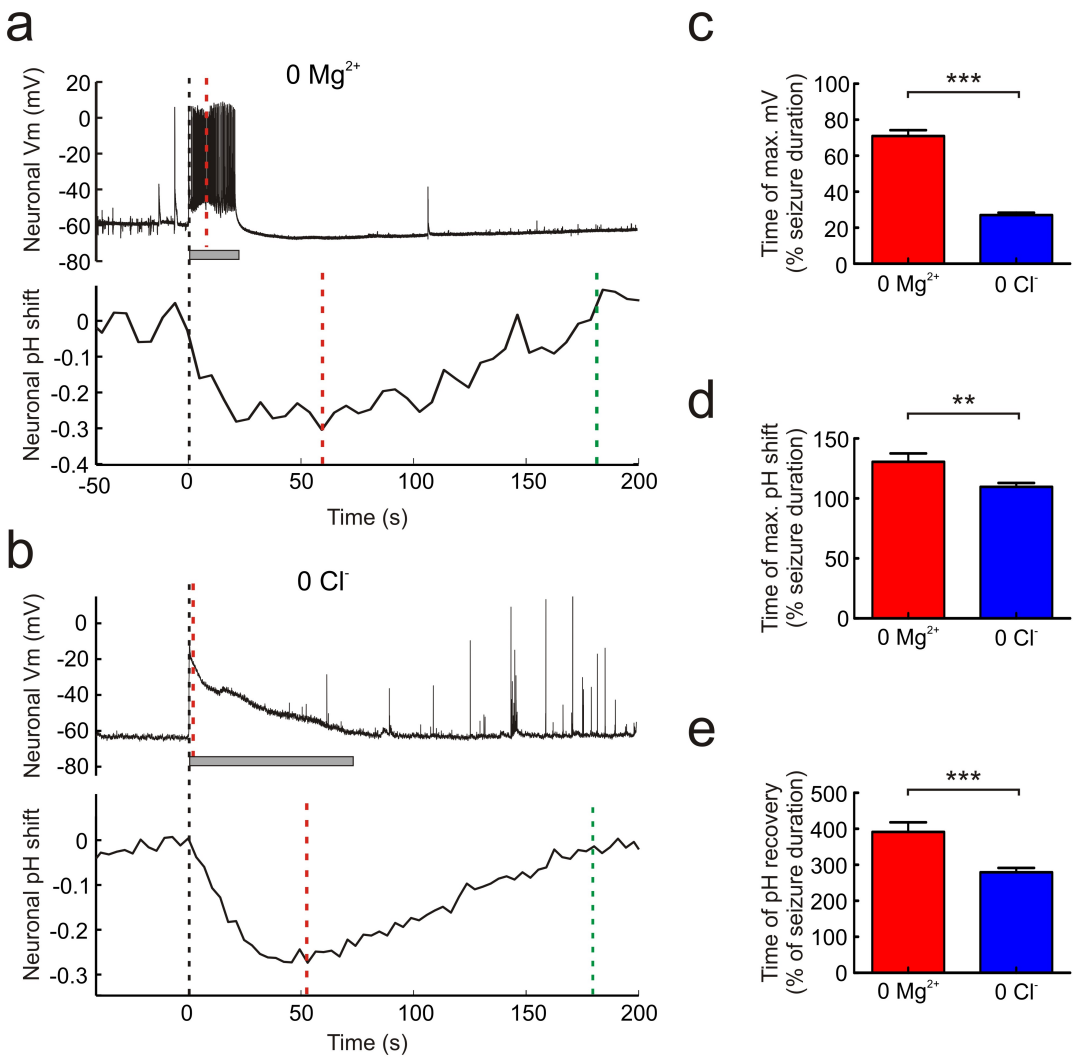
a
0 Mg2+
Neuronal Vm (mV)
20
0
-20
-40
-60
-80
Neuronal pH shift
0
-0.1
-0.2
-0.3
-0.4
-50
0
50
100
150
200
Time (s)
b
0 Cl-
Neuronal Vm (mV)
0
-20
-40
-60
-80
Neuronal pH shift
0
-0.1
-0.2
-0.3
0
50
100
150
200
Time (s)
c
Time of max. mV (% seizure duration)
***
100
80
60
40
20
0
0 Mg2+
0 Cl-
d
Time of max. pH shift (% seizure duration)
**
150
100
50
0
0 Mg2+
0 Cl-
e
Time of pH recovery (% of seizure duration)
***
500
400
300
200
100
0
0 Mg2+
0 Cl-

5.7 Genetic reporters of pH reveal seizure induced intracellular alkaline transients in hippocampal astrocytes

Previous work has suggested that depolarisation induced intracellular pH transients may differ between astrocytes and neurons (Bevensee et al., 1997; Grichtchenko and Chesler, 1994; Pappas and Ransom, 1994; Chesler, 2003). Here, I present the first evidence (to my knowledge) that astrocytes experience substantial alkaline transients during epileptiform activity. As described previously, epileptiform activity within an organotypic hippocampal slice culture was monitored via a whole cell patch recording from a pyramidal cell within 200 μm of the astrocyte of interest. Astrocytes were identified by their location (within Stratum radiatum) and morphology. Two broad morphological groups were observed, the first included cells with small somata and multiple fine processes (protoplasmic astrocytes). The second group included multipolar cells with irregularly shaped, elongated somata with more than two large processes emanating in different directions (fibrous astrocytes). These two groups are consistent with previous reports of astrocytic morphologies in the hippocampus (Benediktsson et al., 2005). A typical example of an astrocyte biolistically transfected with the pH sensor E^2GFP is shown in Fig. 5.6b. Con-

---

Figure 5.5 *(facing page)*: The kinetics of acidic transients and epileptiform activity differ between seizure models. a) The membrane potential (upper trace) of a hippocampal CA1 pyramidal neuron during a 0 Mg^{2+} induced seizure episode (seizure duration of 21 s, indicated by the grey bar). The membrane potential reaches its maximum (red dashed line) midway through the seizure. Simultaneous recording of a neighbouring pyramidal neurons intracellular pH (lower trace) reveals that this does not reach its minimum (red dashed line) until 35 s after the seizure terminates and recovers (green dashed line) by approximately 160 s following the end of the seizure. b) The membrane potential (upper trace) of a CA1 pyramidal neuron during a 0 Cl^- induced seizure episode (seizure duration of 69 s, indicated by the grey bar). Unlike the 0 Mg^{2+} induced seizure, the membrane potential reaches its peak (red dashed line) almost immediately after the seizure begins. Simultaneous recording of a neighbouring pyramidal neurons intracellular pH (lower trace), reveals that the intracellular pH reaches its minimum (red dashed line) 23 s before the seizure ends and returns to baseline (green dashed line) approximately 105 s after the end of the seizure episode. c) The time to reach maximum membrane depolarisation as a percentage of seizure duration was significantly longer for 0 Mg^{2+} as opposed to 0 Cl^- induced seizures (***$P < 0.0001$, *t* test). d) The time to reach maximum intracellular pH shift as a percentage of seizure duration was also significantly longer for 0 Mg^{2+} as opposed to 0 Cl^- induced seizures (**P = 0.0031, *t* test). e) Similarly, the time of pH recovery as a percentage of seizure duration was significantly longer for 0 Mg^{2+} as compared to 0 Cl^- induced seizures (***$P < 0.0001$, *t* test).

focal imaging of this cell revealed that seizure episodes were reliably associated with synchronous intracellular alkaline transients (Fig. 5.6a). Astrocytic intracellular pH was found to increase immediately following seizure onset, and to return to baseline shortly after the end of an epileptiform episode (Fig. 5.6a and Fig. 5.7a,b). In order to confirm the identity of the cell shown in Fig. 5.6a,b it was targeted for whole cell patch recording and its astrocytic phenotype confirmed electrophysiologically. Consistent with previous reports (Kang et al., 1998) the cell exhibited a low resting membrane potential (-81.2 mV), low membrane resistance (41.3 mΩ) and inability to spike in response to large current injection (Fig. 5.6c). To further confirm the accuracy of the identification of astrocytes from morphological criteria, a subset of these cells were whole cell patched and characterised electrophysiologically. In all cases (n = 5 out of 5 cells), a low resting membrane potential (-77 $\pm$ 2.9 mV), low membrane resistance (28.8 $\pm$ 4.9 mΩ) and inability to fire action potentials was confirmed.

Having confirmed the experimental setup I conducted a population study of hippocampal astrocytes in order to quantify the absolute pH changes that occur during two different seizure models. I found that astrocytes undergo a highly significant positive shift in pH during 0 Mg^{2+} induced epileptiform activity ($P < 0.0001$, n = 25, *t* test, pooled data using E^2GFP and deGFP4). Similarly, 0 Cl^- induced epileptiform activity was also associated with a highly significant alkaline shift in astrocytic pH ($P < 0.0001$, n = 63, *t* test, pooled data using deGFP4 and Cl-sensor). As Fig. 5.7a and 5.7b demonstrate, the intracellular pH of hippocampal astrocytes increased from baseline following the onset of epileptiform activity, then re-acidified to pre-seizure levels, at or shortly after, seizure cessation. The mean maximum pH shift in response to 0 Mg^{2+} induced epileptiform activity was 0.19 pH $\pm$ 0.022 units (n = 25, Fig. 5.7e). Similarly, the mean maximum pH change in response to 0 Cl^- seizures was 0.16 $\pm$ 0.012 pH units (n = 63, Fig. 5.7c). The astrocytic alkaline transients elicited by epileptiform activity were not significantly different between the two seizure models used (P = 0.1881, *t* test).

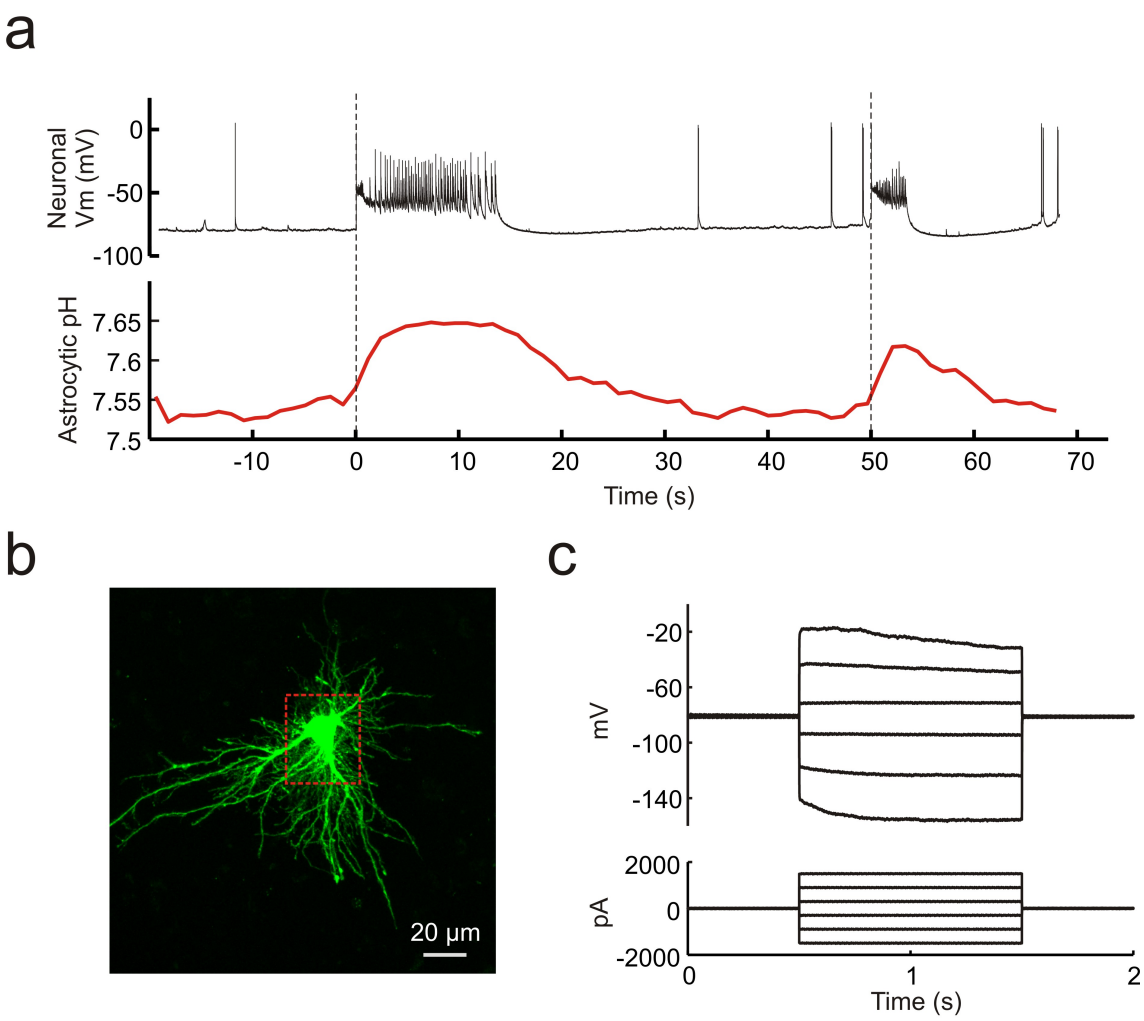

Figure 5.6: Genetic reporters of pH reveal seizure induced intracellular alkaline transients in hippocampal astrocytes. a) Dynamic intracellular pH measurements imaged from the astrocyte shown in 'b' (lower trace). A neuron in close proximity was whole cell patched and the membrane potential recorded over time in current clamp mode (upper trace). Perfusion of the slice with 0 Mg^{2+} induced periods of epileptiform activity characterised by membrane depolarisation and high frequency firing, the onset of which is depicted by dashed lines. Note the marked alkaline shifts in pH that are associated with epileptiform activity. (b) A confocal image of the hippocampal astrocyte in 'a' expressing the pH indicator E^2GFP. The dashed rectangle demarcates the region of interest used to estimate intracellular pH. c) A whole cell patch clamp of the astrocyte in 'b'. Consistent with an astrocytic electrophysiological phenotype, the cell had a low membrane resistance (R_m = 41.3 mΩ), low resting membrane potential (-91.2 mV) and did not exhibit voltage-gated conductances in response to current injection.

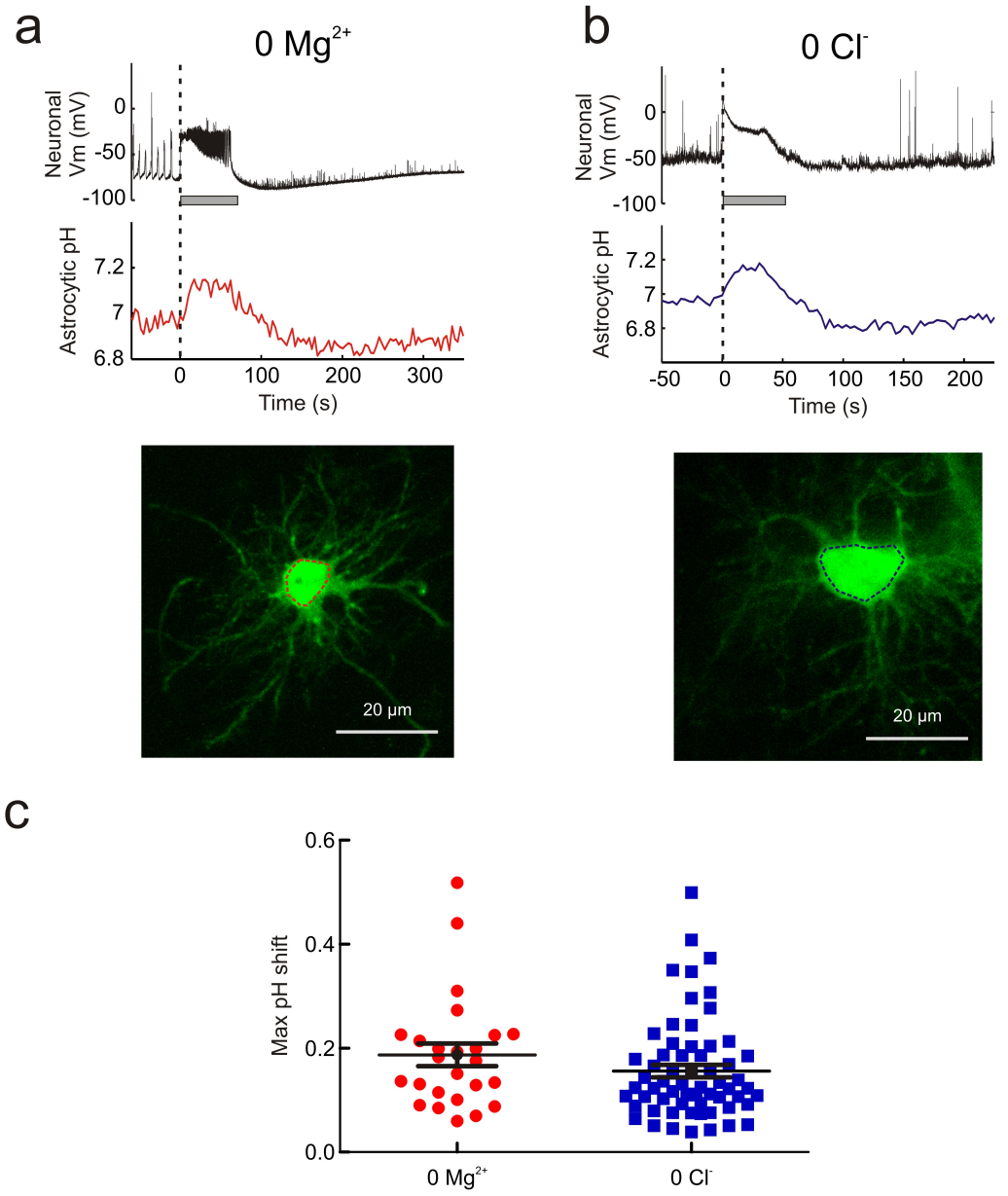

Figure 5.7: The 0 Mg^{2+} and 0 Cl^- seizure models induce alkaline transients in hippocampal astrocytes. a) The intracellular pH of a hippocampal astrocyte transfected with deGFP4 (bottom) recorded during an episode of 0 Mg^{2+} induced epileptiform activity. The onset of epileptiform activity (dashed line) was correlated with the start of an increase in intracellular pH. The pH continued to increase during the seizure, reached a plateau and then recovered to baseline around the time of seizure termination (seizure duration is depicted by the horizontal grey bar). b) Seizure-associated alkaline transients of a similar amplitude were recorded from an astrocyte expressing the pH reporter Cl-sensor (bottom) using the 0 Cl^- model of epileptiform activity. c) Maximum pH shifts across both seizure models had an average amplitude of 0.16 $\pm$ 0.01 pH units. This was not different between the two separate seizure models (P = 0.19, t test).

5.8 Seizure induced intracellular pH transients differ between hippocampal astrocytes and neurons

The data reported above reveal that epileptiform activity results in very different pH changes in hippocampal neurons and astrocytes. In this section I was keen to further examine the differences between neurons and astrocytes. The maximum pH shifts generated by 0 Mg^{2+} seizures in hippocampal astrocytes, as compared to pyramidal neurons, were opposite in direction and highly statistically different (Fig. 5.8a, $P< 0.0001$, *t* test). The same was true for intracellular pH responses recorded during 0 Cl^- induced epileptiform activity (Fig. 5.8a, $P< 0.0001$, *t* test). The examples in Fig 5.8b and Fig. 5.8c depict imaging of intracellular pH dynamics in response to epileptiform activity in a neuron and then an astrocyte within the same hippocampal brain slice. During similar seizure episodes (Fig 5.8b,c, top), the astrocyte (red) became alkaline whilst the neuron (blue) acidified. This was true for seizures generated in 0 Mg^{2+} (Fig. 5.8b left) or 0 Cl^- (Fig. 5.8c right). In order to characterise these different pH responses at a population level, seizures between 15 s and 35 s were selected for pH and membrane voltage averaging. The data for astrocytic and neuronal pH responses for 0 Mg^{2+} (d) and 0 Cl^- (e) seizures is displayed in Fig. 5.8. This population data reveals that for very similar seizure events, the pH shifts are not only opposite in direction for astrocytes and neurons, but they also have different kinetics. Astrocytic pH transients appear to return to baseline more quickly than neuronal pH shifts.

In order to compare the kinetics between the cell types I defined the point of maximum pH change. The point of maximum pH change (pink dashed line in Fig. 5.9a and b) was considerably later in neurons than in astrocytes. During 0 Mg^{2+} seizures, the peak pH shift in astrocytes occurred at 71.27 $\pm$ 5.18% (n = 25) of seizure duration as compared to 134.5 $\pm$ 7.68% (n = 30) in neurons (Fig. 5.9c, $P < 0.0001$, *t* test). This difference was similar in 0 Cl^- seizures where astrocytic pH had shifted maximally by 62.42 $\pm$ 2.707% (n = 63) of seizure length compared to 111.4 $\pm$ 3.15% (n = 85) in neurons (Fig. 5.9c, $P < 0.0001$, *t* test). In summary, while astrocytes reached maximal alkalinity approximately halfway during the seizure, neurons appeared to be most acidic at, or shortly following, the cessation of seizure activity.

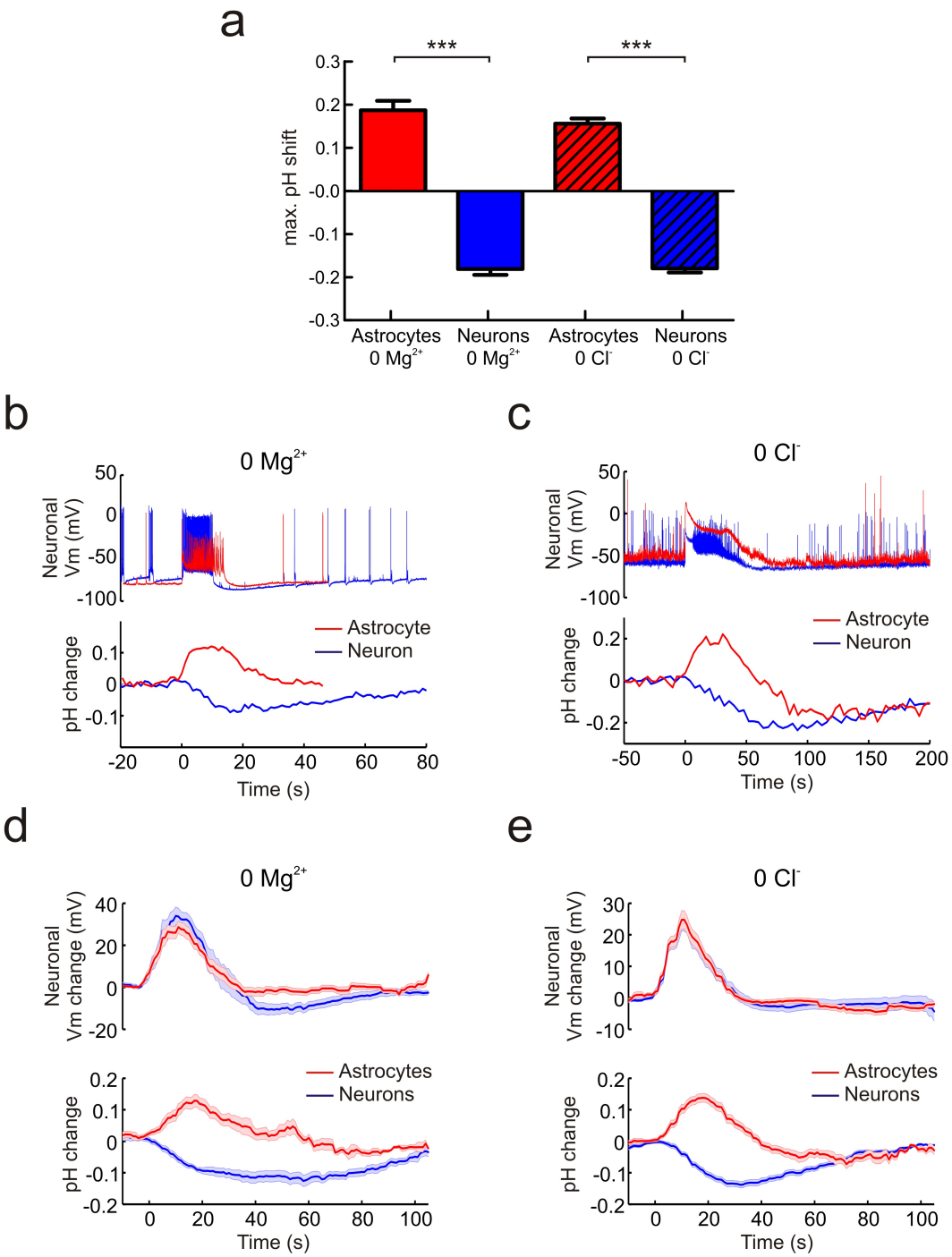
a
***
***
max. pH shift
0.3
0.2
0.1
-0.0
-0.1
-0.2
-0.3
Astrocytes 0 Mg2+
Neurons 0 Mg2+
Astrocytes 0 Cl-
Neurons 0 Cl-
b
0 Mg2+
Neuronal Vm (mV)
50
0
-50
-100
Astrocyte
Neuron
pH change
0.1
0
-0.1
-20
0
20
40
60
80
Time (s)
c
0 Cl-
Neuronal Vm (mV)
50
0
-50
-100
Astrocyte
Neuron
pH change
0.2
0
-0.2
-50
0
50
100
150
200
Time (s)
d
0 Mg2+
Neuronal Vm change (mV)
40
20
0
-20
Astrocytes
Neurons
pH change
0.2
0.1
0
-0.1
-0.2
0
20
40
60
80
100
Time (s)
e
0 Cl-
Neuronal Vm change (mV)
30
20
10
0
-10
Astrocytes
Neurons
pH change
0.2
0.1
0
-0.1
-0.2
0
20
40
60
80
100
Time (s)

The kinetics of pH recovery following epileptiform activity was also found to be delayed in neurons compared to astrocytes (Fig. 5.9). Whilst astrocytes returned to baseline shortly after the end of a seizure, (138.8 $\pm$ 7.47%, n = 25, and 136.1 $\pm$ 3.95%, n = 62, of seizure duration in 0 Mg^{2+} and 0 Cl^- seizures respectively), the intracellular pH of neurons took markedly longer to recover (369.0 $\pm$ 22.75%, n = 21, and 311.5 $\pm$ 14.10%, n = 39). This difference was highly statistically significant for both of the seizure models employed ($P < 0.0001$, *t* test, Fig. 5.9d). This data shows that the kinetics of seizure associated pH transients are different between astrocytes and neurons.

5.9 The astrocytic alkaline transient is mediated by a Na^+ / HCO_3^- cotransporter

Previous work has suggested that the primary mediator of activity dependent alkalinisation in astrocytes is the Na^+/HCO_3^- cotransporter NBCe1 (Bevensee et al., 1997; Chesler and Kraig, 1989). This transporter is electrogenic, meaning that upon glial depolarisation HCO_3^- and Na^+ influx is accelerated. Consistent with the idea that NBCe1 generated the seizure induced alkaline shift, I found that removal of extracellular HCO_3^- (by replacing HCO_3^- with HEPES in the aCSF and bubbling the solution with 100% O_2) resulted in a significant reduction in the magnitude of the astrocytic alkalinisation (P = 0.0135, *t* test, Fig. 5.10a-c). Interestingly, blockade of the astrocytic alkalinisation appeared to reveal an underlying acid transient in the astrocytes similar to that seen in neurons (Fig. 5.10b).

Figure 5.8 *(facing page)*: Seizure induced intracellular pH transients differ between hippocampal astrocytes and neurons. a) Maximal seizure associated pH shifts were in the opposite direction for these two cell types. Whilst intracellular pH became more acidic in neurons in response to epileptiform activity, it became more alkaline in astrocytes. This difference was highly statistically significant regardless of the seizure model employed, $^{***}P < 0.0001$ for both, *t* test. b) Sequential imaging of intracellular pH dynamics in response to epileptiform activity in a CA3 pyramidal neuron (bottom, blue) and an astrocyte (bottom, red) within the same slice. The neuron acidifies, whilst the astrocyte became more alkaline, despite responding to similar 0 Mg^{2+} induced seizure episodes (top). The neuronal membrane potential changes are colour coded depending on the cell type that was imaged concurrently. c) A similar pattern of cell type specific intracellular pH shifts was observed in a different slice where epileptiform activity was induced using 0 Cl^- aCSF. Population data from seizures between 15 s and 35 s duration for 0 Mg^{2+} d) and 0 Cl^- e) seizures confirms the difference between astrocytic and neuronal activity dependent intracellular pH transients.

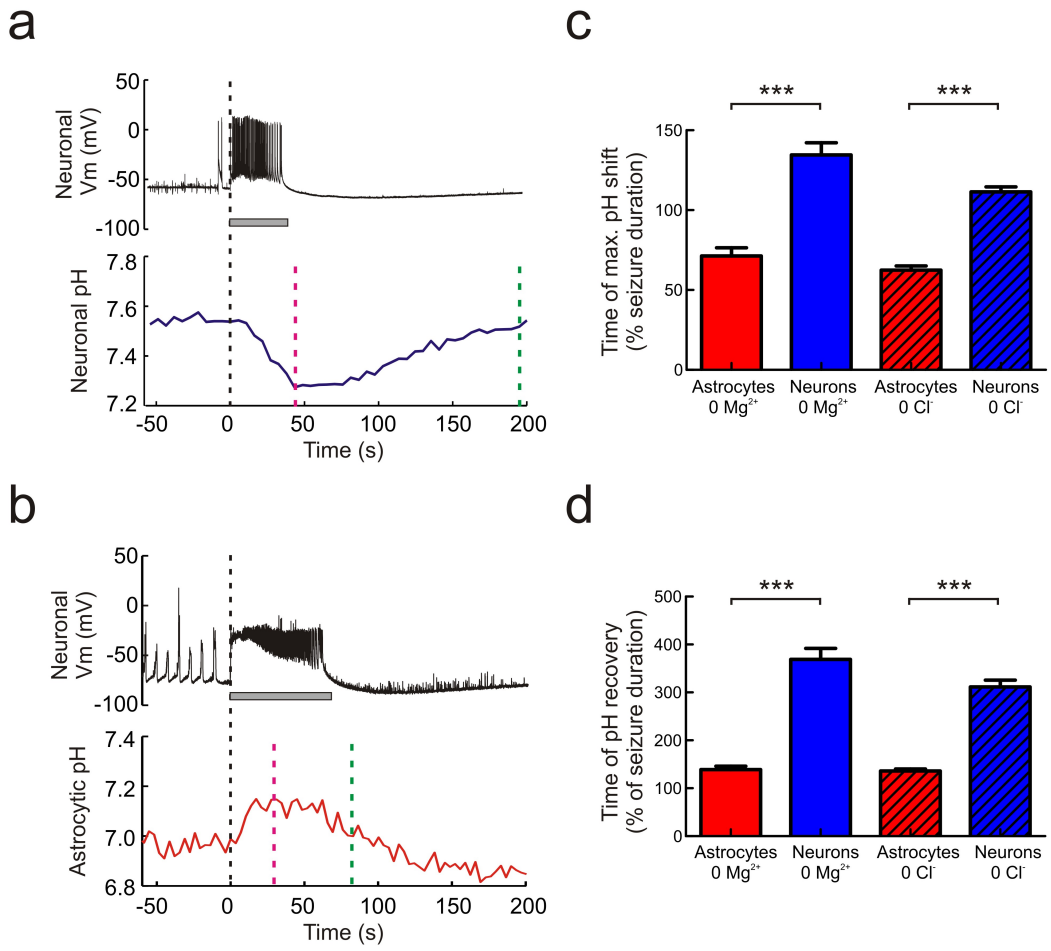

Figure 5.9: The kinetics of seizure induced pH transients differ between hippocampal astrocytes and neurons. a) The membrane potential (upper trace) of a hippocampal CA3 pyramidal neuron during a 0 Mg^{2+} induced seizure episode (seizure duration of 39 s, indicated by the grey bar). Simultaneous recording of a neighbouring pyramidal neuron's intracellular pH (lower trace) revealed that this reached its minimum (pink dashed line) 2 s after the seizure terminated and recovered (green dashed line) approximately 150 s following the end of the seizure. b) The membrane potential (upper trace) of a hippocampal neuron during a separate 0 Mg^{2+} induced seizure episode (seizure duration of 71 s, indicated by the grey bar). Simultaneous recording of a neighbouring astrocyte's intracellular pH (lower trace), reveals that the intracellular pH reaches its maximum (pink dashed line) 43 s before the seizure ends and returns to baseline (green dashed line) approximately 13 s after the end of the seizure episode. c) The time to reach maximum intracellular pH shift as a percentage of seizure duration was significantly shorter for astrocytes than for neurons during both 0 Mg^{2+} and 0 Cl^- induced epileptiform activity (***$P < 0.0001$ for both seizure models, *t* test). d) Similarly, the time for pH to recover to baseline was significantly shorter for astrocytes than for neurons in both seizure models (***$P < 0.0001$ for both 0 Mg^{2+} and 0 Cl^- induced seizures, *t* test).

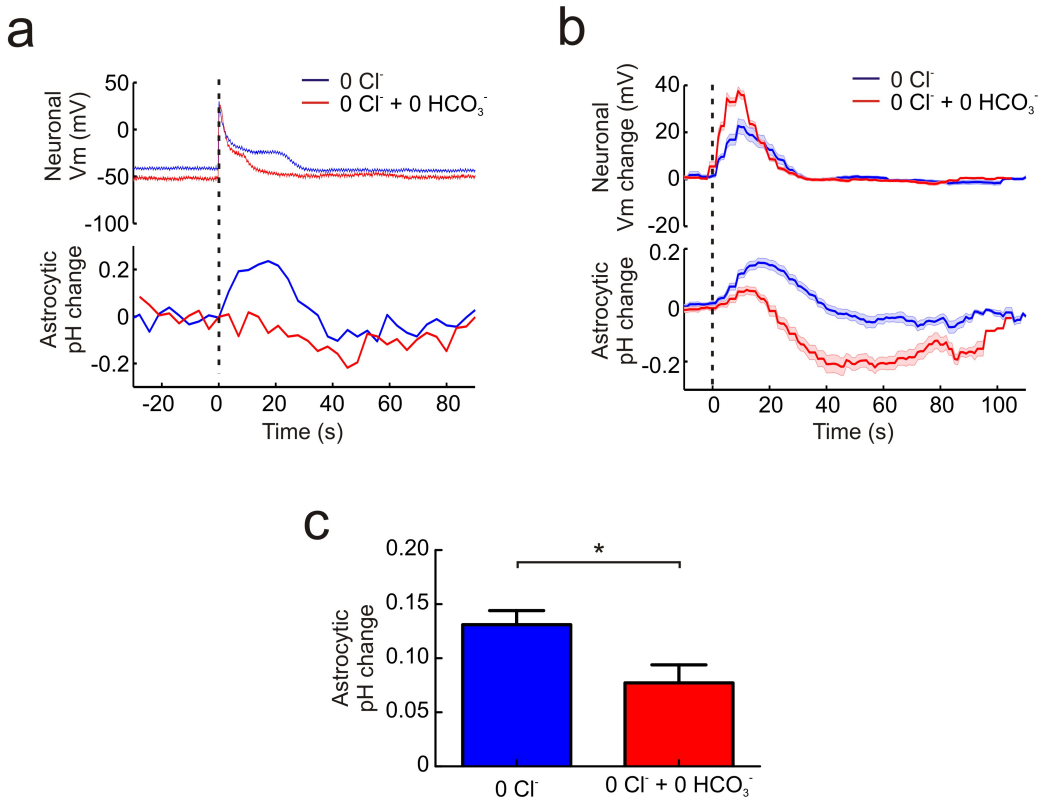

Figure 5.10: The seizure induced alkaline transient in astrocytes depends on HCO_3^-. a) The membrane potential (upper traces) of a hippocampal neuron recorded during a 0 Cl^- induced seizure episode (blue) and the same neuron recorded during a seizure episode with nominal extracellular HCO_3^- (red). Simultaneous recording of a neighbouring astrocyte's intracellular pH (lower traces) revealed that removal of HCO_3^- abolished the seizure induced astrocytic alkaline transient. b) Population data from multiple seizures and cells demonstrates the effect of HCO_3^- removal (lower red trace in 'b') on the magnitude and time course of seizure induced alkaline transients in astrocytes. HCO_3^- removal also appeared to reveal an apparent activity-dependent acidic transient in astrocytes. c) HCO_3^- removal caused a statistically significant reduction in the size of the seizure induced alkaline transient ('c', $*P = 0.0135$, *t* test).

Recent work has shown that the N-cyanosulphonamide compound, S0859, selectively inhibits Na^+ / HCO_3^- cotransport within cardiac tissue (Ch'en, Villafuerte, Swietach, Cobden and Vaughan-Jones, 2008). To test whether this compound has any effect upon astrocytic alkaline transients and / or epileptiform activity within the central nervous system, a full inhibitory concentration of S0859 (50 μM) was added to the slice perfusate following the induction of 0 Cl^- induced seizures. S0859 was found to significantly reduce the magnitude of 0 Cl^- seizure induced alkalinisation in hippocampal astrocytes (P = 0.0012, t test, Fig. 5.11a,c,e) and this was associated with a marked alteration in 0 Cl^- seizure morphology. As Fig. 5.11b and Fig. 5.11d demonstrate, S0859 reduced the amplitude and length of 0 Cl^- induced epileptiform activity, as measured by membrane potential fluctuations in hippocampal pyramidal neurons.

5.10 Discussion

In this chapter I investigated the potential for genetically encoded pH reporters to measure neuronal and astrocytic intracellular pH transients associated with periods of elevated activity. I then used these reporters to quantify the pH dynamics in neurons and astrocytes during seizure activity.

Using a combination of patch clamp recordings and two-photon or single-photon confocal imaging in hippocampal brain slices, I assessed the performance of three different pH-sensitive fluorescent proteins. All three pH sensors were able to report acidic shifts associated with epileptiform activity, although there were differences in terms of their sensitivity, signal-to-noise and utility for activity-dependent studies. For this work, I chose three ratiometric reporters of pH: E^2GFP, deGFP4 and Cl-sensor (Bizzarri et al., 2006; Hanson et al., 2002; Markova et al., 2008). While a number of non-ratiometric GFP-derived pH indicators exist, these are susceptible to measurement artefacts caused by variations in excitation path length, indicator concentration, illumination stability, cell thickness and indicator distribution (Hanson et al., 2002). In addition, non-ratiometric reporters cannot accurately record absolute pH without laborious within cell calibration. In contrast, ratiometric reporters overcome many of these issues. The genetically encoded ratiometric reporters can be classified into two groups, those that are constituted by a single GFP mutant and those that are a fusion of the pH-sensitive YFP with a less

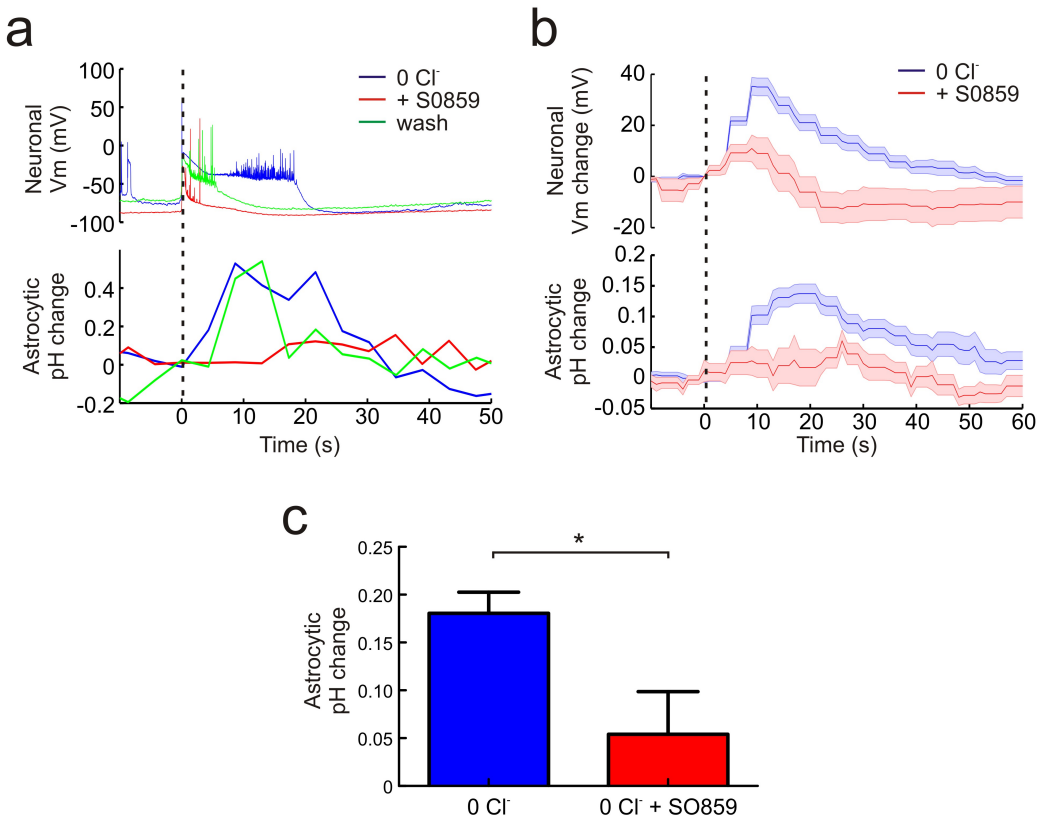

Figure 5.11: S0859 affects astrocytic alkaline transients and 0 Cl^- induced seizures. a) The membrane potential (upper traces) of a hippocampal neuron during 0 Cl^- induced seizures before (blue), during (red) and after (green) application of 50 μM S0859. Simultaneous recording of a neighbouring astrocyte's intracellular pH (lower trace) revealed that S0859 reversibly inhibits seizure induced astrocytic alkalinisation. Population data from multiple seizures and cells demonstrates the effect of S0859 (lower red trace in 'b') on the magnitude and time course of seizure induced alkaline transients in astrocytes. However, S0859 also considerably reduced seizure associated membrane depolarisation, particularly during the later stages of epileptiform activity (top traces in 'a' and 'b'). c) S0859 application caused a statistically significant reduction in the size of the seizure induced alkaline transient ('c', $*P = 0.0012$, t test).

pH-sensitive GFP variant such as CFP (Bizzarri et al., 2009). The former group includes ratiometric pHlourin (RaGFP), deGFP4 and E^2GFP (Miesenböck, 1998; Hanson et al., 2002; Bizzarri et al., 2006). I utilised deGFP4 as it is the only ratiometric pH indicator that has been convincingly established for two-photon use (Hanson et al., 2002). E^2GFP was selected because it is optimally excited with wavelengths that are common to Argon-ion lasers, which facilitates its use with confocal microscopy. Under my imaging conditions I found that deGFP4 and E^2GFP could report intracellular pH with a similar pK_a. However, data gathered using deGFP4 was considerably noisier, most likely due to the weak fluorescence emitted by deGFP4 in the blue wavelength range (Hanson et al., 2002). E^2GFP proved to be an excellent ratiometric indicator by excitation although, as is common to indicators used in this fashion, accurate intracellular pH recordings required correction for independent power fluctuations associated with the two excitation laser lines (see Materials and Methods) (Arosio et al., 2010).

Reporters based upon YFP fusions include YFpH, pHlameleon, clomeleon and Cl-sensor (Awaji and Hirasawa, 2001; Esposito et al., 2008; Kuner and Augustine, 2000; Markova et al., 2008). YFP fluorescence is quenched by both Cl^- and H^+ ions and, as a result, YFP fusion proteins are sensitive to both intracellular pH and Cl^- concentration Jayaraman et al. (2000). This dual sensitivity complicates the interpretation of in vivo measurements using these probes, particularly as neuronal processes often involve either the related, or independent, flux of both Cl^- and H^+ ions (Tabb et al., 1992; Doyon et al., 2011). Attempts to reduce the Cl^- sensitivity of YFP by inducing mutations in the Cl^- binding pocket produced mutants with a low pK_a, that is less suited for physiological pH measurements (Griesbeck et al., 2001). I circumvented the issue of dual sensitivity by utilising a Cl^- free model of epilepsy in order to test the pH sensitivity of the YFP fusion protein, Cl-sensor. This ensured that the activity-dependent fluctuations in fluorescence ratio were more likely to be attributable to changes in intracellular H^+ ion concentration. Under these specific conditions, Cl-sensor proved to be an excellent ratiometric pH indicator by emission, with a signal to noise ratio comparable to that of E^2GFP. This shows that Cl-sensor can be used as a reporter of intracellular pH dynamics and equally that the dual ion-sensitivity of this reporter (and presumably that of closely-related YFP fusion proteins such as Clomeleon; (Kuner and Augustine, 2000), should be considered

when examining activity-dependent changes. One additional point is that despite employing two-photon excitation, pH measurements using Cl-sensor sometimes exhibited slow baseline drift, presumably as a result of the differential bleaching rates experienced by the YFP as opposed to the CFP fluorophore Tramier et al. (2006); Bregestovski et al. (2009).

Previous studies investigating activity-dependent intracellular pH transients have employed either pH-sensitive microelectrodes or pH-sensitive dyes (Rose and Deitmer, 1995; Xiong et al., 2000). Due to their size, the use of microelectrodes to measure pH has been mostly confined to large neurons. pH-sensitive dyes meanwhile are widely used to report intracellular pH and several classes exist including fluoresceins, benzoxanthenes, rhodols and pyrenes. The fluorescein derivatives, 2'-7'-bis(carboxyethyl)-5(6)-carboxyfluorescein (BCECF) and carboxyseminaphthorhodafluor- I (carboxy-SNARF-1) are by far the most popular. These two dyes are suitable for use as ratiometric pH indicators and have desirable optical properties. In addition, both dyes are available as acetoxymethyl (AM) esters, which facilitates intracellular loading without the use of micropipettes. However, fluorescein dyes have a potentially significant disadvantage, which may be particularly relevant to studies of activity-dependent proton fluxes within the nervous system. Fluorescein analogues have been shown to inhibit the Ca^{2+}/H^{+} ATPase Gatto and Milanick (1993); Chesler (2003). This ATP dependent transporter extrudes Ca^{2+} in exchange for H^{+}. As Ca^{2+} influx is a primary feature of neuronal membrane depolarisation, the restoration of low Ca^{2+} via this exchanger is thought to be an important mechanism by which protons accumulate during network activity (Schwiening et al., 1993; Svichar et al., 2011).

Employing three different genetically encoded pH indicators and two separate models of epilepsy I have shown that epileptiform activity lasting on the order of 30 s generates intracellular acidic shifts of between 0.1 and 0.3 pH units. This is an order of magnitude larger than previous estimates (Xiong et al., 2000), and there are several possible explanations for this difference. Firstly, in contrast to Xiong et al. (2000), who employed a non-synaptic Ca^{2+} free model of epileptiform activity, we utilised models that left the majority of synaptic transmission intact and either elevated synaptic excitation (0 Mg^{2+}) or reduced synaptic inhibition (0 Cl^{-}). As Ca^{2+} is known to accompany neuronal activity, the role of H^{+} import via the Ca^{2+} / H^{+} ATPase (see above) may contribute to the observed

difference in acidic transient magnitude observed. Another factor is likely to be the differences in imaging methods. Xiong and colleagues averaged fluorescence changes across regions of tissue, which presumably included different cell types (e.g. neurons and glial cells) and fluorescence from dye that is not exposed to pH changes. By restricting our imaging to individual hippocampal pyramidal neurons, the data from the genetic reporters should more accurately reflect the magnitude of seizure induced intracellular acidic transients, at least in this cell type. These observations suggest that the degree of acidification in neurons is more pronounced than previously appreciated and this should be considered in future studies of network activity and epilepsy.

Simultaneous electrophysiological recordings also enabled me to assess the temporal properties of seizure induced acidic transients in hippocampal pyramidal neurons. Consistent with previous work, I found that the time of maximum acidity correlated with seizure termination (Xiong et al., 2000). This is consistent with the idea that activity-dependent intracellular acidification may serve as a local feedback signal that dampens network excitability (Chesler, 2003). I was also able to detect differences in the temporal properties of pH shifts induced by the two separate seizure models. The 0 Mg^{2+} seizure model resulted in maximum pH shifts and recovery times that occurred relatively later than those induced by the 0 Cl^- seizure model. This most likely reflects the fact that following seizure onset, 0 Mg^{2+} seizures typically displayed a progressive increase in seizure intensity, whilst the 0 Cl^- seizures reached maximum depolarization almost immediately after the start of the seizure. These observations suggest that the pattern of neural activity is linked to the kinetics of pH changes and it will be interesting to explore this relationship in future studies.

These experiments did not investigate the molecular mechanisms underlying seizure induced acidification. However, at least three major processes are likely to be involved. Firstly, as described earlier, a fall in pH is linked to the activity induced entry of Ca^{2+} due to the function of Ca^{2+}/H^+ ATPases located in the plasma membrane and endoplasmic reticulum (Schwiening et al., 1993; Makani and Chesler, 2010*a*). Secondly, prolonged neural activity will increase the production of metabolic acids such as CO_2 and lactate (Wang et al., 1994). And thirdly, the intense $GABA_AR$ activation that accompanies seizure activity has been shown to result in considerable HCO_3^- efflux and a resulting intracellular

acidification (Pasternack et al., 1993; Trapp et al., 1996).

In contrast to the acidic intracellular pH responses seen in neurons, astrocytes have been shown to become more alkaline during membrane depolarisation (Bevensee et al., 1997; Grichtchenko and Chesler, 1994; Pappas and Ransom, 1994; Chesler, 2003). For the first time however, I have shown alkaline pH shifts in astrocytes in response to epileptiform activity. In addition, by leveraging my ability to monitor pH transients in two separate cell types in the same preparation, I have been able to show that neurons and astrocytes display markedly different seizure induced pH kinetics.

Both the 0 Mg^{2+} and 0 Cl^{-} seizure models elicited alkaline pH shifts in astrocytes on the order of 0.2 pH units. This is similar in magnitude to the depolarisation induced positive pH shifts seen in cultured astrocytes (Grichtchenko and Chesler, 1994; Pappas and Ransom, 1994) and astrocytes recorded in vivo during episodes of spreading depression (Chesler and Kraig, 1989). A recent methodological paper has suggested that biolistic transfection of GFP in organotypic slice cultures represents the optimal way of identifying astrocytes morphologically (Benediktsson et al., 2005). This is because sparse labelling of cells and uniform expression of the fluorophore throughout the cytoplasm allow the fine processes typical of astrocytes to be resolved. Taking advantage of this approach, biolistic transfection of GFP-based pH reporters allowed both reliable astrocyte identification and subsequent measurement of intracellular pH dynamics. One concern was that certain interneurons in the stratum radiatum could be mistaken for putative astrocytes (Kang et al., 1998). Therefore, a subset of putative astrocytes were electrophysiologically characterised and in all cases the functional properties were consistent with the astrocytic phenotype.

In addition to the opposite polarity of seizure induced pH responses, the kinetics of pH dynamics were also markedly different between astrocytes and neurons. As described above, peak neuronal acidification correlated well with the termination of seizure episodes before recovering thereafter. In contrast, astrocytic alkaline transients were markedly faster and appeared to track the period of seizure induced membrane depolarisation more closely. Ultimately, this must reflect differences in the mechanisms underlying these two respective pH responses. As described above, neuronal acidification is thought to arise from metabolic processes, the extrusion of Ca^{2+} and $GABA_AR$ activation. The first

two, and possibly the third of these processes are predicted to outlast the seizure. In contrast, astrocytic alkalinisation is thought to arise via a single mechanism; the activity of the electrogenic Na+/HCO_3^- cotransporter NBCe1, which may be more closely linked to membrane depolarisation.

Immunohistochemistry and in situ hybridisation studies have found widespread expression of NBCe1 throughout the brain with especially high expression in astrocytes (Giffard et al., 2000; Schmitt et al., 2000). The stochiometry of NBCe1, at least in hippocampal astrocytes, is two HCO_3^- per Na^+ ion for each transport cycle (Bevensee et al., 1997; O'Connor and Sontheimer, 1994). The electrogenic nature of this transporter means that upon membrane depolarisation HCO_3^- and Na^+ influx is accelerated, which leads to intracellular alkalinisation. Seizure episodes cause extracellular K^+ and glutamate accumulation, which both serve to depolarise astrocytes (Bowman and Kimelberg, 1984; Kaila et al., 1997) and would be predicted to accelerate NBCe1 activity. This is the most likely explanation for why the alkaline shifts in astrocytes demonstrated in this work track the period of seizure induced depolarisation so tightly.

Consistent with the idea that NBCe1 is the primary mediator of the observed seizure induced alkaline transients, removal of HCO_3^- markedly reduced the magnitude of positive pH transients. It should be noted however, that it is impossible to completely remove HCO_3^- from the brain slice preparation as metabolic activity will always produce CO_2, which is rapidly converted to HCO_3^-. Interestingly, by reducing the HCO_3^- dependent alkaline transient, an apparent seizure induced acidic transient in astrocytes was revealed. This might suggest that under normal conditions seizure associated astrocytic proton production, which may be related to increased metabolism, glutamic acid synthesis and Ca^{2+} extrusion is masked by NBCe1 mediated HCO_3^- import.

Finally to further test the role of Na^+ / HCO_3^- transporters in astrocytes I determined the effects of a generic NBC inhibitor (S0859). S0859 has previously been shown to reversibly inhibit NBCs in cardiac tissue (Ch'en, Villafuerte, Swietach, Cobden and Vaughan-Jones, 2008). Consistent with a role for NBC's in the astrocytic pH transient, S0859 was found to significantly reduce seizure dependent alkalinisation. However, it also had a marked effect on the seizures themselves. It is therefore unclear as to the precise chain of causal events. Does a reduction in astrocytic alkalinisation reduce the

length and strength of seizures, or does S0859 have a direct effect upon neural activity and therefore seizure intensity, which results in reduced alkaline transients in astrocytes? For instance, the electroneutral Na^+ / HCO_3^- transporter (NBCn1) is strongly expressed in neurons where it is closely associated with extracellular carbonic anhydrase. These two proteins form what is known as a 'transport metabolon', which greatly facilitates the replenishment of intraneural HCO_3^- in the face of ongoing activity (Alvarez et al., 2003). In neurons, HCO_3^- efflux via $GABA_A$Rs is a major contributor to ongoing depolarisation (Ruusuvuori et al., 2004). If S0859 inhibits NBCn1 in neurons, this would diminish the regeneration of intracellular HCO_3^- and consequently HCO_3^- dependent depolarisation. Consistent with this possibility, seizures recorded in S0859 were shorter and lacked the late stage depolarisation that is most likely mediated by HCO_3^- efflux through $GABA_A$Rs.

In summary, this chapter has demonstrated the utility of employing GFP-derived, genetically encoded pH reporters for quantifying intracellular proton fluxes in the context of changing neuronal activity. This has been used to accurately quantify the magnitude and kinetics of seizure associated pH changes in hippocampal neurons and astrocytes. Epileptiform activity was found to induce acidic transients in neurons but alkaline shifts in astrocytes. The astrocytic alkaline shifts were likely to be mediated by the Na^+ / HCO_3^- cotransporter NBCe1. In the next chapter I discuss the wider implications of these findings and of the other work presented within this thesis.

Chapter 6

General Discussion

In the final chapter of this thesis I recapitulate some of my major experimental findings. These are placed within a broader theoretical framework and their functional implications for basic brain function and pathology are discussed. Lastly, where appropriate, methodological shortcomings are raised and opportunities for future experiments are outlined.

6.1 Cl^- accumulation causes transient changes in the driving force for $GABA_A$Rs

In Chapter 3 of this thesis I demonstrated that large fluxes of Cl^- are able to overwhelm a neuron's ability to maintain a stable transmembrane Cl^- concentration gradient. I confirmed previous reports (Staley and Proctor, 1999; Jin et al., 2005) that intense exogenous activation of $GABA_A$Rs is sufficient to cause considerable Cl^- accumulation and hence a depolarising shift in the reversal potential for $GABA_A$ receptors (E_{GABAA}).

In principle, any factor that affects the rate of Cl^- accumulation during $GABA_A$R activation will affect how rapidly and by how much E_{GABAA} shifts. For example, one would expect that the greater the Cl^- extruding capability of a neuron, the more resistant it would be to activity induced Cl^- accumulation. Several mechanisms have been identified to play a role in Cl^- efflux. These include the Cl^- cotransporter KCC2 (Gamba et al., 2005), the Cl^-/HCO_3^- exchanger (Sterling and Casey, 1999), ATP-driven Cl^- pumps (Inoue et al., 1991) and voltage-sensitive Cl^- channels (Rinke et al., 2010). Despite this wide array of possible Cl^- extruding pathways, my own electrophysiological experiments (see Fig. 3.2

and Fig. 3.9) and those of others have shown that following a Cl^- load, it is possible to fit the recovery of $[Cl^-]_i$ with a single exponent (Staley and Proctor, 1999). This suggests that a single transporter, described by a single exponential process, must play a dominant role in the recovery from Cl^- accumulation. In most adult neurons, KCC2 has been identified as the major player in this process (Blaesse et al., 2009). As one would expect, reducing KCC2 activity within the context of a computational model (Doyon et al., 2011) or experimentally, by genetic knock down or pharmacological inhibition (Zhu et al., 2005; Rivera et al., 1999; Thompson and Gahwiler, 1989*b*; Jarolimek et al., 1999; Doyon et al., 2011), causes a depolarising shift in resting E_{GABAA}. In addition, computational modelling and experimental data suggest that reduced KCC2 activity will hamper a neurons ability to deal with an accumulation of intracellular Cl^- (Jin et al., 2005; Doyon et al., 2011).

What may be under appreciated however, is that KCC2, like all co-transporters, has a limited Cl^- transport capacity (Blaesse et al., 2009). This means that during the short time periods accompanying intense $GABA_AR$ activation, the co-transporter can become saturated. The volume of the compartment into which Cl^- flows and the rate of diffusion into other areas therefore become the most important parameters in governing the extent to which the Cl^- concentration increases intracellularly (Staley and Proctor, 1999). In line with this, I have demonstrated that a given Cl^- load causes a greater depolarising shift of E_{GABAA} within cell dendrites as compared to the cell soma (see Fig. 3.4). This effect was simulated using a biophysically realistic computer model and could be explained by the difference in volume between the two compartments.

These findings are consistent with computational models developed by other groups Doyon et al. (2011); Jedlicka et al. (2011); Staley and Proctor (1999); Qian and Sejnowski (1990), which also predict that for a given amount of synaptic $GABA_AR$ stimulation and its accompanying Cl^- influx, smaller post-synaptic volumes will result in relatively larger increases in $[Cl^-]_i$ and hence depolarising shifts in E_{GABAA}. In a theoretical paper, Qian and Sejnowski (1990) employed this reasoning to suggest that $GABA_AR$-mediated inhibition is likely to be ineffective on dendritic spines. Due to their minute volume, even small amounts of Cl^- influx are predicted to cause a local increase in $[Cl^-]_i$ that would rapidly depolarise E_{GABAA}. Consistent with this idea, it has since been confirmed that most GABAergic synapses are localised to dendritic shafts as opposed to spines (Megías

et al., 2001; Freund and Buzsáki, 1996). In a similar vein, distal dendrites and apical tufts are also predicted to be prone to Cl^- accumulation effects (Doyon et al., 2011). In addition to their small volume, the narrow diameter of these processes means that longitudinal diffusion of Cl^- to other parts of the cell is severely restricted. This implies that multiple GABAergic connections originating from a single cell would have a larger inhibitory effect if the corresponding synapses are distributed throughout the dendritic tree, as opposed to being clustered along a single branch. Once again, such a morphological arrangement appears to be evident in different systems (Doyon et al., 2011; Jedlicka et al., 2011).

An important consideration for multi-compartment models of Cl^- regulation, including those described in this thesis, is the value assigned to the diffusion coefficient of Cl^-. This is a critically important parameter as it determines to what extent Cl^- is able to diffuse between compartments. As a result, it is arguably the most important variable in governing the extent of Cl^- accumulation in small compartments such as dendrites. Published models (Doyon et al., 2011; Jedlicka et al., 2011), as well as my own model, have used a value for Cl^- diffusion based on this ion's diffusion through water (2 - 10 μm/ms). However, it is quite likely that these values of intracellular Cl^- diffusion are significant overestimates. It is more likely that Cl^- moves more slowly within the confines of a densely packed neuronal cytoplasm. Experimentally deriving a value for intracellular Cl^- diffusion is extremely difficult and will likely rely on accurate optical measurements of Cl^- concentration changes in response to a spatially restricted Cl^- load. Future experiments utilising ClopHensor2 will hopefully be able to shed light on this important cellular parameter.

6.1.1 Optogenetics offer a novel approach for modulating intracellular Cl^-

As part of Chapter 3, I showed that one of the latest generation of optogenetic silencers, eNpHR3.0 (eNpHR), can be used to deliver different amounts of Cl^- intracellularly. Indeed I was able to use this approach to investigate how cellular Cl^- homoeostasis mechanisms respond to a Cl^- load. This demonstration of eNpHR as an 'ion modulator' is a significant technical advance for scientists studying Cl^- regulation and synaptic inhibition. Previous mechanisms to challenge cells with Cl^- have relied upon activating $GABA_A$Rs, which has several limitations. Firstly, $GABA_A$R currents are not purely mediated by Cl^-. The permeability of these receptors is roughly 4 to 1 in favour of Cl^- over HCO_3^- (Kaila, 1994).

As such, the proportion of any $GABA_AR$ current that is attributable to Cl^- is a complex function of the relative electrochemical gradients for both Cl^- and HCO_3^- (Staley and Proctor, 1999). In contrast, the current generated by optically activating eNpHR is purely mediated by Cl^- (Seki et al., 2007). This allows the experimenter to precisely quantify the amount of Cl^- delivered to the cell in question. Secondly, delivering large and extended Cl^- loads using activated $GABA_ARs$ is challenging as these receptors rapidly desensitise with continued use (Farrant and Kaila, 2007). In contrast, eNpHR currents can be maintained for minutes or even hours without major attenuation. Lastly, in contrast to methods that employ pharmacological activation of $GABA_ARs$, light-activated pumps offer the potential to deliver precise quantities of $Cl^-$by using eNpHR precise quantities of Cl^- to genetically defined cell types or subcellular compartments.

6.2 Optogenetic silencers differ in their effects on inhibitory synaptic transmission

In this thesis I have demonstrated that an eNpHR induced Cl^- load can significantly increase the probability of spike generation in the period following laser offset. eNpHR's affect on intracellular Cl^-, GABAergic synaptic transmission and hence cellular excitability is particularly relevant for those investigators who wish to use eNpHR as an optogenetic tool to silence neurons. It is likely that enhanced network excitability immediately following the termination of eNpHR photoactivation could have unintended repercussions relevant to a wide array of experimental manipulations (Witten et al., 2010; Goshen et al., 2011). I therefore compared the effect of eNpHR on GABAergic transmission with that of an alternative neural silencer, Arch. Arch causes hyperpolarisation and an inhibition of neural activity by pumping protons out of a cell when activated with light. As such, this optogenetic tool would not be predicted to have as marked an effect on inhibitory synaptic transmission as eNpHR. Indeed, I did not detect a difference in synaptically evoked spike probability before and after laser activation of Arch. In addition, induced Arch photocurrents appeared to have no appreciable effect on E_{GABAA} in organotypic or acute hippocampal slices.

It is theoretically possible that Arch induced proton fluxes could affect network ex-

citability. Extracellular acidic transients are predicted to reduce excitability. For instance, NMDA receptor conductances are reduced by acidity, whilst the opposite is true of $GABA_A$Rs (Pasternack et al., 1996; Tang et al., 1990). And the fact that I did not observe a reduction in stimulus evoked spike probability following extended periods of Arch activation (Fig. 3.11) may be because biolistic transfection results in sparse expression (typically 3-10 Arch expressing cells per slice). It remains a possibility that extracellular changes in pH and their consequent effects upon excitability would be greater under conditions of widespread expression of Arch, such as might be achieved using viral delivery. Therefore, to settle this issue completely, the same experiment would need to be repeated using acute slices containing tissue-wide expression of Arch. That said, the predicted change in network excitability following extended periods of Arch activation would still be the opposite (extended inhibition of network excitability) to that observed using eNpHR (a period of increased excitation).

This caveat aside, my observations establish an important difference between optical silencing strategies, which are relevant to ex vivo and in vitro experiments, and may be helpful in interpreting in vivo experiments. These findings also highlight the usefulness of light-activated proteins as ion modulators, which will be invaluable for exploring the role of ion species in synaptic transmission, development and pathology.

6.3 Steady-state Cl^- regulatory mechanisms

In order to better understand how Cl^- fluxes affect intracellular Cl^- homoeostasis, in Chapter 3 of this thesis I created a single compartment model of a cell with realistic Cl^- transport mechanisms (see Fig. 3.10). Various insights were gained from this approach. The first relates to the mechanisms that control resting Cl^- levels in neurons. It is well known that the activity of Cl^- transporters such as the K^+-Cl^- cotransporter KCC2 play a pivotal role in setting steady state E_{Cl^-} (Blaesse et al., 2009). However, it is perhaps less appreciated that additional Cl^- currents, in particular tonic GABA must play an equally important role in this regard. For instance, in a hypothetical neuron with no tonic $GABA_A$R currents but intact KCC2 transport, E_{Cl^-} would rapidly approximate E_{K^+}. This is because as a K^+-Cl^- cotransporter, the thermodynamic drive on KCC2 is to equilibrate E_{Cl^-} and E_{K^+}. If this scheme is correct, an experimental prediction would be that under conditions of complete

pharmacological blockade of $GABA_A$Rs, E_{Cl^-} (measured optically with a genetic reporter of Cl^-) should approximate E_{K^+}. Conversely, without KCC2 activity and in the presence of tonic $GABA_A$R activity, E_{Cl^-} is predicted to tend toward the resting membrane potential of the neuron. Considering that the properties of tonic $GABA_A$R currents are known to change as a function of developmental age (Vithlani et al., 2011), it is an intriguing question for future research as to whether changes in this cell parameter are an important variable in setting steady state E_{GABAA}.

The second insight gained from the single compartment model of Cl^- homoeostasis relates to how the intracellular Cl^- concentration of a cell changes in response to a prolonged, steady influx of Cl^-. One might predict that prolonged periods of exogenously introduced Cl^-, such as might result from sustained activation of a light-activated Cl^- pump, would flood a cell with Cl^- and ultimately lead to cell swelling via osmotic processes. However, my model revealed that as long as the rate of Cl^- influx is less than the cell's maximum Cl^- extrusion rate, a new stable intracellular Cl^- concentration will be reached within 30 to 50 s (see Fig. 3.10). This new plateau value of $[Cl^-]_i$ is dependent on both the kinetics of Cl^- transport within the cell and the size of the Cl^- influx. Following the termination of the Cl^- load, $[Cl^-]_i$ is predicted to return to resting levels within a minute.

6.4 Short-term alterations in E_{GABAA}

The modelling approach has provided important insights into the conditions under which shifts in Cl^- might occur. However, it still remains to be shown under what physiologically relevant network states changes in E_{GABAA} might occur. Nevertheless, it is interesting to consider what functional effects short-term alterations in E_{GABAA} might have in the context of evolving pathological and physiological network activity. As described above, large depolarising shifts in E_{GABAA} have been shown to play a role in exacerbating and sustaining epileptic seizures (Fujiwara-Tsukamoto, 2006; Fujiwara-Tsukamoto et al., 2003; Lamsa and Kaila, 1997). In addition, it has been observed that high frequency stimulation, of the sort used to induce classic long term potentiation (LTP) at glutamatergic synapses, is sufficient to induce $GABA_A$R mediated depolarisation (Thompson and Gahwiler, 1989*a*). This has led to the suggestion that one function of an activity induced depolarising shift in E_{GABAA} is to modulate the Mg^{2+} block on NMDA receptors. This would suggest that the

short-term GABAergic plasticity described above may play an important role in regulating NMDAR-dependent mechanisms of synaptic plasticity (Staley and Soldo, 1995).

Such functional effects have been demonstrated with large shits in E_{GABAA}, which require induction with patterns of activity of questionable physiological significance. What effect then could smaller shifts in E_{GABAA} (e.g. less than 10 mV), which are more likely to be generated by physiological activity, have on network function? By artificially setting the E_{GABAA} of a neuron, one may investigate how alterations to the ionic driving force for $GABA_A$Rs may impact activity. Previously, this has been performed experimentally either by dialysing neurons during whole-cell recordings with internal solutions of set $[Cl^-]_i$, or by using dynamic clamp to simulate GABAergic inputs with different E_{GABAA} values. Studies performed in this manner have demonstrated that shifting E_{GABAA} to moderately depolarising values can result in enhanced spiking probability and reduced spike latencies in response to GABAergic inputs (Akerman and Cline, 2006; Saraga et al., 2008; Valeeva et al., 2010; Wang et al., 2006). As part of this thesis I have been able to advance these findings by using optogenetic methods to modulate E_{GABAA} intracellularly. By stimulating a hippocampal neuron before and after laser activation of eNpHR, I have demonstrated that an eNpHR induced Cl^- load can significantly increase the probability of spike generation in the period following laser offset.

Developing computational models is also a useful strategy for studying the impact that modest changes in E_{GABAA} might have upon neural signalling. For instance, in Chapter 3 I demonstrated that a multi-compartment model of a pyramidal cell with realistic Cl^- transport mechanisms and biologically relevant glutamatergic and GABAergic synaptic inputs showed changes in spike timing that were dependent upon intracellular Cl^- dynamics. In a similar fashion, Saraga et al. (2008) showed that shifting the E_{GABAA} in a model of a mature CA1 pyramidal neuron from -75 mV to -70 mV results in an increase in action potential firing frequency by approximately 40 percent. And depolarising shifts in inhibitory reversal potentials by as little as 10 mV can considerably shorten the duration of inhibitory inputs at the soma (Jean-Xavier et al., 2007). Small changes to E_{GABAA} are more likely to be functionally significant when a fine balance exists between GABAergic inhibition and excitation. For instance, in neocortical layer 5 neurons and dentate granule cells, E_{GABAA} has been reported to lie at values more depolarised than the resting membrane poten-

tial, but below the action potential threshold (Chiang et al., 2012, Gulledge and Stuart, 2003). This means that small changes in E_{GABAA} can bidirectionally modulate neuronal firing rates and spike times (Chiang et al., 2012; Morita et al., 2006), which could have important consequences for information coding and plasticity (Richards et al., 2010)

An intriguing possibility is that physiological Cl^- accumulation might adjust the processing capacity of a neurons dendritic tree, depending on the amount of information flowing through a particular brain network (Viitanen, 2010). The mechanism would operate as follows. If E_{GABAA} is more negative than the resting membrane potential, then hyperpolarising GABAergic inputs will spread further in time and space than their underlying conductances (Gulledge and Stuart, 2003). During periods of enhanced activity however, synaptic inputs to dendrites would be predicted to cause modest Cl^- accumulation such that E_{GABAA} becomes roughly equal to the resting membrane potential and GABAergic inputs generate an exclusively shunting effect (Jedlicka et al., 2011; Doyon et al., 2011). Such a transition would serve to increase the spatial and temporal precision for integrating synaptic inputs, changing the fidelity of spike generation and effectively increasing the processing capacity of the dendritic compartment (Viitanen, 2010; London and Häusser, 2005). As such, short-term GABAergic plasticity involving shifts in E_{GABAA} could allow a neuron to adjust the information processing capacity of its dendritic tree 'on the fly', to meet the varied computational demands of changing levels of neural activity.

6.5 Cl^- accumulation in pathological states of network activity including epilepsy.

It is well known that many hyperexcitability disorders, such as epilepsy and neuropathic pain, are associated with long-term depolarising shifts in E_{GABA} (Cohen et al., 2002; Pathak et al., 2007; Coull et al., 2005; Lu et al., 2008). What is somewhat less appreciated however, is that short-term changes in E_{GABAA} also play an important role in these disorders. In this thesis I have used a variety of methods to demonstrate that epileptiform activity causes significant Cl^- accumulation and a depolarsing shift in E_{GABAA}. This is consistent with previous and recent reports of similar changes accompanying seizures elicited using a wide-array of in vitro epilepsy models. (Lopantsev and Avoli, 1998;

Fujiwara-Tsukamoto et al., 2003, 2010; Isomura et al., 2003; Ilie et al., 2012; Lamsa and Kaila, 1997; Lillis et al., 2012). These shifts in the action of $GABA_A$Rs are large enough to convert fast synaptic inhibition from being inhibitory and hyperpolarising to depolarising and excitatory (see Fig. 4.1). The primary feature of epileptic activity is the failure of inhibitory systems to contain the generation and spread of neuronal hyperexcitability (McCormick and Contreras, 2001). Therefore, by weakening or even reversing the major source of inhibition within the brain, it is easy to appreciate how transient changes in E_{GABAA} would play an integral role in the pathogenesis of epileptic seizures. Epileptic seizures may be divided into two broad phases; seizure onset, which includes propagation, and seizure termination. I will discuss the implications of Cl^- accumulation for both of these stages.

6.5.1 Cl^- accumulation and seizure onset

The precise mechanisms that describe seizure onset are complex and a complete discussion is beyond the scope of this thesis. At a simplified level, we can consider seizure onset as the high frequency, synchronised activity of a group of excitatory cells, which is allowed to propagate and recruit surrounding neurons due to the failure of accompanying inhibitory systems (Trevelyan et al., 2007). During periods of enhanced physiological network activity, such as 'upstates', runaway excitation is prevented by strong feed-forward and feed-back inhibition. Indeed, upstates have been shown to consist of a dynamic balance between excitation and inhibition (Haider et al., 2006; Mann et al., 2009; Sanchez-Vives and McCormick, 2000). Strong inhibitory input and the activation of $GABA_A$Rs concurrent with membrane depolarisation and excitatory conductances (as occur during upstates) are precisely the conditions under which one would expect Cl^- accumulation to occur. As Cl^- loading proceeds, a 'tipping point' would be reached, as defined by E_{GABAA} exceeding the threshold for action potential generation. This tipping point may represent the moment physiologically controlled network activity switches into a pathological epileptiform state. In this scenario, not only do $GABA_A$R mediated inhibitory mechanisms fail, but they are also subverted to enhance the temporal and spatial propagation of ongoing epileptic activity. As yet, there is limited evidence for this hypothesis of seizure onset. For instance, Lasztóczi et al. (2011) have shown that immediately prior to seizure onset

there is strong synchronisation of GABAergic inputs to CA3 hippocampal pyramidal cells accompanied by Cl^- accumulation. In addition my own work presented in this thesis and a recent paper by Lillis et al. (2012), both using imaging methods, have demonstrated that pyramidal cells accumulate Cl^- at the onset of seizures. These observations are consistent with a Cl^- accumulation induced breakdown in synaptic inhibition. However, future studies are required to investigate the precise role Cl^- accumulation might play during seizure onset. In theoretical terms, E_{GABAA} becoming excitatory could represent a bifurcation point between two stable states - 'quiescent' and 'epileptic'. And just as one can not predict the exact moment of an avalanche, similarly it may be difficult to predict the exact moment of seizure onset - it is inherently a chaotic phenomenon. However, just as the likelihood of avalanches correlates with the amount of snow on a slope, by monitoring the average Cl^- concentration within neurons during ongoing activity, it may be possible to better predict the likelihood of seizure onset.

6.5.2 Mechanisms of seizure termination

It is unclear as to the exact role Cl^- accumulation might play in triggering the onset of an epileptic seizure. However, the intense activation of $GABA_A$Rs in combination with the concurrent membrane depolarisation that occurs during seizures is known to cause rapid, extensive Cl^- accumulation. This has been thoroughly demonstrated in the course of this thesis (Chapter 4) and as part of published work (Lopantsev and Avoli, 1998; Fujiwara-Tsukamoto et al., 2003, 2010; Isomura et al., 2003; Ilie et al., 2012; Lamsa and Kaila, 1997; Lillis et al., 2012). If $GABA_A$R mediated signalling is reinforcing (rather than preventing) excitation during the latter part of a seizure, how then do epileptic seizures terminate?

Although this is once again an extremely broad topic, I will briefly outline two possible mechanisms that are likely to play an important role in this regard. Firstly, whilst Cl^- conductances are rendered excitatory by continued epileptic activity, K^+ conductances will remain inhibitory. As such, signalling systems that derive their inhibitory effect by activating postsynaptic K^+ channels are likely to play a critical role in terminating seizure activity. The presynaptic inhibition of neurotransmitter release is another important mechanism by which excessive activity may be curtailed. The $GABA_B$R and adenosine signalling

systems utilise both of these mechanisms in order to inhibit network activity and terminate epileptiform activity (Boison, 2009). Indeed, data from this thesis has contributed to a recent paper (Ilie et al., 2012) demonstrating that adenosine release during seizures attenuates $GABA_A$ receptor mediated depolarisation and hence contributes to seizure termination.

A second cellular mechanism relevant to seizure termination relates to the control of hydrogen ion concentration. As described in the introduction to this thesis, intra- and extracellular pH changes can have a marked effect on the excitability of neuronal network activity. Indeed, progressive intracellular acidification has been suggested to be an important factor in arresting seizures (Xiong et al., 2000). This is consistent with my observations in Chapter 5, whereby maximal neuronal intracellular acidification was found to be associated with seizure termination (Raimondo, Irkle, Wefelmeyer, Newey and Akerman, 2012). Seizure induced acidification, like adenosine receptor signalling, can also attenuate $GABA_A$ receptor mediated depolarisation, albeit via a very different mechanism. It is perhaps under appreciated that HCO_3^- ions provide a pivotal link between neuronal regulation of Cl^- and pH. For instance, although the enzyme carbonic anhydrase is largely able to regenerate HCO_3^- intracellularly in the face of $GABA_AR$ induced HCO_3^- efflux, the generation of intracellular hydrogen that accompanies seizure activity will shift the equilibrium set point of the carbonic anhydrase catalysed reaction of H_20 and CO_2, to HCO_3^- and H^+. Therefore activity induced acidification is predicted to cause significant reduction in intracellular HCO_3^- and hence a hyperpolarisation of $E_{HCO_3^-}$. As E_{GABAA} is a product of both $E_{HCO_3^-}$ and E_{Cl^-}, this progressive acidification would effectively reduce the depolarising shift in E_{GABAA} that could be activated during intense $GABA_AR$ activation.

These interactions confirm that both intracellular Cl^- and pH are important for understanding how inhibitory synaptic transmission is altered during neuronal activity. As such, a valuable technical contribution of this thesis has been to establish the suitability of genetically encoded pH sensors for investigating activity-dependent pH changes at the level of single cells. A further achievement has been the development of ClopHensor2, a genetic H^+ and Cl^- ion sensor optimised for neuronal use. This reporter's ability to simultaneously measure both of these dynamic variables makes it an exciting tool for future research.

6.6 Activity induced alkaline transients in astrocytes.

Previous sections of this discussion have addressed the implications of intracellular Cl^- and pH changes in neurons during epileptiform activity. In the course of this thesis I have also demonstrated an interesting intracellular pH shift in an alternative cell type, astrocytes. Prior studies have demonstrated that astrocytes and neurons differ in their pH responses to depolarisation (Bevensee et al., 1997; Grichtchenko and Chesler, 1994; Pappas and Ransom, 1994; Chesler, 2003). Whilst neurons become acidic, astrocytes are know to display marked alkaline transients. To my knowledge however, I am the first to demonstrate astrocytic intracellular alkaline shifts in response to epileptiform activity. Chapter 5 suggested that these can be explained by the action of NBCe1, an electrogenic Na^+ coupled HCO_3^- transporter. In the following paragraphs I will attempt to discuss the functional implications of this observed cell-type specific pH transient.

6.6.1 The intracellular effects of astrocytic alkalinisation

Astrocytes are widely known to play a critical role in providing neurons with energy substrates, particularly lactate. The astrocyte-neuron lactate shuttle model (ANLS) describes a mechanism by which astrocytes respond to glutamate receptor activation by increasing their rate of glucose utilisation and release of lactate into the extracellular space, which in turn is used by neurons to sustain their energy requirements (Allaman et al., 2011). The currently accepted mechanism for how this occurs operates as follows: During enhanced network activity synaptic release of glutamate is increased. This glutamate is taken up by glutamate transporters on the astrocytic membrane (EAAT1s/ EAAT2s), which transport a glutamate molecule with 3 Na^+ ions and a proton, in exchange for a K^+ ion (Allaman et al., 2011). In order to maintain the transmembrane Na^+ and K^+ gradients, increased activity of the Na^+/K^+ ATPase effectively reduces the ATP/(ADP+AMP) ratio, leading to allosteric activation of glycolytic enzymes (such as phosphofructokinase - PFK) and an increased production of lactate (Pellerin and Magistretti, 1994; Pellerin et al., 2007). A recent paper by Ruminot et al. (2011) has proposed an interesting and important modification to this canonical model of neurometabolic coupling performed by astrocytes.

PFK is known to be highly sensitive to pH, as such intracellular pH is an important

regulator of glycolytic rate (Trivedi and Danforth, 1966; Ereciska et al., 1995). With this in mind Ruminot et al. (2011) have convincingly demonstrated that depolarisation induced alkaline transients in astrocytes, mediated by NBCe1, are sufficient to greatly accelerate glycolysis and lactate production. An advantage of this proposed mechanism is that astrocytic depolarisation of any kind should be sufficient to accelerate glycolysis (not just glutamate uptake). This is relevant as extracellular K^+, which is believed to accurately 'encode' the level of nearby neuronal activity directly depolarises astrocytes (Ransom, 2000). In addition, as I have demonstrated in this thesis (see Fig. 5.6) astrocytic alkalinisation happens extremely quickly in response to neuronal activity. Therefore, the activity dependent astrocytic alkaline transients described in this thesis provide a rapid mechanism for ensuring neurons receive an increased supply of lactate in the face of enhanced metabolic demand.

I would also like to highlight two further potential effects that could be mediated by activity-dependent intracellular alkaline transients in astrocytes. Firstly, a primary function of astrocytes is to clear released neurotransmitter from the synaptic cleft. As described above glutamate (and GABA) are moved into astrocytes by transporters that utilise predominantly the transmembrane Na^+ gradient, but also the H^+ and K^+ ion gradients to import the relevant neurotransmitter (Zerangue and Kavanaugh, 1996). As such, intracellular alkalinisation, by enhancing the gradient of H^+ across the astrocytic membrane, should serve to increase the clearance of neurotransmitter during heightened network activity. Secondly, astrocytes are known to be extensively gap junction coupled (Zhang, 2010). In addition, gap junction conductance is sensitive to pH with progressive alkalinity enhancing conductance and acidity reducing coupling efficiency (Spray et al., 1981). As a result, astrocytic alkaline shifts of the sort described in this thesis may well serve to enhance gap junction coupling of astrocytes during network activity. This may promote Ca^+ signalling between cells or enhance the ability of astrocytes to spatially buffer extracellular K^+ (Wallraff et al., 2006).

6.6.2 The extracellular effects of astrocytic alkalinisation

In the early 1990's Ransom (1992) proposed a hypothesis whereby astrocytes actually modulate neuronal activity by controlling extracellular pH. In this hypothesis astrocytes re-

spond to neuronal activity with intracellular alkaline transients, which necessarily result in an acidification of the extracellular space. This extracellular acidification is then predicted to serve as a negative feedback signal to reduce network excitability. Many elements of this scheme have since been established. For instance, Na^+ and HCO_3^- dependent, depolarisation-induced astrocytic alkalinisation (DIA) has been confirmed in a variety of studies in addition to the evidence presented in this thesis (Pappas and Ransom, 1994; O'Connor and Sontheimer, 1994; Grichtchenko and Chesler, 1994; Deitmer and Szatkowski, 1990; Chesler and Kraig, 1989). In turn, extracellular pH has been shown to affect the conductance of NMDA receptors (Tang et al., 1990; Traynelis and Cull-Candy, 1990; Vyklicky et al., 1990), $GABA_A$ receptors (Pasternack et al., 1996; Smart and Constanti, 1982; Takeuchi and Takeuchi, 1967) and voltage gated Ca^{2+} channels (Barnes and Bui, 1991; Iijima et al., 1986; Tombaugh, 1998; Tombaugh and Somjen, 1997). Whilst acidosis reduces NMDA receptor conductances, it has the opposite effect on $GABA_A$Rs, the net effect being that extracellular acidity serves to dampen network excitability.

You may also recall from Chapter 5 of this thesis, that neurons undergo profound acidic shifts simultaneous with the astrocytic shifts described above. These neuronal acidic shifts are predicted to have an opposite affect on the extracellular space, causing extracellular alkalinisation. How the opposing proton fluxes in neurons and astrocytes combine in the extracellular space is somewhat poorly understood. Previous work using pH sensitive micro-electordes has demonstrated that seizures and stimulated activity are associated with an initial extracellular alkaline shift followed by a prolonged acidosis (Caspers and Speckmann, 1972; Urbanics et al., 1978). A small number of studies using optical methods have also described a rapid extracellular acidic transient preceding the biphasic response described above (Krishtal et al., 1987). The work in this thesis is unique in that it provides the precise kinetics of intracellular pH transients in two separate tissue compartments (astrocytes and neurons) within the same preparation. This allows a means to predict the kinetics of extracellar pH changes in response to seizure activity. Given the rapid onset of the astrocytic intracellular alkaline shift it is likely that the first extracellular manifestation of activity would be a rapid acidic transient. As neurons become more and more acidic with continued network activation one would expect the extracellular space to shift from being acidic to alkaline. Finally, once seizure activ-

ity has terminated and neurons begin to recover their intracellular pH by extruding acid, extracellular alkalinisation is likely to be replaced by a prolonged acidosis. Indeed, this sort of triphasic extracellular pH shift has been reported in response to seizure activity (Krishtal et al., 1987). Future work would require developing techniques to observe extracellular pH transients, possibly by targeting genetic reporters to the membrane surface. By measuring pH shifts in all three tissue compartments (neurons, astrocytes and the extracellular space) we would be well placed to completely describe proton fluxes in our preparation.

Although many aspects of Ransom (1992) hypothesis linking astrocytic pH transients to the control of network activity have been confirmed, no direct demonstration of this mechanism has yet been described. To investigate this further I would propose the use of the light-activated H^+ pump Arch. The idea would be to express this proton pump only in hippocampal astrocytes using transgenic mouse technologies (Mori et al., 2006). By activating Arch in astrocytes the aim would be to evoke intracellular astrocytic alkalinisation and consequently extracellular acidification. If such a manipulation is then able to modulate epileptiform activity, this would provide direct functional evidence in support of Ransom's two decade old hypothesis.

6.7 Concluding remarks

In the course of this thesis I hope to have convinced the reader that the intracellular concentrations of Cl^- and H^+ are dynamic variables that evolve across both time and space in response to varied patterns of neural activity. This has significant implications for understanding network activity and the balance of synaptic excitation and inhibition. Indeed, I have been able to show that such 'ionic plasticity' is important within the context of epileptiform activity. How these processes contribute to other physiologically important patterns of network activity will provide fertile ground for future research.

Bibliography

Achilles, K., Okabe, A., Ikeda, M., Shimizu-Okabe, C., Yamada, J., Fukuda, A., Luhmann, H. J. and Kilb, W. (2007), 'Kinetic properties of Cl uptake mediated by Na+-dependent K+-2Cl cotransport in immature rat neocortical neurons.', *The Journal of neuroscience : the official journal of the Society for Neuroscience* **27**(32), 8616–27.

Agnati, L., Tinner, B., Staines, W., Väänänen, K. and Fuxe, K. (1995), 'On the cellular localization and distribution of carbonic anhydrase II immunoreactivity in the rat brain', *Brain Res.* **676**(1), 10–24.

Ahmed, Z. and Connor, J. (1980), 'Intracellular pH changes induced by calcium influx during electrical activity in molluscan neurons', *J. Gen. Physiol.* **75**(4), 403–426.

Akerman, C. J. and Cline, H. T. (2006), 'Depolarizing GABAergic conductances regulate the balance of excitation to inhibition in the developing retinotectal circuit in vivo.', *J. Neurosci.* **26**(19), 5117–30.

Alger, B. and Nicoll, R. (1979), 'GABA-mediated biphasic inhibitory responses in hippocampus', *Nature* **281**(5729), 315–317.

Allaman, I., Bélanger, M. and Magistretti, P. J. (2011), 'Astrocyte-neuron metabolic relationships: for better and for worse.', *Trends in neurosciences* **34**(2), 76–87.

Alvarez, B., Loiselle, F., Supuran, C., Schwartz, G. and Casey, J. (2003), 'Direct Extracellular Interaction between Carbonic Anhydrase IV and the Human NBC1 Sodium/Bicarbonate Co-Transporter', *Biochemistry* **42**(42), 12321–12329.

Ambros-Ingerson, J. and Holmes, W. R. (2005), 'Analysis and comparison of morphological reconstructions of hippocampal field CA1 pyramidal cells.', *Hippocampus* **15**(3), 302–15.

Andersen, P., Dingledine, R., Gjerstad, L., Langmoen, I. and Laursen, A. (1980), 'Two different responses of hippocampal pyramidal cells to application of gamma-amino butyric acid.', *J. Physiol.* **305**(1), 279.

Andersen, P., Morris, R. D. A., Bliss, T. and O'Keefe, J. (2006), *The Hippocampus Book*, Oxford University Press.

Anderson, W. W., Lewis, D. V., Swartzwelder, H. S. and Wilson, W. A. (1986), 'Magnesium-free medium activates seizure-like events in the rat hippocampal slice.', *Brain Res.* **398**(1), 215–9.

Arosio, D., Ricci, F., Marchetti, L., Gualdani, R., Albertazzi, L. and Beltram, F. (2010), 'Simultaneous intracellular chloride and pH measurements using a GFP-based sensor.', *Nature methods* **7**(7), 516–8.

Avoli, M., D'Antuono, M., Louvel, J., Köhling, R., Biagini, G., Pumain, R., D'Arcangelo, G. and Tancredi, V. (2002), 'Network and pharmacological mechanisms leading to epileptiform synchronization in the limbic system in vitro.', *Prog. Neurobiol.* **68**(3), 167–207.

Avoli, M., Drapeau, C., Perreault, P., Louvel, J. and Pumain, R. (1990), 'Epileptiform activity induced by low chloride medium in the CA1 subfield of the hippocampal slice.', *J. Neurophysiol.* **64**(6), 1747–57.

Awaji, T. and Hirasawa, A. (2001), 'Novel green fluorescent protein-based ratiometric indicators for monitoring pH in defined intracellular microdomains', *Biochem. Bioph. Res. Co.* .

Bacci, A., Sancini, G., Verderio, C., Armano, S., Pravettoni, E., Fesce, R., Franceschetti, S. and Matteoli, M. (2002), 'Block of glutamate-glutamine cycle between astrocytes and neurons inhibits epileptiform activity in hippocampus.', *J Neurophysiol.* **88**(5), 2302–10.

Barnes, S. and Bui, Q. (1991), 'Modulation of calcium-activated chloride current via pH-induced changes of calcium channel properties in cone photoreceptors', *J. Neurosci.* **11**(12), 4015–4023.

Baumann, S. W., Baur, R. and Sigel, E. (2003), 'Individual properties of the two functional agonist sites in GABA(A) receptors.', *J Neurosci.* **23**(35), 11158–66.

Bear, M. F., Connors, B. W. and Paradiso, M. A. (2007), *Exploring the brain*, number 2008, Lippincott Williams & Wilkins, Philadelphia.

Ben-Ari, Y. (2002), 'Excitatory actions of GABA during development: the nature of the nurture', *Nat. Rev. Neurosci.* **3**(9), 728–739.

Ben-Ari, Y. and Holmes, G. (2005), 'The multiple facets of -aminobutyric acid dysfunction in epilepsy', *Curr Opin Neurol.* .

Benediktsson, A. M., Schachtele, S. J., Green, S. H. and Dailey, M. E. (2005), 'Ballistic labeling and dynamic imaging of astrocytes in organotypic hippocampal slice cultures.', *J. Neurosci. Methods.* **141**(1), 41–53.

Benes, F. and Berretta, S. (2001), 'GABAergic Interneurons Implications for Understanding Schizophrenia and Bipolar Disorder', *Neuropsychopharmacology* **25**(1), 1–27.

Benke, D., Fakitsas, P., Roggenmoser, C., Michel, C., Rudolph, U. and Mohler, H. (2004), 'Analysis of the presence and abundance of GABAA receptors containing two different types of alpha subunits in murine brain using point-mutated alpha subunits.', *J. Biol. Chem.* **279**(42), 43654–60.

Berdichevsky, Y., Dzhala, V., Mail, M. and Staley, K. J. (2011), 'Interictal spikes, seizures and ictal cell death are not necessary for post-traumatic epileptogenesis in vitro.', *Neurobiol. Dis.* **45**(2), 785–774.

Bettler, B., Kaupmann, K., Mosbacher, J. and Gassmann, M. (2004), 'Molecular structure and physiological functions of GABA(B) receptors.', *Physiol Revs.* **84**(3), 835–67.

Bevensee, M., Apkon, M. and Boron, W. (1997), 'Intracellular pH regulation in cultured astrocytes from rat hippocampus', *J. Gen. Physiol.* **110**(4), 467.

Bizzarri, R., Arcangeli, C., Arosio, D., Ricci, F., Faraci, P., Cardarelli, F. and Beltram, F. (2006), 'Development of a novel GFP-based ratiometric excitation and emission pH indicator for intracellular studies', *Biophys. J.* **90**(9), 3300–3314.

Bizzarri, R., Serresi, M., Luin, S. and Beltram, F. (2009), 'Green fluorescent protein based pH indicators for in vivo use: a review', *Anal. Bioanal. Chem.* **393**(4), 1107–1122.

Blaesse, P., Airaksinen, M. S., Rivera, C. and Kaila, K. (2009), 'Cation-chloride cotransporters and neuronal function.', *Neuron* **61**(6), 820–38.

Boison, D. (2009), 'Adenosine augmentation therapies (AATs) for epilepsy: prospect of cell and gene therapies.', *Epilepsy Research* **85**(2-3), 131–41.

Bowman, C. L. and Kimelberg, H. K. (1984), 'Excitatory amino acids directly depolarize rat brain astrocytes in primary culture', *Nature* **311**(5987), 656–659.

Boyarsky, G., Ganz, M. B., Sterzel, R. B. and Boron, W. F. (1988), 'pH regulation in single glomerular mesangial cells. I. Acid extrusion in absence and presence of HCO3-.', *Am. J. Physiol.* **255**(6 Pt 1), C844–56.

Boyden, E. S., Zhang, F., Bamberg, E., Nagel, G. and Deisseroth, K. (2005), 'Millisecond-timescale, genetically targeted optical control of neural activity.', *Nat Neurosci.* **8**(9), 1263–8.

Bragin, D. E., Sanderson, J. L., Peterson, S., Connor, J. A. and Müller, W. S. (2009), 'Development of epileptiform excitability in the deep entorhinal cortex after status epilepticus.', *Eur J Neurosci.* **30**(4), 611–24.

Bregestovski, P., Waseem, T. and Mukhtarov, M. (2009), 'Genetically encoded optical sensors for monitoring of intracellular chloride and chloride-selective channel activity', *Front. Mol. Neurosci.* **2**.

Brumback, A. and Staley, K. (2008), 'Thermodynamic regulation of NKCC1-mediated Cl-cotransport underlies plasticity of GABAA signaling in neonatal neurons', *J. Neurosci.* **28**(6), 1301.

Burgess, N., Maguire, E. A. and O'Keefe, J. (2002), 'The Human Hippocampus and Spatial and Episodic Memory', *Neuron* **35**(4), 625–641.

Burton, R. (1978), 'Intracellular buffering', *Respiration Physiology* **33**(1), 51–58.

Buzsaki, G. (2006), *Rhythms of the Brain*, Oxford University Press.

Caillard, O., Ben-Ari, Y. and Gaïarsa, J. L. (1999), 'Mechanisms of induction and expression of long-term depression at GABAergic synapses in the neonatal rat hippocampus.', *The Journal of neuroscience : the official journal of the Society for Neuroscience* **19**(17), 7568–77.

Cajal, S. (1899), 'Texture of the Nervous System of Man and the Vertebrates'.

Caspers, H. and Speckmann, E. (1972), 'Cerebral pO2, pCO2 and pH: changes during convulsive activity and their significance for spontaneous arrest of seizures', *Epilepsia* pp. 699–725.

Chamberlin, N. L. and Dingledine, R. (1988), 'GABAergic inhibition and the induction of spontaneous epileptiform activity by low chloride and high potassium in the hippocampal slice.', *Brain research* **445**(1), 12–8.

Ch'en, F. F.-T., Villafuerte, F. C., Swietach, P., Cobden, P. M. and Vaughan-Jones, R. D. (2008), 'S0859, an N-cyanosulphonamide inhibitor of sodium-bicarbonate cotransport in the heart.', *British journal of pharmacology* **153**(5), 972–82.

Chen, L.-M., Kelly, M., Parker, M., Bouyer, P., Gill, H., Felie, J., Davis, B. and Boron, W. (2008), 'Expression and localization of Na-driven Cl-HCO3 exchanger (SLC4A8) in rodent CNS', *Neuroscience* **153**(1), 162–174.

Chesler, M. (2003), 'Regulation and modulation of pH in the brain', *Physiol. Rev.* **83**(4), 1183.

Chesler, M. and Kraig, R. (1989), 'Intracellular pH transients of mammalian astrocytes', *J. Neurosci.* **9**(6), 2011.

Chiang, P.-H., Wu, P.-Y., Kuo, T.-W., Liu, Y.-C., Chan, C.-F., Chien, T.-C., Cheng, J.-K., Huang, Y.-Y., Chiu, C.-D. and Lien, C.-C. (2012), 'GABA is depolarizing in hippocampal dentate granule cells of the adolescent and adult rats.', *J. Neurosci.* **32**(1), 62–7.

Chow, B. Y., Han, X., Dobry, A. S., Qian, X., Chuong, A. S., Li, M., Henninger, M. a., Belfort, G. M., Lin, Y., Monahan, P. E. and Boyden, E. S. (2010), 'High-performance genetically targetable optical neural silencing by light-driven proton pumps.', *Nature* **463**(7277), 98–102.

Cohen, I., Navarro, V., Clemenceau, S., Baulac, M. and Miles, R. (2002), 'On the origin of interictal activity in human temporal lobe epilepsy in vitro', *Science* **298**(5597), 1418.

Cooper, D. S., Saxena, N. C., Yang, H. S., Lee, H. J., Moring, A. G., Lee, A. and Choi, I. (2005), 'Molecular and functional characterization of the electroneutral Na/HCO3 co-transporter NBCn1 in rat hippocampal neurons.', *The Journal of biological chemistry* **280**(18), 17823–30.

Cossart, R., Dinocourt, C., Hirsch, J., Merchan-Perez, A., De Felipe, J., Ben-Ari, Y., Esclapez, M. and Bernard, C. (2001), 'Dendritic but not somatic GABAergic inhibition is decreased in experimental epilepsy', *Nat Neurosci.* **4**(1), 52–62.

Coull, J. a. M., Beggs, S., Boudreau, D., Boivin, D., Tsuda, M., Inoue, K., Gravel, C., Salter, M. W. and De Koninck, Y. (2005), 'BDNF from microglia causes the shift in neuronal anion gradient underlying neuropathic pain.', *Nature* **438**(7070), 1017–21.

Davies, C. H., Davies, S. N. and Collingridge, G. L. (1990), 'Paired-pulse depression of monosynaptic GABA-mediated inhibitory postsynaptic responses in rat hippocampus', *J. Physiol.* (1990), 513–531.

DeFelipe, J. and Farinas, I. (1992), 'The pyramidal neuron of the cerebral cortex: morphological and chemical characteristics of the synaptic inputs', *Progress in Neurobiology* **39**(6), 563–607.

Deitmer, J. and Szatkowski, M. (1990), 'Membrane potential dependence of intracellular pH regulation by identified glial cells in the leech central nervous system.', *The Journal of Physiology* **421**(1), 617.

Destexhe, A. (1998), 'Kinetic models of synaptic transmission', *Methods in neuronal modeling* .

Dinocourt, C., Petanjek, Z., Freund, T. F., Ben-Ari, Y. and Esclapez, M. (2003), 'Loss of interneurons innervating pyramidal cell dendrites and axon initial segments in the CA1 region of the hippocampus following pilocarpine-induced seizures.', *J Comp Neurol.* **459**(4), 407–25.

Doyon, N., Prescott, S. a., Castonguay, A., Godin, A. G., Kröger, H. and De Koninck, Y. (2011), 'Efficacy of Synaptic Inhibition Depends on Multiple, Dynamically Interacting Mechanisms Implicated in Chloride Homeostasis', *PLOS Comput. Biol.* **7**(9), e1002149.

Drapeau, P. and Nachshen, D. (1988), 'Effects of lowering extracellular and cytosolic pH on calcium fluxes, cytosolic calcium levels, and transmitter release in presynaptic nerve terminals isolated from rat', *J. Gen. Physiol.* .

Dulla, C. G., Dobelis, P., Pearson, T., Frenguelli, B. G., Staley, K. J. and Masino, S. A. (2005), 'Adenosine and ATP link PCO2 to cortical excitability via pH.', *Neuron* **48**(6), 1011–23.

Dusser de Barenne, J., Marshall, C., McCulloch, W. and Nims, L. (1938), 'Observations on the pH of the arterial blood, the pH and the electrical activity of the cerebral cortex', *American Journal of . . .* .

Dyhrfjeld-Johnsen, J., Berdichevsky, Y., Swiercz, W., Sabolek, H. and Staley, K. J. (2010), 'Interictal spikes precede ictal discharges in an organotypic hippocampal slice culture model of epileptogenesis.', *J. Clin. Neurophysiol.* **27**(6), 418–24.

Dzhala, V., Kuchibhotla, K., Glykys, J., Kahle, K., Swiercz, W., Feng, G., Kuner, T., Augustine, G., Bacskai, B. and Staley, K. (2010), 'Progressive NKCC1-Dependent Neuronal Chloride Accumulation during Neonatal Seizures', *Journal of Neuroscience* **30**(35), 11745.

Eichenbaum, H., Otto, T. and Cohen, N. J. (1992), 'The hippocampus: What does it do?', *Behav Neural Biol* (57), 2–36.

Ereciska, M., Deas, J. and Silver, I. A. (1995), 'The effect of pH on glycolysis and phosphofructokinase activity in cultured cells and synaptosomes.', *Journal of Neurochemistry* **65**(6), 2765–2772.

Esposito, A., Gralle, M., Dani, M., Lange, D. and Wouters, F. (2008), 'pHlameleons: A Family of FRET-Based Protein Sensors for Quantitative pH Imaging', *Biochemistry-US* **47**(49), 13115–13126.

Farrant, M. and Kaila, K. (2007), 'The cellular, molecular and ionic basis of GABAA receptor signalling', *Prog. Brain Res.* **160**, 59–87.

Fedirko, N., Svichar, N. and Chesler, M. (2006), 'Fabrication and use of high-speed, concentric h+- and Ca2+-selective microelectrodes suitable for in vitro extracellular recording.', *Journal of neurophysiology* **96**(2), 919–24.

Fiumelli, H., Cancedda, L. and Poo, M.-m. (2005), 'Modulation of GABAergic transmission by activity via postsynaptic Ca2+-dependent regulation of KCC2 function.', *Neuron* **48**(5), 773–86.

Fleidervish, I. A. and Gutnick, M. J. (1995), 'Paired-pulse facilitation of IPSCs in slices of immature and mature mouse somatosensory neocortex.', *J. Neurophysiol.* **73**(6), 2591–5.

Freund, T. and Buzsáki, G. (1996), 'Interneurons of the hippocampus', *Hippocampus* **6**(4), 347–470.

Fujiwara-Tsukamoto, Y. (2006), 'Comparable GABAergic Mechanisms of Hippocampal Seizurelike Activity in Posttetanic and Low-Mg2+ Conditions', *Journal of Neurophysiology* **95**(3), 2013–2019.

Fujiwara-Tsukamoto, Y., Isomura, Y., Imanishi, M., Ninomiya, T., Tsukada, M., Yanagawa, Y., Fukai, T. and Takada, M. (2010), 'Prototypic Seizure Activity Driven by Mature Hippocampal Fast-Spiking Interneurons', *J. Neurosci.* **30**(41), 13679.

Fujiwara-Tsukamoto, Y., Isomura, Y., Nambu, A. and Takada, M. (2003), 'Excitatory GABA input directly drives seizure-like rhythmic synchronization in mature hippocampal CA1 pyramidal cells', *Neuroscience* **119**(1), 265–275.

Gamba, G., Unit, M. P., Nacional, I. and Me, D. C. (2005), 'Molecular Physiology and Pathophysiology of Electroneutral Cation-Chloride Cotransporters', *Mol. Biol.* pp. 423–493.

Gatto, C. and Milanick, M. A. (1993), 'Inhibition of the red blood cell calcium pump by eosin and other fluorescein analogues', *Am. J. Physiol.* **264**(6), C1577–1586.

Ghandour, M. S., Parkkila, A.-K., Parkkila, S., Waheed, A. and Sly, W. S. (2002), 'Mitochondrial Carbonic Anhydrase in the Nervous System', *Journal of Neurochemistry* **75**(5), 2212–2220.

Giffard, R. G., Papadopoulos, M. C., van Hooft, J. a., Xu, L., Giuffrida, R. and Monyer, H. (2000), 'The electrogenic sodium bicarbonate cotransporter: developmental expression in rat brain and possible role in acid vulnerability.', *J. Neurosci.* **20**(3), 1001–8.

Goshen, I., Brodsky, M., Prakash, R., Wallace, J., Gradinaru, V., Ramakrishnan, C. and Deisseroth, K. (2011), 'Dynamics of Retrieval Strategies for Remote Memories', *Cell* **147**(3), 678–689.

Gradinaru, V., Zhang, F., Ramakrishnan, C., Mattis, J., Prakash, R., Diester, I., Goshen, I., Thompson, K. R. and Deisseroth, K. (2010), 'Molecular and cellular approaches for diversifying and extending optogenetics.', *Cell* **141**(1), 154–165.

Granja, R., Strakhova, M., Knauer, C. and Skolnick, P. (1998), 'Anomalous rectifying properties of diazepam-insensitive GABAA receptors', *Eur J Pharmacol.* **345**(3), 315–321.

Grichtchenko, I. and Chesler, M. (1994), 'Depolarization-induced alkalinization of astrocytes in gliotic hippocampal slices', *Neuroscience* **62**(4), 1071–1078.

Griesbeck, O., Baird, G. S., Campbell, R. E., Zacharias, D. A. and Tsien, R. Y. (2001), 'Reducing the environmental sensitivity of yellow fluorescent protein. Mechanism and applications.', *J. Biol. Chem* **276**(31), 29188–94.

Grynkiewicz, G., Poenie, M. and Tsien, R. Y. (1985), 'A new generation of Ca2+ indicators with greatly improved fluorescence properties.', *J. Biol. Chem* **260**(6), 3440–50.

Gulledge, A. and Stuart, G. (2003), 'Excitatory actions of GABA in the cortex', *Neuron* **37**(2), 299–309.

Gupta, A., Wang, Y. and Markram, H. (2000), 'Organizing principles for a diversity of GABAergic interneurons and synapses in the neocortex.', *Science* **287**(5451), 273–8.

Gutiérrez, R., Armand, V., Schuchmann, S. and Heinemann, U. (1999), 'Epileptiform activity induced by low Mg2+ in cultured rat hippocampal slices.', *Brain Res.* **815**(2), 294–303.

Hablitz, J. J. (1984), 'Picrotoxin-induced epileptiform activity in hippocampus: role of endogenous versus synaptic factors', *J. Neurophysiol.* **51**(5), 1011–1027.

Hafting, T., Fyhn, M., Molden, S., Moser, M.-B. and Moser, E. I. (2005), 'Microstructure of a spatial map in the entorhinal cortex.', *Nature* **436**(7052), 801–6.

Haider, B., Duque, A., Hasenstaub, A. and McCormick, D. (2006), 'Neocortical network activity in vivo is generated through a dynamic balance of excitation and inhibition', *The Journal of neuroscience* **26**(17), 4535.

Hamill, O. P., Bormann, J. and Sakmann, B. (1983), 'Activation of multiple-conductance state chloride channels in spinal neurones by glycine and GABA', *Nature* **305**(5937), 805–808.

Han, X. and Boyden, E. S. (2007), 'Multiple-color optical activation, silencing, and desynchronization of neural activity, with single-spike temporal resolution.', *PloS one* **2**(3), e299.

Hanson, G., McAnaney, T., Park, E., Rendell, M., Yarbrough, D., Chu, S., Xi, L., Boxer, S., Montrose, M. and Remington, S. (2002), 'Green fluorescent protein variants as ratiometric dual emission pH sensors. 1. Structural characterization and preliminary application', *Biochemistry.* **41**(52), 15477–15488.

He, C., Yan, X., Zhang, H., Mirshahi, T., Jin, T., Huang, A. and Logothetis, D. E. (2002), 'Identification of critical residues controlling G protein-gated inwardly rectifying K(+) channel activity through interactions with the beta gamma subunits of G proteins.', *J Biol Chem.* **277**(8), 6088–96.

Henneberger, C., Papouin, T., Oliet, S. H. R. and Rusakov, D. A. (2010), 'Long-term potentiation depends on release of D-serine from astrocytes.', *Nature* **463**(7278), 232–6.

Hines, M. and Carnevale, N. (1997), 'The NEURON simulation environment', *Neural computation* **9**(6), 1179–1209.

Hösli, L., Hösli, E., Landolt, H. and Zehntner, C. (1981), 'Efflux of potassium from neurones excited by glutamate and aspartate causes a depolarization of cultured glial cells', *Neuroscience Letters* **21**(1), 83–86.

Iijima, T., Ciani, S. and Hagiwara, S. (1986), 'Effects of the External pH on Ca Channels: Experimental Studies and Theoretical Considerations Using a Two-Site, Two-Ion Model', *Proc. Natl. Acad. Sci. USA* **83**(3), 654–658.

Ilie, A., Raimondo, J. V. and Akerman, C. J. (2012), 'Adenosine Release during Seizures Attenuates GABAA Receptor-Mediated Depolarization', *Journal of Neuroscience* **32**(15), 5321–5332.

Inoue, M., Hara, M., Zeng, X. T., Hirose, T., Ohnishi, S., Yasukura, T., Uriu, T., Omori, K., Minato, A. and Inagaki, C. (1991), 'An ATP-driven Cl- pump regulates Cl- concentrations in rat hippocampal neurons.', *Neurosci. Lett.* **134**(1), 75–8.

Isomura, Y., Sugimoto, M., Fujiwara-Tsukamoto, Y., Yamamoto-Muraki, S., Yamada, J. and Fukuda, A. (2003), 'Synaptically activated Cl- accumulation responsible for depolarizing GABAergic responses in mature hippocampal neurons.', *Journal of neurophysiology* **90**(4), 2752–6.

Jarolimek, W., Lewen, A. and Misgeld, U. (1999), 'A furosemide-sensitive K+-Cl- cotransporter counteracts intracellular Cl- accumulation and depletion in cultured rat midbrain neurons.', *J. Neurosci.* **19**(12), 4695–704.

Jayaraman, S., Haggie, P., Wachter, R. M., Remington, S. J. and Verkman, A. S. (2000), 'Mechanism and Cellular Applications of a Green Fluorescent Protein-based Halide Sensor', *J. Biol. Chem* **275**(9), 6047–6050.

Jean-Xavier, C., Mentis, G. Z., O'Donovan, M. J., Cattaert, D. and Vinay, L. (2007), 'Dual personality of GABA/glycine-mediated depolarizations in immature spinal cord.', *Proc. Natl. Acad. Sci. USA* **104**(27), 11477–82.

Jedlicka, P., Deller, T. and Gutkin, B. (2011), 'Activity dependent intracellular chloride accumulation and diffusion controls GABAA receptor mediated synaptic transmission', *Hippocampus* **898**(June 2010), 885–898.

Jiang, L., Sun, S., Nedergaard, M. and Kang, J. (2000), 'Paired-pulse modulation at individual GABAergic synapses in rat hippocampus.', *J. Neurophysiol.* **523 Pt 2**(2000), 425–39.

Jin, X., Huguenard, J. and Prince, D. (2005), 'Impaired Clextrusion in layer V pyramidal neurons of chronically injured epileptogenic neocortex', *J. Neurophysiol.* **93**(4), 2117.

Kaila, K. (1994), 'Ionic basis of GABAA receptor channel function in the nervous system', *Progress in Neurobiology* **42**(4), 489–537.

Kaila, K., Lamsa, K., Smirnov, S., Taira, T. and Voipio, J. (1997), 'Long-lasting GABA-mediated depolarization evoked by high-frequency stimulation in pyramidal neurons of rat hippocampal slice is attributable to a network-driven, bicarbonate-dependent K+ transient', *J. Neurosci.* **17**(20), 7662.

Kang, J., Jiang, L., Goldman, S. a. and Nedergaard, M. (1998), 'Astrocyte-mediated potentiation of inhibitory synaptic transmission.', *Nat. Neurosci.* **1**(8), 683–92.

Khalilov, I., Holmes, G. L. and Ben-Ari, Y. (2003), 'In vitro formation of a secondary epileptogenic mirror focus by interhippocampal propagation of seizures.', *Nature neuroscience* **6**(10), 1079–85.

Kirischuk, S., Clements, J. D. and Grantyn, R. (2002), 'Presynaptic and postsynaptic mechanisms underlie paired pulse depression at single GABAergic boutons in rat collicular cultures', *J. Physiol.* **543**(1), 99–116.

Klausberger, T. and Somogyi, P. (2008), 'Neuronal diversity and temporal dynamics: the unity of hippocampal circuit operations.', *Science* **321**(5885), 53–7.

Koncz, C. and Daugirdas, J. (1994), 'Use of MQAE for measurement of intracellular [Cl-] in cultured aortic smooth muscle cells', *American Journal of Physiology-Heart and Circulatory Physiology* **267**(6), H2114.

Krishtal, O. a., Osipchuk, Y. V., Shelest, T. N. and Smirnoff, S. V. (1987), 'Rapid extracellular pH transients related to synaptic transmission in rat hippocampal slices.', *Brain Res.* **436**(2), 352–6.

Kuner, T. and Augustine, G. (2000), 'A Genetically Encoded Ratiometric Indicator for Chloride:: Capturing Chloride Transients in Cultured Hippocampal Neurons', *Neuron* **27**(3), 447–459.

Kyrozis, A. and Reichling, D. B. (1995), 'Perforated-patch recording with gramicidin avoids artifactual changes in intracellular chloride concentration.', *Journal of Neuroscience Methods* **57**(1), 27–35.

Lambert, N. and Grover, L. (1995), 'The mechanism of biphasic GABA responses.', *Science* **269**(5226), 928–9.

Lambert, N. and Wilson, W. (1994), 'Temporally distinct mechanisms of use-dependent depression at inhibitory synapses in the rat hippocampus in vitro.', *J. Neurophysiol.* **72**(1), 121–30.

Lamsa, K. and Kaila, K. (1997), 'Ionic mechanisms of spontaneous GABAergic events in rat hippocampal slices exposed to 4-aminopyridine', *J. Neurophysiol.* **78**(5), 2582.

Lasztóczi, B., Nyitrai, G., Héja, L. and Kardos, J. (2011), 'Synchronization of GABAergic Inputs to CA3 Pyramidal Cells Precedes Seizure-Like Event Onset in Juvenile Rat Hippocampal Slices Synchronization of GABAergic Inputs to CA3 Pyramidal Cells Precedes Seizure-Like Event Onset in Juvenile Rat Hippocampal Slices', *J. Neurophysiol.* .

Lillis, K. P., Kramer, M. a., Mertz, J., Staley, K. J. and White, J. a. (2012), 'Pyramidal cells accumulate chloride at seizure onset.', *Neurobiology of disease* **47**(3), 358–366.

London, M. and Häusser, M. (2005), 'Dendritic computation', *Annu. Rev. Neurosci.* **28**(1), 503–532.

Lopantsev, V. and Avoli, M. (1998), 'Participation of GABAA-mediated inhibition in ictallike discharges in the rat entorhinal cortex', *J. Neurophysiol.* **79**(1), 352.

Lu, Y. M., Mansuy, I. M., Kandel, E. R. and Roder, J. (2000), 'Calcineurin-mediated LTD of GABAergic inhibition underlies the increased excitability of CA1 neurons associated with LTP.', *Neuron* **26**(1), 197–205.

Lu, Y., Zheng, J., Xiong, L., Zimmermann, M. and Yang, J. (2008), 'Spinal cord injury-induced attenuation of GABAergic inhibition in spinal dorsal horn circuits is associated with down-regulation of the chloride transporter KCC2 in rat.', *J. Physiol.* **586**(Pt 23), 5701–15.

Ma, E. and Haddad, G. (1997), 'Expression and localization of Na+/H+ exchangers in rat central nervous system', *Neuroscience* **79**(2), 591–603.

Madisen, L., Mao, T., Koch, H., Zhuo, J.-m., Berenyi, A., Fujisawa, S., Hsu, Y.-w. A., Iii, A. J. G., Gu, X., Zanella, S., Kidney, J., Gu, H., Mao, Y., Hooks, B. M., Boyden, E. S., Buzsáki, G., Ramirez, J. M., Jones, A. R., Svoboda, K., Han, X., Turner, E. E. and Zeng, H. (2012), 'A toolbox of Cre-dependent optogenetic transgenic mice for light-induced activation and silencing', *Nat. Neurosci.* (February).

Majumdar, D. and Bevensee, M. O. (2010), 'Na-coupled bicarbonate transporters of the solute carrier 4 family in the nervous system: function, localization, and relevance to neurologic function.', *Neuroscience* **171**(4), 951–72.

Makani, S. and Chesler, M. (2010*a*), 'Barium Plateau Potentials of CA1 Pyramidal Neurons Elicit All-or-None Extracellular Alkaline Shifts Via the Plasma Membrane Calcium ATPase', *Journal of neurophysiology* **104**(3), 1438.

Makani, S. and Chesler, M. (2010*b*), 'Rapid rise of extracellular pH evoked by neural activity is generated by the plasma membrane calcium ATPase', *J. Neurophysiol.* **103**(2), 667.

Mann, E., Kohl, M. and Paulsen, O. (2009), 'Distinct roles of GABAA and GABAB receptors in balancing and terminating persistent cortical activity', *The Journal of Neuroscience* **29**(23), 7513.

Marandi, N., Konnerth, A. and Garaschuk, O. (2002), 'Two-photon chloride imaging in neurons of brain slices.', *Pflügers Archiv : European journal of physiology* **445**(3), 357–65.

Maren, T. (1967), 'Carbonic anhydrase: chemistry, physiology, and inhibition', *Physiol Revs.* .

Markova, O., Mukhtarov, M., Real, E., Jacob, Y. and Bregestovski, P. (2008), 'Genetically encoded chloride indicator with improved sensitivity', *J. Neurosci. Meth.* **170**(1), 67–76.

Mattis, J., Tye, K. M., Ferenczi, E. A., Ramakrishnan, C., Shea, D. J. O., Prakash, R., Gunaydin, L. A., Hyun, M., Fenno, L. E., Gradinaru, V., Yizhar, O. and Deisseroth, K. (2012), 'Principles for applying optogenetic tools derived from direct comparative analysis of microbial opsins', *Nat. Neurosci.* **2012**(deceMbeR 2011).

Mauro, A. (1954), 'Electrochemical potential difference of chloride ion in the squid giant axon-sea water system', *Fed. Proc* .

McCarren, M. and Alger, B. E. (1985), 'Use-dependent depression of IPSPs in rat hippocampal pyramidal cells in vitro.', *J. Neurophysiol.* **53**(2), 557–71.

McCormick, D. and Contreras, D. (2001), 'On the cellular and network bases of epileptic seizures', *Annual review of physiology* **63**(1), 815–846.

Megías, M., Emri, Z., Freund, T. and Gulyas, A. (2001), 'Total number and distribution of inhibitory and excitatory synapses on hippocampal CA1 pyramidal cells', *Neuroscience* **102**(3), 527–540.

Miesenböck, G. (1998), 'Visualizing secretion and synaptic transmission with pH-sensitive green fluorescent proteins', *Nature* .

Miesenböck, G., De Angelis, D. A. and Rothman, J. E. (1998), 'Visualizing secretion and synaptic transmission with pH-sensitive green fluorescent proteins.', *Nature* **394**(6689), 192–5.

Miles, R., To, K. and Gulya, A. I. (1996), 'Differences between Somatic and Dendritic Inhibition in the Hippocampus', *Neuron* **16**, 815–823.

Min, R. and Nevian, T. (2012), 'Astrocyte signaling controls spike timingdependent depression at neocortical synapses', *Nat Neurosci.* **15**(5), 746–53.

Mody, I., Lambert, J. D. and Heinemann, U. (1987), 'Low extracellular magnesium induces epileptiform activity and spreading depression in rat hippocampal slices.', *J. Neurophysiol.* **57**(3), 869–88.

Mori, T., Tanaka, K., Buffo, A., Wurst, W., Kühn, R. and Götz, M. (2006), 'Inducible gene deletion in astroglia and radial glia–a valuable tool for functional and lineage analysis.', *Glia* **54**(1), 21–34.

Morita, K., Tsumoto, K. and Aihara, K. (2006), 'Bidirectional modulation of neuronal responses by depolarizing GABAergic inputs.', *Biophys. J.* **90**(6), 1925–38.

Moser, E. I., Kropff, E. and Moser, M.-B. (2008), 'Place cells, grid cells, and the brain's spatial representation system.', *Annu Rev Neurosci.* **31**, 69–89.

Mott, D. D., Xie, C. W., Wilson, W. A., Swartzwelder, H. S. and Lewis, D. V. (1993), 'GABAB autoreceptors mediate activity-dependent disinhibition and enhance signal transmission in the dentate gyrus', *J. Neurophysiol.* pp. 674–691.

Noel, J. and Pouyssegur, J. (1995), 'Hormonal regulation, pharmacology, and membrane sorting of vertebrate Na+/H+ exchanger isoforms', *Am J Physiol Cell Physiol* **268**(2), C283–296.

Nusser, Z., Hajos, N., Somogyi, P., Mody, I. and Others (1998), 'Increased number of synaptic GABAA receptors underlies potentiation at hippocampal inhibitory synapses', *Nature* **395**(6698), 172–176.

Nusser, Z., Sieghart, W., Benke, D., Fritschy, J. M. and Somogyi, P. (1996), 'Differential synaptic localization of two major gamma-aminobutyric acid type A receptor alpha subunits on hippocampal pyramidal cells.', *Proceedings of the National Academy of Sciences of the United States of America* **93**(21), 11939–44.

O'Connor, E. and Sontheimer, H. (1994), 'Rat hippocampal astrocytes exhibit electrogenic sodium-bicarbonate co-transport', *J. Neurophysiol.* **72**, 2580–2589.

O'Keefe, J. and Dostrovsky, J. (1971), 'The hippocampus as a spatial map. Preliminary evidence from unit activity in the freely-moving rat', *Brain Res.* **34**(1), 171–175.

Ormond, J. and Woodin, M. a. (2009), 'Disinhibition mediates a form of hippocampal long-term potentiation in area CA1.', *PloS one* **4**(9), e7224.

Overstreet, L. S., Jones, M. V. and Westbrook, G. L. (2000), 'Slow Desensitization Regulates the Availability of Synaptic GABAA Receptors', *J. Neurosci.* **20**(21), 7914–7921.

Owens, D. F. and Kriegstein, A. R. (2002), 'Is there more to GABA than synaptic inhibition?', *Nat Revs Neurosci.* **3**(9), 715–27.

Palma, E., Amici, M., Sobrero, F., Spinelli, G., Di Angelantonio, S., Ragozzino, D., Mascia, A., Scoppetta, C., Esposito, V., Miledi, R. and Eusebi, F. (2006), 'Anomalous levels of Cl- transporters in the hippocampal subiculum from temporal lobe epilepsy patients make GABA excitatory.', *Proceedings of the National Academy of Sciences of the United States of America* **103**(22), 8465–8.

Pappas, C. A. and Ransom, B. R. (1993), 'A depolarization-stimulated, bafilomycin-inhibitable H+ pump in hippocampal astrocytes', *Glia* **9**(4), 280–291.

Pappas, C. and Ransom, B. (1994), 'Depolarization-induced alkalinization (DIA) in rat hippocampal astrocytes', *J. Neurophysiol.* **72**(6), 2816.

Pasternack, M., Smirnov, S. and Kaila, K. (1996), 'Proton Modulation of Functionally Distinct GABAA Receptors in Acutely Isolated Pyramidal Neurons of Rat Hippocampus', *Neuropharmacology* **35**(9-10), 1279–1288.

Pasternack, M., Voipio, J. and Kaila, K. (1993), 'Intracellular carbonic anhydrase activity and its role in GABA-induced acidosis in isolated rat hippocampal pyramidal neurones', *Acta Physiol. Scand.* **148**(2), 229–231.

Pathak, H., Weissinger, F., Terunuma, M., Carlson, G., Hsu, F., Moss, S. and Coulter, D. (2007), 'Disrupted dentate granule cell chloride regulation enhances synaptic excitability during development of temporal lobe epilepsy', *J. Neurosci.* **27**(51), 14012.

Pavlov, I., Savtchenko, L. P., Kullmann, D. M., Semyanov, A. and Walker, M. C. (2009), 'Outwardly rectifying tonically active GABAA receptors in pyramidal cells modulate neuronal offset, not gain.', *The Journal of neuroscience : the official journal of the Society for Neuroscience* **29**(48), 15341–50.

Pellerin, L., Bouzier-Sore, A.-K., Aubert, A., Serres, S., Merle, M., Costalat, R. and Magistretti, P. J. (2007), 'Activity-dependent regulation of energy metabolism by astrocytes: an update.', *Glia* **55**(12), 1251–1262.

Pellerin, L. and Magistretti, P. J. (1994), 'Glutamate Uptake into Astrocytes Stimulates Aerobic Glycolysis: A Mechanism Coupling Neuronal Activity to Glucose Utilization', *Proc Natl Acad Sci U S A.* **91**(22), 10625–10629.

Perea, G. and Araque, A. (2010), 'GLIA modulates synaptic transmission.', *Brain Res Revs* **63**(1-2), 93–102.

Perea, G., Navarrete, M. and Araque, A. (2009), 'Tripartite synapses: astrocytes process and control synaptic information.', *Trends in neurosciences* **32**(8), 421–31.

Perreault, P. and Avoli, M. (1992), '4-Aminopyridine-induced epileptiform activity and a GABA-mediated long-lasting depolarization in the rat hippocampus', *The Journal of neuroscience* **12**(1), 104.

Pouille, F. and Scanziani, M. (2001), 'Enforcement of temporal fidelity in pyramidal cells by somatic feed-forward inhibition.', *Science (New York, N.Y.)* **293**(5532), 1159–63.

Pouille, F. and Scanziani, M. (2004), 'Routing of spike series by dynamic circuits in the hippocampus.', *Nature* **429**(6993), 717–23.

Qian, N. and Sejnowski, T. (1990), 'When is an inhibitory synapse effective?', *Proc. Natl. Acad. Sci. USA* **87**(20), 8145 –8149.

Raimondo, J. V., Irkle, A., Wefelmeyer, W., Newey, S. E. and Akerman, C. J. (2012), 'Genetically encoded proton sensors reveal activity-dependent pH changes in neurons', *Frontiers in Molecular Neuroscience* **5**(May), 1–12.

Raimondo, J. V., Kay, L., Ellender, T. J. and Akerman, C. J. (2012), 'Optogenetic silencing strategies differ in their effects on inhibitory synaptic transmission', *Nature Neuroscience* (June), 1–5.

Ransom, B. R. (1992), 'Glial modulation of neural excitability mediated by extracellular pH: a hypothesis.', *Progress in Brain Research* **94**, 37–46.

Ransom, B. R. (2000), 'Glial modulation of neural excitability mediated by extracellular pH: a hypothesis revisited.', *Progress in Brain Research* **125**, 217–228.

Richards, B. A., Voss, O. P. and Akerman, C. J. (2010), 'GABAergic circuits control stimulus-instructed receptive field development in the optic tectum.', *Nat. Neurosci.* **13**(9), 1098–106.

Rinke, I., Artmann, J. and Stein, V. (2010), 'ClC-2 voltage-gated channels constitute part of the background conductance and assist chloride extrusion.', *J. Neurosci.* **30**(13), 4776–86.

Rivera, C., Li, H., Thomas-Crusells, J., Lahtinen, H., Viitanen, T., Nanobashvili, A., Kokaia, Z., Airaksinen, M. S., Voipio, J., Kaila, K. and Saarma, M. (2002), 'BDNF-induced TrkB activation down-regulates the K+-Cl- cotransporter KCC2 and impairs neuronal Cl- extrusion.', *J Cell Biol.* **159**(5), 747–52.

Rivera, C., Voipio, J. and Kaila, K. (2005), 'Two developmental switches in GABAergic signalling: the K+Cl- cotransporter KCC2 and carbonic anhydrase CAVII', *J. Physiol.* **562**(1), 27.

Rivera, C., Voipio, J., Payne, J. A., Ruusuvuori, E., Lahtinen, H., Lamsa, K., Pirvola, U., Saarma, M. and Kaila, K. (1999), 'The K+/Cl- co-transporter KCC2 renders GABA hyperpolarizing during neuronal maturation.', *Nature* **397**(6716), 251–5.

Rivera, C., Voipio, J., Thomas-Crusells, J., Li, H., Emri, Z., Sipilä, S., Payne, J. A., Minichiello, L., Saarma, M. and Kaila, K. (2004), 'Mechanism of activity-dependent downregulation of the neuron-specific K-Cl cotransporter KCC2.', *J Neurosci.* **24**(19), 4683–91.

Romero, M. F., Hediger, M. A., Boulpaep, E. L. and Boron, W. F. (1997), 'Expression cloning and characterization of a renal electrogenic Na+/HCO3- cotransporter.', *Nature* **387**(6631), 409–13.

Rose, C. R. and Deitmer, J. W. (1995), 'Stimulus-evoked changes of extra- and intracellular pH in the leech central nervous system. II. Mechanisms and maintenance of pH homeostasis', *J. Neurophysiol.* **73**(1), 132–140.

Ruminot, I., Gutiérrez, R., Peña Münzenmayer, G., Añazco, C., Sotelo-Hitschfeld, T., Lerchundi, R., Niemeyer, M. I., Shull, G. E. and Barros, L. F. (2011), 'NBCe1 mediates the acute stimulation of astrocytic glycolysis by extracellular K+.', *J. Neurosci.* **31**(40), 14264–71.

Russell, J. (2000), 'Sodium-potassium-chloride cotransport', *Physiological Reviews* **80**(1), 211.

Ruusuvuori, E., Li, H., Huttu, K., Palva, J., Smirnov, S., Rivera, C., Kaila, K. and Voipio, J. (2004), 'Carbonic anhydrase isoform VII acts as a molecular switch in the development of synchronous gamma-frequency firing of hippocampal CA1 pyramidal cells', *J. Neurosci.* **24**(11), 2699.

Sanchez-Vives, M. and McCormick, D. (2000), 'Cellular and network mechanisms of rhythmic recurrent activity in neocortex', *Nature neuroscience* **3**(10), 1027–1034.

Saraga, F., Balena, T., Wolansky, T., Dickson, C. T. and Woodin, M. a. (2008), 'Inhibitory synaptic plasticity regulates pyramidal neuron spiking in the rodent hippocampus.', *Neuroscience* **155**(1), 64–75.

Schmitt, B. M., Berger, U. V., Douglas, R. M., Bevensee, M. O., Hediger, M. a., Haddad, G. G. and Boron, W. F. (2000), 'Na/HCO3 cotransporters in rat brain: expression in glia, neurons, and choroid plexus.', *J. Neurosci.* **20**(18), 6839–48.

Schwiening, C., Kennedy, H. and Thomas, R. (1993), 'Calcium-hydrogen exchange by the plasma membrane Ca-ATPase of voltage-clamped snail neurons', *Proc. Biol. Sci.* pp. 285–289.

Seki, A., Miyauchi, S., Hayashi, S., Kikukawa, T., Kubo, M., Demura, M., Ganapathy, V. and Kamo, N. (2007), 'Heterologous expression of Pharaonis halorhodopsin in Xenopus laevis oocytes and electrophysiological characterization of its light-driven Cl-pump activity', *Biophys. J.* **92**(7), 2559–2569.

Shaner, N. C., Steinbach, P. A. and Tsien, R. Y. (2005), 'A guide to choosing fluorescent proteins.', *Nature methods* **2**(12), 905–9.

Sieghart, W. and Sperk, G. (2002), 'Subunit composition, distribution and function of GABA(A) receptor subtypes.', *Curr. Top. Med. Chem.* **2**(8), 795–816.

Slemmer, J., Matsushita, S., De Zeeuw, C., Weber, J. and Knöpfel, T. (2004), 'Glutamate-induced elevations in intracellular chloride concentration in hippocampal cell cultures derived from EYFP-expressing mice', *European Journal of Neuroscience* **19**(11), 2915–2922.

Smart, T. G. and Constanti, A. (1982), 'A Novel Effect of Zinc on the Lobster Muscle GABA Receptor', *Proc R Soc Lond B Biol Sci.* **215**(1200), 327–341.

Solstad, T., Boccara, C. N., Kropff, E., Moser, M.-B. and Moser, E. I. (2008), 'Representation of geometric borders in the entorhinal cortex.', *Science* **322**(5909), 1865–8.

Somogyi, P. and Klausberger, T. (2005), 'Defined types of cortical interneurone structure space and spike timing in the hippocampus.', *J Physiol* **562**(Pt 1), 9–26.

Spray, D., Harris, A. and Bennett, M. (1981), 'Gap junctional conductance is a simple and sensitive function of intracellular pH', *Science* **211**(4483), 712.

Staley, K. and Proctor, W. (1999), 'Modulation of mammalian dendritic GABAA receptor function by the kinetics of Cl- and HCO3- transport', *J. Physiol.* **519**(3), 693.

Staley, K. and Soldo, B. (1995), 'Ionic mechanisms of neuronal excitation by inhibitory GABAA receptors', *Science* **30428**.

Sterling, D. and Casey, J. (1999), 'Transport activity of AE3 chloride/bicarbonate anion-exchange proteins and their regulation by intracellular pH.', *Biochem. J.* **229**, 221–229.

Stoppini, L., Buchs, P.-A. and Muller, D. (1991), 'A simple method for organotypic cultures of nervous tissue', *Journal of neuroscience methods* **37**(2), 173–182.

Straub, H., Köhling, R., Lücke, A., Fauteck, J.-D., Speckmann, E.-J., Moskopp, D., Wassmann, H., Tuxhorn, I., Wolf, P., Pannek, H. and Oppel, F. (1996), 'The effects of verapamil and flunarizine on epileptiform activity induced by bicuculline and low Mg2+ in neocortical tissue of epileptic and primary non-epileptic patients', *Brain Res.* **733**(2), 307–311.

Supuran, C. T. (2008), 'Carbonic anhydrases: novel therapeutic applications for inhibitors and activators.', *Nat Revs.* **7**(2), 168–81.

Svichar, N., Esquenazi, S., Chen, H.-Y. and Chesler, M. (2011), 'Preemptive regulation of intracellular pH in hippocampal neurons by a dual mechanism of depolarization-induced alkalinization.', *J. Neurosci.* **31**(19), 6997–7004.

Svichar, N., Waheed, A., Sly, W. S., Hennings, J. C., Hübner, C. A. and Chesler, M. (2009), 'Carbonic anhydrases CA4 and CA14 both enhance AE3-mediated Cl–HCO3-exchange in hippocampal neurons.', *J Neurosci.* **29**(10), 3252–8.

Tabb, J., Kish, P., Van Dyke, R. and Ueda, T. (1992), 'Glutamate transport into synaptic vesicles. Roles of membrane potential, pH gradient, and intravesicular pH', *J. Biol. Chem.* **267**(22), 15412–15418.

Takeuchi, A. and Takeuchi, N. (1967), 'Anion permeability of the inhibitory post-synaptic membrane of the crayfish neuromuscular junction', *J Physiol.* **191**(3), 575–590.

Tamás, G., Buhl, E. H., Lörincz, A. and Somogyi, P. (2000), 'Proximally targeted GABAergic synapses and gap junctions synchronize cortical interneurons.', *Nature neuroscience* **3**(4), 366–71.

Tang, C., Dichter, M. and Morad, M. (1990), 'Modulation of the N-Methyl-D-Aspartate Channel by Extracellular H+', *Proc. Natl. Acad. Sci. USA* **87**(16), 6445–6449.

Taube, J., Muller, R. and Ranck, J. (1990), 'Head-direction cells recorded from the postsubiculum in freely moving rats. I. Description and quantitative analysis', *J Neurosci.* .

Thomas, R. C. (2008), 'The plasma membrane calcium ATPase (PMCA) of neurones is electroneutral and exchanges 2 H+ for each Ca2+ or Ba2+ ion extruded', *The Journal of Physiology* **587**(2), 315–327.

Thompson, S. and Gahwiler, B. (1989*a*), 'Activity-dependent disinhibition. I. Repetitive stimulation reduces IPSP driving force and conductance in the hippocampus in vitro', *J. Neurophysiol.* **61**(3), 501.

Thompson, S. and Gahwiler, B. (1989*b*), 'Activity-dependent disinhibition. II. Effects of extracellular potassium, furosemide, and membrane potential on ECl-in hippocampal CA3 neurons', *J. Neurophysiol.* **61**(3), 512.

Tombaugh, G. C. (1998), 'Intracellular pH Buffering Shapes Activity-Dependent Ca2+ Dynamics in Dendrites of CA1 Interneurons', *J Neurophysiol* **80**(4), 1702–1712.

Tombaugh, G. C. and Somjen, G. G. (1997), 'Differential Sensitivity to Intracellular pH Among High- and Low-Threshold Ca2+ Currents in Isolated Rat CA1 Neurons', *J Neurophysiol* **77**(2), 639–653.

Tramier, M., Zahid, M., Mevel, J.-C., Masse, M.-J. and Coppey-Moisan, M. (2006), 'Sensitivity of CFP/YFP and GFP/mCherry pairs to donor photobleaching on FRET determination by fluorescence lifetime imaging microscopy in living cells.', *Microsc. Res. Techniq.* **69**(11), 933–9.

Trapp, S., Luckermann, M., Brooks, P. A. and Ballanyi, K. (1996), 'Acidosis of rat dorsal vagal neurons in situ during spontaneous and evoked activity.', *J. Physiol.* **496**(Pt_3), 695–710.

Traynelis, S. F. and Cull-Candy, S. G. (1990), 'Proton inhibition of N-methyl-D-aspartate receptors in cerebellar neurons', *Nature* **345**(6273), 347–350.

Treiman, D. M. (2001), 'GABAergic Mechanisms in Epilepsy', *Epilepsia* **42**, 8–12.

Trevelyan, A. J., Sussillo, D. and Yuste, R. (2007), 'Feedforward inhibition contributes to the control of epileptiform propagation speed.', *The Journal of neuroscience : the official journal of the Society for Neuroscience* **27**(13), 3383–7.

Trivedi, B. and Danforth, W. H. (1966), 'Effect of pH on the kinetics of frog muscle phosphofructokinase.', *The Journal of Biological Chemistry* **241**(17), 4110–4112.

Tsodyks, M. V. and Markram, H. (1997), 'The neural code between neocortical pyramidal neurons depends', *Proc. Natl. Acad. Sci. USA* **94**(January), 719–723.

Tyzio, R., Minlebaev, M., Rheims, S., Ivanov, A., Jorquera, I., Holmes, G. L., Zilberter, Y., Ben-Ari, Y. and Khazipov, R. (2008), 'Postnatal changes in somatic gamma-aminobutyric acid signalling in the rat hippocampus.', *The European journal of neuroscience* **27**(10), 2515–28.

Urbanics, R., Leniger-Follert, E. and Ltibbers, D. (1978), 'Time course of changes of extracellular H+ and K+ activities during and after direct electrical stimulation of the brain cortex', **53**, 47–53.

Valeeva, G., Abdullin, A., Tyzio, R., Skorinkin, A., Nikolski, E., Ben-Ari, Y. and Khazipov, R. (2010), 'Temporal coding at the immature depolarizing GABAergic synapse.', *Front. Cell. Neurosci.* **4**(July), 1–12.

Varela, J., Sen, K., Gibson, J., Fost, J., Abbott, L. F. and Nelson, S. B. (1997), 'A quantitative description of short-term plasticity at excitatory synapses in layer 2/3 of rat primary visual cortex', *J. Neurosci.* **17**(20), 7926–7940.

Vasseur, M., Frangne, R. and Alvarado, F. (1993), 'Buffer-dependent pH sensitivity of the fluorescent chloride-indicator dye SPQ', *American Journal of Physiology-Cell Physiology* **264**(1), C27.

Viitanen, T. (2010), 'GABA A Receptor Mediated Signalling in the Brain: Inhibition, Shunting and Excitation', *Phd Thesis* (June).

Viitanen, T., Ruusuvuori, E., Kaila, K. and Voipio, J. (2010), 'The K+-Cl cotransporter KCC2 promotes GABAergic excitation in the mature rat hippocampus.', *J. Physiol.* **588**(Pt 9), 1527–40.

Vithlani, M., Terunuma, M. and Moss, S. J. (2011), 'The Dynamic Modulation of GABAA Receptor Trafficking and Its Role in Regulating the Plasticity of Inhibitory Synapses.', *Physiological reviews* **91**(3), 1009–22.

Vyklicky, L., Vlachova, V. and Krusek, J. (1990), 'The effect of external pH changes on responses to excitatory amino acids in mouse hippocampal neurones.', *J. Physiol.* **430**(1), 497–517.

Wallraff, A., Köhling, R., Heinemann, U., Theis, M., Willecke, K. and Steinhäuser, C. (2006), 'The impact of astrocytic gap junctional coupling on potassium buffering in the hippocampus.', *The Journal of neuroscience : the official journal of the Society for Neuroscience* **26**(20), 5438–47.

Wang, G. J., Randall, R. D. and Thayer, S. A. (1994), 'Glutamate-induced intracellular acidification of cultured hippocampal neurons demonstrates altered energy metabolism resulting from Ca2+ loads', *J. Neurophysiol.* **72**(6), 2563–2569.

Wang, L., Kitai, S. T. and Xiang, Z. (2006), 'Activity-dependent bidirectional modification of inhibitory synaptic transmission in rat subthalamic neurons.', *J. Neurosci.* **26**(28), 7321–7.

Wilson, M. A. and McNaughton, B. L. (1994), 'Reactivation of hippocampal ensemble memories during sleep', *Science* **265**(5172), 676–679.

Witten, I. B., Lin, S.-C., Brodsky, M., Prakash, R., Diester, I., Anikeeva, P., Gradinaru, V., Ramakrishnan, C. and Deisseroth, K. (2010), 'Cholinergic interneurons control local circuit activity and cocaine conditioning.', *Science* **330**(6011), 1677–1681.

Woodin, M. A., Ganguly, K. and Poo, M.-m. (2003), 'Coincident pre- and postsynaptic activity modifies GABAergic synapses by postsynaptic changes in Cl- transporter activity.', *Neuron* **39**(5), 807–20.

Wright, R., Raimondo, J. V. and Akerman, C. J. (2011), 'Spatial and temporal dynamics in the ionic driving force for GABA(A) receptors.', *Neural plasticity* **2011**, 728395.

Xiong, Z., Saggau, P. and Stringer, J. (2000), 'Activity-dependent intracellular acidification correlates with the duration of seizure activity', *J. Neurosci.* **20**(4), 1290.

Yamamoto, C. (1972), 'Intracellular study of seizure-like afterdischarges elicited in thin hippocampal sections in vitro.', *Exp. Neurol.* .

Yamamoto, C. and Kawai, N. (1967), 'Seizure discharges evoked in vitro in thin section from guinea pig hippocampus', *Science* .

Yamamoto, C. and Kawai, N. (1968), 'Generation of the seizure discharge in thin sections from the guinea pig brain in chloride-free medium in vitro.', *Jpn. J. Physiol.* .

Yamamoto, C. and Kawai, N. (1969), 'Origin of the seizure discharge evoked in vitro in thin sections from the guinea pig dentate gyrus.', *Jpn. J. Physiol.* .

Yang, Y., Ge, W., Chen, Y., Zhang, Z., Shen, W., Wu, C., Poo, M. and Duan, S. (2003), 'Contribution of astrocytes to hippocampal long-term potentiation through release of D-serine.', *Proc Natl Acad Sci U S A.* **100**(25), 15194–9.

Yizhar, O., Fenno, L. E., Davidson, T. J., Mogri, M. and Deisseroth, K. (2011), 'Optogenetics in neural systems.', *Neuron* **71**(1), 9–34.

Yu, X., Carroll, S., Rigaud, J. and Inesi, G. (1993), 'H+ countertransport and electrogenicity of the sarcoplasmic reticulum Ca2+ pump in reconstituted proteoliposomes', *Biophysical Journal* **64**(4), 1232–1242.

Zerangue, N. and Kavanaugh, M. P. (1996), 'Flux coupling in a neuronal glutamate transporter.', *Nature* **383**(6601), 634–637.

Zhang, F., Wang, L.-P., Brauner, M., Liewald, J. F., Kay, K., Watzke, N., Wood, P. G., Bamberg, E., Nagel, G., Gottschalk, A. and Deisseroth, K. (2007), 'Multimodal fast optical interrogation of neural circuitry.', *Nature* **446**(7136), 633–9.

Zhang, Y. (2010), 'Astrocyte heterogeneity: an underappreciated topic in neurobiology', *Current Opinion in Neurobiology* **20**(5), 588–594.

Zhu, L., Lovinger, D. and Delpire, E. (2005), 'Cortical neurons lacking KCC2 expression show impaired regulation of intracellular chloride.', *J. Neurophysiol.* **93**(3), 1557–68.

Zucker, R. M. and Price, O. (2001), 'Evaluation of confocal microscopy system performance.', *Cytometry* **44**(4), 273–94.

Zucker, R. S. and Regehr, W. G. (2002), 'Short-term synaptic plasticity.', *Ann. Rev. Physiol.* **64**, 355–405.